ANALYSIS OF THE ACCURACY AND PRECISION OF MAGNETIC AZIMUTHS MEASURED BY DIFFERENT CAVE SURVEYING INSTRUMENTS

Peter Tarsoly, PhD.
Alba Regia Technical Faculty of Óbuda University, Székesfehérvár, Hungary
tarsoly.peter@amk.uni-obuda.hu

Abstract **- By cave surveying playing important roles those instruments, which are able to determine the direction of the magnetic meridian or the angle, between the line of sight and the magnetic north. The field surveying data, like the magnetic azimuths determine directly the accuracy of a cave map, so it is important to know exactly the precision and accuracy of a magnetic azimuth**

After testing four instruments (Süss-compass, Sokkia SET 230 R with a tubular-bussola, simple compass, Quechua C100 bussola with a dioptre), I involved in the precision and accuracy examinations two instruments: the Sokkia SET 230R mounted with a tubular-bussola and a Quechua C100 bussola. The precision of the tubular-bussola is 17'40", which is significantly worse, as given in the owner's manual (3-7'). The precision of the magnetic azimuth measured by the C100 bussola is 45', which is very good, when we take into account the non-precise setting up possibility of this instrument, and the disadvantages of the pointing with a dioptre. The circumstances in the caves rarely allowed to measure longer directions as 50 meters; in the most occasions the lengths of directions are between 0 and 15 meters. Take into account this distance-interval, the accuracy of magnetic azimuths, measured with the tubular-bussola will be between 0-8 cm, and measured with the Quechua C100 bussola will be between 0-20 cm.

I. INTRODUCTION

The most relevant documentation of a cave surveying campaign is the resulted map. By the field surveying we need to determine the angle between the line of sight and the magnetic north. For the determination of the magnetic azimuth we are using compasses and bussole (it is a compass, which has a sighting equipment, like a dioptre). Among the bussole we can find also some special instruments, like the tubular-bussola, which is an orientation bussola. It can be mount on the top of the alidade of a total station and is appropriate to show the direction of the magnetic meridian. When we set zero reading into this direction, we are able to measure directly magnetic azimuths on the field.

There are three different cave surveying methods, which are widely used: the chase-method, the TS (Total Station)-surveying and laser scanning [3]. By the chase-method and the TS-surveying we are using magnetic azimuths for the orientation of polygon lines. Only in rare occasions are we able to use points, with given coordinates in the national grid system (in Hungary this is the EOV) for the orientation. By laser scanning we are using pass points given in a local network or with coordinates given in the national grid system. Before the scanning we must determine the coordinates of the pass points, using some surveying methods, like TS-surveying or GNSS-measurements.

By cave surveying playing important roles those instruments, which are able to determine the direction of the magnetic meridian or the angle, between the line of sight and the magnetic north. The field surveying data, like the magnetic azimuths determine directly the accuracy of a cave map, so that is why it is important to know exactly the precision and accuracy of a magnetic azimuth.

II. THE STRUCTURE AND USE OF COMPASSES AND BUSSOLE

The bussola is a compass, which has a sighting equipment. In the surveying practice we are using circle bussole and orientation bussole. The most important part of a bussola is a wolfram or chrome-steel needle. The needle, and its pivot-point is built in a conic agate cup [4]. To ensure proper and prolonged operation of the needle, pivot point and cup, the needle can be fixed by pressing the cup to the glass with a catch. The magnetic needle must has a great magnetic remanency and a little coercitive force.

Due to the strength of the magnetic field of the Earth, the magnetic needle points to the magnetic north (N_M), which differs from the astronomical north (N_A) by the Δ magnetic declination (Fig.1). The declination is positive, when the magnetic north points to the east form the astronomical north. The magnetic needle deviates from the horizontal with an angle, called magnetic inclination.

The circle bussola contains counter-clockwise increasing graduations on its perimeter. When we rotate the bussola clockwise, the readings taken by the opposite ends of the needle are increasing, and are showing the magnetic azimuth of the collimation axis, which is parallel with the 0° - 180° graduations. By some bussola

types the graduated circle and the needle are fastened, and are making rotation and swinging in a cup, which is full with shock absorber liquid, like oil. In this occasion the graduation of the circle is increasing clockwise, and the reading, taken on the index, mounted on the magnetic needle-house, shows directly the value of the magnetic azimuth. The tubular-bussola does not contain any graduations. The opposite ends of the needle are tend 90° upwards, and can be adjust in coincide with the help of a little mirror over the needle, using the small motion screw of the total station [4]. When the ends of the needle coincide, the collimation axis of the total station points to the magnetic north. When we store the reading for this direction, or set zero reading for it, than we record the direction of the magnetic meridian, as an orientation point for the further measurements and calculations. By some other types of tubular-bussole the free-swinging needle can bring into the centreline of two parallel, vertical index lines using the horizontal small motion screw of the instrument. When the needle coincide with the centreline, the line of sight points to the direction of the magnetic north.

The angle between the N_A astronomical north and the N_G grid north is the μ convergence of the meridians. The meridian convergence is positive, when the grid north points to the east form the astronomical north.

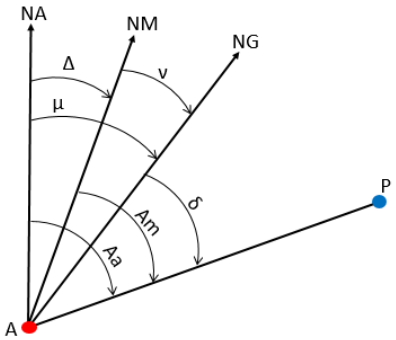

Figure 1. The relationship between the N_A astronomical, N_G grid and N_M magnetic norths

The angle between the N_M magnetic north and the N_G grid north is the ν magnetic orientation angle. It is positive, when the grid north points to the east form the magnetic north. For the mapping we need bearings (δ), also the angle between the line of sight and the grid north. To derivate astronomical azimuth from the magnetic azimuth we must reduce it using the magnetic declination, and the using meridian convergene we can derive from the astronomical azimuth bearing. When we know the value of the magnetic orientation angle, we can calculate directly the bearing from the magnetic azimuth:

$$\delta = A_m - \vartheta = A_m + \Delta - \mu \qquad (1)$$

The magnetic north at any particular place varies over a period of a century by tens of degrees, the complete cycle taking as much as for centuries or more. Such variation is referred to as the secular change. The annual change of the magnetic declination in Europe is on the average something like 5', westerly is currently diminishing while easterly declination is increasing [6]. There is also a diurnal variation which, in the middle latitudes of Hungary, may be as much as 15', in summer this value is greater than in winter and greater in the northern parts than in the southern parts of our country [8]. The magnetic declination may be also effected by magnetic disturbances or magnetic storms induced by different effects f.e. aurora borealis, solar activity etc. The magnetic needle's readings are also strongly influenced by the place of observation in areas of magnetic ore deposits. Such departures from the mean value of magnetic declination are described as magnetic anomalies. Great care should be taken not to work in areas where is a large amount of iron in the vicinity of a railway, ferroconcrete, fence or high-tension power line etc. The observers in the neighbourhood of the instrument could not have tools made of iron (hammer, axe, peg or penknife etc.) on them.

The magnetic declination varies in time and space. To calculate it, the plainest procedure is to use some free databases published on the Internet, like ngdc.noaa.gov; geomag.nrcan.gc.ca etc. The effect of the magnetic inclination is balanced with a weight, which is on the same offset situation on the magnetic needle, in the whole are of Hungary. The value of the meridian convergence does not varies in time, it depends only from the place and the used grid system. In Hungary, using the national grid system, the EOV, its value varies between -2° and +2°. His calculation is regulated by the A1 Grid Regulation (MÉM OFTH Surveying Department 63619/2/1975. direction).

III. TESTING OF A SURVEYOR'S COMPASS AND BUSSOLA

The surveyor's compass or bussola should meet the following requirements [5]:

1. the graduation of the horizontal circle must be adequately accurate,
2. the magnetic needle should be properly charged, the pivot point well sharpened, and the cup polished,
3. the magnetic needle should be straight,
4. the rotation axis of the magnetic needle should pass through the centre of the graduated circle.

The bussola in terms of the over mentioned points should be tested.

1. Let us pull an optional line on a paper, and let us fit always another graduate to this. If the readings agree within the range of the least count, than the graduations of the horizontal circle are adequate accurate.
2. To test this take readings on the graduated circle from the opposite ends of the needle when it has settled. Then place an iron object next to the needle and on removing it take a second reading once the needle has again settled. If the readings agree and the needle settles after a few swings (30") the requirement is met. If the needle settles quickly but the readings fail to agree, it shows that either the pivot point is dulled or the agate cup is badly polished. Should the needle swing

for a long time before it settles, this means that it is badly charged.

3. The magnetic needle is straight, when the readings making from the opposite ends of the needle, differs exactly with 180°. The admissible variance should be 0.3° (18'), because it falls out by the diametral readings. If the difference is not 180°, the reason could be the eccentricity of the needle, too.
4. Rotate the horizontal circle within a range of 10° clockwise, and take readings from opposite ends of the needle from different parts of the graduated circle. If the difference of the readings is exactly 180°, the needle is straight and his axis pass through the centre of the graduated circle. If the differences are uniform, the axis of the needle pass through the centre of the graduated circle, but is not straight. When the axis of the needle is eccentric, the reading differs from 180° with different, but symmetric values on the different places. If the differences are not symmetric, than the needle is not straight and is eccentric. To rule out the effect of eccentricity and roundabout of the needle we have to calculate the arithmetical mean of the readings taken from both ends of the magnetic needle.

IV. THE INSTRUMENTS USED FOR THE EXAMINATION

I used four instruments for the examination: Sokkia SET 230R total station with a tubular-bussola, a compass manufactured by Süss, Quechua C100 bussola with a diopter, and a simple compass with an unknown trademark (Fig.2).

The angular measurement accuracy of the Sokkia SET 230R total station is 2", the magnification is 30°. The tubular-bussola can be mount on the alidade. The tubular-bussola is not a coincide-structured bussola. The free-swinging needle can bring into the centreline of two parallel, vertical index lines using the horizontal small motion screw of the instrument. When the needle coincide with the centreline, the line of sight points to the direction of the magnetic north. The precision of the tubular-bussola is 3-7' [7].

The compass, manufactured by Süss can be mount also on the top of the alidade of an instrument. It can be also use directly on the ground by the chase-method. It is graduated counter-clockwise from the South, the least count is 20'.

By Quechua C100 bussola the graduated circle and the needle are fastened, and are making rotation and swinging in a cup, which is full with shock absorber liquid. The graduation of the circle is increasing clockwise from the North, the least count is 5°. We should take the readings in ticks, then 64 ticks are equal with 360°. The least count is 0.2 tick, and we could estimate the reading by 0.1 tick. One tick is equal with 5°37'30", 0.1 is equal with 0°33'45". So when we take the reading in ticks, the least count is 0°33'45".

The graduation of the circle of the simple compass is increasing clockwise from the north, the least count is 2°.

Figure 2. The Sokkia SET 230R total station with a tubular-bussola (a), the compass manufactured by Süss (b), Quechua C100 bussola (c) and the simple compass (d)

V. TESTING THE INSTRUMENTS USED FOR THE EXAMINATION

By the Süss-compass and by the simple compass it was possible to do the full examination process. By the Quechua C100 bussola it was possible to do the first and second examination steps, because the structure of the instrument does not allowed the third and the fourth steps. By this instrument we supposed, that the magnetic needle is centered and straight (it was insured in the course of the production process already). By the tubular-bussola is neither opportunity nor need for this kind of examination, because this instrument deals only for setting out the direction of the magnetic meridian. The Table 1. contains the results of the examination.

Table 1. Testing the instruments used for the examination

Instruments	Graduation accuracy	Charge		Straightness	Centring
		Settle time["]	RMSE [°]		
Compass (Süss)	good	14	1	yes	yes
Simple compass	good	4	2	yes	no
Quechua C100	good	11	0.3	-	-

The graduated circle of the Süss-compass does not have graduation errors, the magnetic needle is straight and centered, but the magnetic needle is badly charged and either the pivot point is dulled or the agate cup is badly polished. The age of this instrument is more than 100 years, so it can be explained, that the remanency of the needle decreased, and the pivot point dulled. The graduated circle of the simple compass does not have graduation errors, the needle is well charged, the pivot point is not dulled, the cup is well polished, the needle is straight but not centered. The readings taken from opposite ends of the needle differs symmetric, the root mean square error of the readings takes 4°. The graduated circle of the Quechua C100 bussola does not have graduation errors, the needle is well charged, the pivot point is not dulled, the cup is well polished, the needle is straight and centered.

Summarizing the results, from the further investigations I exclude the Süss-compass, because the badly charged magnetic needle, and the simple compass,

because of its eccentric needle. Further reason is, that this type of instruments does not have any sighting equipment.

VI. THE ACCURACY AND PRECISION OF THE MAGNETIC AZIMUTHS MEASURED BY THE DIFFERENT BUSSOLA TYPES

By the Sokkia SET 230 R total station, mounted with a tubular-bussola, and by the Quechua C100 bussola I investigated the accuracy and precision of the measured magnetic azimuths. I set out a 12 meters long reference line in the surveying practise room at the Alba Regia Technical Faculty of Óbuda University, Department of Geoinformatics. On one end of this line I set up the instrument, and on the other end I fixed a plastic surveying mark on the wall. I measured 15-th time the magnetic azimuth of this direction with the two instruments. Before each sighting I centered again and again the mark of the tubular-bussola, and I made also again and again a whole sighting process with the Quechua C100 bussola. By the tubular-bussola I set zero reading into this direction, and so I measured directly the magnetic azimuths. By the C100 bussola I was taken the readings in ticks, and then I convert these values to the 360° system. For the calculation of the precision of the azimuth I used the numerical method of the equally accurate measurements of the same quantity, for the calculation of the precision of the angle between the magnetic north and the line of sight I used the terms of error theory [1]. The results of the calculations contains the Table 2.

Table 2. The precision of the magnetic azimuths and the derived angles measured with the Sokkia SET 230 R total station, mounted with a tubular-bussola and with the Quechua C100 bussola

	RMSE	
Instruments	Azimuth	Angle
Tubular-bussola – Sokkia SET 230 R	±0°17'40"	±0°25'00"
Quechua C100	±0°45'08"	±1°03'50"

Based on the values of the Table 2. we can declare, that the precision of the tubular-bussola is significantly worse, as given in the owner's manual (3-7'). The instrument has 2" reading precision from the horizontal circle; by magnetic azimuth measurements we can't take advantage of this characteristic. Measured from the initial target point, the precision of the other directions will be equal with 2", because without the initial direction, the further directions will be the part of a traditional round of directions. The precision of the magnetic azimuth measured by the C100 bussola is 45', which is very good, when we take into account the non-precise setting up possibility of this instrument, and the disadvantages of the pointing with a dioptre.

I defined the accuracy with a viewing angle based on the value of the root mean square error of the magnetic azimuth and a linear bias, imagined at the correct point location. The value of the linear bias writes the accuracy down, which depends from the value of the viewing angle, and the distance between the station and the aimed point. Take into account the circumstances of cave surveying, I calculated the accuracy from 0 to 50 meters using 5 meters intervals. I based the calculation of the equation of the linear bias [2]. The Table 3. contains the results of the accuracy calculations.

Table 3. The accuracy of the magnetic azimuths measured with the Sokkia SET 230 R, mounted with a tubular-bussola, and with the Quechua C100 bussola

	Accuracy [cm]									
Instruments	5m	10m	15m	20m	25m	30m	35m	40m	45m	50m
Tubular-bussola – Sokkia SET 230 R	3	5	8	10	13	15	18	21	23	26
Quechua C100	7	13	20	26	33	39	46	53	59	66

Based on the values of the Table 3. we can declare, that both instrument is suitable for cave surveying. The circumstances in the caves rarely allowed to measure longer directions as 50 meters; in the most occasions the lengths of directions are between 0 and 15 meters. Take into account this distance-interval, the accuracy of magnetic azimuths, measured with the tubular-bussola will be between 0-8 cm, and measured with the Quechua C100 bussola will be between 0-20 cm.

REFERENCES

[1] Detrekői Á.: „*Kiegyenlítő számítások*", Tankönyvkiadó, Budapest, p. 684., 1991

[2] Deumlich F., Sraiger R.: „*Instrumentenkunde der Vermessungstechnik*", Wichmann Verlag, ISBN 10: 3879073058 ISBN 13: 9783879073054, Berlin, p. 426., 2002

[3] Eszterhás I., Tarsoly P.: „*Kisméretű barlangok térképezése*", MKBT Vulkánszpeleológiai Kollektívájának évkönyve, Isztimér, pp. 39-62, 2015

[4] Fialovszky L.: „*Geodéziai műszerek*", Műszaki Könyvkiadó, Budapest, pp. 181-186, 1979

[5] Hazay I. szerk.: „*Geodéziai kézikönyv*", II. kötet, Közgazdasági és Jogi Kiadó, Budapest, pp. 409-412, 1957

[6] Maslov A.V., Gordeev A.V., Batrakov Yu. G.: „*Geodetic Surveying*", MIR Publisher, Moscow, p.652., 1984

[7] Sokkia Operators Manual Series 30R: Sokkia B.V. European headoffice, 1300 BG Almere, Netherlands, p. 90., 2002

[8] Völgyesi L.: „*Geofizika*", Műegyetemi Kiadó, Budapest, pp. 22-33., 2002

Accuracy analysis of Glacial Isostatic Adjustment models using for satellite gravimetry

L. Földváry[*,**] and A. Kiss[***]
[*] Institute of Geoinformatics, Alba Regia Faculty of Engineering, Óbuda University, Székesfehérvár, Hungary
[**] MTA-CSFK Geodetic and Geophysical Institute, Sopron, Hungary
[***] Department of Geodesy and Surveying, Budapest University of Technology and Economics, Budapest, Hungary
foldvary.lorant@amk.uni-obuda.hu, kiss.annamaria@epito.bme.hu

***Abstract*—Ice mass balance investigations in Antarctica with the use of GRACE monthly gravity models should take into account the GIA process of the Antarctic lithosphere. In the present study visual and statistical comparison of most recent and regularly used GIA models is performed. According to the results, the difference of the models is in the range of mm/yr of equivalent water column height. Since GRACE has detected Antarctic ice mass variations of 2-3 mm/yr, the choice of the GIA model may completely dominate the result. Therefore GIA models must be treated with reservation.**

I. Introduction

A. History of the Antarctic ice cover

It is known from geological (sediment records, permanent ice records) and geomagnetic evidences that starting in the Proterozoic eon (from 2500 to 542 million years ago (Ma)) the Earth regularly goes through glaciations interrupted by interglacial periods. There have been five major glacial periods so far, they are summarized in Table I.

The Antarctic continent (or the equivalent region within Gondwana before its breakup 160 to 23 Ma) has been affected by the ice ages to different extent. During the Andean-Saharan and Karoo ice ages Antarctica has been located at tropical latitudes, then it has started to move to the Southern pole [1] arriving to approximately its present position about 70 Ma (still merged with Australia). That time due to the global subtropical climate no ice formation could be developed. Gradual cooling has started 55 Ma, the first signs of Antarctic ice dates to 35 Ma (during this period Antarctica has split with Australia 40 Ma). Intensive ice formation periods can be detected from sediments about 13 Ma and also about 7-5 Ma. Antarctic ice has continuously developing until the Last Glacial Maximum (LGM) of the Quaternary glaciation occurring between approximately 110,000 to 12,000 years ago. Then it has started to melt, and it is in constant melting also in the present.

Obviously, the Antarctic ice has been developed independently from the glacial periods, c.f. Table I, approximately for 55 Ma, it has only been amplified by the Quaternary glaciation (in fact, glaciation on the Northern hemisphere has exclusively been formed by this glaciation event). Thus, Antarctic ice is the consequence of a regional features, which is can be explained by the opening of the Drake passage 20-25 Ma ago creating the Antarctic Circum Current (ACC), which blocks heat transport to the tropics, cooling the whole continent down [2]. As the ACC is the main factor of the Antarctic climate, present day climate changes due to global warming may essentially occur due to its changes.

B. The effect of permanent ice loading

Fig. 1 shows the thickness of the ice cover over Antarctica from on the BEDMAP project [3]. Obviously, the thickness of the ice sheet is more than 4 km at the central part of East Antarctica, which is a huge amount of frozen fresh water. According to an estimate of [4] the present volume of the Antarctic ice is 27.000.000 km^3.

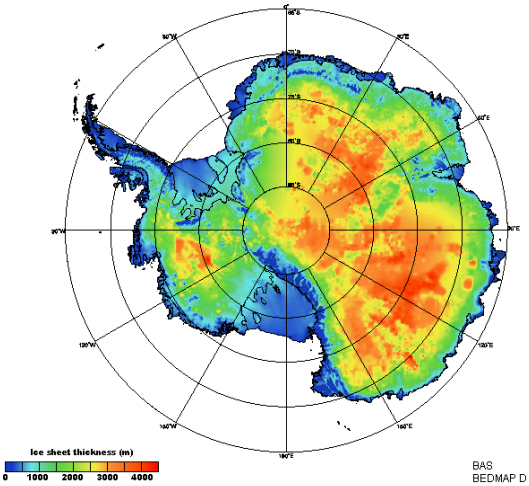

Figure 1. Thickness of the ice cover, source: [3]

TABLE I.
List of major ice ages

glaciation	eon	era	era	period
Huronian	Proterozoic	Paleoproterozoic	Siderian, Rhyacian	from 2400 Ma to 2100 Ma
Cryogenian	Proterozoic	Neoproterozoic	Cryogenian	from 720 Ma to 635 Ma
Andean-Saharan	Phanerozoic	Paleosoic	Ordovician, Silurian	from 450 Ma to 420 Ma
Karoo Ice Age	Phanerozoic	Paleosoic	Carboniferous, Permian	from 360 Ma to 260 Ma
Quaternary	Phanerozoic	Cenozoic	Quaternary	from 2.58 Ma to present

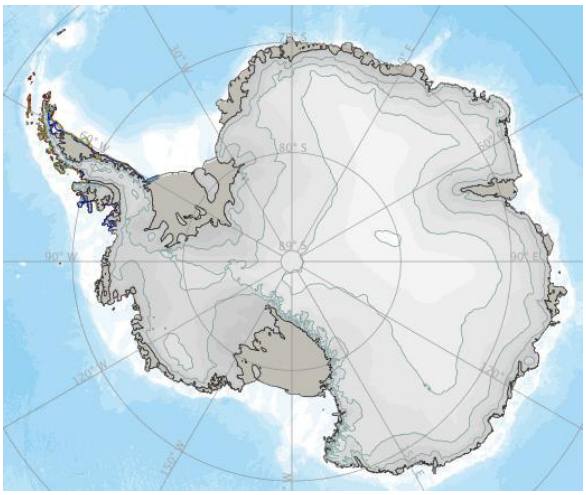

Figure 2. Surface topography

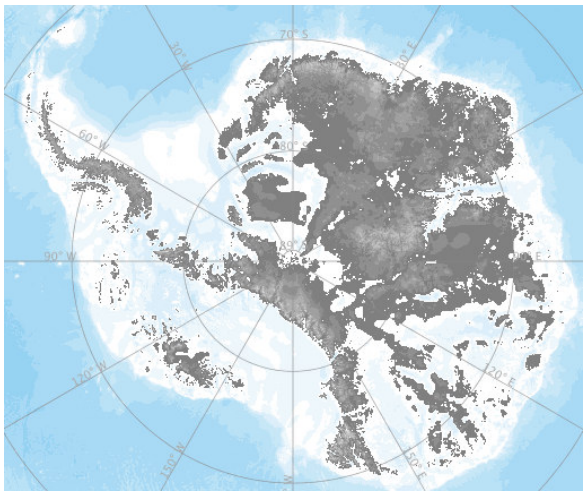

Figure 3. Bed topography

This incredible amount of ice mass pushes the upper rigid layer of the Earth, the lithosphere (composed of the earth crust and some part of the upper mantle), which is floating on an underlying viscous layer, the asthenosphere. The lithospheric plates on the asthenosphere are in equilibrium, each blocks of the lithosphere are dipping into the asthenosphere depending on their mass, on the viscosity and the elasticity of the underlying asthenosphere. The huge amount of ice load adds to the mass of the lithosphere, and depresses the lithospheric plate into the asthenosphere. Due to the additional mass load, several regions of the Antarctic continent lay below the sea level. Fig. 2 shows the Antarctic topography, while Fig. 3 displays the topography below the ice cover generated from BEDMAP data [3]. Obviously, most are of the West-Antarctic part is under the sea level.

However, situation shown on Fig. 1-3 is just a permanent situation, which may change drastically by time. As glacials and interglacials are changing, the ice content may change, changing the centre of mass of the lithospheric plate. The LGM has been "quickly' ended approximately 12,000 Ma ago, which means that (in geologic time scales) over a very short time a huge amount of ice mass has disappeared from the continent. The centre of mass of the lithospheric plate moved up relevantly, resulting in a real time isostatic uplift of the lithosphere. The viscosity of the asthenosphere is, however, essentially different from those fluids we consider as 'liquids' in daily life; for clarification the difference: while water has a viscosity of 8.94×10^{-4} Pa·s, the viscosity of the asthenosphere is approximately 7×10^{19} Pa·s [5], so 23 orders of magnitude difference in resistance to shear stress and tensile stress. This means that isostatic compensation takes notable time. In fact, isostatic compensation of the lithospheric plate due to the end of the LGM (this is the so-called Post-Glacial Rebound, abbreviated as PGR) at several locations of the Earth has not been completed yet. The apparently affected regions by PGR are Northern Eurasia (particularly Scandinavia), Northern America (surroundings of the Hudson Bay), Patagonia, and Antarctica.

When PGR is mentioned, it purely refers to the unloading after LGM. In reality change in ice mass content is more dynamic: even during the Quarternary glaciation there have been several glacial and interglacial periods, which may have been affected the amount of ice by unloading or uploading it. Each process has influenced the vertical motion of the lithosphere. Furthermore, recent ice mass changing processes also affects the motion. Also, the solid Earth also suffers deformations due to the loading, making the whole uploading and unloading phenomenon quite complex. The term used for this complex phenomenon is Glacial Isostatic Adjustment (GIA).

The complexity of GIA process is challenging in theoretical level, while observing it is challenging in practical level: due to plate tectonics, vertical plate motions, and the ceaseless changes of the sea level, there is no fix point to compare to. Still, observations regarding to GIA process can be obtained by geodetic control networks (which are usually interpreted with certain assumptions and feasible for certain regions only). Instead of leaning on observations, GIA modeling is based on theoretical considerations. Assuming certain glaciation history for the whole globe (including an assumptions on ice mass distribution at a starting historical epoch), fixing certain Earth parameters, such as total mass, mean radius, angular velocity of the rotation, defining a mantle viscosity model, delineating the delineation and the ocean bed topography for every geological era, circumscribing all subsequent glacial events with climate parameters, then integrate all this information into a global flow model (the so-called 'Sea-Level Equation'), one can derive a GIA model for the whole Earth (a detailed description is provided by [6]. It is a very complex methodology, which depends notably on the preconceptions and arbitrary parameterization. Indeed, in some cases not a singular GIA model is determined by the same group of researchers, but a set of reliable scenarios, e.g. [7] has delivered 6 slightly different versions for their IJ05_R2 model.

At the end, the measure of the reliability of the GIA models derived in such a way is its validation with observed deformations by geodetic control measurement results, remote sensing satellites and present observations of climate change. As GIA models fits better at different regions, no globally most reliable model has been found by any validation so far. In this study, a statistical intercomparison of those GIA models is presented, which are most commonly used for Antarctic ice mass balance investigations.

The comparison is performed with the purpose of using the GIA models for satellite gravimetric investigations. As GRACE satellites enables investigation of mass variation in a monthly basis [8], elimination of GIA process from actual mass variations, such as ice mass variations, is unavoidable. Thus in this study GIA model are processed in a way to be appropriate for satellite gravimetric use.

II. METHODOLOGY

Surface mass anomaly, $\Delta\sigma$ can be calculated by the formula derived by [9]:

$$\Delta\sigma(\vartheta,\lambda) = \frac{a\rho_E}{3}\sum_{l=0}^{L}\sum_{m=0}^{l}\frac{2l+1}{1+k_l}\bar{P}_{lm}(\cos\vartheta)\cdot$$

$$\cdot\left(\Delta C_{lm}\cos m\lambda + \Delta S_{lm}\sin m\lambda\right) \quad (1).$$

In equation (1) ϑ and λ are co-latitude and longitude, a and ρ_E are mean radius and average density of the Earth, l and m are degree and order of the spherical harmonics, L is the maximal degree of the harmonic expansion, k_l is the load Love number, $\bar{P}_{lm}$ is the Legendre function, ΔC_{lm} and ΔS_{lm} are Stokes coefficients describing relative variations of surface mass density. Surface mass anomaly describes mass variation over time e.g. in *Gt/yr* unit, which can be converted to equivalent vertical crust motion. The unit of surface mass anomaly is thus *mm/yr* as that of the vertical uplift [10].

Surface mass anomaly from each GIA models was calculated according to the methodology used by [11]. The calculation was performed in a *100 km* × *100 km* grid, altogether in 1333 pixels. The elastic loading was taken into account by the standard manner using elastic Love numbers, c.f. [9]. The calculated mass variations were smoothed by a Gaussian filter with *300 km* radius [12].

III. COMPARISON OF GIA MODELS

In order to quantify the uncertainties GIA models, statistics of the following models are derived: ICE-6G model [13], W12 model [14], IJ05 Revision 2 models [7] and the combined GIA model used in [15]. In order to differentiate the IJ05 Revision 2 models, the key parameters are hidden in the model name: the first number after the R2 tag refers to the assumed lithospheric thickness (65 km is more consistent with the West Antarctica rift system, while 115 km with the East Antarctic craton), afterwards different values for η_{UM} viscosity at the upper mantle, finally for η_{LM} viscosity at the lower mantle – both values should be implemented in 10^{21} Pa·s unit.

As in most GRACE applications a Gaussian smoothing is applied during the processing, in this analysis only the smoothed versions of the different models are compared. The smoothed models are displayed on Fig. 4-12. Looking at these figures, obvious spatial differences can be found. In case most of these models, there are two local maxima of the GIA velocity in West Antarctica, however their exact location is variable by model. Obviously, the second peak is much smaller in case of the IJ05 R2 models. Another regular difference among these models is the emphasis of the East Antarctic coastal area: while ICE6G doesn't show here relevant uplift, all other models find

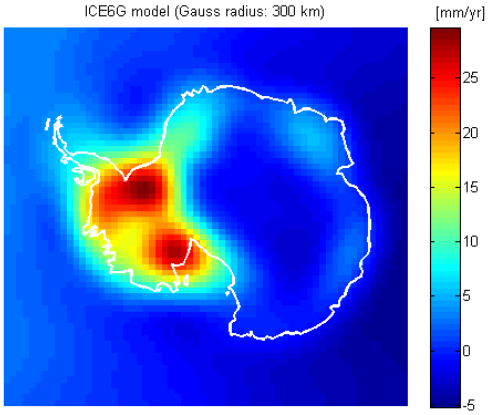

Figure 4. Linear trends calculated from ICE6G model with Gaussian filter of 300 km applied.

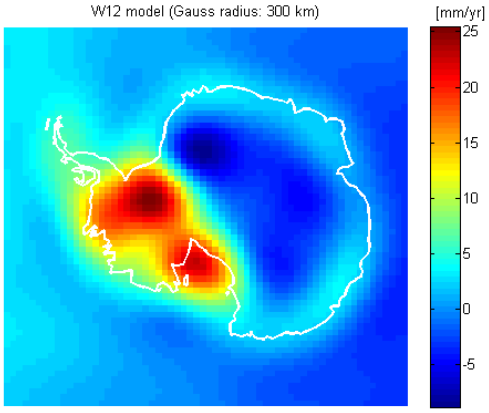

Figure5. Linear trends calculated from W12 model with Gaussian filter of 300 km applied.

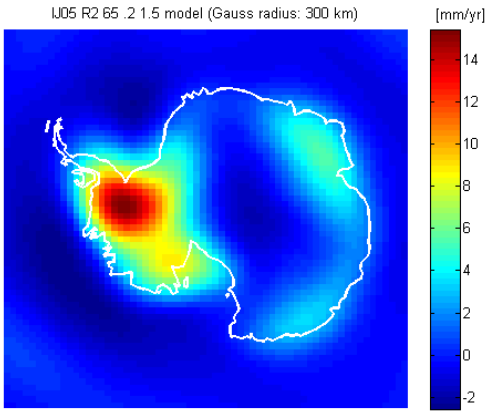

Figure 6. Linear trends calculated from IJ05 Revision 2 version 1 model with Gaussian filter of 300 km applied.

these regions in definite rise. Particular difference can be found in Enderby Land (located along the coast at the upper right corner of these figures).

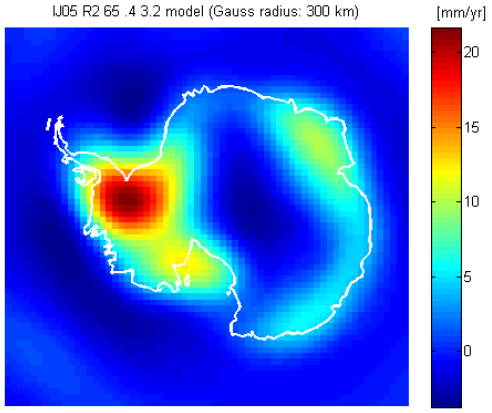

Figure 7. Linear trends calculated from IJ05 Revision 2 version 2 model with Gaussian filter of 300 km applied.

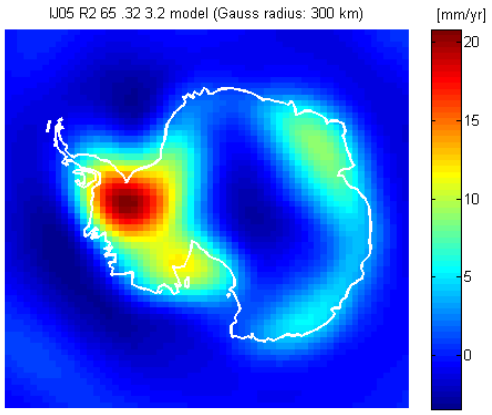

Figure 8. Linear trends calculated from IJ05 Revision 2 version 3 model with Gaussian filter of 300 km applied.

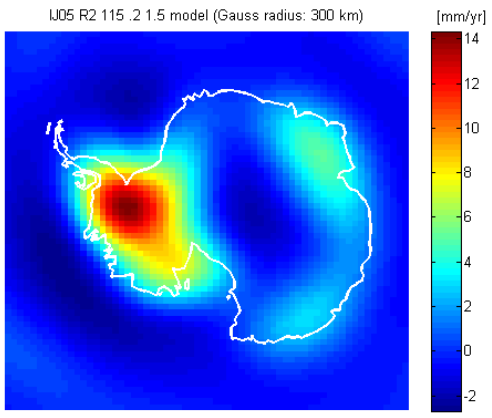

Figure 9. Linear trends calculated from IJ05 Revision 2 version 4 model with Gaussian filter of 300 km applied.

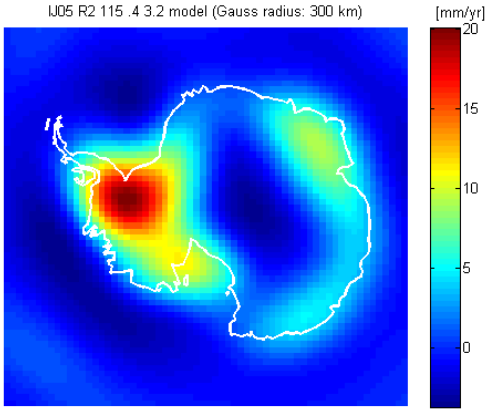

Figure 10. Linear trends calculated from IJ05 Revision 2 version 5 model with Gaussian filter of 300 km applied.

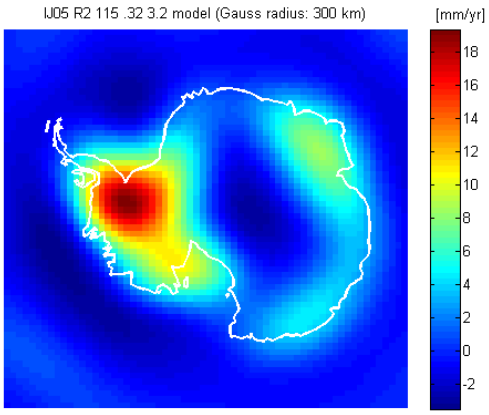

Figure 11. Linear trends calculated from IJ05 Revision 2 version 6 model with Gaussian filter of 300 km applied.

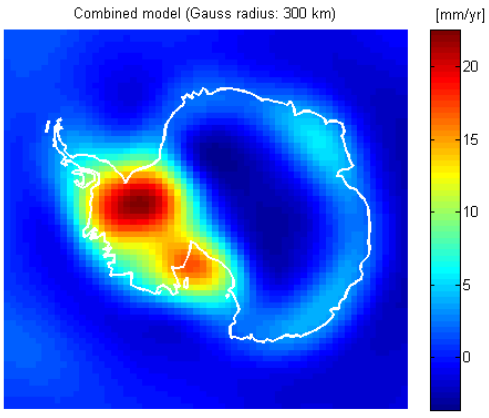

Figure 12. Linear trends calculated from combined model of [15] with Gaussian filter of 300 km applied.

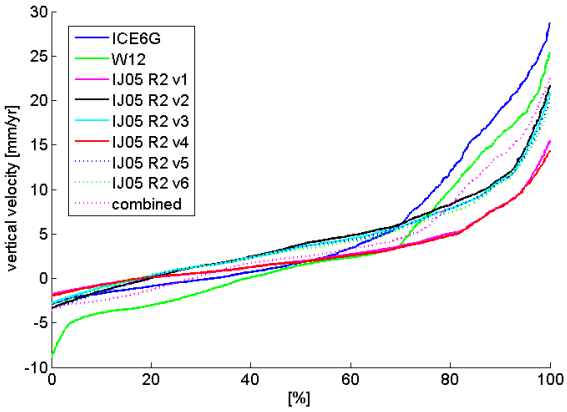

Figure 13. Velocity values derived from different GIA models for the area of Antarctica arranged in increasing order.

TABLE II.
AREAL MEAN AND RMS OF GIA MODELS

	GIA model	mean [mm/yr]	RMS [mm/yr]
1	ICE6G	5.18	± 7.89
2	W12	3.32	± 7.47
3	IJ05 R2_65_.2_1.5	2.84	± 3.52
4	IJ05 R2_65_. 4_3.2	4.44	± 5.07
5	IJ05 R2_65_.32_3.2	4.31	± 4.78
6	IJ05 R2_115_.2_1.5	2.74	± 3.42
7	IJ05 R2_115_. 4_3.2	4.16	± 4.83
8	IJ05 R2_115_.32_3.2	4.06	± 4.59
9	combined GIA	3.88	± 5.97

Further comparison on the range of GIA velocity values of these models is provided by Fig. 13. This figure has been derived by arranging all GIA velocities over the continent into a vector, then sorting them in increasing order. The figure shows in percentage that how much of area uplifts with a certain (or less) velocity. According to the figure, ICE6G model shows generally the largest extent of vertical uplift, while IJ05 R2 models are the least dynamic showing the smallest values and slightest variability.

The statistical description of the content of these models is provided in Table II. The areal mean of the data represents the typical GIA trends of the continent according to the models. The RMS column of Table II refers to the quadratic mean of the differences with respect to the areal mean. It describes the variability of the GIA trends over the Antarctic continent. According to Table II, no consensus on the *mm/yr* level can be detected, neither in the average velocity nor in its spatial variability.

The comparison of the models to each other is summarized in Table III. The difference in every grid point was calculated, then the typical difference was estimated by areal mean. The number of the models, i.e. the first row and the first column, refers to the numbers defined in the first columns of Table II. The similarity of the IJ05 R2 models to each other, i.e. no. 3 to 8 models, is obvious: they difference is less than *2 mm/yr*. The combined model, no. 9, includes one of the IJ05 R2 models and the W12a model as well, thus it differs slightly from both; the difference is in the *2-3 mm/yr* interval. The ICE6G model is not included in the combined model, but its processor, ICE5G was involved. Thus the difference of the combined and ICE6G models is also not so much, only *3.44 mm/yr*. Finally, comparison of GIA models with independent origins, i.e. ICE6G, IJ05 R2 and W12a with each other are discussed. These differences slightly exceed the *4-5 mm/yr* interval. This is the essential property, since these models can be assumed to be uncorrelated.

IV. CONCLUSIONS

State-of-the-art GIA models have been compared with each other visually and with simple statistics. As it turned out, the differences of independent GIA models are in the range of *4-5 mm/yr*, which thus can be considered as an empirical error estimate of GIA process modeling. This is a huge difference, since GRACE has detected the areal mean of Antarctic ice mass variations to be *±2-3 mm/yr* [11], thus these estimates may completely been dominated by the choice of the used GIA model. According to [16], all modelling errors of Antarctic ice mass balance may reach the *±11 mm/yr* level, in which the uncertainties of the GIA model takes a notable share. Therefore, GIA models must be treated with reservation to make use of the accuracy of the GRACE models. But whatever result is provided by a GRACE-borne Antartic ice mass balance study, it should be considered to be relevantly influenced by the choice of the GIA model.

TABLE III.
STATISTICS OF GIA MODELS

No.	2	3	4	5	6	7	8	9
1	3.82	5.13	4.63	4.62	5.18	4.67	4.66	3.44
2		5.04	4.78	4.74	5.04	4.77	4.73	2.30
3			1.76	1.38	0.28	1.52	1.21	2.97
4				0.40	1.90	0.39	0.67	2.50
5					1.53	0.32	0.35	2.45
6						1.62	1.31	3.01
7							0.35	2.49
8								2.46

REFERENCES

[1] Torsvik, T.H., Gaina, C. and Redfield, T.F., Antarctica and Global Paleogeography: From Rodinia, through Gondwanaland and Pangea, to the birth of the Southern Ocean and the opening of gateways. In Cooper, A. K., P. J. Barrett, H. Stagg, B. Storey, E. Stump, W. Wise, and the 10th ISAES editorial team (eds.) Antarctica: A Keystone in a Changing World. *Proceedings of the 10th International Symposium on Antarctic Earth Sciences*. Washington, DC: The National Academies Press, 125-140, 2008.

[2] Ruddiman, W.F., "Earth's Climate: Past and Future", W. H. Freeman; First Edition edition, pp. 465 pages, ISBN-10: 0716737418, ISBN-13: 978-0716737414, 2000.

[3] Lythe, M.B., Vaughan D.G. and the BEDMAP Consortium, BEDMAP: A new ice thickness and subglacial topographic model of Antarctica, *Journal of Geophysical Research*, 106(B6), 11,335–11,351, 2001.

[4] Fretwell, P., H.D. Pritchard, D.G. Vaughan, J.L. Bamber, N.E. Barrand, R. Bell, C. Bianchi, R.G. Bingham, D.D. Blankenship, G. Casassa, G. Catania, D. Callens, H. Conway, A.J. Cook, H.F.J. Corr, D. Damaske, V. Damm, F. Ferraccioli, R. Forsberg, S. Fujita, Y. Gim, P. Gogineni, J.A. Griggs, R.C.A. Hindmarsh, P. Holmlund, J.W. Holt, R.W. Jacobel, A. Jenkins, W. Jokat, T. Jordan, E.C. King, J. Kohler, W. Krabill, M. Riger-Kusk, K.A. Langley, G. Leitchenkov, C. Leuschen, B.P. Luyendyk, K. Matsuoka, J. Mouginot, F.O. Nitsche, Y. Nogi, O.A. Nost, S.V. Popov, E. Rignot, D.M. Rippin, A. Rivera, J. Roberts, N. Ross, M.J. Siegert, A.M. Smith, D. Steinhage, M. Studinger, B. Sun, B.K. Tinto, B.C. Welch, D. Wilson, D.A. Young, C. Xiangbin and A. Zirizzotti, BEDMAP2: improved ice bed, surface and thickness datasets for Antarctica, *The Cryosphere*, 7:375–393, DOI:10.5194/tc-7-375-2013, 2013.

[5] Fjeldskaar, W., Viscosity and thickness of the asthenosphere detected from the Fennoscandian uplift. *Earth and Planetary Science Letters*, 126 (4): 399–410, 1994.

[6] Peltier, W.R., Ice Age Paleotopography, *Science*, New Series, 265(5169): 195-201, 1994.

[7] Ivins, E. R., James, T. S., Wahr, J., Schrama, E. J. O., Landerer, F. W., Simon, K. M., Antarctic contribution to sea level rise observed by GRACE with improved GIA correction *Journal of Geophysical Research*, Solid Earth, 118: 1-16, 2013.

[8] Tapley, B. D., S. Bettadpur, M. Watkins, and C. Reigber, The gravity recovery and climate experiment: Mission overview and early results, *Geophysical Research Letters*, 31(9): L09607, 2004.

[9] Swenson S. and Wahr, J., Methods for inferring regional surface-mass anomalies from Gravity Recovery and Climate Experiment (GRACE) measurements of time-variable gravity. *Journal of Geophysical Research*, Solid Earth, 107 (B9), 2002.

[10] Wahr, J., M. Molenaar, and F. Bryan, Time-variability of the Earth's gravity field: hydrological and oceanic effects and their possible detection using GRACE, J. Geophys. Res., 103, 30,205-30,230, 1998.

[11] Földváry, L., Kiss, A., Su, Z. X., Wang, G. C., Wang, L., Accuracy investigations of GRACE-borne ice mass variations in Antarctica, (in Chinese), *Earth Science Frontiers*, 22(4): 239-246, 2015.

[12] Swenson, S. and Wahr, J., Post-processing removal of correlated errors in GRACE data. *Geophysical Research Letters*, 33: L08402, doi:10.1029/2005GL025285, 2006.

[13] Peltier, W.R., Argus, D.F., Drummond, R., Space geodesy constrains ice-age terminal deglaciation: The global ICE-6G_C (VM5a) model. *Journal of Geophysical Research*, Solid Earth, 120, 450-487, doi:10.1002/2014JB011176, 2015.

[14] Whitehouse, P.L., Bentley, M.J., Milne, G.A., King, M.A., Thomas ,I.D., A new glacial isostatic adjustment model for Antarctica: calibrated and tested using observations of relative sea-level change and present-day uplift rates. *Geophysical Journal International* 190, 1464-1482, 2012.

[15] Shepherd, A., Ivins, E. R., A, G., Barletta, V. R., Bentley, M. J., Bettadpur, S., Briggs, K. H., Bromwich, D. H., Forsberg, R., Galin, N., Horwath, M., Jacobs, S., Joughin, I., King, M. A., Lenaerts, J. T. M., Li, J., Ligtenberg, S. R. M., Luckman, A., Luthcke, S. B., McMillan, M., Meister, R., Milne, G., Mouginot, J., Muir, A., Nicolas, J. P., Paden, J., Payne, A. J., Pritchard, H., Rignot, E., Rott, H., Sørensen, L. S., Scambos, T. A., Scheuchl, B., Schrama, E. J. O., Smith, B., Sundal, A. V., van Angelen, J. H., van de Berg, W. J., van den Broeke, M. R., Vaughan, D. G., Velicogna, I., Wahr, J., Whitehouse, P. L., Wingham, D. J., Yi, D., Young, D., and Zwally, H. J., A Reconciled Estimate of Ice-Sheet Mass Balance. *Science*, 338: 1183–1189, doi:10.1126/science.1228102, 2012.

[16] Kiss, A., Földváry, L., Uncertainty of GRACE-borne long periodic and secular ice mass variations in Antarctica, *Acta Geodaetica et Geophysica*, submitted, 2016.

ÍRISZ – the Smart Communication System

Hatalyák Dezső, Seebauer Márta, Ivanics József
Óbuda University/ Alba Regia Technical Faculty, Székesfehérvár, Hungary
seebauer.marta@amk.uni-obuda.hu, hatalyak.dezso@amk.uni-obuda.hu, ivanicsjozsef94@gmail.com

***Abstract* — For improving the quality of the customer relation services a higher education institution cannot keep off the introducing a smart communication system. The aim of this paper is to describe the project "Írisz" carried out by the Alba Regia Technical Faculty of Óbuda University. The project focuses on the support of communication between university's offices, under-graduated and graduated students, representatives of the labor market, and also the local government. The topics of the paper includes the aim of the project, the software architecture and development methodology chosen for the application, the constraints of data management, the main functions of the smart communication system, and the queries of output data, as well.**

I. Introduction

The by demographic crises caused competition for the student candidates, the fulfillment of labor market needs, the reforms performed in higher education are brought new challenges for the universities and colleges. One of the methods – besides on elementary requirements on improving the education quality – is the introducing new communication channels between the representatives of the higher education and the labor market.

The president of Commerce and Industry Chamber, László Parragh in several publications and interviews recommended the institutions of higher education to open the doors in the direction of labor market, to make the education more offend and practice-oriented [1].

The Ministry of Human Resources supported this idea and responded to this challenge with the starting the pilot program of dual education not only in professional high school branch but in higher education, too. Several activities of Széchenyi 2020 program had set the goal to support this purposes.

Figure 1. The starting page of Írisz 2.0 System on a desktop PC

Figure 2. The starting page of Írisz 2.0 on a mobile phone with small (720p) resolution

II. The Írisz project

The introducing of dual education, and also the more intensive organization if traineeship programs for the students increased the amount of administrative task for the university's officers. The local government, and personally the Mayor took active part in the motivation of firms, and organization on participation in dual education. The increasing administrative work indicated the development and introducing of a smart and modern communication system.

A. Applied Software Development Methodology

The main features of software design were a tried and stabile data base system. a thin client-server architecture, also a user interface with attractive graphical elements. The most important point of view was the responsive design, ensuring that the page can be shown correctly on many different type of devices (like mobile phones, televisions, laptops, tablets, etc.) with the same code.

Figure 3. The student's registration page on a mobile phone

Figure 4. The company's registration page

First of all, the aim was to develop a responsive Web-site. This is the reason why the design was based on Bootstrap. This is a new technology, invented by two developers from the Company Twitter. It is based on Cascade Style Sheets (CSS).

The application was developed using PHP programming language with object oriented language components. The database manipulation carried out with the built-in PHP Data Objects functions (PDO) which is not the fastest way to data selecting from databases but it's got a big advantage. The database can be changed behind the scene and the Web-site continues to work correctly.

Secondly, a new database schema was designed to store more type of data over students and companies.

B. Basic Data

By the development of data base, the intentions and constraints of data management regulation of Hungarian National Statue about the Higher Education [2], and also the Data Security Regulations of Óbuda University [3] must be satisfied.

The users of the communication system are the following:

- system administrator
- university teachers
- university officers
- undergraduate students
- graduated students
- representatives of organizations, firms, and companies
- representatives of local government.

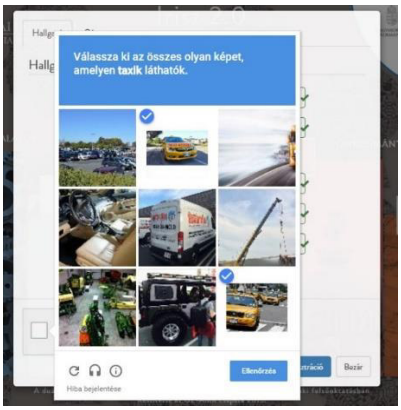

Figure 5. Captcha from Google at the registration screen

The registration and data entering is voluntary for the users. The users are distributed in three user group

- administrator
- private user (Fig.3)
- company (Fig.4).

The basic data can be imported from the user's Facebook profile, as well. The registration page contains an anti-robot control picture test – developed by Google. These captcha programs are very useful to avoid a denial of service attack. (Fig.5)

In the base data the students can maintain their profile specifying the personal skills, practices and fields of interest.

C. Workflow

The main function of the system is the communication between the registered users. The main communication channels are shown on the Fig.6.

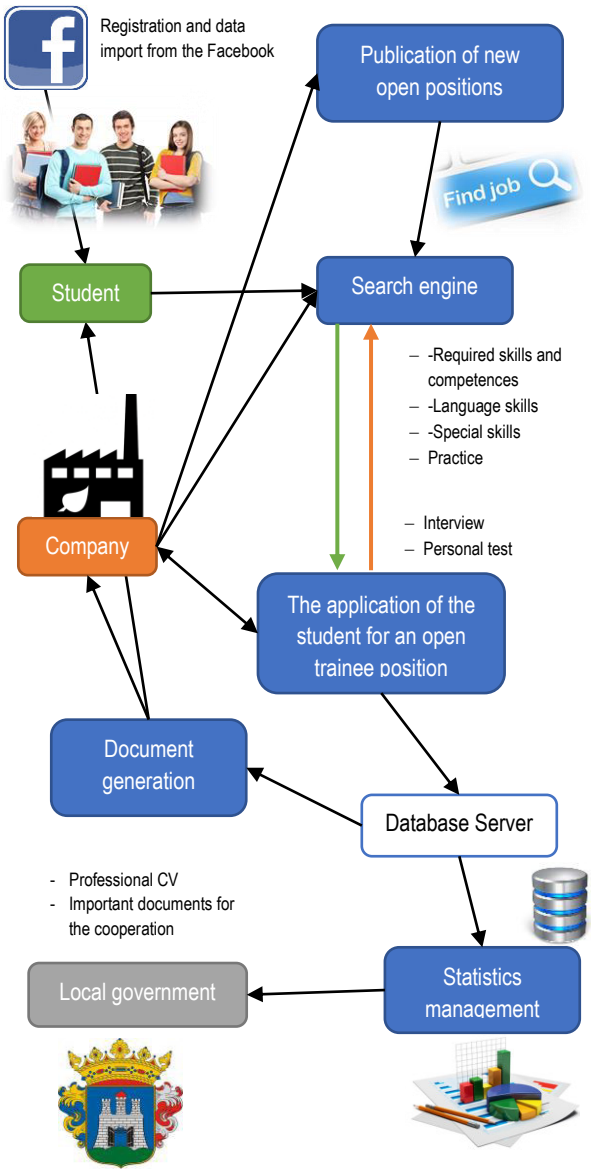

Figure 6: Írisz 2.0 – Tuned for cooperation

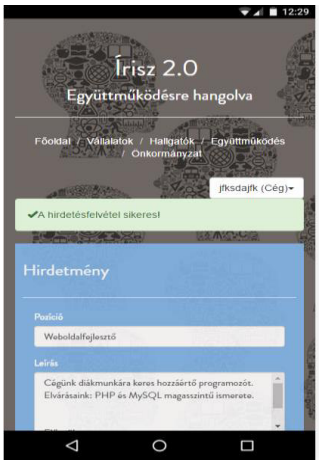

Figure 7. Job announcement on mobile phone

The communication system allows the companies

- to upload their free places for trainee programs or open job positions in which they define exactly the required professional skills, the level and type of foreign language, several practices
- announces projects or themes for final thesis's
- to choose competent worker.

The communication system helps

- the undergraduate students to brows in appropriate trainee places
- the graduated student to brows in several jobs
- to find a convenient trainee program or job for graduated students
- to find an interesting project or theme for final thesis.

The communication system supports

- the university administration in organization and management of the trainee-programs (Fig 8)
- the local government in supervising of labor market.

Fig. 9 shows the data query using the special search engine developed special for this system. The requirements of the companies for the different jobs are compared with the abilities of the students. As soon as a student is logging in to the system, the search engine automatically lists the positions, that are relevant for the student's interest and skills.

We had a big dilemma by the developing of the search-engine. First we wrote an algorithm that generated only the positions with exactly strait language skill requirements for the students.

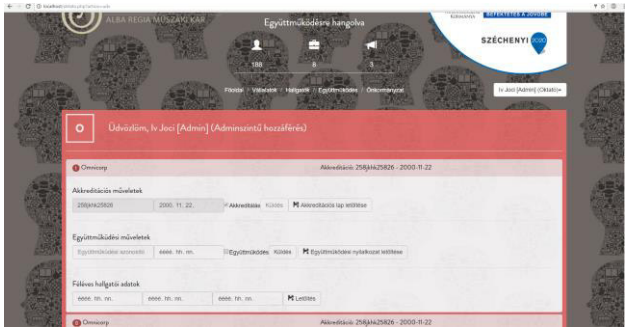

Figure 8. Management of company's processes

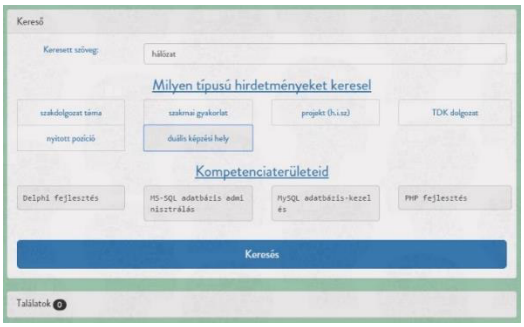

Figure 9. Data queries

This way we got only a few hits by every running time. The program code was so modified that every different level of language skill is shown for the students, not only their own level.

1.) Szak, tagozat megjelölése

szak pontos megnevezése	*tagozat*	*szakirány*	*modul*
Mérnökinformatikus BSC	**Nappali**		-

2.) Az általam tervezett terület (az ismert adatok megadását kérjük)

cég neve:	**Omnicorp**
cég akkreditációs száma*:	**258jkhk25826**
székhelye:	**Úrhida Budapest út 7/4.**
kapcsolattartó neve:	**Kun Béla**

3.) A megjelölt gyakorlati helyen teljes munkaidőben veszek részt a gyakorlaton.
4.) A gyakorlatot teljesítő hallgató adatai:

név:	**Ivanics József**
neptunkód:	**DG4N5C**
tanulmányi félév megjelölése:	**0. félév**
telefonszám:	**+36305531111**
e-mail cím:	**ivj94@freemail.hu**
gyakorlat teljesítésének tervezett időintervalluma:	
az abszolutóriumhoz csak a szakmai gyakorlat teljesítése hiányzik	**igen / nem**

Figure 9. Student's application data sheet

D. Output Data

Every user – who has been registered – in the system can print in pdf format the required documents, that are needed to make a successfully cooperation between our university and the members of the business life.

The students can apply for the announced places by sending professional CV and application data sheet generated in system. (Fig.9)

The companies have fourteen days to accept or reject the student's application. This is a period for the company to call the students for personal interview. If the student is rejected by the company, he/she can choose another free position. Fig.10. shows the list for admitted applicants by the company.

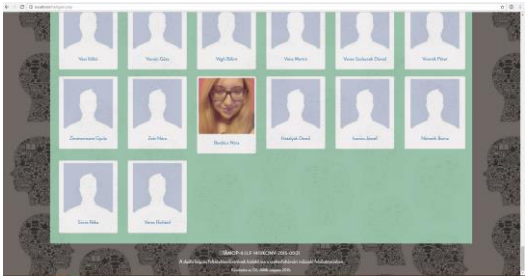

Figure 10. The list of students

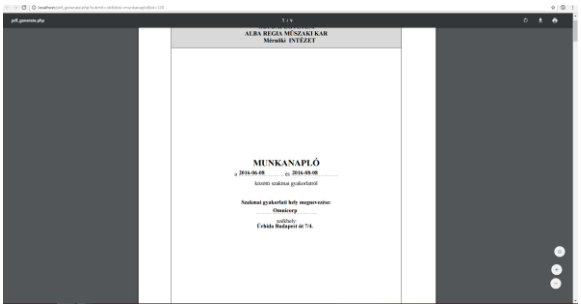

Figure 11. Student's work log

For the accepted by a company student the system generates the related documentation, for example the work log. (Fig.11)

The collaboration between the companies and the university based on cooperation agreement registered official by the Education Office of the Ministry of Human Resources. This agreement can be generated by the Írisz system, too. (Fig.12)

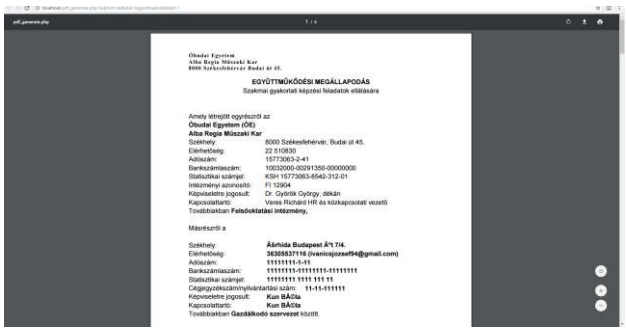

Figure 12. Cooperation agreement between a company and the university

Different type of statistics about the cooperation of higher education institute and representatives of labor market can be generated by the new version of the program. These statistics were required by the local government. (Fig. 13)

III. Conclusion

The introducing a smart communication system brings a new age into the administration process. The development team hope that the using of the system makes more easy the communication between the parties in education process.

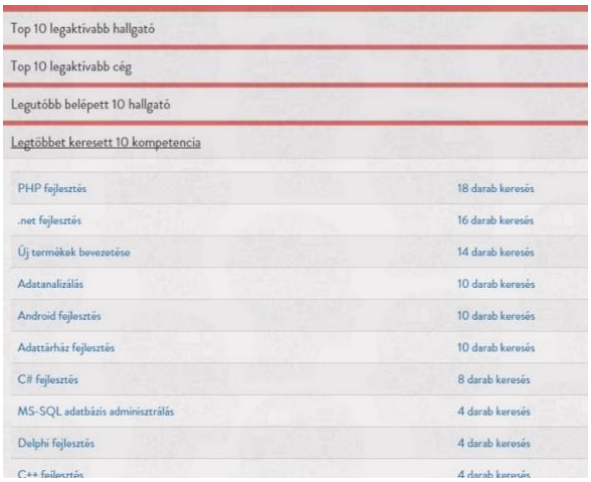

Figure13. Statistics

Acknowledgment

The authors of this paper express their thanks and appreciation to the members of Írisz project's software development team.

The original version of Írisz 1.0 system was developed by Kertész Gábor. The development project was sponsored by TÁMOP 4.2.3/12/KONV-0039 activity of the Széchenyi 2020 program. The general goal of this activity was to force the application of student candidates and the development of teaching staff.

The new version, the Írisz 2.0 system was developed by Ivanics József, Németh Barna, Zsobrák Krisztián, with the team leader Hatalyák Dezső. The development of the new version was sponsored by TÁMOP-4.1.1.F-14/1/KONV-2015 activity of the Széchenyi 2020 program. The aim of this project was the introduction of dual education system in the Alba Regia Technical Faculty of Óbuda University.

References

[1] Parragh László: A fejlődés záloga a minőségi felsőoktatás - Informatika a Társadalomért konferencia, Balatonfüred, 2016.11.08-10. See more at: http://autopro.hu/oktatas/Parragh-Laszlo-a-fejlodes-zaloga-a-minosegi-felsooktatas/12330/#sthash.2pSRqsyE.dpuf

[2] CCIV. Hungarian National Statue about the Higher Education. 2011. évi CCIV. törvény a nemzeti felsőoktatásról. http://net.jogtar.hu/jr/gen/hjegy_doc.cgi?docid=A1100204.TV

[3] The Data Security Regulations of Óbuda University. Az Óbudai Egyetem Adatvédelmi Szabályzata. See more at: http://uni-obuda.hu/files/private/regulation/488/obudai-egyetem-adatvedelmi-szabalyzata.pdf

Statistical Survey of Influenza and Influenza-Like Diseases in a Rural General Practitioner Database

Hatalyák Dezső, Nagyné Dr. Hajnal Éva, Dr. Seebauer Márta
Óbuda University Alba Regia Technical Faculty, Székesfehérvár, Hungary
hatalyak.dezso@amk.uni-obuda.hu, hajnal.eva@amk.uni-obuda.hu,
seebauer.marta@amk.uni-obuda.hu

Abstract — **A rural general practitioner's database was investigated to create statistics about influenza and influenza like diseases. The number, gender, vaccination and age distribution of patients were collected and analyzed. The collected dataset is homogenous from the aspects of medical persons and originates from a small rural town. We created a time series of data between 2007 and 2015. The distributions of vaccination and illnesses were visualized and interpreted.**

I. Introduction

Increasingly severe economic and social problem is that the European population is getting rapidly older. The same problem can be detected also in Hungary. The number of the medical supply obliged people at the end of the year 2015 was the next: in the 0-17 years old age group: 1 716 600 person, in the 18-22 age group: 476 900 person, in the 23-39 age group: 2 086 500 person, in the 40-61 age group: 2 889 800 person, and finally in the age group over 62 years: 2 147 500 person [1].

The health-state of Hungarian people was on average compared to the European Union's population. This state is different in the different part of the country. In given sector the g.p. has got a significant role to survey and maintain the health-state of the people.

It is clearly observable [2], that the healing of human population is a big expense for the country. In the consequence it is a very sensitive problem. Every political leadership wants to change the state of the medical supply. In the focus of our paper the influenza and influenza like disease are investigated.

Influenza, varicella (in older ages shingles), and rubeola – three viruses of them – are such kind of viruses, that have 100 percent of contagiousity. The Spanish-snuffles was one subgenus of influenza viruses. We realized, that in the circle of specific kind of risk factor living people, the chance of the illness is much more smaller caused by the influenza viruses. It could be very interesting, to take act of the vaccination of the whole population, and to search for the group of people, where the chain of the virus infection could be broken.

The viruses of influenza is not the only one, but one of the most important viruses, what can be transform into a world contagious disease. The importance of it is not only the infection of whole countries or continents, the more dangerous fact is, that the runoff can be very fast.

The Epidemiology Center of Hungary collects data about the facts of illnesses caused by the influenza viruses since 1931. This institution makes surveys in the field of epidemiology since 1937. From the doctor's practices collected samples are tested and analyzed for influenza. The statistics of influenza-infected people are published for the information on the Web-site week after week.

II. Bouts of influenza

For the first time it is very important to explain why the g.p.'s aren't able to recognize with certainty of 100 percent that one or more of his patients are infected with influenza viruses.

Let's see the definition of it: „the influenza is a respiratory disease caused by the influenza viruses. The most relevant symptoms are: high temperature, headache, coughing, sore throat, pain in the articulation and in the muscular system, general depression, as well. Not all patients are suffering from these symptoms. The influenza is a heavy weight disease, more dangerous than a simple snuffle. The clinical image can varied from the minor, to the very serious one. In the worst case, is getting pneumonia, brain-fever or septicemia. These symptoms are caused by influenza viruses, but the weak and ill organism can get additional bacterial or viral infections". [3]

Table I. compares the symptoms of general snuffles and influenza.

By the time we are speaking about vaccinating, is very important to mention the behavior of the influenza viruses. The virus is changing himself year for year. The construction of the new influenza viruses and the built-in viruses in the vaccine will be reviewed by specialists yearly. These two type will be compared, and analyzed.

I. Data and Methods

The origin of data was a rural g.p. database of the praxis between 2007 and 2015, the queries are no containing any name and personal identification data. The database was written in dBase and FoxPro, queries were run on the own graphical interface of the medical information system. The g.p.'s program was able to execute queries including date period and BNO code. (BNO is the international classification of diseases.) We had to ask different BNO codes one by one with different queries. For results we got the patient number and ratio of gender.

TABLE I. THE COMPARISON OF SNUFFLES AND INFLUENZA [3]

Symptoms	Snuffles	Influenza
fever	Not typical, but sometimes the patient has got low fever (38°C and under).	common with high temperature (38°C and above)
pain in the muscles and in the limbs	rare	common
weariness and general exhaustion	rare	common
headache	common	common
snuffles	nearly always	Common, but this is a symptom with small importance.
sneeze	nearly always	Common, but this is a symptom with small importance.
tears	common	a symptom with small importance
sore throat	nearly always	a symptom with small importance
coughing	common	common

The resulted data sets were collected in Excel spreadsheets. Diagrams and statistical calculations were made by using Microsoft Excel 2013. The influenza and influenza-like diseases were stood into the center of the investigation. The count of male and female patients and their illnesses and vaccination data were collected. The count of total cases and the patient numbers was got. The total case number is a count, that shows how many times the g.p. was visited by the patients with influenza-like diseases. If a patient falls back in a disease, he/she can repeatedly visit the g.p. The patient count shows the number of different people who was suffering in influenza-like diseases.

One of the most difficult methodological problem was the data querying, because the most relevant BNO codes had to choose from the database. The Table I. shows, that a g.p. can shuffle snuffles and influenza very easily. The viruses of influenza can be detected only in laboratory conditions. Before the g.p. could get the results of the tests, he/she has to order the corresponding medication for patients, and to start the treatment.

This is the reason, why this article deals not only with influenza, but also with influenza-like diseases. According to this, a whole group of BNO-codes was queried from the database, not only the influenza's. In the treated database was only a few BNO-codes with influenza.

TABLE II. BNO (ICD-10 2016) CODES OF INFLUENZA [4]

BNO-code	Description of the illnesses
J1000	Influenza with pneumonia, seasonal influenza virus identified
J1010	Influenza with other respiratory manifestations, seasonal influenza virus identified
J1080	Influenza with other manifestations, seasonal influenza virus identified
J1100	Influenza with pneumonia, virus not identified
J1110	Influenza with other respiratory manifestations, virus not identified
J1180	Influenza with other manifestations, virus not identified

The g.p. has got the right for free decision-making in choosing of appropriate BNO-code for the current case. The most relevant BNO-codes for influenza are shown in the Table II.

There are a group of BNO-numbers that can be also used by the g.p. in the praxis in influenza like cases. These codes were collected in Table III. To get the relevant BNO codes for the further data-requesting, we discussed a lot with our g.p about the type of illnesses, that can be concern here. Another problem was caused with the doctor's software system, because we could access the data only in separated queries, while the system did not support the complex query terms.

TABLE III. BNO (ICD-10 2016) CODES OF INFLUENZA-LIKE DISEASES CODED BY THE G.P.[4]

BNO-code	Description of the illnesses
B3490	**Viral infection, unspecified**
J0410	**Acute tracheitis**
J0420	**Acute laryngotracheitis**
J0100	**Acute maxillary sinusitis**
J0110	**Acute frontal sinusitis**
J0140	**Acute pansinusitis**
J0290	**Acute pharyngitis, unspecified**
J0390	**Acute tonsillitis, unspecified**
J0680	**Other acute upper respiratory infections of multiple sites**
J0690	**Acute upper respiratory infection, unspecified**
J2090	**Acute bronchitis, unspecified**

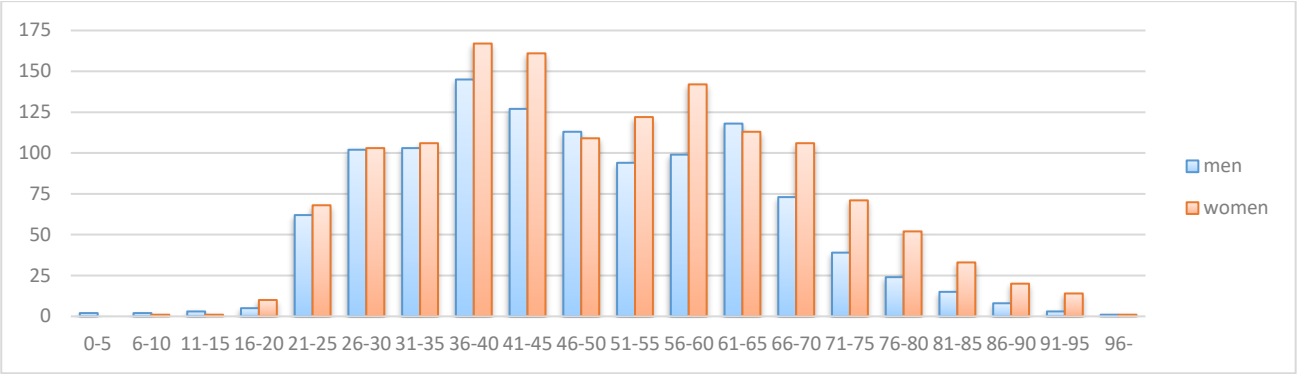

Figure 1. Age-distribution diagram of the praxis' patients in year 2016

The Fig. 1. shows the age distribution graph of the patients in surveyed praxis. The diagram is divided into the number of male-female patients and shows the distribution of the different age-ranges. The praxis contains total 1138 male and 1400 female patients.

The age distribution is very important, because influenza-like diseases are detected primarily in the group of young adults and pensioners. The consequence of this fact is the reason, why these age groups are vaccinated.

II. Results and Discussion

In the most of cases the people are infected by influenza viruses between the 40th and the 20th week of a calendar year. Data about the total amount of patients and the number of vaccination between October and May can be seen on the Fig. 2. Generally, the vaccination prevents from the infection and so there is an inverse relationship between them. The number of vaccinated people in the current g.p.'s praxis is shown on the Fig. 3.

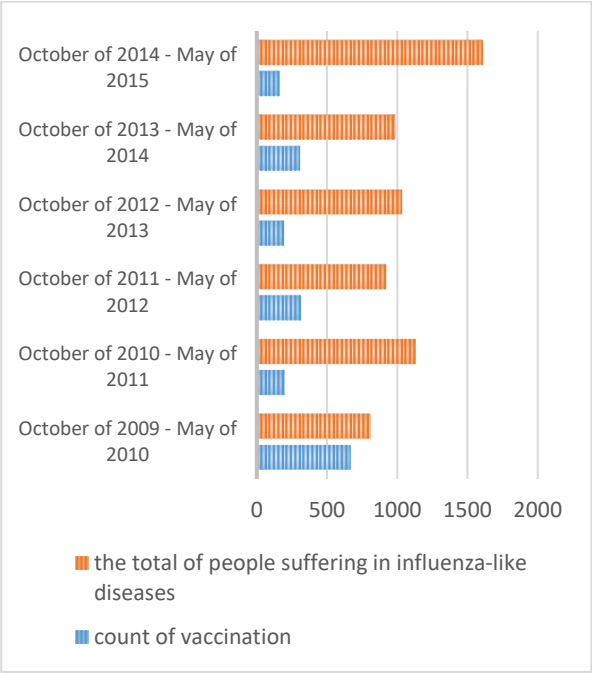

Figure 2. The amount of vaccinated patients and case numbers caused by influenza-like diseases in the praxis

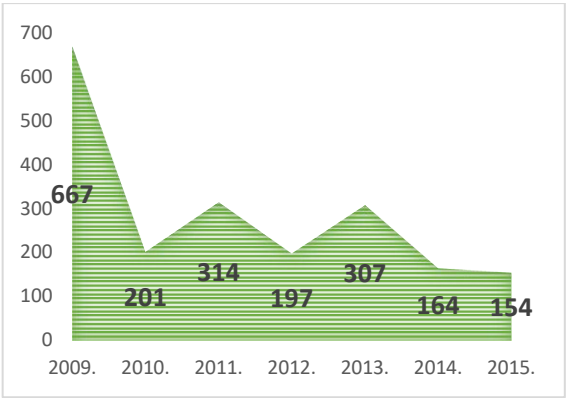

Figure 3. The number of vaccinated people between 2009 and 2015

There was written a study in the United States in the year 2010, where the researcher got interesting results. 90 percent of the vaccinated people in the age group over 65 years should be vaccinated, and 60% of the high risk adults in the age group between 18 and 64 years. [5] But these results can be reached only in the dreams of the doctors.

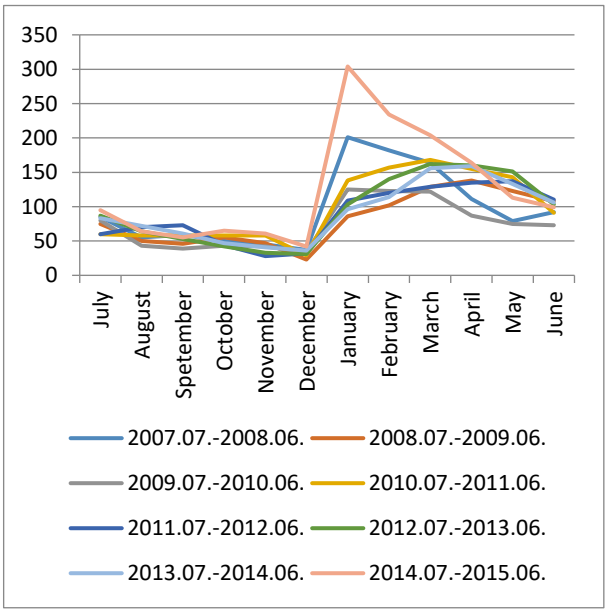

Figure 4: The number of different patients infected by influenza-like viruses

Analyzing the data on Fig. 4. and 5., we can conclude very interesting things. In every December the amount of morbidity is very small, but the count of causes highly increases in January.

There can be found a few different reasons for this phenomenon. In first of all, on the last week of December there are no surgery hours. The ill people are provided by the Emergency Centre and not by the g.p.

Secondly the people on Christmas holiday won't go to the doctor, and are trying to solve their medical problems at home.

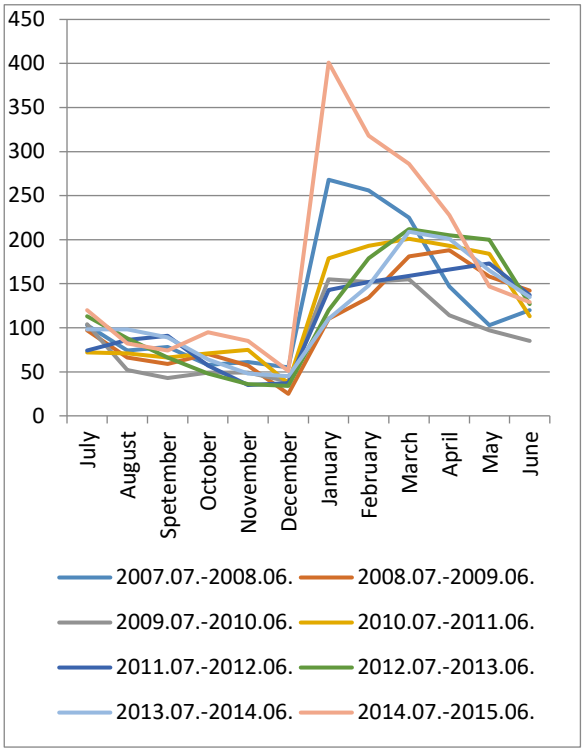

Figure 5: The total case number

Thirdly elementary school-children and children from kindergarten age are spending the most of time at home in these days and only a few time in the community. They can easily infect the family members but hard to get infection from their age range. It can change the infection patterns.

The g.p. is visited by patients only in January in most of cases. The most typical reason is that the patients want to get sickness benefit at this time. At the end of December, the local factories aren't working. Ill people doesn't need to get to the g.p. In the other group are people, who don't get better during the Christmas-holiday, and are still ill in January.

Usually people are infected by influenza-like diseases in the period of February-March, because vitamin-resources of the human body are exhausted at that time. At spring the outside temperature is ideal for virus-propagation. Furthermore, to the end of winter people are weaken.

It's interesting to analyze the data of the year 2015. In the vaccinating period before January only a little part of patients was vaccinated. In this January there was an explosion among the people infected by influenza-like disease. The missing vaccination process led to a heavy epidemic.

It seems, if the vaccinated part of population is not reached a threshold, then the next year occurs a big enhancement in the virus propagation.

In addition, some other relationships have been identified. If the amount of cases presented in September and October is low than at the beginning of the next year befalls an enhancement. If the infected number of people is higher in the autumn than the case number will show a decreasing tendency in the next year.

We weren't satisfied with the current data-analysis explanations of January 2015 therefore we were looked after other reasons. The ambulant patient scale was investigated (See Fig. 6.).

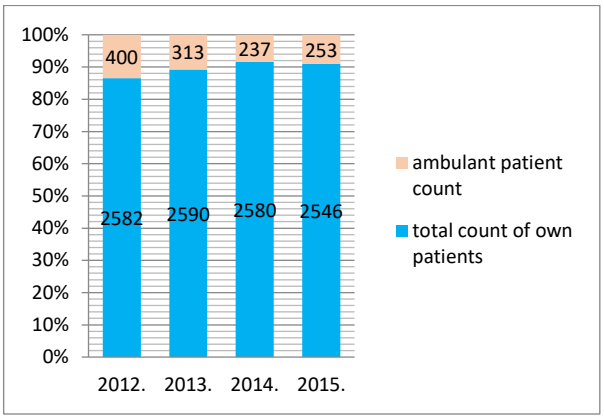

Figure 6. The number of patients from the own praxis and ambulant patients between 2012 and 2015

Firstly, it can be seen that only 10% of the patient visits was made by the ambulant people. Secondly, the total amount of patients was not significantly changed during the last years.

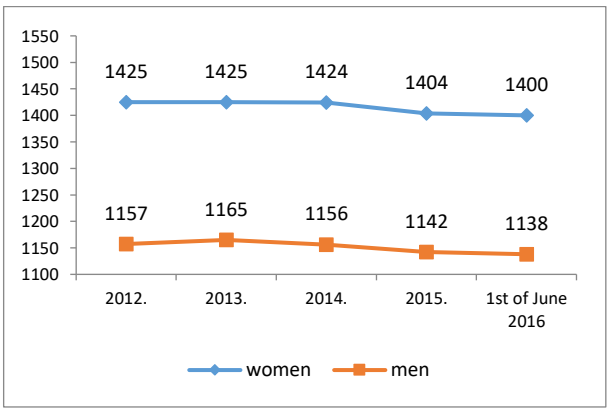

Figure 7. The rate of men and women in the last four years in the praxis

Thirdly, the gender rate of praxis wasn't changed in the last years. (See Fig. 7.)

III. Conclusions

In this paper the influenza and influenza-like diseases data of a g.p. database were investigated. The number of patients in gender groups, the vaccination data were collected between 2007 and 2015. The general trends

were analyzed. It was shown that global data are matching to the references and supports the generally accepted infection models. However, some local patterns can be observed according to temporal changes of the infection and to the vaccination efficiency. It was raised that only quite large number of vaccination can prevent the infection. In the future it is important to find the lower bound of vaccinated patients amount to moderate the epidemic's propagation.

Further questions will be planned by our survey. It can be very interesting to monitor the vaccinated patients, and watch the scale of influenza-infected amount of them.

Our data are coherent from the aspect of medical experts and geographically because the origin of data is a small city. The consequence of that, our data are useful for local model creation and testing.

REFERENCES

[1] OEP Statistical Book, year 2015, page 3

[2] OEP Statistical Book, year 2015, page 5

[3] The webpage of Epidemical Center of Hungary – Questions and answers about Influenza http://www.oek.hu/oek.web?to=1667&nid=1057&pid=1&lang=hun

[4] The resource of BNO-codes: ICD-10 Version 2016 http://apps.who.int/classifications/icd10/browse/2016/en#/J10

[5] Danielle C. Ompad, Sandro Galea1, and David Vlahov: Distribution of Influenza Vaccine to High-Risk Groups Oxford Journals – Epidemic Reviews – March 20, 2006 http://epirev.oxfordjournals.org/content/28/1/54.full

Investigation of Full-waveform Lidar Data Segmentation

A. Kimlei*, A. Barsi**
* Doctoral School of Applied Informatics and Applied Mathematics, Óbuda University, Budapest, Hungary
** Department of Photogrammetry and Geoinformatics, Budapest University of Technology and Economics, Budapest, Hungary
kimlei.annamaria@gmail.com, barsi@eik.bme.hu

***Abstract*— Many of the recent laser scanners are capable of digitizing the full waveform of the received signal. Full waveform laser scanners provide a lot of new opportunities. Analyzing the registered waveforms further geometric and material properties of the reflected surface can be derived. These waveforms can be used for multiple purposes. The full waveforms of backscattered signals are different when coming back from grass, canopy, road or oblique roof, so they can be used for classification tasks. Increased number of reflections can support classifying forested areas where the tree type or canopy size is to be determined. This technology leads to enormously increased data volume, which requires totally new processing methodologies. In this paper several processing techniques have been investigated that are able to provide remarkable results in segmentation. Obviously, these methods require further investigations to exploit their full potential.**

I. INTRODUCTION

Laser scanning is a dynamically developing part of remote sensing. We can get information about target objects without direct contact.

In the last few decades new airborne laser scanners appeared, which could measure not only discrete points, but the whole backscattered signal of every emitted pulse.

During the full waveform processing the whole backscattered pulse is computed with a given resolution, so the detailed vertical resolution of the backscattered pulse is produced. This new technology gives the opportunity to increase the reliability, accuracy, and resolution of the impulse-detection. These Lidar (Light Detection and Ranging) systems provide more possibilities to the users to determine physical properties.

A. History

In the 1980s the first full-waveform systems were designed to measure bathymetric data [2].

As an experimental system, topographic devices appeared in the middle of the 1990s, and have been commercially available for a few years later.

The first useful topographic system was designed by the NASA in 1999. It was called LVIS (Laser Vegetation Image Sensor); it was an improved version of the previous SLICER satellite system. The purpose of SLICER was to describe the vertical structure of the vegetation in huge areas.

The LVIS data processing proved the efficiency of characterizing wooded areas and measuring ground topography even beneath the vegetation.

The first commercial full wave-form system was released in 2004. Full wave-form topographic Lidar systems mainly differ in footprint size, pulse energy and repetition frequency (PRF). Small- and large footprint systems collect different information over the same area (Fig. 1):

- small-footprint system with higher PRF: high point density, accurate altimetric description. In the case of these systems tree tops are often missing, and it's difficult to determine ground points under dense vegetation.
- large footprint systems: the probability, that the impulse hits both the canopy top and the ground, is higher. The returned waveform gives the vertical distribution of the recorded surface, because none of the levels between the ground and the top are missing.

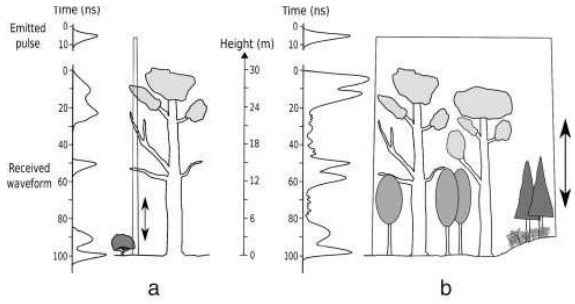

Figure 1. Emitted and returned pulses in the case of small and large footprints at wooded area [2]

B. Recording the data

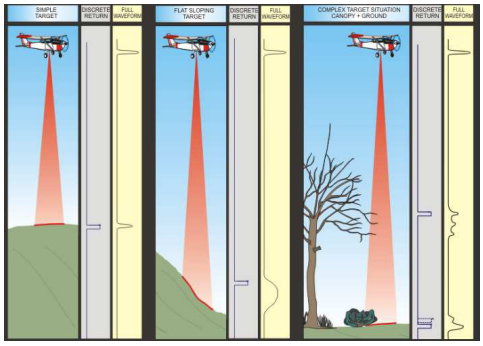

Figure 2. Recording the full waveform of different surfaces[1]

The recording of the backscattered waves is a function of time. The manufacturers of Lidar equipments have added digitization modules to their systems (for example Leica uses a separate digitization module, while Riegl has built it into the system).

The coordinates of the points, intensity values, number of all backscatters, direction of progress, scanning angle, GPS time, wave packet index, wave packet and the waveform are also recorded.

The waveform is characterized by the amplitude and width of the backscattered pulse. The amplitude depends on the signal intensity, which depends on the distance, atmospheric effects, and the reflection properties of the object. The width of the impulse depends on the height differences and the surface roughness of the object.

During the full waveform processing the whole backscattered pulse is computed with a given resolution, so the detailed vertical resolution of the backscattered pulse is produced.

The intensity values have no units, the intensity of the emitted and the backscattered pulse is between 0-255.

The waveforms are digitized on 8 bit, which means 2^8 (0-255) wave samples are stored for each points. It can be done by other sampling rates, but this option needs to be given before the data recording [2].

The digitization sampling period is between 1 and 10 ns, which is the time between the consecutive waveforms.

The main limit of full waveform Lidar recording is the storage capacity. The instruments record a few million points on each flying. The general frequency of sampling is 50-100 kHz. If the whole backscattered pulse to each emitted signal has been stored, the storage need could increase highly. (For example: one minute of full waveform laser-scanning about 4 million of recorded waveforms means 580 MByte data besides the 460 MByte of navigation data (GPS time, latitude, longitude, elevation, pitch, roll, direction, etc.). It can be easily computed that a 3 hour long data recording means 180 GByte of data to be stored) [3].

C. Data proccessing

There are two approaches to process the vertical profiles. According to the first one, the waveform is decomposed into components or echoes to analyze the different objects hit by the laser.

The goal of this method is to maximize the detection efficiency of the relevant peaks, to generate a denser 3D point cloud, and to optimize the processing capabilities by supporting information extraction from raw data. The increasing number of 3D points is important for e.g. forestry applications. More extracted information can be useful for segmentation and classification in both wooded and urban areas. Beside the more accurate determination of peaks the density of the point cloud can be increased and previously not found local maximums in the merging waveforms with more backscattered pulses can be determined.

On the other hand, the whole waveform is preserved, information is gathered from the full waveform by spatio-temporal analysis. This method is useful at urban areas, where the geometry is regular.

The last opportunity has been barely investigated, most researches have their focus on 3D point cloud processing [2].

II. METHODOLOGY

A. Data

The raw data (4 flight bands with 4-bit sampling, full waveform data at every second impulse) was given by the Remote Sensing Research Institute of the Károly Róbert Collage. The recording was taken by a CESSNA C-206 “Skywagon” aircraft, and covered the center of Mátrafüred. A Leica AL70-HP scanner was used for the airborne laser scanning. It is a specially designed instrument for general topographic surveys at high altitude with high accuracy. With a WDM65 digitization module attached the full waveforms of the impulses can be stored. Furthermore, this system contains a Leica RCD30 camera with 60 MPixel resolution to take pictures at the same time.

The four flight bands contain too much points, therefore the processing was done by a smaller cutoff area to shorten the processing time.

Properties of the cutoff area:

- Area: 22 000 m^2,
- Number of points: 300 000,
- Number of full waveform points: 94 624,
- Rate of full waveform points: 31,5%
- Average point density: 13,6 points/ m^2,
- Density of full waveform points: 4,3 points/ m^2.

B. Proccessing

There are basic differences between the backscattered waveforms depending on the reflective surface, but the most important distinction is the number of backscatters. The waveforms are very different, but probably there is correlation between the waveform and the material of the reflective surface, thus the form of the wave backscattered from grassy area is different than from an urban area.

In this case, the task is clustering using the full waveform data (with Matlab) followed by a classification of the results.

Many of the researches deals with decomposing the waveforms to echoes using Gaussian function [2]. This method is used not just to increase the efficiency of peak detection, but to distinguish between vegetation and non-vegetation using Gaussian parameters (like amplitude).

In the study [5] Authors have fit Gaussian functions to the backscattered waveforms. In another Article [6] it was used generalized Gaussian and lognormal functions to model the signals.

In the study [3] Researchers have compared different peak detection methods to find more peaks (backscatters) in the full waveform data during the post-processing. It has a dual purpose: the first one is to increase the accuracy of the point cloud definition, the second one is to support the later classification tasks. Peak detection methods are indispensable for determining return time. Because of that, there are several existing peak detection techniques. The simplest methods are looking for the maximum values of intensity, but only the detection of one peak is possible. Another frequently used method is the fix threshold technique: if the backscattered signal is uprising to the threshold, a peak detection occurs (highly depending on the amplitude of the waveform). A better choice is, when

the threshold is not a fix value, but it is set at the half of the actual maximum amplitude. There are several solutions to determine the center of the returning wave: correlation technique, first derivatives based filters, or fitting a function can determine the peaks of the returning wave. Function fitting is the most efficient algorithm; it can find the most number of peaks. Great advantage of this method is serving with the parameters (like width, flattening) being useful information for the later classification.

In the study [4] Authors could successfully do the segmentation of vegetation and built environment using full waveforms, but they didn't get satisfying results in the case of the sidewalks and roofs. They have determined that identifying roofs depend on the material and slope.

Relying on these statements the determination of the Gaussian curve parameters to each waveform was done. The exact value and position of the peak were important. After the peak detection the Gaussian function was fitted based on the environment of the peaks.

The used generalized Gaussian function was:

$$y = f(x) = a * \exp\left(\frac{-x^2}{b}\right) + c \qquad (1)$$

An indirect measurement based adjustment has been used to determine the parameters.

The Gaussian function determines only the parameters of the highest peak of each wave.

First the Gaussian parameters to each point (each waveform) were calculated, then a SOM (self-organizing-map) neural network was used with them as inputs. In the first approach of SOM network a 4×4 neuron matrix with hexagonal-cell topology was used. The input data set was extended by other parameters like elevation, waveform or intensity.

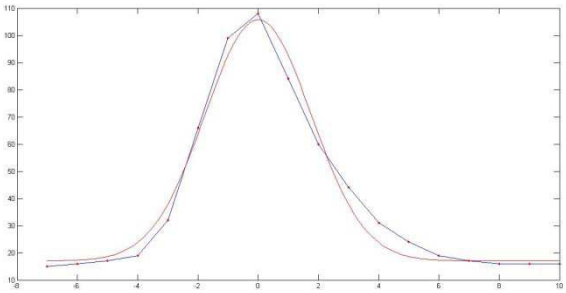

Figure 3. Fitting Gaussian function to a waveform

There were several segmentation attempts using the following parameters:

1. Only Gaussian parameters (a, b, c),
2. Height and Gaussian parameters (a, b, c),
3. Height and Gaussian parameters (a, b),
4. Height, the first 80 wave samples, Gaussian parameters (a, b, c),
5. Height, the first 10 wave samples, Gaussian parameters (a, b, c),
6. Intensity, Gaussian parameters (a, b, c).

C. Results

Fig. 4-9 show the results of the segmentations of the aforementioned parametrizations. Every figure shows the first 8 output images. One can notice that the output in cases 1-5 can't be ordered to any class. There are some results, which could be identified almost as a class (e.g. street in Fig. 5/2.), but accepting these are still not possible because of wrong identified points. Using intensity values in input data set results (dataset 6) outlining object contours (see Fig. 9). At Fig. 9/6, the points of the segmented image are mostly wooded area.

As a control, image 9/6. was acceptable; we have checked the result on a raster image in QGIS (Fig. 10).

It shows that the function can almost separate trees from other objects. Of course, there are mistakes between the points (e.g. misinterpretations on roofs), but the rate of wrongly identified points are small.

Of course, this method needs further researches and tests. Neither of the classes could be separated clearly. It could have different reasons:

- Gaussian parameters was assigned to a wrong data;
- The full waveforms should be proccessed not from the first wave sample or,
- A bigger radiometric resolution results different or better output.

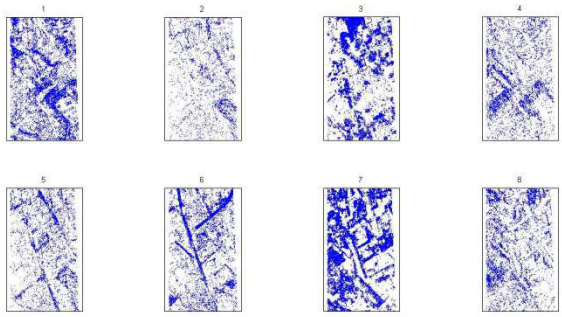

Figure 4. Segmentation by only Gaussian parameters (a, b, c)

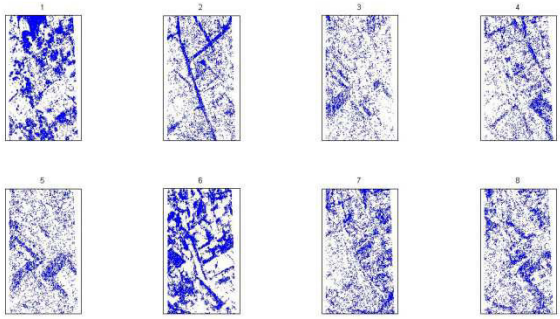

Figure 5. Using Height and Gaussian parameters (a, b, c)

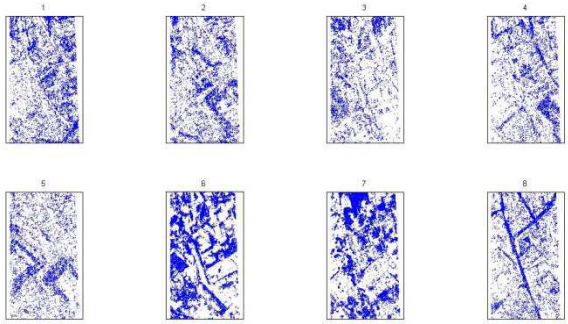

Figure 6. Using Height and Gaussian parameters (a, b)

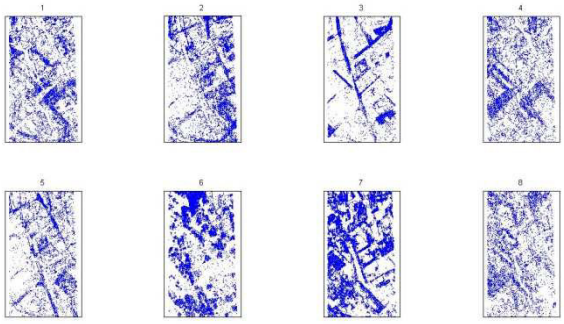

Figure 7. Using Height, the first 80 samples of the wave and Gaussian parameters (a, b, c)

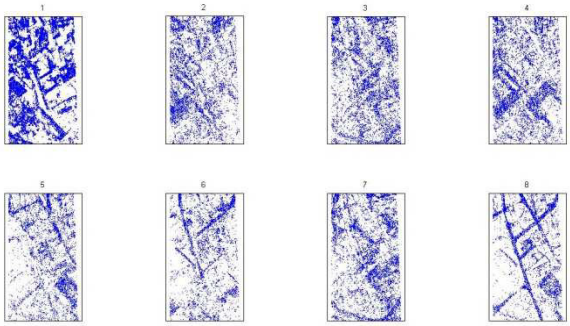

Figure 8. Using Height, the first 10 samples of the wave and Gaussian parameters (a, b, c)

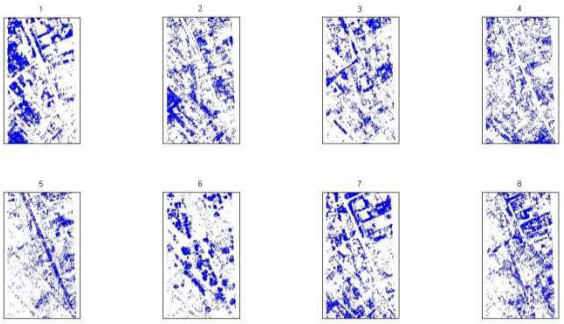

Figure 9. Using Intensity and Gaussian parameters (a, b, c)

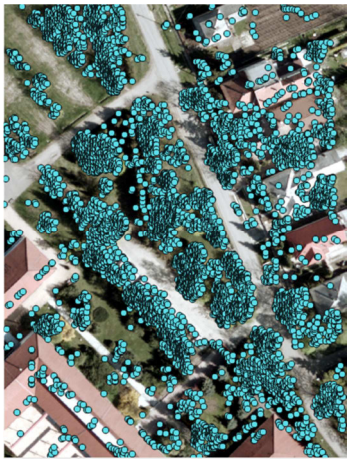

Figure 10. Segmented results in QGIS

III. CONCLUSIONS

In this paper the full waveform laser scanning and its possible usage have been shown. As an example the properties and classification possibilities of the full waveform data were analyzed.

The extremely high amount of data was the biggest difficulty during the processing, therefore a cutoff area was created and the methodology was applied there.

The processing of the full waveform Lidar data is not an easy task, because well-established methods with exact and accurate results are failing. Thus the main task was to achieve the best result from the received data. As a future research it should be worthy to investigate, whether a bigger radiometric resolution of waveforms results increased accuracy or not, and further analysis with additional parameters is recommended.

REFERENCES

[1] Verőné Wojtaszek M. (2010): Fotointerpretáció és távérzékelés, Tankönyvtár.

[2] Clément Mallet, Frédéric Bretar (2009): Full-waveform topographic lidar: State-of-the-art, ISPRS Journal of Photogrammetry and Remote Sensing
http://recherche.ign.fr/labos/matis/pdf/articles_revues/mallet_IJPRS09.pdf

[3] Zaletnyik P., Laky S., Charles K. Tóth (2011): Csúcskeresési eljárások teljes hullámalakos lézerszkenner adatok feldolgozásához, Geomatikai közlemények XIV/1

[4] Bodon F. - Adatbányászati algoritmusok tanulmány

[5] Wagner, W., Ullrich, A., Ducic, V., Melzer, T., Studnicka, N., (2006): Gaussian decomposition and calibration of novel small-footprint full-waveform digitizing airborne laser scanner. ISPRS Journal of Photogrammetry & Remote Sensing 60 (2), 100-112.

[6] Chauve, A., Mallet, C., Bretar, F., Durrieu, S., Pierrot-Deseilligny, M., Puech, W. (2007): Processing full-waveform lidar data: Modelling raw signals. International Archives of Photogrammetry, Remote Sensing and Spatial Information Sciences 36 (Part 3/W52), 102-107.

A diagram to illustrate the distribution of slope and aspect of an area

G. Nagy*
*Óbuda University, Alba Regia Technical Faculty, Institute of Geoinformatics
nagy.gabor@amk.uni-obuda.hu

***Abstract*—The slope and the aspect are an important property of the terrain in the agriculture related geospatial analysis. The distribution of this values in a determined area can be demonstrated by different tools. This paper describes a diagram and its generating method, that can show the slope and aspect in a geomtrically correct layout, which use a polar coordinate system.**

***Index Terms*—digital elevation model, slope, aspect**

I. Introduction

In many cases, the slope and the aspect are a very important property of the terrain. For example, when we look for the ideal place of a vineyard or a orchard, we search areas, which aspect is south or south-east and the slope is also an ideal value, not too steep but neither too plain. The slope and aspect are also very important in the ecological research like [1], [2], [3], [4], [5].

These important properties determine the ideal location together, the representation of the distribution of slope and aspect also show these two properties together. In this paper, the author demonstrates a trivial solutions of this problem, and the problems of this simple methods. After this, I suggest a diagram for this problem.

II. Classical methods

In this section, I demonstate the distribution of the slope and the aspect by some classical methods. The sample area is a vineyard area near Enying, in Fejér county, Hungary. The coordinates of the center of this area are E18°13'53" and N46°55'32". (See the Figure 1.)

I calculated the slope and aspect data of this area (see the Implementation section) and showed it by some classical tool.

A. Tables

The different slope and aspect surfaces can be counted by category in an area, and the result of this computing can be presented in a table. For example, the data of the sample area are in the Table I. The columns of this table represent the categories by the slope (between 0 and 2.5 degrees, between 2.5 and 5 degree, etc.), and the rows represent the categories by the aspect (between 0 and 22.5 degrees, between 22.5 and 45 degrees, etc.). One field of this table represents the total area of the surfaces, where the slope and the aspect are also in the specified interval.

The last column and the last row contain summas.

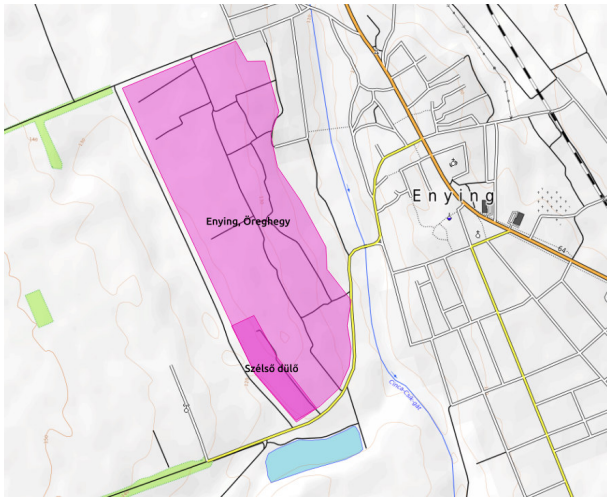

Figure 1. The location of the sample area with the OpenTopoMap data.

Table I
The total areas (hectares) with different slope (horizontal) and aspect (vertical) in the sample area

	0.0°-2.5°	2.5°-5.0°	5.0°-7.5°	7.5°-10.0°	10.0°-12.5°	SUM
0.0°-22.5°	2.45	1.10	0.00	0.00	0.00	3.55
22.5°-45.0°	3.40	2.45	0.15	0.00	0.00	6.00
45.0°-67.5°	4.15	6.95	2.40	0.25	0.05	13.80
67.5°-90.0°	5.20	9.40	3.95	0.65	0.10	19.30
90.0°-112.5°	4.75	6.25	1.75	0.35	0.00	13.10
112.5°-135.0°	3.30	2.35	0.25	0.00	0.00	5.90
135.0°-157.5°	3.10	1.15	0.00	0.00	0.00	4.25
157.5°-180.0°	2.25	0.80	0.00	0.00	0.00	3.05
180.0°-202.5°	2.30	1.90	0.15	0.00	0.00	4.35
202.5°-225.0°	2.15	3.05	1.65	0.25	0.00	7.10
225.0°-247.5°	2.00	3.80	2.15	0.20	0.00	9.00
247.5°-270.0°	1.75	2.55	1.15	0.05	0.00	5.90
270.0°-292.5°	2.05	0.85	0.15	0.00	0.00	3.00
292.5°-315.0°	1.75	0.75	0.00	0.00	0.00	2.50
315.0°-337.5°	2.05	0.60	0.00	0.00	0.00	2.65
337.5°-360.0°	1.60	0.65	0.00	0.00	0.00	2.25
SUM	45.45	44.60	13.75	1.75	0.15	105.70

This table contains many useful data about the terrain of the studied area, but it is not too spectacular. A solution is needed for showing this data in a suitable diagram.

B. Classical diagrams

The classical spreadsheet software (in this case LibreOffice Calc) can be applied to create a diagram from the data series of the Table I. This diagram may be an 3D column diagram,

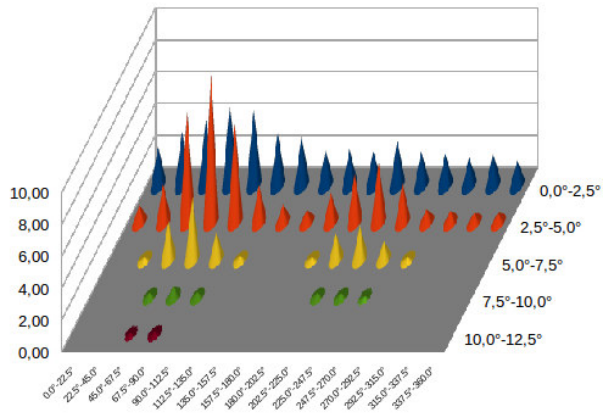

Figure 2. The distribution of the slope and the aspect in a classical diagram. The areas are in hectares. (Created by LibreOffice from the data of the Table I.)

where the X coordinate is the categories of the aspect, the Y coordinate is the categories of the slope and the Z coordinate is the total area of the surfaces. This diagram is in the Figure 2. Using of cones instead of columns are much preferable, because the cones cover smaller area from the elements in the background.

This diagram shows the distribution of the slope and the aspect in the examined area, but there are some problems.

The aspect is an azimuth-like value. The categories of 0°-22.5° and the 337.5°-360° are neighbours, but in the Figure 2. these categories are located in the opposite sides of the diagram. Another problem is that the distance between different aspects are equal in any slope category, but the impact of the difference is higher in larger slope.

III. The proposed diagram

The ideal diagram of the distribution of slope and aspect eliminates the mistakes of the classical diagram (Figure 2.). The places of an element of the diagram have to satisfy two criteria: the places around the north direction (or any other direction) have to be located close to each other, and two places with different aspects have to be located further, where the slope is larger.

The Figure 3. shows my proposal to this diagram.

A. The coordinate system of the diagram

The diagram recommended by the author use a polar coordinate system to perform the described requirements. (See the Figure4.)

The angular coordinate is equal to the aspect. Both of these values are an azimuth-like number, the application in a polar coordinate system is simple.

The distance in this polar coordinate system is proportional to the slope. A function defines the relationship between the slope and the distance in the diagram, for example:

$$d = \frac{w_d s}{2 s_{max}} \tag{1}$$

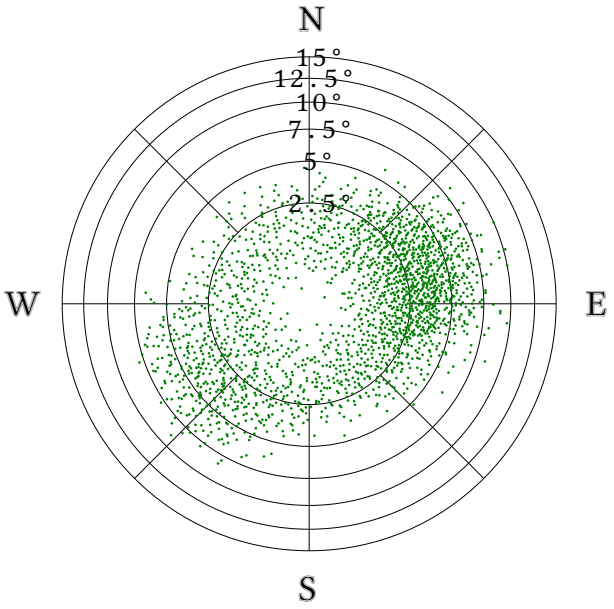

Figure 3. The proposed diagram of the sample area. The slope is proportional to the distance from the centre of the diagram. The aspect is equivalent to the direction from the centre of the diagram. Twenty dots represent one hectar.

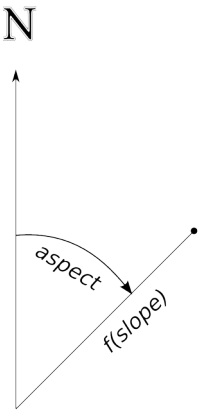

Figure 4. The polar coordinate system of the diagram.

where d is the distance in the diagram, w_d is the width of the diagram, s is the slope, and s_{max} is the maximal slope, which is shown in the diagram. The d and the w_d are in the units of the diagram (millimeters, pixels or other units), the s and s_{max} are in degrees.

Another possible example:

$$d = \frac{w_d}{2} \sqrt{\frac{s}{s_{max}}} \tag{2}$$

B. The distribution of the diferent slope and aspect surfaces of the area

The fields of TableI belong to a sector of the diagram. (The angle and the distance are limited by the values of the intervals

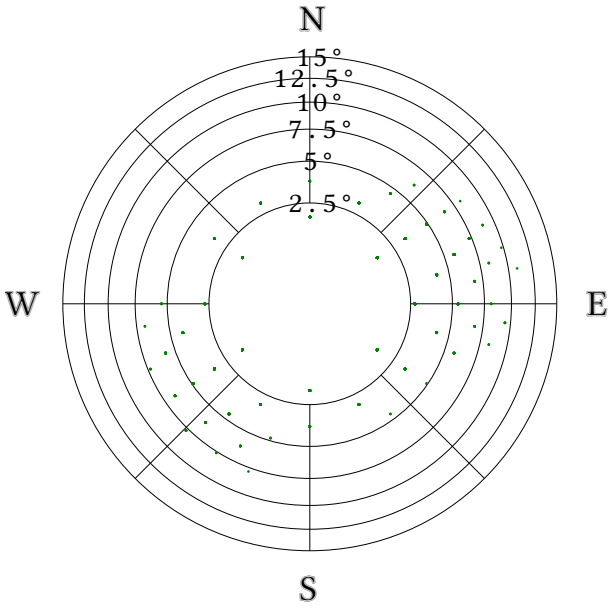

Figure 5. The diagram of the sample area without (quasy-) random modification of the dot's places.

of the table.) This sectors can be colored in proportion to the area, or a dot density representation can be applied.

Each pieces of the suface of the area has a dot in the diagram, the slope and the aspect of this surface element determines the place of the dot in the diagram. If we use the equation (2), the areas of the sectors are equal, and the dot density impression's will be like a coloring with a scale from light to dark.

IV. Implementation

A Python 3 application was written for creating the above described diagram. This program reads the data of areas from a CSV file and the digital elevation model (DEM) data from a one arc second SRTM ([6], [7], [8]) file. The polygons of the areas are descripted by an WKT (well-konwn text) in the CSV file. The program reads the elevation data directly from the 1×1 degree SRTM tiles without any transformation.

The SRTM dataset contains elevations rounded to whole numbers in meter, because of the slope and the aspect will be only quantized values. The places of this values can be viewed in the Figure 5. The points of this diagram are in determined places, and we can not see, how many points are a position.

The program uses a pseudo-random shift in the points to the points of the result will not be in overlapped positions. I use a 2,3 Halton sequence ([9]) for generate a quasy-random point sequence for this step.

The program creates SVG files as output. The dots are circles in this file. The fill of this circles may be transparent, because the overlapped places will be darker in this solution, and the output will be specious. (See in Figure 6.)

The program contains more different slope scales, and choice by the maximal slope value. The legend of the isoslope lines are in the northern part of the diagrams, because the important locations usually are in the southern part.

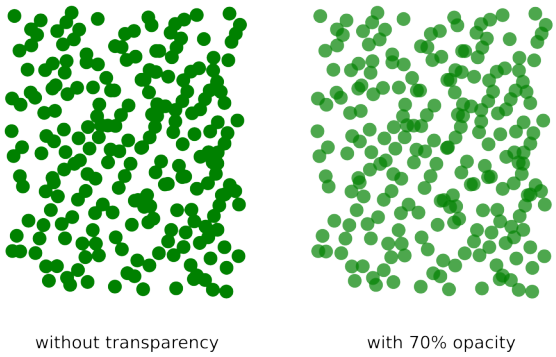

Figure 6. The dots without transparency and with transparent drawing.

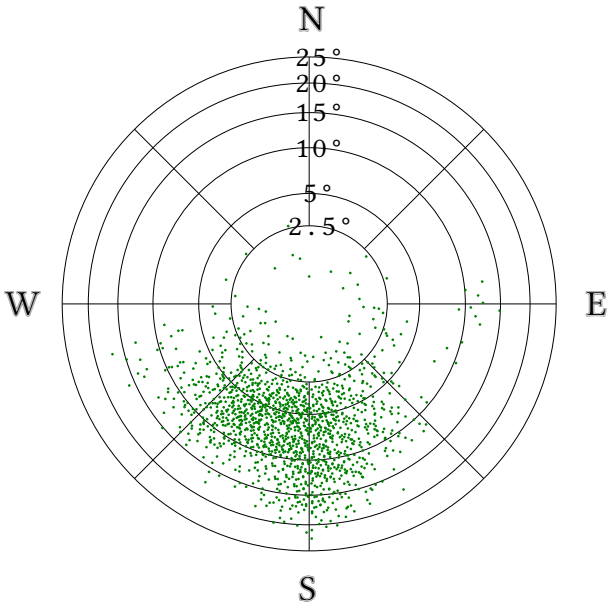

Figure 7. The diagram of an vineyard area Tokaj, Hungary. Twenty dots represent one hectar.

V. Examples

I create some diagram from other areas. The Figure 7. represents a vineyard area from Tokaj, the famous Hungarian wine-grower city.

Another example are in the Figure 8. This is a wine and fruit grower area near in Csór, not too far Székesfehérvár.

VI. Conclusion

The proposed diagram shows the distribution of the slope and the aspect together. This diagram can be used, when we want to demostrate the distribution these properties in an area. This may be useful when we search an ideal place for a vineyard, an orchard or an solar power plant.

The set of ideal slope and aspect can be delimit in the polar coordinate system of the diagram. The viewer can see the ideal distribution and the real distribution together.

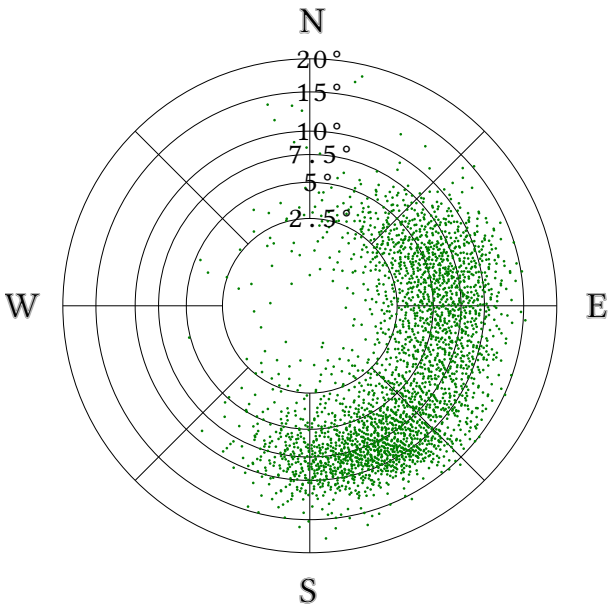

Figure 8. The diagram of an vineyard area in Csór, Hungary. Twenty dots represent one hectar.

REFERENCES

[1] J. J. Armesto and J. A. Martínez, "Relations between vegetation structure and slope aspect in the mediterranean region of chile," *The Journal of Ecology*, pp. 881–889, 1978.

[2] J. Bennie, B. Huntley, A. Wiltshire, M. O. Hill, and R. Baxter, "Slope, aspect and climate: spatially explicit and implicit models of topographic microclimate in chalk grassland," *Ecological Modelling*, vol. 216, no. 1, pp. 47–59, 2008.

[3] X. Gong, H. Brueck, K. Giese, L. Zhang, B. Sattelmacher, and S. Lin, "Slope aspect has effects on productivity and species composition of hilly grassland in the xilin river basin, inner mongolia, china," *Journal of arid environments*, vol. 72, no. 4, pp. 483–493, 2008.

[4] V. Lieffers and P. Larkin-Lieffers, "Slope, aspect, and slope position as factors controlling grassland communities in the coulees of the oldman river, alberta," *Canadian Journal of Botany*, vol. 65, no. 7, pp. 1371–1378, 1987.

[5] A. R. Stage and C. Salas, "Interactions of elevation, aspect, and slope in models of forest species composition and productivity," *Forest Science*, vol. 53, no. 4, pp. 486–492, 2007.

[6] J. J. Van Zyl, "The shuttle radar topography mission (srtm): a breakthrough in remote sensing of topography," *Acta Astronautica*, vol. 48, no. 5, pp. 559–565, 2001.

[7] E. Rodriguez, C. S. Morris, and J. E. Belz, "A global assessment of the srtm performance," *Photogrammetric Engineering & Remote Sensing*, vol. 72, no. 3, pp. 249–260, 2006.

[8] A. Jarvis, H. I. Reuter, A. Nelson, E. Guevara *et al.*, "Hole-filled srtm for the globe version 4," *available from the CGIAR-CSI SRTM 90m Database (http://srtm. csi. cgiar. org)*, 2008.

[9] J. Halton and G. Smith, "Radical inverse quasi-random point sequence, algorithm 247," *Commun. ACM*, vol. 7, p. 701, 1964.

Cost-effective WiFi controlled mobile robot

J. Katona*, A. Kovari**
* University of Dunaujvaros/Institute of Computer Engineering, Dunaujvaros, Hungary
** University of Dunaujvaros/Institute of Engineering, Dunaujvaros, Hungary
katonaj@uniduna.hu, kovari@uniduna.hu

Abstract — **In this article, a simple-designed mobile robot built up from cost-effective parts is introduced. The mobile robot can be controlled via WiFi wireless network with the help of a simple application. Due to the cheap and simple design of the robot, it may be a useful developing tool for those, who can not afford themselves a much more expensive robot. Its ESP8266 chip based (manufactured by Espressif Systems) modules are cost-effective tools of performing WiFi wireless control functions, so the control of this robot has been achieved by applying this chip. That such designed device may be a quite useful example in education as well, regarding the fields of informatics and meachatronics, where the programming and applying of the embedded systems can be introduced through practical examples.**

I. INTRODUCTION

Mobile robots are getting more and more important in our everyday life. By the development of electronics, embedded systems and informatics, the price of mobile robots significantly decreased, while their field of use increased.

One of the domestic uses of mobile robots is the field of hoovers or lawn mowers [1]. Hardware design of such a robot is not too complicated, so the simplified version of such a robot containing its control system and sensors required for moving can be assembled using cheap parts.

By the development of telecommunication technologies and ICs, there are several opportunities to perform wireless control, taking into consideration, that through this communication channel, transfer of complex information might be necessary, like continuous transfer of signals of some specific sensors beyond control signals, or even video signals. This means, that during communication, the proper speed of wireless transfer may reveal other opportunities in performing control of the mobile robot.

For controlling mobile robots, low-cost Bluetooth communication was applied in most cases [2], but the bandwidth of Bluetooth wireless transfer is not good enough and its range is only some meters either. There have been such ICs capable of WiFi communication available for some years, which support WiFi 802.11n transfer standard with appropriate encryption contrary to their relatively low prices, and their ranges are higher as well.

In this article, a simple-designed mobile robot assembled from cost-effective parts is introduced, which can be controlled via WiFi wireless network by a simple application.

II. HARDWARE OF THE MOBILE ROBOT

During the development of the mobile robot, simple design, upgradeability, and wireless control were the main goals. In case of educational use, the application of modern ICT based technology and knowledge transfers are very offer new possibilities [4]-[6]. The developed device can be used well in education, because simple and clearly arranged layout, control features have to be achieved. Motor control of the mobile robot and the WiFi wireless communication are usually performed by two separate units; one unit, which performs motor control, is generally a microcontroller, while WiFi communication is ensured by a separate communication unit [3]. In case of a cheap, easy construction mobile robot, such a solution is preferable, where the microcontroller and WiFi communication units are achieved in one IC. For example such a cost-effective IC is the ESP8266 chip based modules (manufactured by Espressif Systems), available since 2014. When creating the mobile robot, this module was chosen. The main features of ESP8266 IC are summarized in Table 1.

The device is available in differently designed modules, for development purposes the ESP-12E was chosen, which contains integrated antenna, and important outputs of the IC are available. For the module, a 2nd generation LoLin development board was chosen, which contains the 3.3V voltage controller required for USB power supply, and USB-UART serial converter based on CH340G IC for programming via USB port. (Figure 1). Connection of other external modules to LoLin developer chip is made easier by a separate I/O adapter module (Figure 2).

TABLE I.
MAIN FEATURES OF ESP8266 WIFI CHIP

Unit	Param	Other
Microcontroller	32 bit RISC CPU	Tensilica Xtensa LX106 running at 80 MHz
Internal memory	64 kB program, 96 kB data	RAM
External memory	512 kB – 4 MB	Flash
WiFi communication	IEEE 802.11 b/g/n	WEP vagy WPA/WPA2 authentication
I/O	16 GPIO, 1 analog	
Interfaces	SPI, I2C, I2S, UART	

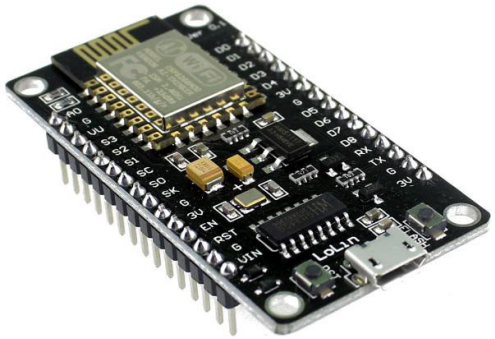

Figure 1. LoLin ESP8266 development module

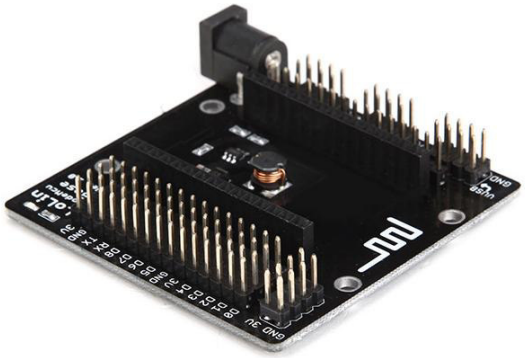

Figure 2. I/O adapter module

Programming of the device can be accomplished via UART connection, so for programming, no special (and usually expensive) programmer tool is necessary.

For the main purpose of the mobile robot, primarily the simple-design, upgradeable chassis and the control of mechanic movement was preferred. Thus, for performing control mechanism, driven front wheels and a free rear wheel was chosen. For chassis of the mobile robot, such design is expedient, which makes placing other accessories required for further developments, and sensors possible. On the international market, several kits containing the chassis of the mobile robot are available, and such solution was chosen, where the battery holder responsible for power supply can be placed on the lower part of the chassis, leaving more free space for other units on the upper part of the chassis (Figure 3 and 5).

Figure 3. 2 Wheel Drive Mobile Robot Kit

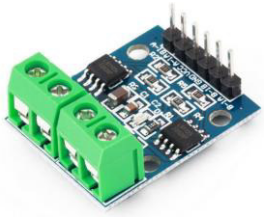

Figure 4. L9110S motor control module

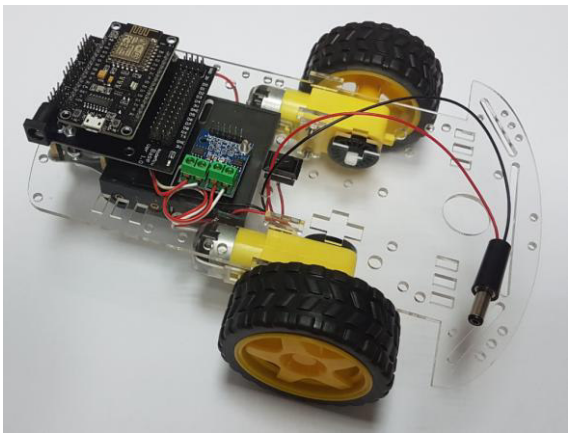

Figure 5. Assembled mobile robot

The mobile robot kit contains a removable coated transparent plexi chassis, two driven wheels, two direct current motors with 1:48 transmission ratio, one free wheel, battery holder and other accessories required for assembly. In the battery holder, 4 pcs AA type 1.5 V battery can be inserted, so the supply current is appr. 6 V. The current of the direct current motors measured during operation are below 500 mA, so for their supply, a module built on L9110S motor controller's IC was chosen, whose operating voltage range is between 2.5 and 12 V, while its continuous output current is 800 mA (Figure 4). The assembled mobile robot containing modules placed on the chassis, and also the motor and power supply input is shown on Figure 5.

III. SOFTWARE OF THE MOBILE ROBOT

For programming ESP8266 IC, there are several developer environments available. For the development of embedded systems' software, generally C or C++ programming languages are used, which are also supported by the freeware Arduino development environment, so this one was chosen. (Figure 6).

In the development environment, the ESP-12E module is not among the supported developer tabs, but with the help of 'Boards Manager', it can be easily added. For programming the developer tab, driver of CH340G IC performing USB-UART conversion needs to be installed, which creates a virtual serial port on the computer. For programming, the proper serial port has to be selected in the development environment, as well as the 115.2 kbit/s bandwidth.

Programming is supported by the ESP8266WIFI function library. By the function library, connection to WiFi network, creation of server making the connection of external clients possible, and the client-server data connection can be handled easier.

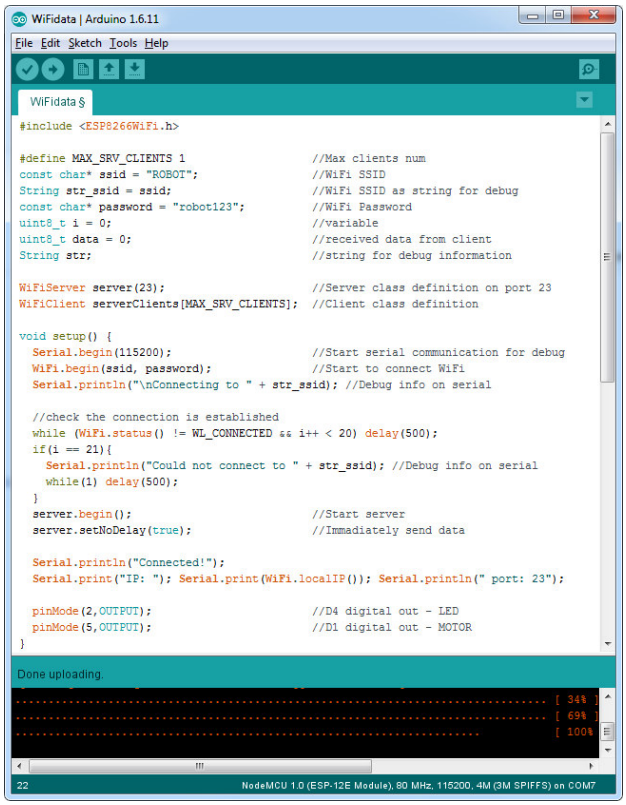

Figure 6. Arduino IDE

The PC control software, sends the speed parameters of the robot motors (in the range of 0...100), connecting to the control unit of the mobile robot (as server) as a client, via TCP/IP connection. The speed of the mobile robot is defined by the speed of the controller-motor unit supplying each wheels, which in case of permanent magnet direct current motor. In case of permanent load the supply voltage of the motor is proportional to the speed. The effective, low-loss control of the motor's speed is performed by switching operation, the speed control was performed by pulse width modulation (PWM). Digital outputs of ESP8266 IC are capable of creating direct pulse width modulated signal, whose default base frequency is 1 kHz. So in the program code, speed control was performed by the value defining the duty cycle of PWM output sent by the PC control software. The flow chart of the program ensuring speed control of the mobile robot is shown on Figure 7.

The application managing TCP/IP-based connection and performing the control of the mobile robot is built up by two classes. In the first class, there is the description of TCP/IP connection , where the responsibility of the object of TcpClient class is to establish, maintain and close new connections on the IP address and port nr.: 23 (defined in the mobile robot program). In the second class, there is the description of performing control of the mobile robot by cursor keys. NetworkStream class is responsible to send the speed parameters for the mobile robot via the already created object. The application interface of the program is very simple. The user has to define the IP address of the robot and click on the connect button. When the connection is established the state of the connection is changing from Inactive to Active. When the connection is active the cursor keys can be used to control the robot. The application windows can be seen in the Figure 8.

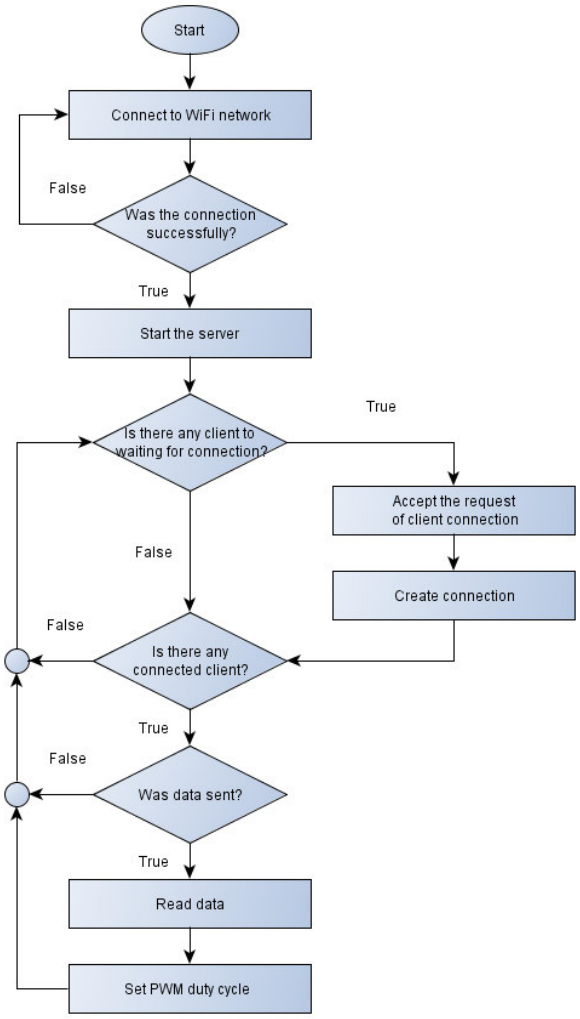

Figure 7. Flow chart of the mobil robot's control program

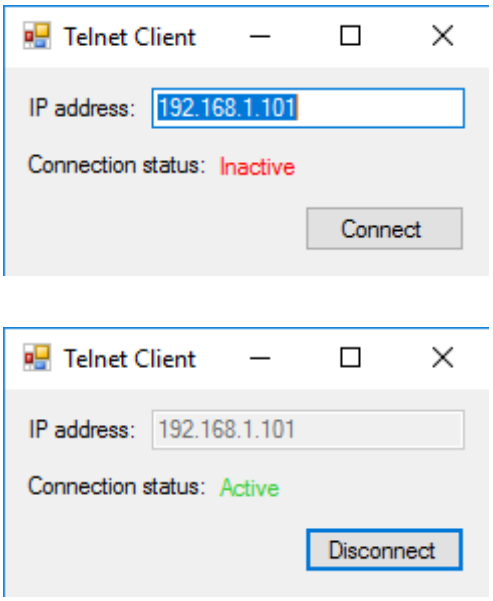

Figure 8. PC control software

IV. SUMMARY

A simple-designed mobile robot assembled from cost-effective parts introduced in this article, can be well-used as a tool for those, who are interested in this field of mechatronics and informatics. This cheap, easy-to-build system even for students can be well-used for educational purposes too to support ICT based learning [4] and knowledge transfer [5], which helps to understand the design, and the application, programming and wireless communication use of embedded systems through practical examples.

For creating the mobile robot, modules based on ESP8266 chip are enable cost-effective design and WiFi wireless control features.

REFERENCES

[1] Jordi Palacín, José Antonio Salse, Ignasi Valgañón, and Xavi Clua, "Building a Mobile Robot for a Floor-Cleaning Operation in Domestic Environments," IEEE TRANSACTIONS ON INSTRUMENTATION AND MEASUREMENT, vol. 53, no. 5, pp. 1418–1424, 2004.

[2] S. Kahar, R. Sulaiman, A. S. Prabuwono, N. A. Ahmad and M. A. A. Hassan, "A Review of Wireless Technology Usage for Mobile Robot Controller", 2012 International Conference on System Engineering and Modeling (ICSEM 2012), IPCSIT vol. 34, IACSIT Press, Singapore, pp. 7-12, 2012.

[3] A. Aneiba and K. Hormos, "A model for Remote Controlled Mobile Robotic over Wi-Fi network using Arduino technology," Frontiers of Communications, Networks and Applications (ICFCNA 2014 - Malaysia), International Conference on, Kuala Lumpur, 2014, pp. 1-4.

[4] György Molnár: Modern ICT based teaching and learning support systems and solutions in higher education practice, In: Milan Turčáni, Martin Drlík, Jozef Kapusta, Peter Švec (ed.) 10th International Scientific Conference on Distance Learning in Applied Informatics. 654 p. Praha: Wolters Kluwer Law and Business, 2014, pp. 421-430.

[5] András Benedek, György Molnár: Supporting the m-learning based knowledge transfer in university education and corporate sector, In: Prof Inmaculada Arnedillo Sánchez, Prof Pedro Isaías (ed.) PROCEEDINGS OF THE 10th INTERNATIONAL CONFERENCE ON MOBILE LEARNING 2014. Madrid: IADIS Press, 2014, pp. 339-343.

[6] Anikó Kálmán, "Learning - in the New Lifelong and Lifewide Perspectives", Tampere: Tampere University of Applied Sciences, 2016, 139 p.

A Special Robust Solution for Battery Based Power Supply

György Györök[1], Tihomir Trifonov[2], Alexander E. Baklanov[3], Bertalan Beszédes[1]
Svetlana V. Grigoryeva[3], Aizhan Zhaparova[3]

1 Óbuda University, Alba Regia Technical Faculty, Budai Str. 45, H-8000 Székesfehérvár
{gyorok.gyorgy, bertalan.beszedes}@amk.uni-obuda.hu
2 St. Cyril and St. Methodius University of Veliko Tarnovo,
Department of Computer Systems and Technologies and National Military University Vasil Levski,
Department of Communication and Information Systems,Veliko Tarnovo, Bulgaria
tihomirtrifonov@ieee.org
3 D. Serikbayev East Kazakhstan State Technical University
Instrument Engineering and Technology Automation, Protozanov Str. 69, Ust-Kamenogorsk, Kazakhstan
ABaklanov@ektu.kz, sgrigorieva@inbox.ru, atj-43@mail.ru

***Abstract*—The use of mobile devices has become general, their spread is self-evident. As a Power-source either an accumulator or a battery is used. (The next, we do not differentiate between the rechargeable accumulator and battery, only referring to a battery.) In either case, if the devices do not work, do not work properly, replace them. In either case, if the electronic devices do not work, do not work properly, the batteries are charge, or we replace batteries.**

In this paper, we examine whether a discharged battery is really empty. If not, what can be more possible to extract from it the total energy. All of these activities as a result of power supply devices and mobile devices become more robust operation.

I. Introduction

The usual approach to the battery power-supply model is shown in Figure (1). On the figure U_g is source voltage of the chemical cells, R_g the internal resistance of the battery, R_l is internal resistance of the device, of load, U_l is voltage of load.

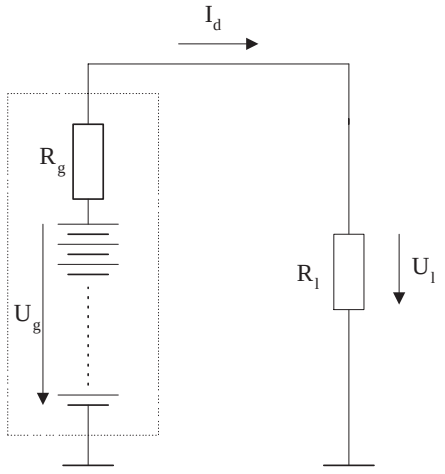

Fig. 1. Usual battery based power-supply model.

During the operation, I_d discharge current flows according equation 1;

$$I = \frac{U_g}{R_g + R_l} e^{-\frac{t}{C_b(R_g+R_l)}}; \tag{1}$$

where C_b is capacity of battery. If we put on that voltage (U_b), and current (I_b) of capacitor are constant, can be calculated value of stored energy with equation 2;

$$E = U_b \cdot I_b \cdot t. \tag{2}$$

As we know the greatness in a capacitor stored energy is in equation 3

$$E = \frac{1}{2} C_b U_b^2. \tag{3}$$

For example if a battery has 1,5V source voltage, and 2000mAh capacity, by equation 2 can calculate stored energy, it is 10800J. Wit equation 3 from result of equation 2 is calculable capacity of battery, it is in example; 9,6kF.

Thus, on the basis of the model of Figure (1) is an approximate function of time can define to the battery voltage changes at continuous discharge

(equation 4).

$$U_l = U_g \cdot e^{-\frac{t}{C_b(R_g+R_l)}}. \tag{4}$$

In the figure (2) is shown as a function of battery voltage in time at discharge [14] .

The equations that are used previously (equations 2 and 3), have a significant approximations. If you are an approximation

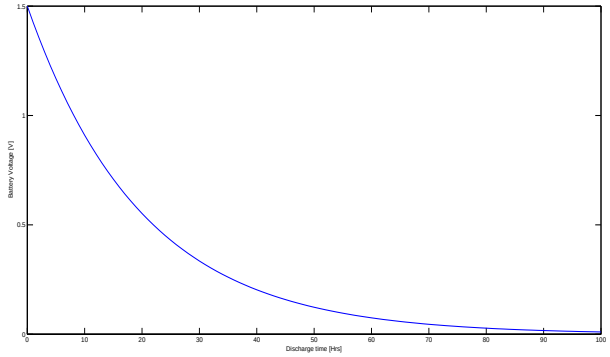

Fig. 2. The change voltage of the battery at discharge in idealized state.

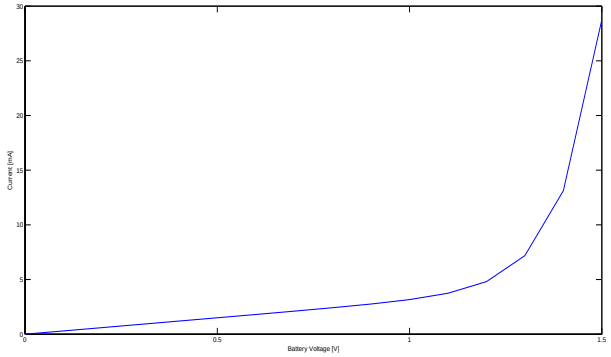

Fig. 4. supply voltage and supply current characteristics of a MP3 player electronic equipment in standby mode.

of the physical, electronically content to be carried out, it would be the correct way to write these (5, 6).

$$E = \int_0^T \big(U(t) \cdot I\big) dt. \tag{5}$$

$$E = \frac{1}{2} C_b \int_0^T \big(U(t)^2\big) dt. \tag{6}$$

Together with the previous approaches can be applied, in terms of further examinations.

II. Really model of electronic devices

On Fig. 3 is seen really power relation model of semiconductor based electronic devices [20]. In the figure U_g and R_g are voltage and inner resistance of battery, U_l and R_l equivalent parameters of electronic device.

A typical semiconductor-based electronic devices can operate in the event of a battery voltage is greater than a semiconductor specific threshold voltage (U_s). Its value depends on the type of semiconductor (manufacturing technology of silicon structures, Shottky or not, BJT or FET…etc.) and the circuit environment [16].

Thus, the electronic equipment from power-supply side is viewed it were an internal voltage generator ($U_s = I_s R_{ll}$). It follows that the equipment voltage-current characteristic is nonlinear [15].

Fig. 4 shows a supply voltage and supply current characteristics of a semiconductor-based really electronic equipment [18]. It can be observed that below the threshold voltage the internal resistance is greater (R_{ll}) as above (R_{ll}).

According in equation 4 described voltage-time function now is definable in equation 7;

$$U_l = (U_g - U_s) \cdot e^{-\frac{t}{C_b(R_g + R_l)}} + U_s, \tag{7}$$

and is seen on Fig. 5.

This also means that at normal application the battery is only to the threshold voltage can discharge [9]. Thus, using the former approach greatness of remaining energy in the battery is (equation 8);

$$E = \frac{1}{2} C_b U_s^2. \tag{8}$$

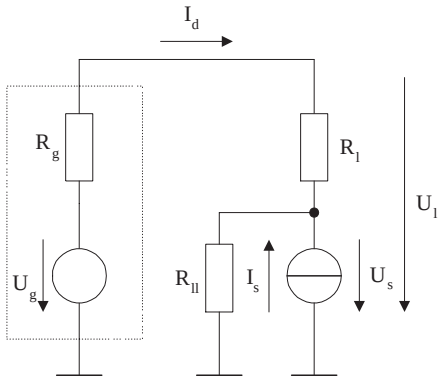

Fig. 3. Really power relation model of semiconductor based electronic devices.

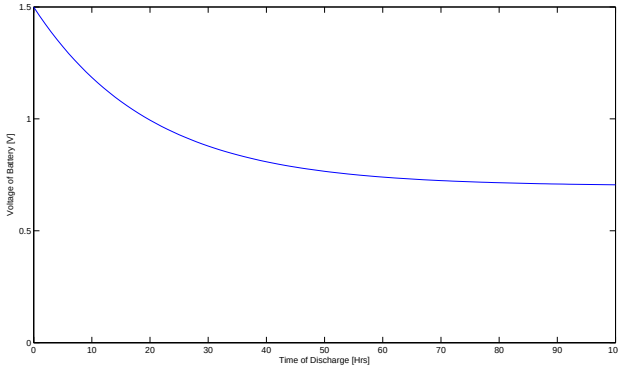

Fig. 5. The discharge characteristic of a battery in case of a semiconductor-based device.

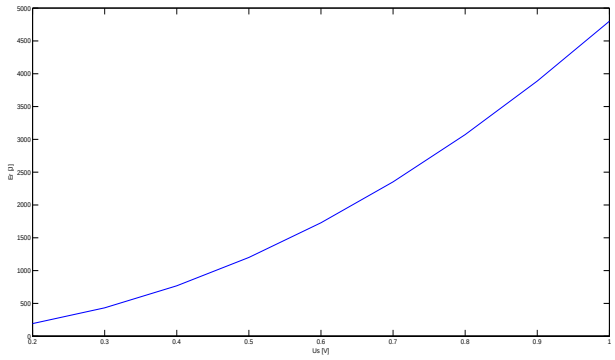

Fig. 6. Remaining energy in function of discharge voltage case at 200mAh battery.

In our previous example, if the $U_s = 0,5V$, and battery capacity is 9,6kF, the rested energy (E_r) is approximately 1200J, and if $U_s = 0,8V$ than $E_r = 3000$J. It is hardly plausibility but this is highly wasteful, inefficient solution, with large environmental component.[13] [17]

Fig. 6 shows a function of remaining energy of battery (E_r) and discharge voltage (U_s).

III. Proposed Solution

The appropriate solution is a switching-mode power supply (SMPS) that can operate at very low voltages and on output can produce the desired voltage value, together with own power voltage [5].

The proposed arrangement is shown on Fig. 7. The power supply operates by I_d current of battery and its output produces a stabilized voltage [1]. Because the power supply is also consists semiconductors, so it has its minimum operating voltage (U_{ss}). If manage to achieve that (9);

$$U_{ss} << U_s, \tag{9}$$

so from battery obtained energy is larger.

The structure of the proposed power supply is shown on Fig. 8. Battery (U_s, R_s) connect to input of SMPS, and on output is a load (R_l). The power supply unit boost type, therefore, the output voltage may be higher than the input voltage [12].

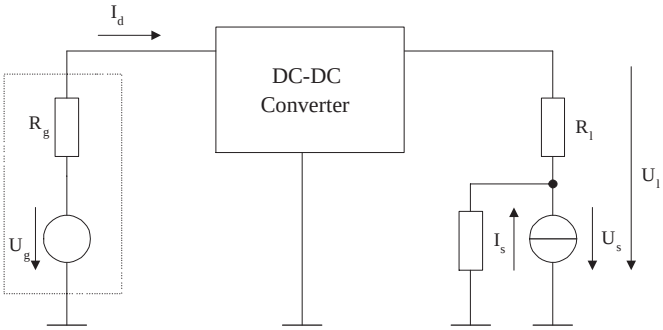

Fig. 7. Proposed arrangement to extracting more energy from battery.

The pulse width modulation (PWM) unit gets feedback signal from the output, which is also the operating voltage as well [4]. If the PWM control unit opens the FET (T_s), the coil (L_b) builds a magnetic field [2]. If the FET is closed the energy of coil trough a diode (D_s) gets to the load [19]. If the output voltage is too high, the PWM's pulse width decreases, while otherwise grow [3]. C_f a filter capacitor for suppress the high frequency component in DC voltage at output.[6] [7] [8]

So that the a switching-mode power supply unit able work case of low input voltage we must use appropriate semiconductors in position T_s, D_s. Nowadays choice of the appropriate components, this value can be down to 200mV.

And now calculated with the 0,2V voltage at 9,6kF battery 200J is obtained. The results show significant improvement. It is important to note that the power supply's operation need energy, but we are sure that the balance is still high.The robustness of this solution is operating with a lower supply voltage range. [10] [11]

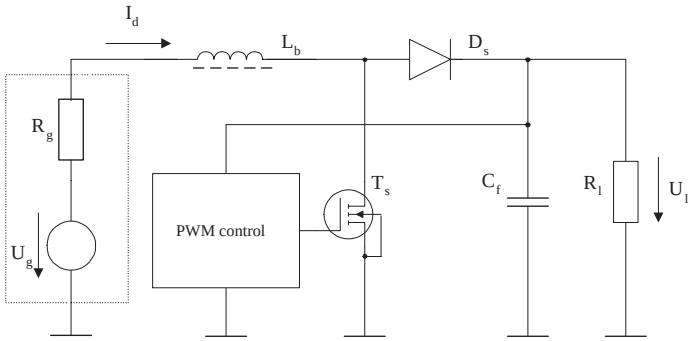

Fig. 8. Structure of boost type switching-mode power supply, with battery and load.

IV. Conclusions

The price of the devices, because need an additional power supply, is increased, but at expensive devices just a few percent [4].

At proposed method is an important aspect of above discussed discharge voltage levels, power demand of device, how often should replaced batteries.

Further work is needed to elaborating a proposed switching-mode power supply unit [2].

In the future, we will deal with the possibility of a greater operating range, thus increasing the robustness of the method.

References

[1] N. Ádám. Single input operators of the df kpi system. *Acta Polytechnica Hungarica*, 7(1):73–86, 2010.

[2] Gy. Györök, M. Makó, J. Lakner. Combinatorics at electronic circuit realization in FPAA. *Acta Polytechnica Hungarica, Journal of Applied Sciences*, 6(1):151–160, 2009.

[3] Gy. Györök. Self configuration analog circuit by FPAA. *Proc. 4th Slovakien – Hungarien Joint Symposium on Applied Machine Intelligence (SAMI2006)*, pages 34–37, January 2006.

[4] Gy. Györök. A-class amplifier with FPAA as a predictive supply voltage control. *Proc. 9th International Symposium of Hungarian Researchers on Computational Intelligence and Informatics (CINTI2008)*, pages 361–368, November 2008.

[5] Gy. Györök. Crossbar network for automatic analog circuit synthesis. *Proceedings (Liberios Vokorokos, Ladislav Hluch, Jnos Fodor szerk.) of the IEEE 12th International Symposium on Applied Machine Intelligence and Informatics (SAMI 2014). IEEE Computational Intelligence Society, Budapest: IEEE Hungary Section, ISBN:978-1-4799-3441-6*, pages 263–267, January 2014.

[6] J. Kopják. Dynamic analysis of distributed control network based on event driven software gates. *IEEE 11th International Symposium on Intelligent Systems and Informatics, Subotica, Serbia*, ISBN: 978-1-4673-4751-8:p. 293–297, 2013.

[7] J. Kopják and J. Kovács. Implementation of event driven software gates for combinational logic networks. *IEEE 10th Jubilee International Symposium on Intelligent Systems and Informatics, Subotica, Serbia*, ISBN: 978-1-4673-4751-8:p. 299–304, 2012.

[8] K. Lamár. A világ leggyorsabb mikrovezérlöje. *ChipCAD Kft.*, page 96, January 1999.

[9] K. Lamár and Veszprémi K. A mikroszámítógépek térnyerése a villamos hajtások szabályozásában. *Proceedings of the Kandó Conference 2002, Budapest, Hungary*, pages 1–7, January 2002.

[10] K. Lamár and J. Neszveda. Average probability of failure of aperiodically operated devices. *Acta Polytechnica Hungarica*, 10.(8.):pp. 153–167, 2013.

[11] L. Madarász and Zivcak J. Aspects of computational intelligence: Theory and applications. *Revised and Selected Papers of the 15th IEEE International Conference on Intelligent Engineering Systems 2011, Springer-Verlag , Berlin Heidelberg*, ISBN 978-3-642-30667-9:p. 436, 2011.

[12] L. Madarász and Fözö R. Intelligent technologies in modelling and control of turbojet engines. *New Trends in Technologies : Control, Management, Computational Intellingence and Network Systems, Rijeka, Croatia*, ISBN 978-953-307-213-5:p. 17–38, 2011.

[13] T. Orosz. Analysis of sap development tools and methods. *15th IEEE International Conference on Intelligent Engineering Systems (INES)*, pages pp. 439–443, 2011.

[14] Malcolm Bailey David A. Foster Peter R. Green, Peter N. Green. Design and delivery of a microcontroller engineering teaching theme. *International Journal of Electrical Engineering Education*, 50.(3.):pp. 231–238, 2013.

[15] A. Pilat and J. Klocek. Programmable analog hard real-time controller [programowalny sterownik analogowy]. *Przeglad Elektrotechniczny*, 89(3 A):38–46, 2013. cited By (since 1996) 0.

[16] Adam Pilat. Control toolbox for industrial programmable analog controllerembedding state feedback controller. pages 1–4, 2012.

[17] A. Selmeci and T. Orosz. Usage of soa and bpm changes the roles and the way of thinking in development. *IEEE 10th Jubilee International Symposium on Intelligent Systems and Informatics (SISY)*, pages pp. 265–271, 2012.

[18] S. Sergyán. Useful and effective feature descriptors in content-based image retrieval of thermal images. *LINDI 2012 - 4th IEEE International Symposium on Logistics and Industrial Informatics, Proceedings*, pages 55–58, 2012.

[19] Z. Vámossy. Thermal image fusion. *2012 IEEE 10th Jubilee International Symposium on Intelligent Systems and Informatics, SISY 2012*, pages 385–388, 2012.

[20] L. Vokorokos, N. Ádám, and B. Madol. The process control for p-single operators. *19th International Workshop on Robotics in Alpe-Adria-Danube Region, RAAD 2010 - Proceedings*, pages 119–123, 2010.

Data collection and analysis of activity patterns with W2 Activity Tracker

Balazs Borbely[1], Attila Safar[1] and Jozsef Halasz[1,2]
1. Obuda University, AMK, Szekesfehervar, Hungary
2. Vadaskert Child Psychiatry Hospital, Budapest, Hungary

balazs.borb@gmail.com
safar.attila@amk.uni-obuda.hu
halasz.jozsef@amk.uni-obuda.hu

Abstract— **Data collection of different biological signals became easily accessible with commercially available smart instruments. Still, the interpretation and validation of the acquired data create a major debate in the usage of smart instruments in scientific data collection. The aim of the present study was to perform a reliability analysis of the W2 Activity Tracker, and to establish differences according to different locations, like location of the devices at arm and hip. In the first set of experiments, data from the W2 Activity Tracker was compared with data acquired from the Xiaomi Mi Band, and with data from a GPS device. In the second set of experiments, diurnal data collection was performed with W2 Activity Trackers in identical locations. In the third set of experiments, the arm and hip movement was compared during sport classes, data were collected from ten male university students.**
Our results indicate that the examined device has a high level of reliability (in identical locations). Additionally, there was a significant difference in the activity counts according to the origin of data (arm or hip). This major effect has to be considered in the interpretation of activity data collected by different instruments.

Keywords: Activity tracker, Data collection, Laterality, Locomotion pattern, Reliability.

I. INTRODUCTION

A. Activity trackers and their application

Several applications involving the e-health sector became available recently, targeting and continuously monitoring biological signals as heart rate, body temperature, skin conductance, blood pressure, and even daily activity patterns [1]. The interpretation of these biological signals is related to big data analysis, and the optimal strategies for data collection with widely available instruments was not verified. One major problem of these equipment is not only the lack of guidelines for scientific data collection strategies, but the scientific validation of the collected data.

3-D accelerometers were widely used to establish different human locomotion patterns, and the signal acquisition and transformation seems verified [2, 3]. Human locomotion patterns have high importance in establishing daily physical activity, and physical locomotion activity per se. Movement disorders have a major impact on locomotor abilities, but different cardiovascular and chronic conditions might alter locomotion patterns. E.g., the prognosis and cross-sectional condition could be monitored with daily physical activities in patients with Parkinson's disease, patients with heart failure and patients with renal failure [4-6]. Physical activity in itself might be able to help in the recovery in certain chronic conditions [7]. In this respect, these instruments might also be used for motivational purposes both in different populations with certain chronical conditions and healthy individuals [4, 8].

Theoretically, the application of accelerometers might have major importance in conditions where the daily activity patterns are crucial (and not just indicator) symptoms. According to the data of two major meta-analyses, attention deficit/hyperactivity disorder (ADHD) is the most common neurodevelopmental disorder, with a worldwide prevalence rate of 5-7 percent [9, 10]. The core symptoms of the disorder are inattention, hyperactivity and impulsivity [11, 12]. The diagnosis of the above condition is based on clinical symptoms, so far no systematic measure was applied to characterize the physical extent of hyperactivity (the exact locomotion pattern). Additionally to the basic symptoms, children and adolescents with ADHD might have multiple comorbid psychiatric conditions including externalizing and internalizing disorders [13], and even certain aspects of social dysfunction in patients with ADHD emerged. Data also suggest that impaired social skills and behavioral problems in children and adolescents with ADHD are also present [14, 15]. Thus, ADHD symptom severity does not end with hyperactivity per se, but is related with serious consequences. Monitoring the precise nature of locomotion patterns might help to characterize other type of difficulties in affected individuals.

Earlier papers used different validation/reliability strategies. E.g., Holowachuk validated Tritac with both a similar instrument and a questionnaire [16]. In the above

paper a rather large (day-based) time frame was chosen, as an activity questionnaire could not be established for rather short time frame (hours or even minutes). Later studies focused on smart-instrument activity data collection in different populations [17, 18], and the description of validation strategies between instruments from different providers was also documented [19, 20]. Still, certain elements were not targeted so far.

To our best knowledge, earlier validation strategies did not apply identical instruments in different locations (like arm and hip), and reliability analysis (instruments with same locations, at different time points) was not performed. Additionally, the above papers used instruments that were capable of collecting data with a relatively large time frame (like hours, days, or weeks), and this time frame can not be used for a relative smooth discrimination in problems like ADHD, were parallel neuropsychological measures might have crucial importance. Thus, our major intention was to use an instrument what could be used for a relatively smooth (minute resolution) data collection.

B. Aims

The aims of the present experiments were to perform a validation and reliability analysis of the W2 Activity Tracker, what later can be used in real life experimental design in children and adolescents with ADHD and externalization problems. The experiments were used as preliminary experiments for the Grant "Dimensional approach in externalization disorders".

II. METHODS

The W2 Activity tracker was chosen for (i) capability for a rather smooth data collection (2-min intervals) and (ii) the relatively easy accessibility of the output file for scientific data analysis (Fig. 1). The majority of commercially available instruments use internal statistical procedures, what is not sufficient for deeper interpretation of the data.

Fig. 1. The devices used during the measures. From left to right, Xiaomi Mi Band, and W2 devices. The W2 devices were labeled with a special string, and that was used as color code of a given device.

With the built-in high sensitivity 3D acceleration sensor, the device can capture every tiny movement of the pedometer, which provides more accurate functioning. The smartband can track the burned calories, exercise steps, moved distance, and also can set the query of the movement goal completion. The strap can be set by the built in USB2.0 interface, which is fully plug and play. It has a built in large capacity storage space (up to 16GB), which can be used as mobile hard disk, and the strap has motion data memory function. The watch can be charged by USB interface, and replenish the built-in rechargeable (95mAh) battery.

Three sets of experiments were performed. For easier discrimination, 'color codes' were used. Altogether, the codes green, orange, blue, black represent individual W2 Activity Trackers.

In the first set of experiments (Experiment1), data collection was performed with W2 devices in different arm and hip locations, while a Xiaomi Mi Band activity tracker was also used. During the experiment, the data collector was walking a circumscribed distance of 110 meters. The procedure was repeated 20 times, while a GPS tracker was also used (Fig. 2). The Xiaomi Mi Band was located at the dominant arm, while one of the W2 Activity Trackers at the dominant arm, and an additional W2 Activity Tracker at the hip. During Experiment1, green code was used for the subdominant arm, and orange code was used for the hip. The major aim in Experiment1 was to establish correlation patterns between different devices and locations. The highest correlation was suggested between identical localizations, in spite of the differences of the providers.

In the second set of experiments (Experiment2), spontaneous diurnal data collection was performed with different W2 devices. In a subset of the experiment, a data collector (B. B.) was continuously wearing W2 activity trackers, but for constant data collection, the capacity of the setup could not bear over 14 hours in preliminary experiments. Thus, a single device was used for 12 hours (from 7a.m. to 7 p.m.), than an additional W2 Activity tracker was used (from 7 p.m. to 7 a.m.). In the other subset of Experiment2, three parallel devices were used for a week from 7 a.m. to 7 p.m., at the dominant arm (green), directly near the green in proximal position (blue), and at the subdominal arm (black, Fig. 2). This experiment had a major importance in the validation strategy for spontaneous daily activities, comparing data between dominant and subdominant locations, with internal control (setup at proximal dominant position).

In the third set of experiments (Experiment3), a 30-min controlled sport activity was used for data collection, with two W2 Activity Trackers at arm (green/black) and at hip (orange/blue) location, after informed consent in 10 male university students (ages between 18-24 years, average: 21.1 years). The heights and weights were also registered. The students were free to discontinue the experiment, but none of them dropped from the data collection. The data collection was approved by Obuda University, Alba Regia Technical Faculty. Part of the data collection was also used as diploma work one of the Authors [1], and as we stated

earlier, data collection was used as preliminary experiment for the Grant "Dimensional approach in externalization disorders".

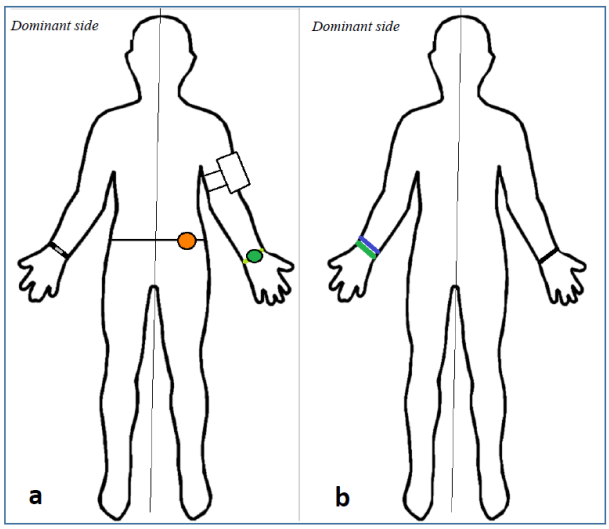

Fig. 2. The localization of the devices during Experiment 1 (a) and during Experiment2 (b). In Experiment1, a Xiaomi Mi Band was located at the dominant arm, while 2 W2 devices were located at the hip (orange) and at the subdominant arm (green). In Experiment2, 2 W2 devices were located at the dominant arm, while an additional w2 was located at the subdominant arm.

Statistical analysis. Statistica 7.0 was used to analyze datasets. In Experiment1, Spearman correlation was performed between different devices in different locations. Additionally, a General Linear Model (GLM) was also used. In Experiment2, diurnal sets from different W2 devices were analyzed in a GLM-based testing. Two factors were used: a time (hours) and a location factor. In Experiment3, a repeated measure design was applied, basically in 2-min datasets, but also in 10-min and 30-min intervals. The level of significance was set at p=0.05.

III. RESULTS

In Experiment1, Spearman correlation was significant between activity counts from Xiaomi Mi Band and the green W2 Activity Tracker (Spearman R=0.602, p<0.005), while no significant correlation occurred between other locations. Activity counts in identical locations did not show significant differences ($F_{(1,38)}$=3,60; p=NS; Xiaomi Mi Band and green W2 Activity Tracker).

Table 1. Data from Experiment1, Spearman correlations.

	Valid N	Spearman R	p-level
W2Gr & W2Or	20	0,383	0,096
W2Gr & Xiaomi	20	0,602	0,005
W2Gr & GPS (m)	20	0,298	0,202
W2Or & Xiaomi	20	0,012	0,958
W2Or & GPS (m)	20	0,215	0,364
Xiaomi & GPS (m)	20	0,326	0,165

Spearman correlation data from Experiment1. In Experiment1, the devices were used on a fixed distance of 100 meters in a repeated order. A GPS tracker was located at the subdominant arm, Xiaomi Mi Band was located at the dominant arm, W2Gr (W2, green string) was located at the hip. Strong correlation occurred only between devices from different origin but with identical (mirror) location (W2Gr and Xiaomi).

In Experiment2, significant differences could be observed in diurnal variations ($F_{(11,72)}$=9.01; p<0.00001). During the day, two major activity peaks could be observed (Fig. 3). Day and night activities were clearly visible during data collection. When data collection was repeated on a daily basis with 3 W2 Activity Trackers, a similar pattern in the diurnal variation emerged (data not shown), but no significant differences occurred between different setups (F=0.066; p=NS; Fig. 4).

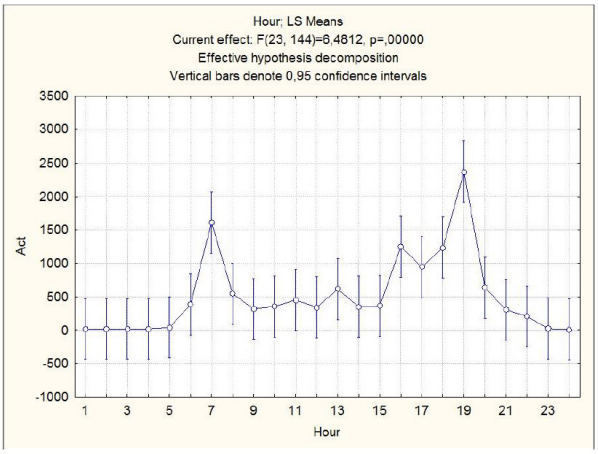

Fig. 3. Summary of the data (from Statistica 7.0, hour averages and 95% confidence intervals) from Experiment2. Two daily activity peaks could be clarified.

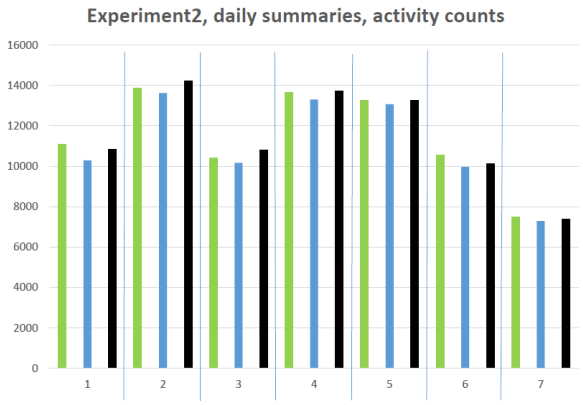

Fig. 4. Daily activity count summary data (for seven days) during Experiment2, with 3 W2 devices. Green, distal dominant arm, Blue, proximal dominant arm, Black, subdominant arm. No statistical difference occurred between the W2 devices labeled with different strings during Experiment2.

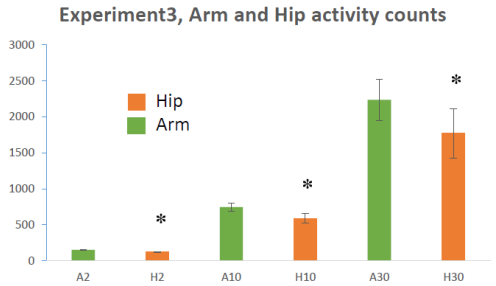

*Fig. 5. Activity count averages and SEM values during Experiment3, with 2 different W2 devices. Green, subdominant arm, Orange, hip. Distributions for 2, 10 and 30 minutes were presented. *, significantly different (p<0.05) from subdominant arm activity count values.*

In Experiment3, major differences occurred between different locations, irrespective of the time frame (2-min, $F=89.349$; $p<0.0000001$; 10-min, $F=38.779$; $p<0.00001$; 30-min, $F=15.905$; $p<0.004$). The most sensitive was the smooth data collection, and the average difference between hip and arm activity was 26% (Fig. 5).

IV. Discussion

The main results of the present study were the followings. First, the correlation patterns between activity counts were strongest in identical locations, irrespective to the origin/provider of the setup. Second, stable daily activity patterns could be observed, and no differences occurred between the activity counts data from subdominant and dominant arms. Third, major differences could be observed in activity counts during a limited (30-min long) sport activity, when W2 Activity Trackers could be localized at arm or at hip.

The activity count patterns between identical setups in different locations (Experiment1, green vs. orange, Table 1) was shown significantly weaker correlation patterns than activity count patterns measured with different setups and identical locations (Xiaomi Mi Band and (green) W2 Activity Tracker). This information was underlined in Experiment2, where the activity differences from 3 identical setups (dominant arm, proximal position, dominant arm, distant position and subdominant arm) shown differences of 0.05% during a week of data collection. Thus, identical locations (even if the dominant and subdominant arm movement theoretically could not be considered completely identical) resulted in very small alterations. Surprisingly, activity patterns (W2 Activity Tracker) were highly different during a 30-min sport activity in male university students, having 26% more activity counts registered at arm compared to the activity counts registered at hip. Identical locations (hip) were also tested by Noah et al, where highly reliable data were emerged from different providers [20].

Earlier validation and reliability analyses focused mainly on the comparison of two different systems [16, 17, 20]. E.g., Sasaki et al compared the estimated energy expenditure used by the Fitbit Activity Tracker and the Oxycon Mobile portable system [17]. Importantly, the hip-based registration (no other registration point was tested) significantly underestimated energy expenditure compared to the Oxycon system in the majority of the tested conditions. Thus, the localization should be weighted in the algorithms used for calculation.

These data were crucial in order to plan later data collection strategies in children and adolescents with ADHD, where a core symptom of the condition is hyperactivity [11, 12]. Localization of the activity tracker was crucial in our experiments, and should be considered during experiments planned in the future. In Experiment3, where different sport activities could be observed, data indicate that intensive running and leg-activities might change the differences between hip and arm data. Interestingly, when the data analysis was performed without the data of a professional runner, the difference between arm and hip activities was further increased, thus this effect also should be considered.

The limitations of the study were the followings. During Experiment1 and Experiment2, a repeated measure design was applied, and the data collector was repeatedly the same person, one of the Authors of the present manuscript (B.B.). Albeit this design was inevitable during the validation procedure, the present measures could have been repeated with more people. In Experiment3, the sport experiment was freely chosen for the individuals, and the nature of sport activity was not unified. As we stated above, running, free activity and badminton were also among the sport activities. Thus, our design could be considered as soft in this respect, but still major significant differences occurred. It is assumed that data collection in case of targeted activities (like systematically comparing running, badminton) might significantly increase our knowledge on terms of activity counts on different body parts, but this was not a direct target of our present study. In future studies, these issues also should be addressed.

V. Summary

In the present paper, the validation and reliability analysis of the W2 Activity Tracker was performed. According to our data, W2 Activity tracker was highly reliable in identical locations, but differences in data collection locations (like arm or hip) was accompanied by major differences in activity counts. This effect should be considered during later data collections, and also has to be considered in the planned data collection in children with ADHD and externalization problems.

VI. Acknowledgment

The authors declare no conflict of interest. The work was supported by OTKA Grant No. 108336. The authors would like to express their gratitude to those university students who participated in the project.

References

[1] B. Borbely, “Parametric data configuration of an activity tracker”, diploma work, Obuda University, 2016.

[2] F. Foerster and J. Fahrenberg, “Motion pattern and posture: correctly assessed by calibrated accelerometers”, *Behav. Res. Methods Instrum. Comput.,* vol. 32, pp. 450–457, 2000.

[3] N. Ravi, N. Dandekar, P. Mysore and M.L. Littman, “Activity recognition from accelerometer data”, *I.A.A.I.,* pp. 1541–1546, 2005.

[4] M. van Nimwegen, A.D. Speelman, S. Overeem, B.P. van de Warrenburg, K. Smulders, M.L. Dontje, G.F. Borm, F.J.G. Backx, B.R. Bloem and M. Munneke, “Promotion of physical activity and fitness in sedentary patients with Parkinson’s disease: randomized controlled trial”, *B.M..J.,* vol. 346, doi: 10.1136, 2013.

[5] M.L. Dontje, M.H.L. van der Wal, R.P. Stolk, J. Brügemann, T. Jaarsma, P.E.P.J. Wijtfliet, C.P. van der Schans and M.H.G. de Greef, “Daily physical activity in stable heart failure patients”, *SJ. Cardiovasc. Nurs.,* vol. 29, pp. 218–226, 2014.

[6] K.L. Johansen, G.M. Chertow, A.V. Ng, K. Mulligan, S. Carey, P.Y. Schoenfeld and J.A. Kent-Braun, "Physical activity levels in patients on hemodialysis and healthy sedentary controls", *Kidney Int.,* vol. 57, pp. 2564–2570, 2000.

[7] G. Hu, N.C. Barengo, J. Tuomilehto, T.A. Lakka, A. Nissinen and P. Jousilahti, "Relationship of physical activity and body mass index to the risk of hypertension: a prospective study in Finland", *Hypertension,* vol. 67, pp. 693–700, 2016.

[8] M. Iwane, M. Arita, S. Tomimoto, O. Satani, M. Matsumoto, K. Miyashita and I. Nishio, "Walking 10000 steps/day or more reduces blood pressure and sympathetic nerve activity in mild essential hypertension", *Hypertens. Res.,* vol. 23, pp. 573–580, 2006.

[9] G. Polanczyk, M.S. de Lima, B.L. Horta, J. Biederman and L.A. Rohde, "The worldwide prevalence of ADHD: a systematic review and metaregression analysis", *Am. J. Psychiatry,* vol. 164, pp. 942–948, 2007.

[10] E.G. Willcutt, "The prevalence of DSM-IV attention-deficit/hyperactivity disorder: a meta-analytic review", *Neurotherapeutics,* vol. 9, pp. 490–499, 2012.

[11] American Psychiatric Association, "Diagnostic and Statistic Manual of Mental Disorders, DSM-5", New York, American Psychiatric Publishing, 2013.

[12] National Institute for Health and Care Excellence, "Attention deficit hyperactivity disorder. Diagnosis and management of ADHD in children, young people and adults", British Psychological Society and The Royal College of Psychiatrists, *National Clinical Guideline Number 72,* pp. 1–664, 2016.

[13] E.J. Costello, S. Mustillo, A. Erkanli, G. Keeler and A. Angold, "Prevalence and development of psychiatric disorders in childhood and adolescence", *Arch. Gen. Psychiatry,* vol. 60, pp. 837–844, 2003.

[14] J. Uekermann. M. Kraemer, M. Abdel-Hamid, B.G. Schimmelmann, J. Hebebrand, I. Daum, J. Wiltfang and B. Kis, "Social cognition in attention-deficit hyperactivity disorder (ADHD)", *Neurosci. Biobehav. Rev.,* vol. 34, pp. 734–743, 2010.

[15] J.S. Nijmeijer, R.B. Minderaa, J.K. Buitelaar, A. Mulligan, C.A. Hartman and P.J. Hoekstra, "Attention-deficit/hyperactivity disorder and social dysfunctioning", *Clin. Psychol. Rev., vol. 28,* pp. 692–708, 2008.

[16] D.R. Holowachuk, "Field validation of the Tritac-3D Activity Monitor for the assessment of physical activity in older children", diploma work, University of Saskatchewan, 1998.

[17] J.E. Sasaki, A. Hickey, M. Mavilia, J. Tedesco, D. John, S.K. Keadle and P.S. Freedson, "Validation of the Fitbit wireless activity tracker for prediction of energy expenditure", *J. Physical Act. Health,* vol. 12, pp. 149–154, 2014.

[18] S.S. Paul, A. Tiedemann, L.M. Hassett, E. Ramsay, C. Kirkham, S. Chagpar and C. Sherrington, "Validity of the Fitbit activity tracker for measuring steps in a community-dwelling older adults", *B.M.J. Open, Sport, Exercise and Medicine,* doi: 10.1136, 2015.

[19] A. Giannini, "Comparison of the Fitbit Zip to the Actical accelerometer in children and adults", diploma work, University of Delaware, 2013.

[20] J.A. Noah, D.K. Spierer, J. Gu and S. Bronner, "Comparison of steps and energy expenditure assessment in adults of Fitbit Tracker and Ultra to the Actual and indirect calorimetry", *J. Med. Eng Technol.,* doi: 10.3109, 2013.

Comparative analysis of navigation GPS receiver by GPS/GLONASS/EGNOS

Anita Karika
Department of Physical Geography and Geoinformatics
University of Debrecen
Debrecen, Hungary
karika.anita@science.unideb.hu

Gergely Szabó
Department of Physical Geography and Geoinformatics
University of Debrecen
Debrecen, Hungary
szabo.gergely@science.unideb.hu

Dániel Balla
Department of Landscape Protection and Environmental Geography
University of Debrecen
Debrecen, Hungary
balla.daniel@science.unideb.hu

***Abstract*—This research is all about horizontal and vertical accuracy of five navigation GPS receivers, which were set up on the sport field of the University of Debrecen in February 2016. We used 37 points to determine positional accuracy. We compared the horizontal and vertical accuracy of the receivers in different modes. We estimated the point accuracy combined with GPS and GLONASS, with and without EGNOS. The EGNOS usages compare to the autonomous mode provide better accuracy horizontally, but not vertically. The average horizontal accuracy error values were between 0 and 3 m. The vertical component of absolute error showed that all satellites with EGNOS combination had the worst result. The vertical component of absolute error provided similar result in autonomous mode and in EGNOS-corrected mode between 0-4 m.**

Keywords—GPS accuracy; Global Positioning System; GPS receivers; positioning; horizontal; vertical

I. INTRODUCTION

The Global Positioning System (GPS) has been used in the consumer and professional field too; that is why there are a lot of expectations of them. The accuracy of the GPS is dependent on the price of the receivers, or any other receiver specifications. The environment and outside factors can change the precision of the receivers (objects, trees, shape or deformation of the Earth, ionospheric electron content tropospheric water vapor). According all these factors the accuracy of the receivers changes constantly. The accuracy of the GPS can be provided by some applications e.g. single GPS satellites, GPS with GLONASS, EGNOS, different correction etc. In this paper the accuracy was compared by autonomous mode, GPS system, GPS with GLONASS system, application and not application of EGNOS system. Næsset found that the accuracy of the GPS combined with GLONASS, was much better than the accuracy obtained from single GPS measurements [1]. We can improve the accuracy with base stations. Basically the precision can provide extended number of the available satellites [2]. The condition of the receivers, the constellation of the satellites and the canopy can make different HDOP and VDOP [3]. In most cases GPS accuracy was tested by two methods, by autonomous mode and by Wide Area Augmentation System (WAAS). This system is the US-corresponding version of EGNOS. WAAS can improve the accuracy in clear sky condition, but it does not work well under forest canopy [4]. The use of WAAS has increased the value of the precisions with low-cost recreational-grade units, but it is difficult to forecast the rate and the affect in some cases [5]. WAAS availability is not appropriate near buildings or underneath tree canopy, because the receivers cannot accept signal near buildings or under tree canopy [6]. In research of Londe was mentioned that using WAAS got better horizontal component of the absolute error with Garmin unit [10]. Nevertheless, there are other options that improve the precision. Used the GPS–GLONASS simultaneously increased the accuracy [3, 5]. The GPS and COMPASS combination also can improve the positioning accuracy with some signal attenuation and limited satellite visibility condition [7]. Most of researches were based on the horizontal accuracy, but just few of them paid attention on the vertical accuracy [8, 9].

II. MATERIAL AND METHODS

A. Survey instrumentation

In this study five different types of commercial GPS receivers were used: Garmin eTrex 30, Trimble GeoExplorer XM, Trimble Juno SB, Ashtech Mobile Mapper 10, Stonex S9 and Focus 8 total station. There are different specifications for each receiver. I. Specifications of Ashtech Mobile Mapper 10: code phase, 20 channels, L1 antenna, low-cost receiver. II. Specifications of Garmin eTrex 30: code phase, 12 channels, L1 antenna, lowest-cost receiver between five of them. III. Specifications of Trimble Juno SB: post-processing correction, code phase, 12 channels, L1 antenna, medium - cost receiver. IV. Specifications of Trimble GeoExplorer XM: post-processing correction, code phase, L1 antenna, medium-cost receiver. V. Equipment's specifications of Stonex S9: real-time kinematic (RTK), carrier phase, 220 channels, L1, L2, L5 antennas, high-cost receiver. The coordinate system was

Hungarian EOV (EPSG: 23700). The reference positions were recorded by leveling equipment and Focus 8 total station.

B. *Study area*

The study area was a smooth and flat sport pitch, located in Debrecen, Hungary, at the University of Debrecen. This test consisted of 37 points in L-shaped "Fig. 1".

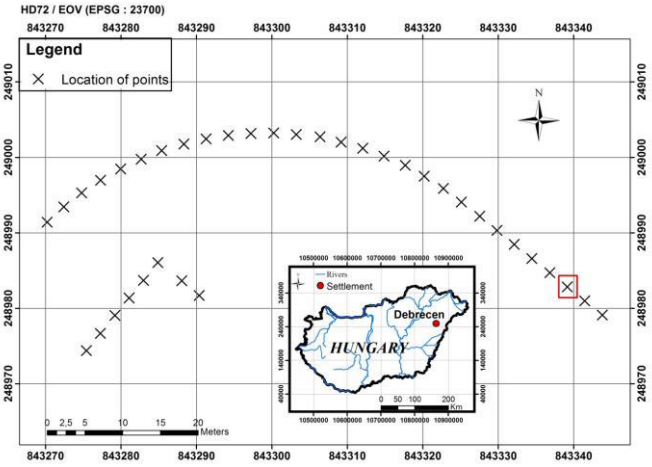

Fig. 1. Location of study area.

C. *Data collection*

Data collection was divided into two main parts. First collection was in autonomous mode, second part was the EGNOS, GPS-GLONASS, GPS-GLONASS and EGNOS combination. The recorded period was 1 minute. The data of the Garmin eTrex 30 and Trimble receivers provided data in WGS84 that is why we used an official online calculator named "EHT 2014 V.1.0" [11]. We used leveling equipment (with 28x zoom) and Focus 8 total station for reference data "Fig. 2".

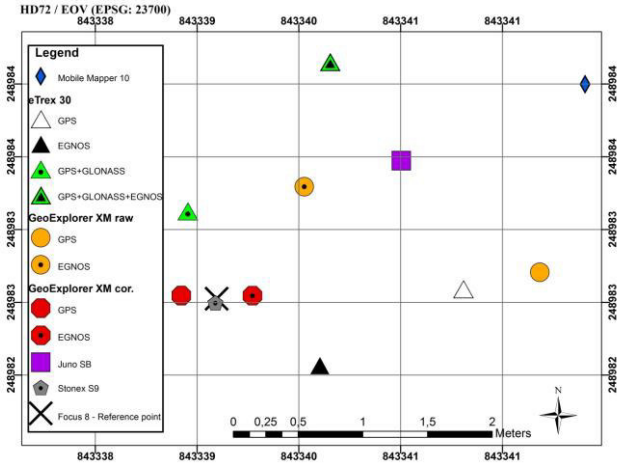

Fig. 2. Study area with some sample points.

D. *Horizontal and vertical analysis*

We calculated the horizontal and vertical accuracy among each GPS receivers and among approaches. Basic analysis was generated in Microsoft EXCEL as the mean, minimum, maximum, standard deviation of the distinctions one by one for each of the receivers.

First, we separated all measurements into two parts. The first part was the vertical accuracy, and second part was the horizontal accuracy. We used the total station and the leveling equipment for the vertical accuracy.

The horizontal accuracy also split into other two parts. The first one comprises of all autonomous measurements with each of the GPS receivers. The main value of this part is the mean accuracy for each of receivers, other category is all the measurements with Garmin eTrex 30 and Trimble GeoExplorer XM, which include the surveys with EGNOS correction.

III. Results and Discussion

A. *Vertical accuracy*

First comparisons were for databases of the Stonex S9, Garmin eTrex 30, the Trimble GeoExplorer XM data collection in code-corrected mode with vertical accuracy, which were based on the Focus 8 and the levelling equipment. The Trimble Juno SB collected only horizontal measurements for accuracy analysis. The results indicated that there is a difference among the two GeoExplorer XM files (between the original raw file and the differentially corrected files).

The mean vertical accuracy in 4 cases (1. eTrex in autonomous mode; 2. GeoExplorer correction in autonomous; 3. EGNOS-corrected mode; 4. Stonex S9) were less than 1 m. The Mobile Mapper 10 had the largest bias with 9.89 m, all in other case the mean was around 3-4 m. The range of standard deviation of the vertical accuracy is wide, the eTrex 30 in GPS+GLONASS logging mode had more straggler or outlier value than the other surveying. The GeoExplorer XM corrected data without EGNOS and with EGNOS-corrected mode, and the Stonex S9 surveys were more stable with smaller biases (less than 0.3 m) "Fig. 3".

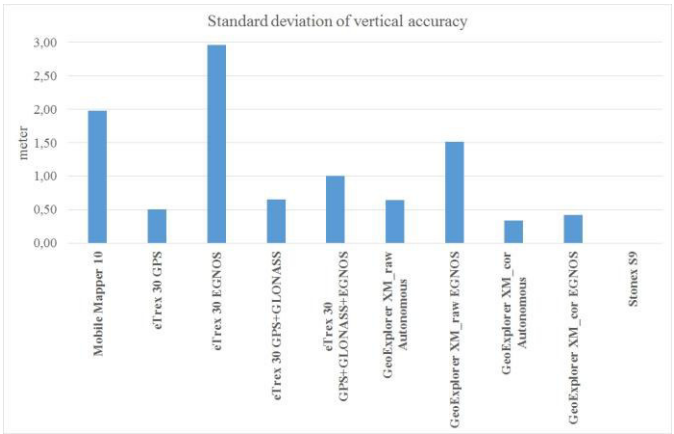

Fig. 3. Standard deviation of the vertical accuracy for Stonex S9, Garmin eTrex 30, Trimble GeoExplorer XM with 2 basis station values (GeoExplorer XM_raw, GeoExplorer XM_cor.).

The minimum and maximum vertical accuracy showed us similar distribution. Stonex S9 had the lowest result, as we

expected (min: 0.0 m). The GeoExplorer, with code correction provided less than 2 cm bias in both cases. As we did not expect, the highest vertical deviation is more than 13 m with the Mobile Mapper 10 "Fig. 4". As we show below, these excessive values of this equipment will appear at horizontal accuracy as well "Fig. 5". The second highest value is the 8.78 m by the eTrex 30 in GPS + GLONASS mode.

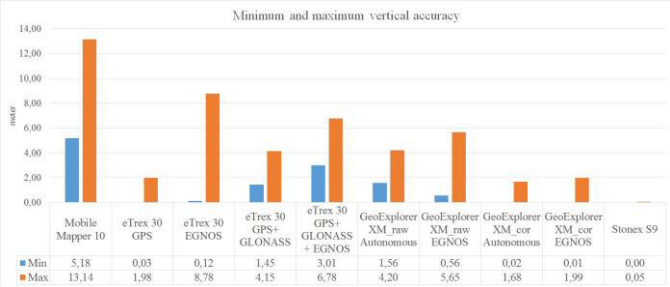

Fig. 4. Minimum and maximum vertical accuracy.

B. *Horizontal accuracy*

The study showed remarkable differences among these receivers. Hand-held receivers collected the horizontal accuracy in autonomous mode simultaneously. This ensured that the receivers provide more accurate result during the same condition.

The lowest result of the horizontal accuracy was provided by the GeoExplorer XM with EGNOS correction (0.61 m, "Fig. 5". The eTrex 30 with EGNOS correction did not improve the horizontal accuracy. Andersen [5] mentioned the same conclusion that low-cost units had not real influence of the WAAS at the accuracy, just like in our case with EGNOS. Remarkable that the highest bias was with the GeoExplorer XM unit in autonomous mode; regarding the high quality of this receiver. After the differential correction the accuracy became fairly better. The status of satellite geometry or the number of the available satellites can modify the accuracy, as Næsset and Habrich determined before [1, 2]. That is why some combinations (such as the GPS and GLONASS combination) can modify and decrease the accuracy of the GPS receivers. Our results are the same as Andersen [5] had that using GLONASS can improve the accuracy. On the other hand, those values, when we used the 3 satellite systems (GPS, GLONASS, EGNOS) simultaneously, were the least favorable result among all the values. Using those one by one can improve the accuracy, but this combined satellite method doesn't lead to higher accuracy. Furthermore, enhancing measuring interval can increase the accuracy as well. Our surveying's interval was 1 minute, but most of other authors measured during 5-10-20-30 minutes or 1-2 hours, which can give better accuracy. Valbuena determined that with more than fifteen minutes recording can improve the accuracy [3]. Weih measured around 2 hours by Garmin eTrex and Juno, and his horizontal accuracy was enhanced comparing to ours, which proved the fact that longer surveying time can improve the accuracy [6].

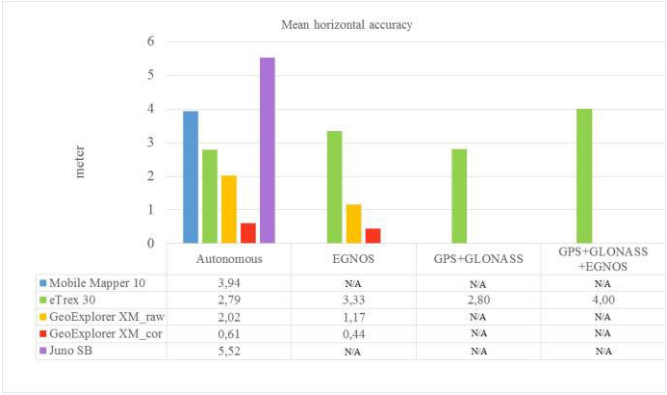

Fig. 5. Mean horizontal accuracy in different mode.

IV. CONCLUSION

This study showed that GPS, GLONASS and EGNOS system can modify the accuracy of receivers in different way in different aspect. The horizontal accuracy is not determined by the level of professionality of device by all means. Weih found the same conclusion that the interaction between accuracy and the cost of the receivers is minimal [6]. These results showed that the GPS error could be increased by some obstructions: the differential correction can decrease some GPS errors, but cannot handle the multipath or the receiver errors. We would require lower accuracy, especially with the GeoExplorer XM case. The GPS and GLONASS combination is a good option to improve the horizontal accuracy, using these 3 methods together (GPS, GLONASS, EGNOS), cannot improve the result. In case of the horizontal accuracy we can state out that using EGNOS is giving us the lowest result, so the EGNOS can increase the accuracy horizontally, but not vertically in our case. The EGNOS signal has an advantage by the GeoExplorer XM receivers, but did not show any improvement in case of eTrex 30.

REFERENCES

[1] Næsset, E., Bjerke, T., Øvstedal, O. and Ryan, L.H., Contributions of Differential GPS and GLONASS observations to point accuracy under forest canopies, Photogrammetric engineering and remote sensing 66 (4), (2000) 403-407

[2] [2.]Habrich H., Curtner W., Rothacher M., Processing of GLONASS and combined GLONASS/GPS observations, Advances in Space Research 23, (1999) 655-658

[3] Valbuena R., Mauro F., Rodriguez-Solano R. and Manzanera J. A., Accuracy and precision of GPS receivers under forest canopies in a mountainous environment, Spanish Journal of Agricultural Research. 8(4), (2010) 1047-1057

[4] Karsky, D., Comparing four methods of correcting GPS data: DGPS, WAAS, L-Band, and postprocessing, US For. Serv. Gen. Tech. Rep. 0471-2307-MTDC. Missoula Technology and Development Center, (2004) Missoula, MT. 6p.

[5] Andersen, H.E., Clarkin, T., Winterberger, K., Strunk, J., An accuracy assessment of positions obtained using survey- and recreational-grade Global Positioning System receivers across a range of forest conditions within the Tanana valley of interior Alaska, Western Journal of Applied Forestry 24(3),(2009) 128-136

[6] Weih R.C., Gilbert Jr., M., Cross J., and Freeman D., Accuracy assessment of recreational and mapping grade GPS receivers, Journal of the Arkansas Academy of Science 63, (2009) 163-168

[7] Changsheng, C., Yang, G., Lin, P., Wujiao, D., , An analysis on combined GPS/COMPASS data quality and its effect on single point positioning accuracy under different observing conditions, Advanced in Space Research 54, (2014) 818-829

[8] Wing M. G., Eklund A., Elevation measurement capabilities of consumer-grade global positioning system (GPS) receivers, Journal of Forestry 105 (2), (2007) 91-94

[9] Hall, K. W., Cooper, J.K., Lawton, D.C., GPS accuracy: Hand-held versus RTK. CREWES Research Report 20, (2008) 1-10

[10] Londe, M., D. Baseline accuracy assessments of Garmin Recreational GPS Receivers: http://www.blm.gov/pgdata/etc/medialib/blm/wy/programs/cultural/docs.Par.1458.File.dat/garminaccuracy.pdf (Downloaded: 02. February 2014.)

[11] EHT2014 V.1.0 coordinate calculator: http://eht.gnssnet.hu/index.php/site/coordByKeyIn

Discover a black hole in the classroom: the "Pear-Star" Project

Cs. Fülöp*, Zs. Horváth**
* Madách Imre Gimnázium , Budapest, Hungary
** Kosztolányi Dezső Gimnázium, Budapest, Hungary
*,** Physics Education Programme, Ph.D. School of Physics, ELTE TTK, Budapest
fulcsilla@gmail.com, hosu@pro.hu

Is the notion of black hole only a part of a theory called astrophysics? If they are black, and swallow everything, how can we find them? How the method, photometry is used in research? Can also we use the shots made by the Faulkes telescope? By the way, what are the Faulkes telescopes? Is it difficult to learn SalsaJ? These questions above and similar ones will be discussed spiced with students' in-situ measurements. And, what do these do with a pear, you will find out.

I. INTRODUCTION

The concept of black holes is a very popular one. Our students can meet it in science fiction movies and surely in computer games. It is frequently in the media, also in the news. In our days it is an important scientific topic.

Last year the gravitational waves were discovered. These results were announced in the beginning of this year. In the researchers opinion the cause of the detected gravitational waves is two black holes moving closer and closer to each other, and finally colliding.

This discovery has an exceptional role in many aspects. One of this is that black holes are invisible. They can be detected exclusively by their effects.

No question, this topic is highly motivating for the students.

Many dedicated science and physics teachers are eager to teach or at least mention this topic in their classrooms. Rosa Doran and her colleagues recognized this need for help in the society of teachers. They called a project to life: the Galileo Teacher Training Program [1].

Figure 1. The logo of GTTP

Each year GTTP organizes sessions for physics and science teachers with other societies to promote their methodological solutions worked outr especially in the fields of astrophysics and cosmology. We had a possibility to participate in one of these sessions, namely the one that was organized in Leiden in 2014 in cooperation with ESA. In the workshops we met many results and useful methodological tools of their didactical research, including SalsaJ and Stellarium [2] programs. SalsaJ enables us to identify black holes also by analyzing the brightness of stars.

II. POSSIBLE REASONS FOR THE CHANGES OF BRIGHTNESS OF STARS

It is important to overview why the brightness of stars can change. As the "Twinkle twinkle little star…" rhyme says the change in brightness of stars is called twinkling in everyday life. The change (=twinkling) can be either non-periodic or periodic.

Twinkling in the scientific context is an irregular effect caused by the changes of the atmosphere. It must be considered in all ground-observations. There are one-fold glazings too, for example:

- the explosion of novas or supernovas
- gravitational lensing or microlensing
- starpots.

The phenomena of periodic changes in brightness can be interpreted with numerous reasons. These reasons can be internal (we call these intrinsic variability) or external (we call these extrinsic variability). We can see one of the groupings in figure 2.

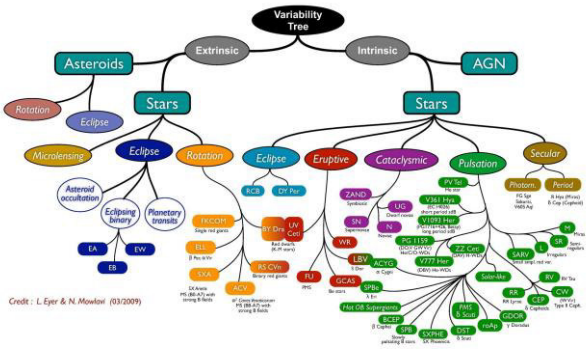

Figure 2. The Eyer-Mowlavi graph

There are many types of variable stars. We propose a site in English, where our students can broaden their knowledge:

https://www.aavso.org/education/vsa

We focus on systems containing at least one star. Since more stars may belong to a system we need to restrict our studies to binaries. In secondary school education the topic of binaries is also a challenging task. Our "pear-star" project is dedicated to them.

Both members of the binary may be a star, a star and an exoplanet, or a star and a black hole. Two celestial bodies can affect one another in a number of ways. The spectacle informs us about the types of binaries:

- astrometry binaries
- spectroscopic binaries
- eclipsing binaries
- ellipsoidal binaries

If a star "wobbles" in the sky, it is a gravitational influence of a companion (astrometry binaries). If spectral lines move due to the Doppler Effect, we speak about spectroscopic binaries. In photometric measurement a periodic change in the apparent magnitude implies eclipsing binaries. If two celestial bodies are very close to one another, the shape of the star may alter to an ellipsoidal one. The light curve of this is very important in our project. We can study this in Figure 3.

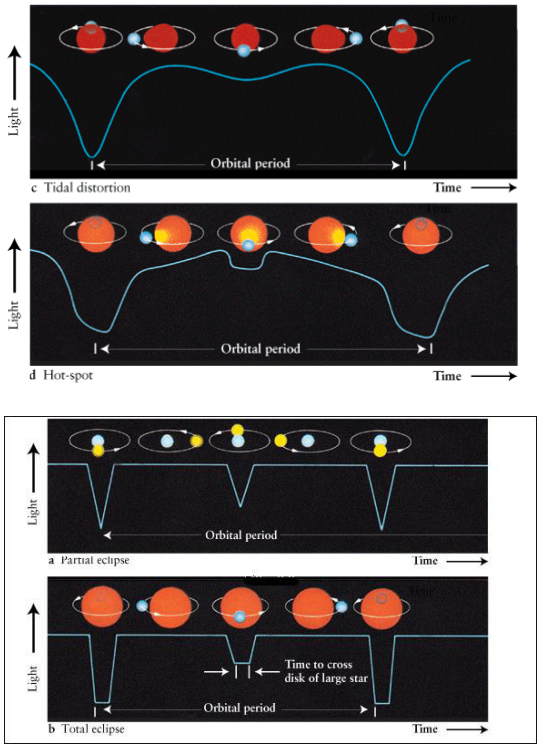

Figure 3. The light curves of eclipsing binaries [3]

The light curve is similar even if one of the celestial objects is a black hole. This is one clue for detecting the effect of black holes.

III. THE "PEAR-STAR" PROJECT

A. *What do we need?*

First of all we need to overview what will be needed for our project. Surely, we can't work without a series of real pictures that were taken of the astronomical objects that we want to study. Also a program is needed for doing the actual analysis.

Dr. Martin C. "Dill" Faulkes (figure 4.) raised the Faulkes Educational Project to support the Faulkes Telescope Project (FTP).

Figure 4. Dill Faulkes, the businessman, who supports telescopes

The FTP provides free access to 1 500 hours of observation time on two 2-meter class telescopes. These are located in Hawaii and Australia (figure 5.). First it was available for students and teacher in the UK, but recently has been opened for studies in Europe and the USA as well. Any group from the mentioned areas can register and take advantage of the possibility for free. It has been so since 2004. Detection time can be booked and the requested images are available via the internet, even online.

Figure 5. One of the Faulkes telescopes

For analyzing the data we may have gained, for example, from the FTP we need a simple program that is able to measure quantities like the magnitude of a star. A Java application, called SalsaJ is appropriate for the task. It is excellent for teaching purposes. We can demonstrate the work of astronomers, to give a hint about present-day astronomical research, and still is not overcomplicated. We can download it for free from this link:

http://www.euhou.net/index.php/salsaj-software-mainmenu-9

This application is user and student-friendly (figure 6.). It is not only multi-platform, but also multi-lingual. We can find versions with or without associated images for Windows, Linux and Mac OS X as well.

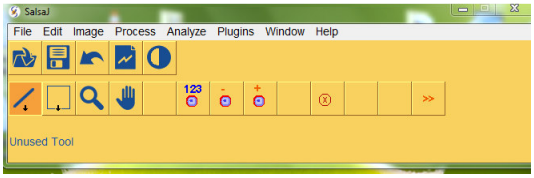

Figure 6. The window of the SalsaJ program

We can also find video manual on the site in the following topics:

1. How to open a file
2. How to display the properties of an image
3. How to set the scale of an image
4. How to measure distances inside an image
5. How to create an animation with several images
6. How to measure the flux inside an image
7. How to process a spectrum

SalsaJ is presented in the framework of EU-HOU SRT Network Project. On the site we can find inspiring projects that can give us ideas or are free to be repeated. We highlight a few from our favourites that gave us courage to have a go with our "pear-star" project in a secondary technical school:

1. From Doppler effect to exo-planets
2. A black hole lurked at the centre of our Galaxy?!
3. Life cycles of a star -- Plotting your own HR diagram!
4. Discover an exo-planet: the transit method

B. Dispelling a misconception

The study of misconception is one of the leading areas of science didactics research. First we decided to introduce the SalsaJ program with a task in service of this. Our students tend to think that most stars should be seen red because of the well-known effect, called red-shift, while some stars should be visibly blue because of the similar reason. Also many find it disappointing to make personal observations with a telescope since the spectacle falls short to the magnificent ones that are in most albums or on the title-pages of magazines.

First we can open the SalsaJ program with our students. We can give them a picture (figure 7) like this one:

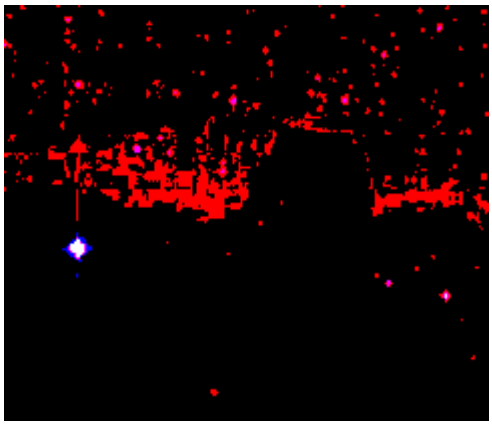

Figure 7. What is on the picture?

It is very unlikely that anybody can identify what is on their screen. Now, we can show them that that using this program we can make things visible, and doing so they can understand that the same picture can stay hidden from us if we use different filters, use different brightness or contrast settings. In the program we follow this route:

image / adjust / brightness & contrast

We reveal our "hidden" picture in a famed form: the Horse-Head Nebula (figure 8.).

Figure 8. The Horse Head nebula

We ask our students to check that the information in the image doesn't change as we change the spectacle of the given picture by pulling the sliders. We do this following these steps and comparing the data:

image / show info

We can enjoy this session with our student very much. They are eager to change the sight and test each other on images of actors, their own pictures, etc. Surely, it isn't a crucial part of the project, still necessary for the oncoming steps. It proves to be a time consuming task, still we make fun whilst helping our students to acknowledge very important steps of processes in the fields of astronomy and its popularization.

C. Discover a Black Hole

We had a series of 60 pictures that were evenly shot in time and made by a Faulkes Telescope. These were asked for our specific purpose to give our students a possibility to discover a black hole.

Our students get this series. Each image is similar to this one, not necessarily in an easily recognizable format, but now they understand that no information changes as they choose a spectacle more likeable or more comfortable to work with.

In the middle of our images (figure 9.,10.) there are four stars that form a rhombus.

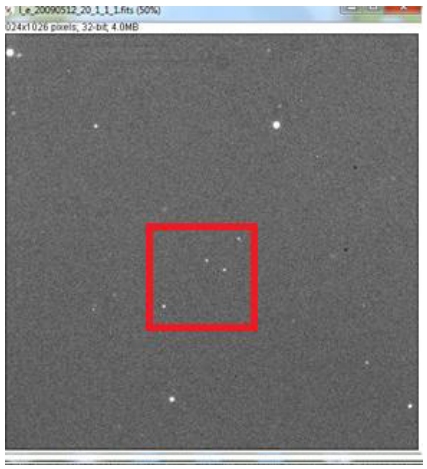

Figure 9. One of the 60 images

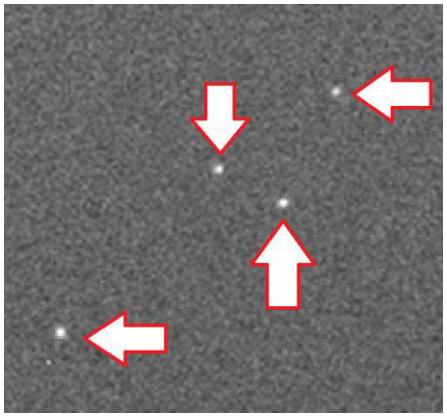

Figure 10. The four stars forming a rhombus

We can measure the luminosity (or brightness) of these four stars easily by these steps in SalsaJ:

analyze / photometry /click

We copy our results into Microsoft Excell. This program also provides the completion of the next task: plotting intensity versus time graph. These are the light curves for each of the chosen stars.

The results of our measurements are these:

For star we called Right-Top is (figure 11.):

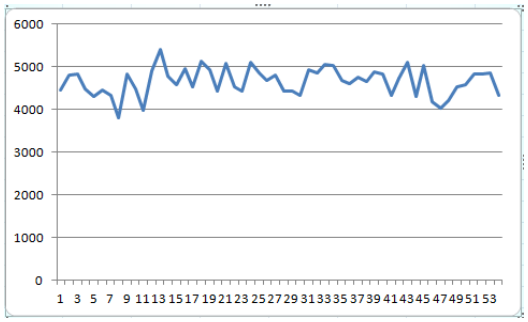

Figure 11. The graph for star “RT”

For the star we called Middle-Top is (figure 12.):

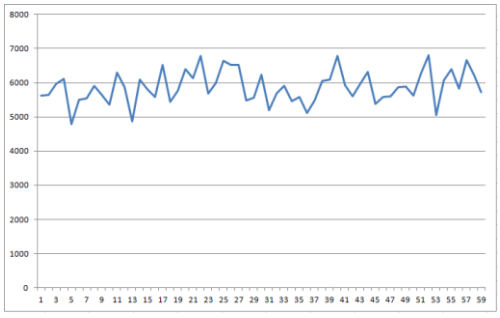

Figure 12. The light curve for the “MT” star

The light curve for star Left-Under is shown in figure 13..

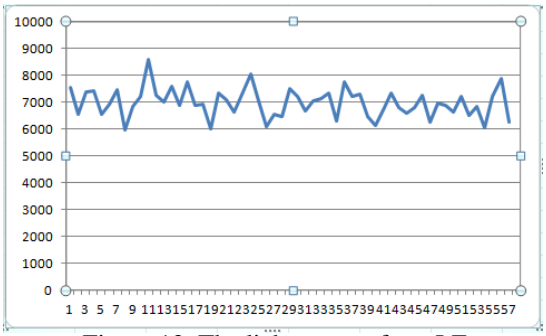

Figure 13. The light curve of our LF star

And, finally the curve for the Middle-Lower star is as follows (figure 14.):

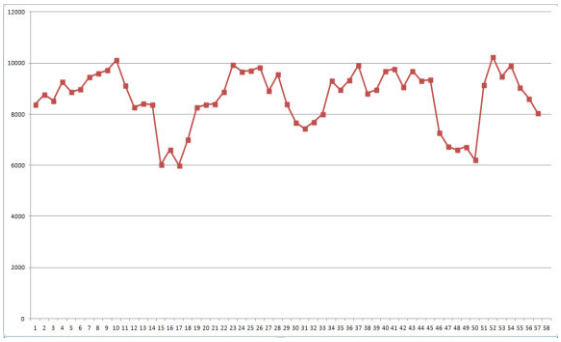

Figure 14.The light curve of ML star

We can discuss the size of the measured data and the extent and pattern of the dispersion of the results for each star.

It is obvious to notice that our ML star has a particular period in the results of magnitude. We can estimate the time period to 30 picture-times and the biggest difference about 50%.

We note that units are unusual in the physics classroom, but our purpose is to a give a hint for the methods of astronomical research rather than give an exact analysis. Those students who are interested can make a deeper study by using the information that is encoded in the images.

Also it is obvious that the period consists of a smaller and a bigger decrease of magnitude. From this we can conclude the possible form of the star we are studying. Our students can easily figure out or accept that this shape could be one of a pear. From each side to us the magnitude is at its maximum. When the “calyx” is to us a bigger decrease in the magnitude can be measured. When the stem is to us a smaller decrease can be detected. That’s why the name of the project is the “pear-star” project.

Now, that we know the shape of the “pear-star”, we can go back to some of our images and recognize that our star is not in the same place in the images. It wobbles slightly. By checking what we can find close to the star we don’t find another star that could be the partner in a double-star duplex (binary). By checking the spectrum and thus disqualifying other possibilities that could explain this phenomenon, we get closer and closer to the idea that our “pear-star” has its shape because of a black hole.

D. *The implementation*

We announced in Trefort Ágoston Technical Secondary School, Budapest the "pear-star" project in the spring of 2015. We had an eager group of 14 students who showed interest in the topic and also had a good command of English. These boys were all students of IT in the bilingual section (figure 15.).

Figure 15. IT students in mentor class

First, we visited the TIT Budapest Planetarium [6], where we watched two shows: Wonders of the sky and Hubble Universe. We also had a session there with one the astronomers (Mr. Gyula Nyerges) of the institution to promote the project.

In one of the IT seminar rooms we spent a nice afternoon together getting to know SalsaJ and finding The Black Hole (figure 16.).

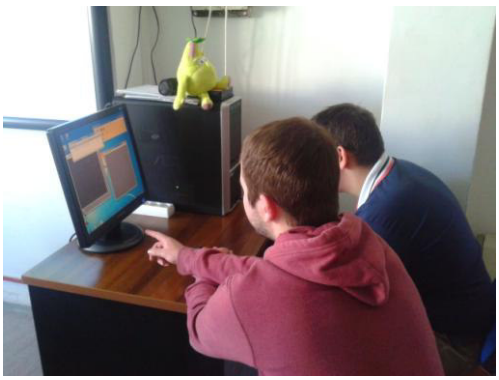

Figure 16. Tamás and Tomi analyzing the intensity data of one of the appointed stars

IV. SUMMARY

The concept of black holes is an up-to-date one so in research as in our everyday life. Teenagers are highly motivated to study the subject. Today's innovations in information technology do open a whole new world in didactics and methodology.

We planned and carried out a project, called The "Pear-Star" project for eager secondary school students of IT. We visited a Planetarium, where our astronomer also lead us into the details of their informatics in use. We registered to the Faulkes Telescope Project to get a series of images. We got these in e-mail. We downloaded a Java Application, named SalsaJ. We used it on our computers in the school's seminar room. We utilized Microsoft Excel to collect the data of 240 measurements, and also to plot a graph that we could analyse. During the project we found a lot of other educational and astronomical sites that we could examine together, and made good use of the most.

Our idea could not have turned into practice without computers and the internet. IT promoted our project in astrophysics.

ACKNOWLEDGMENT

We express our gratitude to

- our PhD consultants, Dr. Judit Illy (ELTE), and Dr. Bálint Érdi (ELTE),
- friend and colleague Mr. Gyula Nyerges, the astronomer of TIT Bp. Planetárium,
- Dr. Rosa Doran and her fellow teacher training mentors at GTTP,
- the Headmasters and Headmistress of our secondary schools: Ms. Eszter Bodor (Kosztolányi Dezső Gimnázium, Budapest), Mr. Károly Varsóci (Trefort Ágoston Bilingual Technical Secondary School, Budapest), and Mr. Csaba Mészáros (Madách Imre Gimnázium, Budapest),
- each of the students who participated in The Pear-Star Project

REFERENCES

[1] http://galileoteachers.org/
[2] http://www.stellarium.org/hu/
[3] http://plato.acadiau.ca/courses/phys/1523/jan18/JAN18.HTM
[4] http://www.euhou.net/index.php/salsaj-software-mainmenu-9
[5] https://en.wikipedia.org/wiki/Faulkes_Telescope_Project
[6] http://www.faulkes-telescope.com/
[7] http://www.planetarium.hu/english

Overview of IPv6 transition solutions and possible migration plans

Péter Bálint
Department of Telecommunications
Széchenyi István University
Győr, Hungary
Peter.Balint4@gmail.com

***Abstract*— In the 1990s it became obvious that the 32-bit address size of the IPv4 protocol would be too small in the near future, so IETF started working on an updated version of the address space with larger addresses, and the result of it was the introduction of IPv6. Unfortunately, the resulting protocol is not backward compatible with IPv4, so there was a need for additional tools to allow the transition from IPv4 to IPv6. Then IETF started introducing transition technologies for making the transition easier. The best way is still not defined. Could we find it? Or do we have to use a mixture of transition strategies and suit or change them according to the situation's requirements? In this paper, the most important IPv6 transition technologies are surveyed and their typical application situations are introduced. Two case studies are presented about the possible IPv6 transition scenario an industrial and an Internet Service Provider.**

Keywords—IPv6 transition, Mixing transition technologies, Possible Industrial and ISP migration plan, IPv6 migration design

I. INTRODUCTION

We are at the point when the Internet has outgrown the IPv4 address space. In the year 2011 the Internet Assigned Numbers Authority (IANA) delegated the last five "/8" IPv4 address blocks to the five Regional Internet Registries [1]. In the last 20 years, service providers tried to postpone the time of transition with different solutions like NAT44 or NAT444, and because of this practice the migration process went very slowly. The change comes at the depletion of the IPv4 address pool, which speeds up the process.

II. IPV6 TRANSITION TOOLS

In the history of the Internet, there was only one successful protocol change that happened in a short period of time/moment. This was in 1983, when the ARPANET was migrated from NCP to TCP/IP. This type of change is impossible today because of the very heterogeneous structure of the network and the huge amount of network devices [2].

So we could speak about a long term step-by-step process, that is to say parallel usage of IPv6 and IPv4. The process started in the 90s with very low pressure, but the depletion of IPv4 brought a big change in attitude.

The IPv6 transition includes the integration of, co-existence of and inter-operation between IPv4 and IPv6 networks and equipment and it is a very broad subject. First, we give a brief overview of the most common tools. The term 'IPv6 transition' is a bit misty: it could mean a transition or migration from IPv4-only operation to IPv6-only operation, but in practice, IPv6 deployment will be a step-by-step process. The IPv4 and IPv6 co-existence will be a medium-term strategy. The transition technologies need to handle a variety of different scenarios of IPv4 and IPv6 interworking.

There are three main classes of transition:

- Dual-stack – here network elements use both protocols and can communicate with each other using either protocol.
- Tunnels – these generally involve encapsulating IPv6 over IPv4, or IPv4 over IPv6, to allow separated protocol islands to communicate over the other protocol's paths. This requires free paths on firewalls, routers and other network elements.
- Translation – is a solution for communicating between IPv6-only and IPv4-only areas. The translation is a method of remapping one IP address space into the other and the conversion of the IP header between IPv4 and IPv6.

A. *Dual-stack*

Dual-stack technology is one of the most direct methods. The dual-stack protocol equips partial hosts or routers with two protocol stacks, an IPv4 and an IPv6. It can communicate with the system of IPv4, and also with the system of IPv6.

In the dual-stack case routers have to use the two independent (IPv4 and IPv6) routing protocols, and maintain two routing tables, an IPv4 and an IPv6. The IPv4 packets are forwarded according to the IPv4 routing table, and the IPv6 packets are forwarded in accordance with the IPv6 routing table. (Figure 1.)

Most of the European and international NRENs (National Research and Education Network) have deployed IPv6 dual-stack on their backbone networks. Deploying dual-stack assumes enough IPv4 addresses are

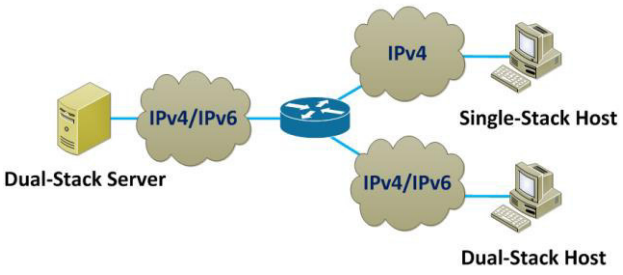

Figure 1. Dual-stack architecture.

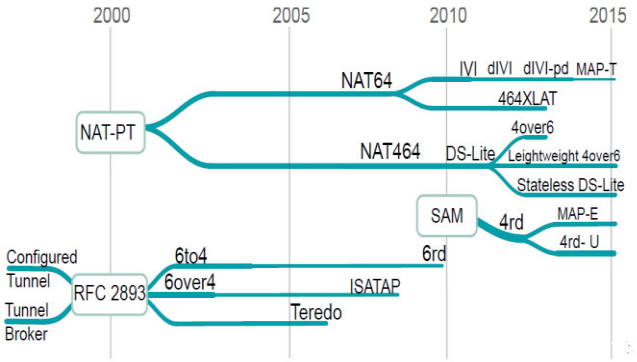

Figure 2. Evolution of IPv6 transition protocols. [4]

available, but it is also perfectly possible to deploy IPv6 with global addresses alongside IPv4 and NAT. [3] The biggest disadvantage of dual-stack networking is the complexity. All network elements, their management and monitoring systems need to support dual-stack operation. An important consideration for dual-stack is security. A good summary of IPv6 transition security issues can be found in reference 5 [5].

Before the description of translation and encapsulation technologies, we show the evolution of them in Fig. 2.

B. *Translation technologies*

We use the word "translation" when we convert the traffic between the two protocols from IPv4 to IPv6 or vice versa, that is to say transforming the headers and payload. This mechanism can be established at different layers in the protocol stack, consisting of network, transport, and application layers. The translation process can happen in the end systems or in network devices.

There are four well known types of translation:

- NAT-PT (now obsolete)
- Stateless NAT64
- Stateful NAT64
- 464XLAT

1) *NAT-PT*

NAT-PT (Figure 3.) has two types [6]. The traditional-NAT-PT allows hosts within a V6 network to access hosts in the V4 network. The traditional-NAT-PT sessions are uni-directional, supporting outbound communication from the V6 network. The other type is the Bi-directional-NAT-PT, which permits sessions in both directions, inbound

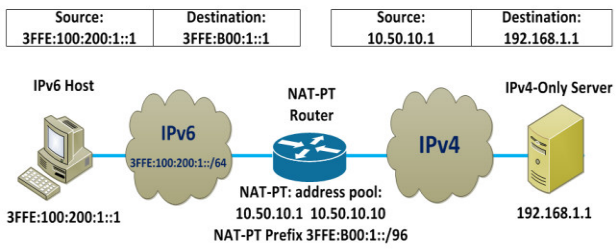

Figure 3. NAT-PT architecture

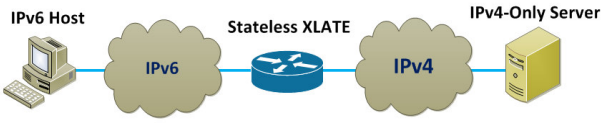

Figure 4. Stateless NAT64 architecture

and outbound. There are a lot of significant issues with NAT-PT, so NAT-PT was retired.

2) *Stateless NAT64*

The stateless NAT64 [7] architecture is shown in Fig. 4. The main features are:

- each IPv6 address is translated into a corresponding IPv4 address
- only ICMP packets and IP headers are translated

3) *Stateful NAT64*

Stateful NAT64 [8] (or "NAT64" for short), the architecture shown in Fig. 5., masks several IPv6 nodes behind a few IPv4 addresses. Its main features are:

- It is very similar to PAT (stateful NAT44)
- Individual TCP and UDP sessions + ICMP replies are translated
- Source and destination IPv6 addresses + port numbers used in lookups
- It should be used with DNS64 [9], which embeds the IPv4 address of the IPv4-only server into an IPv6 address so that it can be used by the IPv6-only client.

4) *464XLAT*

464XLAT [10] (Fig. 6.) combines the Stateful protocol translation in the core (PLAT) and stateless protocol translation at the edge (CLAT). It is a simple and scalable

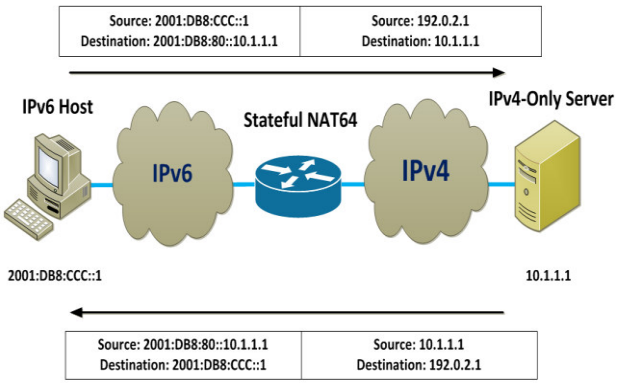

Figure 5. Stateful NAT64 architecture

Figure 6. 464XLAT architecture

TABLE I. . COMPARISON OF STATEFUL AND STATELESS NAT64

Stateless NAT64	Stateful NAT64
1:1 translation	N:1 translation
No conservation of IPv4 address	Conserves IPv4 address
Assures end-to-end address transparency and scalability	Uses address overloading, hence lacks in end-to-end address transparency
No state or bindings created on the translation	State or bindings are created on every unique translation
Requires IPv4-translatable IPv6 addresses assignment (mandatory requirement)	No requirement on the nature of IPv6 address assignment

technique to quickly deploy limited IPv4 access service to IPv6-only edge networks without encapsulation.

- PLAT is a provider-side Stateful NAT64 translator. It translates N:1 global IPv6 addresses to global IPv4 addresses, and vice versa.
- CLAT is a customer-side Stateless NAT64 translator. It translates 1:1 private IPv4 addresses to global IPv6 addresses, and vice versa.

C. Tunneling Technologies

The concept behind tunneling is not new; many people use tunneling daily. For example, many companies use IPsec or Secure Sockets Layer (SSL) tunnels to secure information when it is being transmitted over an untrusted network.
Many tunneling methods are available to support IPv4 over IPv6 or IPv6 over IPv4 tunneling. The type depends on the specific implementation details. There are two main types of tunnel: Manual tunnels and Automatic tunnels.

1) Manual tunnels

Manual tunnels are manually configured and configuration is required at both ends of the tunnel. The Administrator will always know how their tunnels are created. From a management perspective, manual tunnels are good for implementation, but from a configuration perspective they are a little bit more time consuming.

2) Automatic tunnels

Automatic means that tunnel configuration is carried out with no additional management. This method is considered as the most popular choice in the field of automatic tunneling techniques.
Types of automatic tunnels:

- 6to4 (RFC 3056)
- 6rd (RFC 5569)
- Teredo (RFC 4380)
- ISATAP (RFC4214)
- TSP (RFC 5572)

III. REAL-LIFE INDUSTRIAL EXAMPLE

We introduce a real-life migration concept based on [12]. The authors define a 3-stage process driven by several motivational factors which could be very useful in other migration scenarios as well:

- Minimize network topology change
- Simplify upgrading process
- Endpoint upgrade is independent of network change
- Protect investment on existing machine endpoints for a longer period

Stage 1 – Migrating IPv4-Only Network to Dual-Stack Network (2-3 years)

The process involves the provisioning and configuration of NAT64 gateways and DNS64 servers, including:

- Replace regular layer-3 routers and gateways with NAT64-capable devices via HW and/or SW upgrade
- Replace IPv4 DNS servers with DNS64 servers
- Install DHCPv6 servers to serve stateful DHCP requests
- Use a central NMS (Network Management System) to manage all NAT64 Gateways and DNS64 Servers and ensure consistent configuration across all systems

Stage 2 – Migrating IPv4-Only Endpoints to IPv6 (5-15 years)

- Upgrade servers, employee desktops, laptops and important IT assets to IPv6
- Upgrade Historian and other assets on the Supervisory network to IPv6
- Upgrade PLCs, Drives and other I/O devices to IPv6

Stage 3 – Migrate Dual-Stack Network to IPv6-Only Network (1-2 years)

Stage 3 begins when all the endpoints on the network support IPv6. At which point, network operators can simplify the network management and configuration by removing or disabling NAT64-related functionality and infrastructure. To ensure a smooth transition, a phased approach is also recommended:

- Selectively disable NAT64 functionality on NAT64 gateways and DNS64 servers and test drive an IPv6-only network
- Create small IPv6 pockets by replacing NAT64 gateways with regular IPv6 gateways. Merge small IPv6 pockets into bigger IPv6-only subnets
- Remove all IPv4 and NAT64 infrastructure assets
- If we would like to access IPv4 Internet, NAT64 installation is needed in LAN-IPv4 Internet edge

This migration scenario could be good for small- and medium-sized companies, but the migration is not so simple and fast for service providers, large enterprises and big companies.

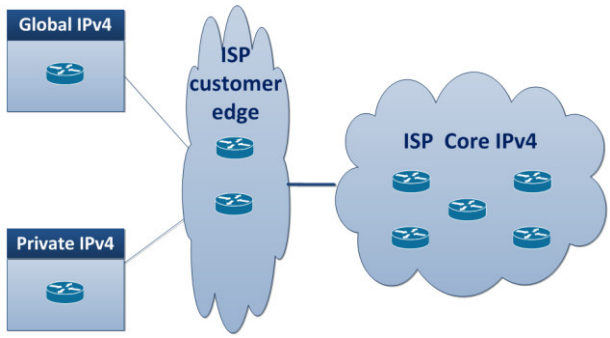

Figure 7. Only IPv4 ISP architecture

Next we will introduce a possible migration process for a service provider.

The depletion of the IPv4 address space affected strongly the service provider segment. The reasons: it makes harder the delivery of new internet services, meaning it is hard to increase the number of new customers. On the other hand, demand increases strongly because of the decreasing internet costs and the boom of IoT.

IV. POSSIBLE ISP MIGRATION PLAN

The ISPs have two types of customers (Fig. 7.):

1. Customer with Global IPv4 address.
2. Customer without Global IPv4 address. This type was unknown earlier. Earlier there was Global Fix and not Fix-IP-based internet service, and due to the depletion of IPv4 address space the providers introduced this type in order to delay the introduction of IPv6. This is a temporary solution with disadvantages. The target customer groups are the internet surfers and normal mobile subscribers.

According to our experiences, we defined a 3-step migration process for an ISP

Step 1. - Provide IPv6 addresses for customers

In this step, the ISP handles 4 types of traffic (Fig. 8.):

1. (yellow) IPv4 customer to IPv4 Internet: Global IPv4 only routing at customer edge, Private IPv4 NAT44 at customer edge
2. (red) IPv4 customer to IPv6 Internet: Global IPv4-only routing needed, Private IPv4 NAT44 at customer edge and stateful or stateless (the type is decided by the requested service and customer needs) NAT46 at V6 Internet edge
3. (purple) IPv6 customer to IPv4 Internet: Stateful or stateless NAT64 at customer edge (the type is decided by the requested service and customer needs)
4. (green) IPv6 customer to IPv6 Internet: Tunneling 6to4 between customer and v6 Internet edge

NAT46 was not mentioned earlier as we could find only draft RFC [11] in this topic, and at design phase we have to investigate the usage of NAT46 or other possible solutions. Nevertheless it could happen that all of the IPv6 servers will support Dual-stack, this scenario makes unnecessary the usage of NAT46. The time period of the first step is strongly influenced by new address needs and the growth of the number of customers.

Step 2. - Migration of ISP core

We can speak about 4 types of traffic too (Fig. 9.):

1. (yellow) IPv4 customer to IPv4 Internet: 4in6 Tunneling between customer and v4 Internet edge, the Private IPv4 addresses NAT44 at customer edge
2. (red) IPv4 customer (or private IPv4 customer) to IPv6 internet Stateful or stateless NAT46 at customer edge (the type is decided by the requested service and customer needs)
3. (purple) IPv6 customer to IPv4 Internet: Stateful or stateless NAT64 at v4 Internet edge (the type is decided by the requested service and customer needs)
4. (green) only routing needed

As above mentioned before using of NAT46, we have to ponder the opportunities.

Step 3. - Retire IPv4

As the last step (Fig. 10.), we migrate to an IPv6-only

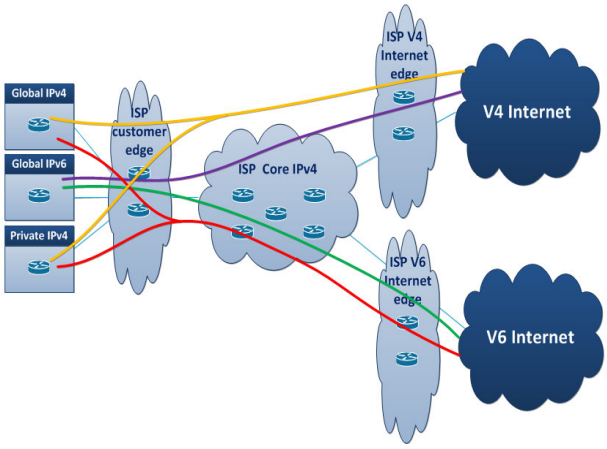

Figure 8. Step 1. architecture

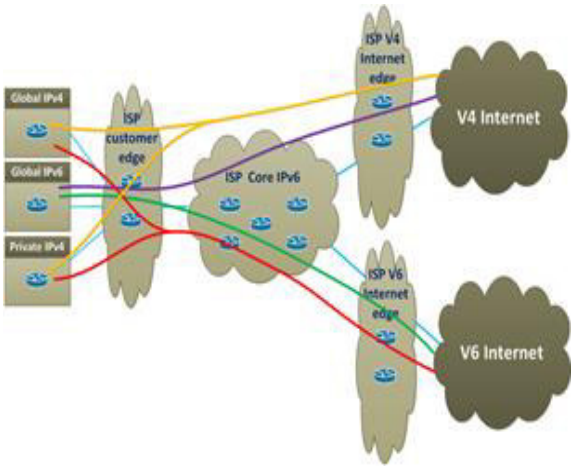

Figure 9. Step 2. architecture

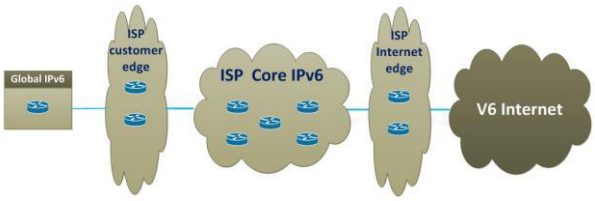

Figure 10. Step 3. architecture

network. It is not sure that the Internet will ever retire IPv4, possible never. If yes, this could be the last step.

V. THE ISP MIGRATION PROJECT

The 3 steps mentioned above define the frame of migration; the real process has many more phases. A good way is to divide every step into three different phases:

- design phase
- implementation phase
- cyclic operation phase

Design phase

The main activities in this phase:

- Traffic analysis and estimation
- Scaling the hardware and software elements according to the needs
- Design the implementation plan
- Define the threshold criterion to start the preparation for the next step

Implementation phase

We implement the new architecture and go live.

Cyclic operation phase

In the operation phase, we continously monitor and analyse the network and make changes to satisfy needs. A good example: if an increase in the number of IPv6 customers leads to the address translation capacity getting close to its limit, then we have to enhance the system capacity.

If the system reaches the threshold where the usage of the next step architecture is more efficient, then we start the design phase of the next step.

Next I investigate some usable resourse at design. We can find several publications about performance analysis and hardware resource optimatization for different solutions. For tunneling, we could use a Linux-based solution to satisfy the requirements [13].

For address translation, there are two important NAT64 solutions which offer the performance and stability to satisfy ISPs' needs, namely the PF (Packet Filter) of OpenBSD and the TAYGA+iptables under Linux [14]. As for NAT64, we have to consider the port number consumption as well: this is a crucial parameter at design [15]. For name server functionality, BIND is a good software to satisfy production network needs [16].

VI. CONCLUSION

We are at the time when we can not avoid the usage of IPv6. The lack of IPv4 addresses strongly affects the ISPs. In this paper, we introduced the different IPv6 transition solutions and two migration plans, the introduced plans could be very useful if a company or service provider start the preparation to a migration. Finally, we defined the main phases of a possible migration project and then presented some useful resources for the design phase.

REFERENCES

[1] The Number Resource Organization, "Free pool of IPv4 address space depleted" http://www.nro.net/news/ipv4-free-pool-depleted

[2] G. Lencse, S. Répás, A. Arató, *IPv6 és bevezetését támogató technológiák*, 1st. ed. Budapest: HunNet-Média Kft., 2015. DOI: 10.18660/ipv6-b1.2015.9.1

[3] T. Chown, "IPv6 Technical Guide", [Online] Available: https://community.jisc.ac.uk/system/files/487/ipv6-tech-guide-for-web.pdf

[4] M. Georgescu, *Evolution of Translation and Encapsulation Technologies*, PhD dissertation, NAIST, 2016.

[5] E. Davies, S. Krishnan, P. Savola, "IPv6 Transition/Coexistence Security Considerations", RFC 4942, DOI: 10.17487/RFC4942

[6] G. Tsirtsis, P. Srisuresh, "Network Address Translation - Protocol Translation (NAT-PT)", RFC 2766. DOI: 10.17487/RFC2766

[7] X. Li, C. Bao, F. Baker, "IP/ICMP Translation Algorithm", RFC 6145. DOI: 10.17487/RFC6145

[8] M. Bagnulo, P. Matthews, I. van Beijnum, "Stateful NAT64: Network Address and Protocol Translation from IPv6 Clients to IPv4 Servers", RFC 6146 DOI: 10.17487/RFC6146

[9] M. Bagnulo, A. Sullivan, P. Matthews, and I. Beijnum, "DNS64: DNS extensions for network address translation from IPv6 clients to IPv4 servers", IETF RFC 6147. DOI: 10.17487/rfc6147

[10] M. Mawatari, M. Kawashima, C. Byrne, 464XLAT: Combination of Stateful and Stateless Translation RFC 6877. DOI: 10.17487/RFC6877

[11] D. Liu, H. Deng, "NAT46 considerations", Expired Internet-Draft, 2010, [Online], Available: https://tools.ietf.org/html/draft-liu-behave-nat46-02

[12] X. Yang, M. Dalal, "Migrating Industrial IPv4 Network to IPv6", ODVA 2014 Industry Conference & 16th Annual Meeting 2014, March 11-13, Phoenix, Arizona, USA, [Online], Available: https://www.odva.org/Portals/0/Library/Annual_Meeting_2014/2014_ODVA_Conference_Yang%20Dalal_%20Migrating_Industrial_IPv4_Network_to_IPv6_FINAL.pdf

[13] S. Répás, V. Horváth and G. Lencse, "Stability Analysis and Performance Comparison of Five 6to4 Relay Implementations" *Infocommunications Journal*, vol 8. no. 2. pp. 1-10

[14] G. Lencse and S. Répás, "Performance Analysis and Comparison of the TAYGA and of the PF NAT64 Implementations", *Proceedings of the 36th International Conference on Telecommunications and Signal Processing (TSP 2013)*, Rome, Italy, 2013. July, 2-4. Brno University of Technology, pp. 71-76. DOI: 10.1109/TSP.2013.6613894

[15] S. Répás, T. Hajas and G. Lencse, "Port Number Consumption of the NAT64 IPv6 Transition Technology" *Proceedings of the 37th International Conference on Telecommunications and Signal Processing (TSP 2014)*, Berlin, Germany, 2014. July, 1-3. Brno University of Technology, pp. 66-72. DOI: 10.1109/TSP.2015.7296411

[16] G. Lencse, and G. Takács, "Performance Analysis of DNS64 and NAT64 Solutions" *Infocommunications Journal*, vol. IV, no. 2,. June, 2012, pp. 29-36.

Developing an E-learning Course for Teaching Digital Technology

Nikoletta Tolner and András Dávid

Campus of Alba Regia Technical Faculty of Óbuda University
H-8000 Hungary Székesfehérvár, Budai str. 45, Hungary
tolner.nikoletta@amk.uni-obuda.hu
david.andras@amk.uni-obuda.hu

Abstract: We have been teaching Digital Technology to full time and correspondent students for several years. Based on this experience, we attempted to compile a course that is easy to use. We also took into consideration the fact that our students' needs have changed. We use the MOODLE system at the Obuda University, so we developed Digital Technology Course 1. and 2. within the frames of this system. Our courses cover the same topics that are taught to full time electrical engineer students in their courses with the same name. In the beginning Digital Technology 1. and 2. were only used in the KMOOC system (Carpathian Basin Massive Open Online Courses), as an optional subject. Now we also use it in full time education as a supplementary material, with certain necessary alterations. In the present article we describe the process of developing the courses, and also our experiences of using them.

I. INTRODUCTION

A) The subject of Digital Technology in brief

Digital Technology is a subject that we teach at Obuda University to Electrical Engineering, Informatics Engineering and Engineering Management students. It is a foundation subject, part of the core material. Electrical Engineering students study Digital Technology I. in the first term in the following schedule: 2 lectures and one lab practice lesson per week (4 credits). In the second term Digital Technology II. takes up 2 lectures per week (3 credits).

Informatics Engineering students study Digital Technology in the second term in 2 lectures and 2 lab practice lessons per week (4 credits).

Engineering Management students study the subject under the name of Analog and Digital Technology in 2 lectures and 2 lab practice lessons per week (5 credits). The main aim of the subjects is to give basic hardware knowledge required for designing digital circuits. To this end, students deepen their theoretical knowledge though practical tasks.

During the course students

- Learn about Boolean algebra, the mathematical language used for describing the operation of networks
- Learn about the main types of circuit components
- Learn and practice the steps of designing combination networks
- Gain knowledge in identifying and eradicating hazard phenomena
- Learn about the operation of arithmetic circuits
- Learn about the operation and description of sequential networks
- Get knowledge of elementary synchronous and asynchronous sequential networks
- Get knowledge of and practice the steps of planning sequential networks
- Learn to identify and eradicate competitive situations
- Practice how to analyse time operation of sequential networks
- Learn about different types of memory, and how to use them for planning sequential networks

B) Survey of student needs

We tried to gauge student needs before developing our supplementary materials. Although the survey was not representative, we got some significant results:

The supplementary materials should be

- electronic, rather than printed
- easy to reach anywhere and anytime
- short, concentrating on the essence of the material
- theoretical material should be supplemented by practical examples and exercises
- it should contain self-monitoring tasks providing immediate feedback

We all know that students' learning habits have changed. Research of teaching methodology has also produced new results. More and more educational institutions are developing an electronic curriculum.

In the field of public education, the work of the Education Research and Development Institute (OFI) is outstanding. This institute has developed new textbooks, supplementary materials and teaching aids, among which you can find electronic materials [1], too. Higher education institutions also began to develop electronic curriculum. The Hungarian Virtual University Network Association has been formed to represent the e-learning system of 19

higher education institutions. Obuda University is also a member of this Association [2].

The Association aims to establish a cooperation framework that provides support for the development of distance learning and e-learning.

II. GOALS AND OBJECTIVES

A) The development objective

Taking into consideration students' needs, we started developing the curriculum. Several teaching methodology questions arose during the process. Our main goal was to create a material that is best suited to meet the needs of the student. We studied the possibilities of developing e-learning materials, as this was one of the students' requests. At that time, an opportunity emerged to use our material as an elective course in KMOOC. Our application was accepted, so we modified the material in a way that it could be used as an independent online course. As a result of this work, Digital Technology I came out in September 2015., then Digital Technology II. in September 2016. The material of the two courses completely covers the same courses for Electrical Engineer students. The two courses are worth 4 credits.

B) Steps of developing the e-learning course

1. We studied resources on how to compile easy-to-use e-learning materials. [3], [4], [5]
2. We tried to use this knowledge for the topic of Digital Technology. The basis of our material was a course book written by one of our colleagues. [6]
3. We also studied already existing e-learning materials available at Obuda University.
4. We looked for tools and programs that could be used for designing and testing digital circuits. Logisim [9], [10].
5. We created Digital Technology I. online course.
6. Digital Technology I. had been successfully operating for a year, when we created Digital Technology II. (It was also realized within the frames of KMOOC.)
7. We built in the material of online courses into the curriculum of full-time Electrical Engineering students. It is used as a supplementary material in full-time education.

III. METHODS

A) What kind of e-learning materials can you find?

E-learning materials available in higher education are usually in pdf format, with a few self-test questions at the end. They do not really meet students' needs. A smaller part of materials contain theoretical explanation, practical examples and self-tests, too.

B) The possibilities offered by Moodle

Obuda University uses the Moodle system, so we created Digital Technology I. and II. courses in this system. Moodle is a freely available e-learning framework, written in PHP language [7]. There is a "community-based, globally supported Moodle community" [8], which provides its members with useful information.

First we had to find out what opportunities are provided by this system. What kind of educational materials, activities and tests can we include in our material?

We have created a question bank containing nearly 1,500 questions. Then we compiled self-tests and knowledge evaluation tests using this question bank. We used the following types of questions and tasks: embedded answers, essay, multiple choice, true or false, open ended questions, matching tasks, select missing words, numerical, drag and drop onto image and drag and drop into text. We also created video materials: animated ppt and classroom videos. We also set complex requirements for students to pass the test.
Questions are randomly selected for midterm tests and final tests, so it cannot happen that one student gets the same question twice.

C) Logisim [9], [10]

During the development of the courses we considered it important that students can test and simulate the operation of the designed combination and sequential networks. We looked for a program that is free, easy to learn, and is suitable for simulating combination and sequential networks. After examining several programs, we chose Logisim. At the beginning of both courses we teach students how to use Logisim by the help of videos. This program can be perfectly used for simulating combination networks, it can simulate sequential networks on a basic level, but unfortunately it cannot be used for drawing time diagrams. We created sample circuits for each module, these are available for students, too.

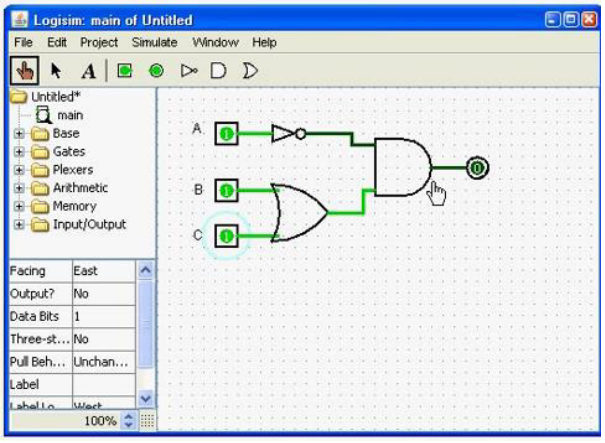

Figure 1: An example of the implementation of a combination network with Logisim program

D) Camtasia program

Camtasia Studio are software suites, created and published by TechSmith, for creating video tutorials and presentations directly via screencast, or via a direct recording plug-in to Microsoft PowerPoint. The screen area to be recorded can be chosen freely, and audio or other multimedia recordings may be recorded at the same time or added separately from any other source and integrated in the Camtasia Studio component of the product. Both versions of Camtasia started as enhanced screen capture programs and have evolved to integrate screen capture and post-processing tools targeted at the educational and information multimedia development marketplace. Camtasia program was also used in the online (recorded) course material (Figure 2,3). Animated ppt files, which can be used multiple functions, has also been produced with this program.

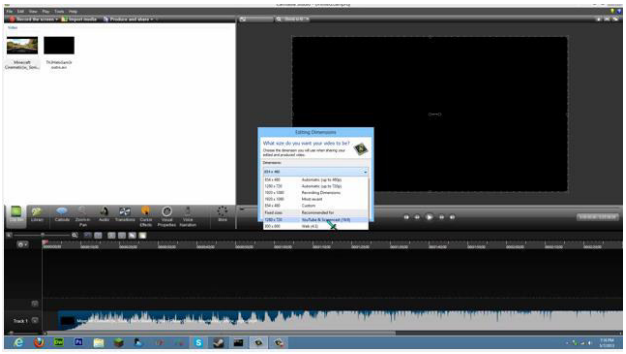

Figure 2: Camtasia Studio program

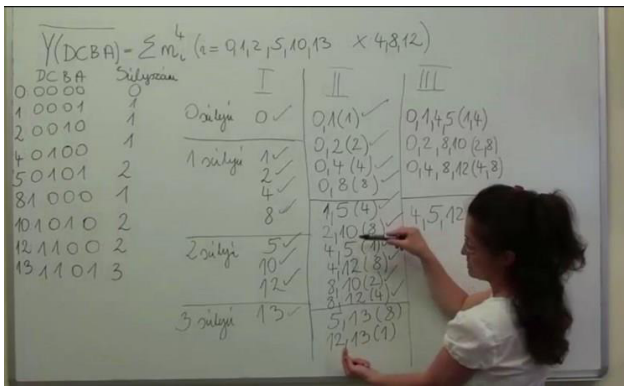

Figure 3: Video with Camtasia program

IV. RESULT

A) Creating online course for Digital Technology I.

After examining the opportunities, the Digital Technology 1. online course was prepared, and was divided into 12 modules (Figure 6 and 7):

Module 1: The concept of logic network and its function, its standard makes, its description opportunities

Module 2: Number systems, coding systems for digital technology

Module 3: The Boolean algebra

Module 4: The logic network, and the description of its function with equations. Disjunctive, conjunctive canonical forms

Module 5: Universal logic functions and implementing these building blocks

Module 6: Simplification of logic functions with Karnaugh table

Module 7: Simplification of logic functions with digital minimization (Quine-McCluskey)

Module 8: Design and analysis of combinational networks. Hazardous phenomena

Module 9: The ideal and the real circuit blocks, the features of the real circuit blocks. TTL and CMOS technology

Module 10: Different types of outputs and their connectivity

Module 11: Multiplexers, demultiplexers

Module 12: Arithmetic circuits

B) Creating online course for Digital Technology II.

Digital Technology I. online course had been operating for a year, when we started to compile Digital Technology II. Because of this we were able to take into consideration the feedback and suggestions we got from our students. Digital Technology II. is also divided into 12 modules.

Module 1: The concept of sequential network, its types and methods of description (synchronous and asynchronous sequential networks, Mealy model, Moore model, state table, state graphs)

Module 2: Basic sequential networks (R-S, Rnegated-Snegated storage, D, T, J-K, J-Knegated flip-flops)

Module 3: Steps of designing synchronous sequential networks

Module 4: Steps of designing asynchronous sequential networks (stable, unstable states, critical, non-critical conditions)

Module 5: Designing a synchronous sequential network using flip-flops

Module 6: Designing networks with shift register (ring, Johnson, modulo numerator)

Module 7: Designing networks with synchronous counters

Module 8: Designing networks with asynchronous counters

Module 9: Examination of the operation time of synchronous sequential networks

Module 10: Time operation of synchronous sequential circuits with shift registers

Module 11: Time operation of synchronous sequential circuits with synchronous counters

Module 12: Memories and their usage in sequential circuits

In the beginning of the course students can see only Module 1. They can go on to the next module only if they reach the required result in the Final Module Test. The required results are the following:

Digital Technology I.

Modules 1, 2, 3, 4, 5, 9: minimum 60%

Modules 6, 7, 8, 10, 11, 12: minimum 50%

Digital Technology II.

Modules 1, 2: minimum 60%

Modules 3 to12 minimum 50%

If students reach the required results in the first 6 Final Module Test, they can sit the first Mid-term Test. They can go on studying the next modules even if they fail the first Mid-term Test. The structure of all modules is the following (Figure 4.):

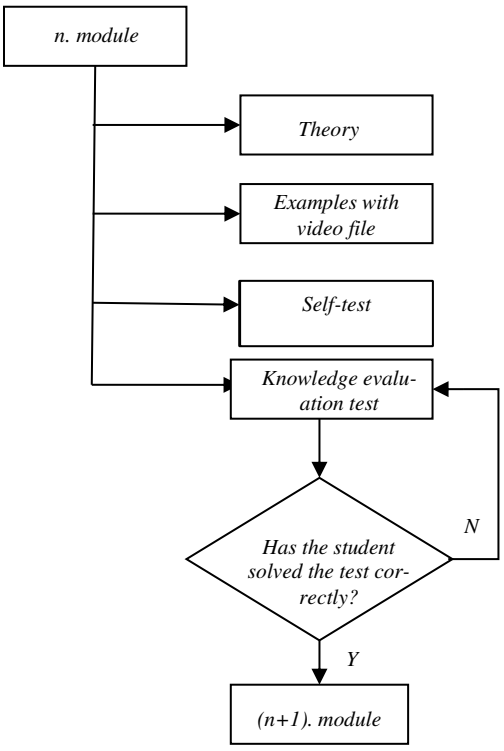

Figure 4: The structure of modules

The order of the modules is carefully designed, we recommend students to study the modules in the given order. They have to understand the theoretical part first, then they can move on and study the practical examples. Video materials are also provided, so students can follow a teacher's explanation, as if they were sitting in a classroom. The next step is the self-test, which gives students opportunity to evaluate their knowledge of the module. It is possible to do the self-tests (Figure 5.) several times, so students are given the possibility to practise their skills. Then they can do the Final Module Test, which is marked by teacher. This kind of test can be done only 3 times (in the case of the first 3 modules) or twice (in the case of rest of the models).

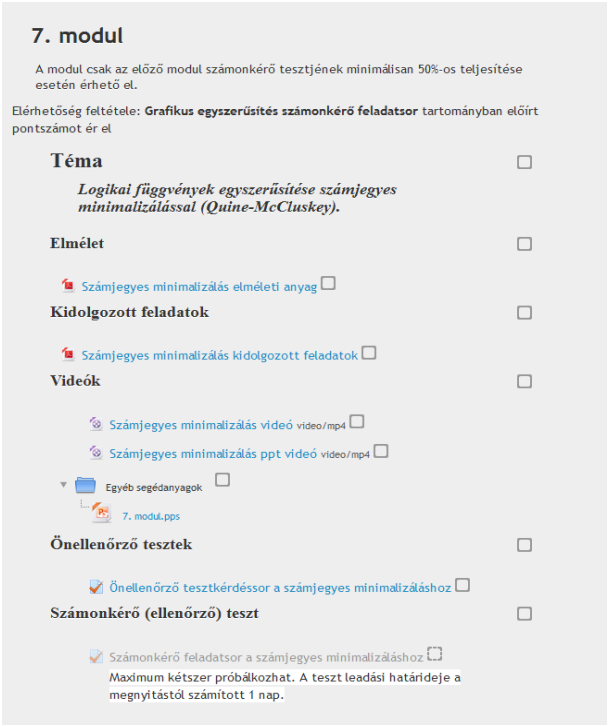

Figure 5: An example an module of the Digital Technology I. online course

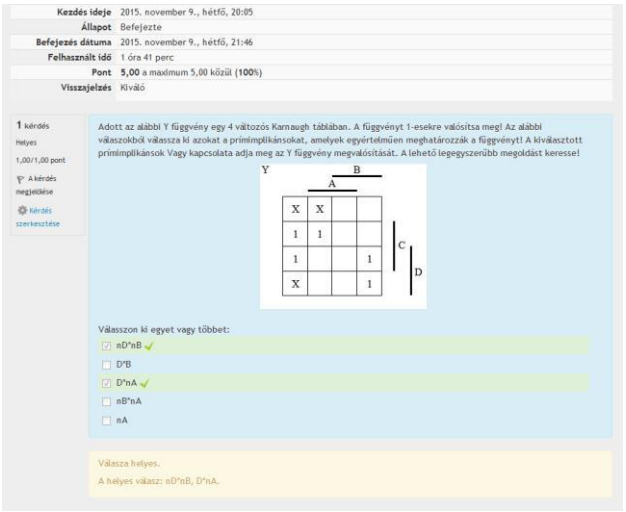

Figure 6: An example of a self-test of the Digital Technology I. online course

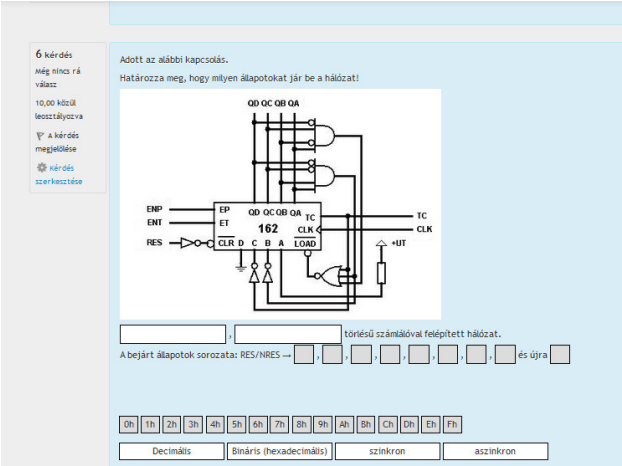

Figure 7: An example of a Final Module Test of the Digital Technology II. online course

C) Evaluation of students' achievement

For both courses we designed two mid-term tests, one after the 6th, the other after the last module. Mid-term tests can be reached by students only on certain days and only for a certain period of time.

We did not give a time limit for studying the modules, as our experience is that students can learn the material in their own pace. Giving a time limit puts unnecessary stress on students with a slower pace. Most mid-term tests are designed in a way that students can get immediate response about their result (passed of failed). Some tests are more complex and have to be marked by a teacher, which takes more time.

Completion of the course will be considered successful if students pass all their tests and do their written homework with the required result. If students fulfil these conditions, they get a mark from their teacher. The mark is based on the following results:

30% of the mark: written homework and Final Module Test results

70% of the mark: Mid-Term Tests results

Mid-term tests must be written by students at the University Campus. Obuda University's goal is to provide students with the opportunity to study all subject online, not only the elective courses.

V. DISCUSSION

A lot of work is also associated with not only the creation, but with the management of an online course. Certain tasks cannot be evaluated automatically. The teacher has much work after the completion of the course. It is necessary to correct the incoming tasks, it is necessary to have information about the results. This should be done completely electronically. In the regular full-time education, a lot of things can be used from the online course material. In this case, personal feedback can be provided, which can be interpreted more precisely. In the case of an online course the teacher has no chance to check whether it was the registered student or someone else who solved and sent in the Final Module Test.

VI. FEEDBACK FROM STUDENTS

Students achieve surprisingly good results when doing Final Module Tests of elective courses. This can probably be explained by the fact that only those students choose these courses who are really interested in the topic. We keep receiving a lot of positive feedback from students, they also point out errors if they discover any. We try to correct these errors as quickly as possible. We started using the course materials in full-time education in 2016 and so far we have received only positive feedback.

VII. REFERENCES

[1] http://ofi.hu/

[2] http://e-university.hu/network/

[3] Harangi László, Kelner Gitta, Csoma Gyula: Az e-learning szerepe a felnőttoktatásban és –képzésben, Magyar Pedagógia Társaság, Budapest, 2003

[4] Kovács Ilma: Az elektronikus tanulásról a 21. század első éveiben

[5] Az Óbudai Egyetem Moodle rendszere Felhasználói kézikönyv oktatóknak:

https://elearning.uni-obuda.hu/kmooc/ pluginfile.php/56099/mod_resource/content/1/Az%20%C3%93budai%20Egyetem%20Moodle%20rendszere.pdf

[6] Grosz Imre: Élő digitronika című jegyzete

[7] https://hu.wikipedia.org/wiki/Moodle

[8] https://moodle.org/

[9] http://www.cburch.com/logisim/

[10] https://www.youtube.com/watch?v=dYZ-Hwbcnq4

Pixel-based 3D Object Reconstruction

A. Somogyi, A. Barsi
Department of Photogrammetry and Geoinformatics,
Budapest University of Technology and Economics, Budapest, Hungary
somogyi.arpad@epito.bme.hu, barsi.arpad@epito.bme.hu

***Abstract*— The photogrammetric object reconstruction seems to find its modern Holy Grail in the pixel-based technology. The great offer of sophisticated software packages prove that the formerly developed computer vision and photogrammetric functions can efficiently be combined to support an accurate object reconstruction. In the paper the general theory and workflow of the methodology is discussed followed by seven in-house projects. These projects show up big variety in the application: ancient wood and current stone sculptures, medieval cathedral and fortress or famous tourist places can be found as supporting case studies. The authors wanted to demonstrate also the independency from the image capture, which was proven the applied image sources: internet-based image data base, UAV-mounted action camera, high quality mirrorless and digital single-lens reflex (DSLR) camera, but also smartphone camera or YouTube video stream. The attached figures intentionally illustrate also the three processing steps: camera alignment, reconstruction and visualization.**

I. INTRODUCTION

It is no wonder that the Hollywood film *Avatar* from James Cameron is so famous and popular. Visual effect companies, like *Industrial Light & Magic* or *Weta Digital* use computer techniques based on the reality. Their technology is an implementation of the methodology currently used by the photogrammetry and computer vision community. Because this methodology is rapidly developing and spreading we do want to draw a sketch about its essence.

The very brief summary of the methodology is simple: only a series of pictures must be taken about an object and this technology can deliver the real spatial 3-dimensional model. The black-box technology has been realized in several commercial and free software packages, where the users can or need to have basic knowledge about the workflow. In the paper a draft overview is given followed by examples taken from our practice.

II. METHODOLOGY

A. 3D reconstruction workflow

The exact spatial reconstruction of an object is a very hard challenge. Images with suitable amount and quality must be captured in acceptable recording geometry. This means that convergent imagery must be shot about the object, possibly at high geometric and radiometric resolution. The more overlapping images cover the object, the better will be the reconstructed model.

An overview about the whole theoretic procedure can be seen in Fig. 1. The first step is the loading of these images into the processing environment. All of the images must be processed searching for matching features. Such features can be points (or corners) delivered by interest operators like Harris, Förstner etc. but can be complex ones being invariant against scaling or rotation, like HOG (Histogram of Oriented Gradients), SIFT (Scale Invariant Feature Transform) or SURF (Speeded Up Robust Features) [1], [2], [3]. These features are rugged enough to be found in more images and being able to connect them.

So the following step is the matching of images using these features. One can imagine that by increasing the number of images, the number of the features and much more the amount of the possible combinations increase. To cope this problem effective search strategies are deployed.

These strategies are either locally or globally "effective". The first group is best represented by the Normalized Cross Correlation (NCC) technique, while the second one by a cost-function based optimization, e.g. Dynamic Programming (DP). The most known algorithms are of the global group: Graph Cut (GC), Dynamic Programming (DP), Belief Propagation (BP) and Semi Global Matching (SGM) [4], [5]. These global algorithms deliver esthetically and computationally better reconstruction.

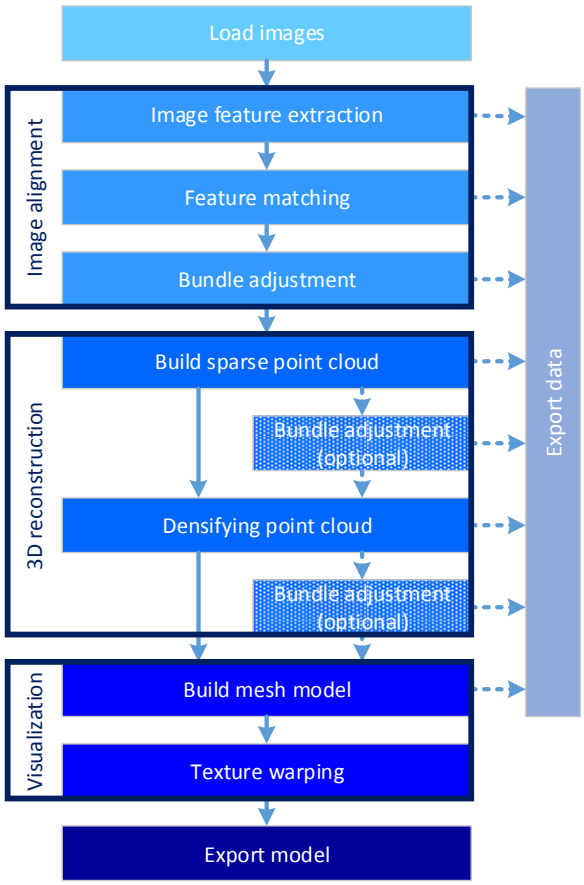

Figure 1. Flowchart of the spatial reconstruction methodology

After getting the matchings among the images, all of their pose, i.e. the positions of their projection centers and orientations can be computed. Because the matching may have some anomalies, the result of these orientation isn't error-free. The quality of the orientation is generally improved by sophisticated bundle adjustment. These last three steps belong to the Image Alignment phase of the procedure.

The 3D object reconstruction can be started now: first a rapid and draft solution is given, which results a sparse point cloud. In several cases an optional bundle adjustment can refine the orientation parameters prior the densification of the point cloud. These lastly mentioned step is the core of the Multi View Stereo (MVS) systems, because the reality-near point density of the object is achievable just by this step. Because the densifying requires very much computing power (significantly more than image alignment – see examples!), different realizations have been developed: Clustering Views for MVS (CMVS), Patch-based MVS (PMVS) or more sub-versions of them. (The visual effect companies in Hollywood are strongly interesting in these methods, because the film production can efficiently be supported by them.) [6], [7]

The result of the sparse and dense point cloud building is adequate for modeling the spatial relation of the object. For example, the surface model of a statue can be the output, which can be transferred into visualization modules. Sometimes the reconstruction software serves with visualization functionality, then point cloud meshing and texturizing is also included. The procedure finishes by the exportation of the digital object model for example in *obj* or *ply* format. This model can be then used for 3D printing or in on-line visualization embedded into a web portal or pdf-document. The users usually have the option to export all computed results (e.g. camera pose parameters, rotation matrices, essential and fundamental matrices, bundle adjustment data, point clouds). [8]

B. Reconstruction based on still images

The above described general method is implemented in the commercial and free software packages. Agisoft Photoscan, VisualSFM, 3DF Samantha, Colmap or Autodesk Remake were the mostly applied software tools. To test the applicability and the packages we have conducted several projects. Two main sources were used to feed the software packages: still images and frames taken from video streams. The most important descriptors are collected in Table 1.

TABLE I.
RECONSTRUCTION PROJECT PROPERTIES

Project name	Number of images	Number of points in dense model	Number of mesh elements
BME sculpture	11	638.588	1.272.362
Parliament	63	117.267	24.353
Heroes' Square	1626	663.268	n.a.
Ócsa aerial photos	15	2.310.794	462.148
Sirok	1042	13.544.267	2.609.077
Ócsa aerial video	583	795.463	90.919
Madonna	1804	2.667.782	533.556

n.a. – not available

The next part of the chapter will introduce the reconstruction projects. The *BME sculpture* has a stone sculpture next to the main entrance of the university's main building. It is a sitting woman figure allegorizing the civil engineering discipline. The sculpture is 3.3 m high and weights more than 9 tons. The sculpture images were taken by a Sony Nex-7 camera under clouded weather circumstances. The resolution of the images was 3376 × 6000 pixels. The rendered textured model can be seen in Fig. 2.

Figure 2. Textured model of the sitting woman sculpture at BME main building

The *Parliament* and the *Heroes' Square* projects had an unconventional image source: the necessary images were downloaded by a self-developed software tool from the Flickr image data base. Flickr belongs to Yahoo Group and its data base contains photos taken by anybody, who uploaded them. The downloader tool could get the images with a highest resolution of 1024 × 1024 pixels. Unfortunately, the image size was mostly much lower and the quality was very heterogeneous. The biggest problem was the automatic selection of the downloaded photos covering outdoor scenes, instead of indoor event contents. Wrong image tags, poor light circumstances, blurred images have to be removed before starting the reconstruction. The camera centers in Heroes' Square are shown in Fig. 3. One can notice that most tourists capture the view from the square's main axis; it seems that people are very sensitive on the symmetry in their pictures. The viewing angle is mostly about 40° or less, which is not a perfect configuration, only a single side can be reconstructed using these photos. On the Heroes' Square the farthest camera position is roughly 140 m from the colonnade. Because of the lower quality of dense point cloud, no mesh was obtained.

In case of the Parliament the nearest photos were taken from the Pest side, whilst the nearest pictures from Buda were ~ 400 m far from the building. There were more photos taken from a distance of 700-800 m. Pictures of longer distance were dropped by the software because the object was too small in the images (do not forget the image size!).

Because the input images have low geometric resolution, the derived model is quite noisy. As an illustration of the power of the spatial reconstruction even under so hard conditions (poor resolution and low quality), the Danube view

of the Parliament building was achieved (Fig. 4). The resulting model has enough detail to derive sections from e.g. Cupola [9]. The given number of mesh elements in Table 1 are also only from cupola.

Figure 3. Computed camera centers with orientation in the Heroes' Square project

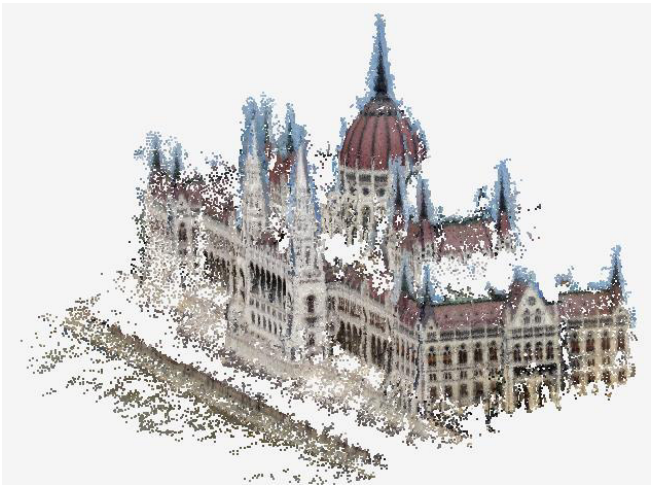

Figure 4. Reconstructed Danube view of the Parliament building from crowd-sourced images

The project *Ócsa aerial photos* was based on the excellent camera shots from an airplane. The involved images were capture by a Fuji FinePix S3Pro camera with a resolution of 4256 × 2848 pixels. This project has been started newly; the goal is to test the combination of terrestrial and aerial images with terrestrial laser scanning. The object is a medieval cathedral, which was part of a Premonstratensian monastery. The construction of the cathedral was started in the 13th century in roman style. It has a layout forming a Latin cross: nave, aisles, transept and 3 apses. The ownership of the cathedral was changed: since the 16th century it belongs to the Calvinistic church. Between 1986 and 1992 the cathedral was totally renovated. The cathedral is about 40 m long, 25 m wide and the towers are roughly 25 m high.

The photo projection centers were computed during the alignment phase giving a feed-back that the used imagery has nice uniform distribution around the object.

The dense point model can be directly visualized in the web by Potree, see Fig. 5.

Figure 5. Potree viewer with the point cloud about the ancient cathedral in Ócsa

To illustrate the computing time, the following data can be given. The derivation of feature vectors and pairwise matching took 1 minute, the alignment of all image pairs, the connected bundle adjustment and the creation of the sparse point cloud 1 second, while the production of the dense point cloud was 9 seconds followed by a processing time of 2 minutes 46 seconds for meshing and further 1 minute for building texture.

In the *Sirok* project a GoPro Hero3+ Black Edition camera was mounted on a DJI Phantom platform and was flown around the ruins of the ancient castle. The fortress stands on a 296 m high hill; the first citations are from 1320 AD. Since that time it was continually developed till 1713, when the Habsburgs have destroyed. Now the ruins are in an area of almost 3000 m^2. The width of the remained wall segments is between 1.5 and 2.5-3.5 m in the upper and the lower castle respectively. There were 4 m deep and 4.5 m wide pits along the northern wall as well as 25-30 m high cliffs.

The resolution of the taken photos was 4000 × 3000 pixels. Figure 6 shows the full size meshed and textured terrain model about the working area. [10]

Figure 6. Textured model about Sirok

The Sirok project was the largest of the evaluated ones. The processing times are therefore interesting, even in comparison to the previously presented project. The feature vector extraction and pairwise matching required 10 hours 12 minutes, the basic alignment with sparse point cloud 2 hours

10 minutes, while the dense point cloud needed 1 whole day and 17 hours processing time on our dedicated workstation! The mesh step took then 7 minutes and the texturizing 3 hours 32 minutes respectively.

C. *Video-based reconstruction*

The processing of video streams has great similarity to the technology of still image processing. The main difference is the frame extraction, which must be performed by a sampling step. Each recorded movies must be played and every n^{th} image frame must be cut off and save as still image in a dedicated directory. There can be quality differences between image streams, so the sampling frequency is depending mainly from the recording camera.

The two presented cases are therefore interesting in the capturing aspects. The *Ócsa aerial video* project was focused on the crowd-source, namely a YouTube video stream was download. The stream has a length of 9 minutes and 42 seconds. The framerate is 25 fps, the recording is full-HD (1920 × 1080 pixels). The supposedly action cam captured video was taken from a UAV. After executing all camera alignment and 3D reconstruction steps it is really worthy to go through all visualization phases, because the final model is very sculpturesque, "almost touchable" (Fig. 7).

Figure 7. The Ócsa cathedral model after all reconstruction steps

In the *Madonna* project a Samsung Galaxy S5 mobile phone was used as a camera. The wood sculpture was made by an unknown Italian master from Fabriano in the 14^{th} century. The 153 cm high painted wood Madonna holds the child Jesus in her hand. On the backside of the sculpture there is a roughly 20 cm big padded niche presumably for keeping valuable relic.

The stream was recorded as full-HD video. Every 10^{th} frame was sampled and saved for later processing. Two trajectories were applied around the head of the Madonna sculpture: 31 s and 34 s long streams were stored. More details about the modeling and results, see [11]. Fig. 8 illustrates the two trajectories around the reconstructed Madonna-head. It isn't necessary to mention that the dense projection centers strongly correlate with the camera movement, so the image capture can easily be checked. In this project the very end was reached by the 3D printing of the head model.

Figure 8. Madonna-head with the camera poses in two circular trajectories

The presented projects were computed on a computer with double Intel Xeon E5-2650 @ 2.0 GHz CPU, 64 GB RAM and NVidia Quadro K5000 video card with CUDA support.

III. CONCLUSIONS

In this paper the big picture of the spatial object reconstruction was drawn. The main components of the methodology have been presented followed by a collection of divergent case studies. These cases aimed to show that the technology can be involved universally for images captured from smaller indoor objects (like a wood art treasure) to a bigger outdoor objects (like a fortress on a hill). The origin of the images can have also great variety, the image alignment and point cloud production can achieve the expected outputs.

REFERENCES

[1] http://en.wikipedia.org

[2] MathWorks Matlab, Computer Vision Toolbox

[3] Barsi, Á. (2013): Application of image segmentation techniques in remote sensing [in Hungarian], Geomatikai Közlemények, XVI, pp. 83-88

[4] Unger, Ch. (2013): Contributions to Stereo Vision, PhD thesis, Technical University Munich, p. 152

[5] Hirschmüller, H. (2008): Stereo Processing by Semiglobal Matching and Mutual Information, IEEE Transactions on Pattern Analysis and Machine Intelligence, Vol. 30, No. 2, pp. 328-341

[6] http://www.di.ens.fr/cmvs/

[7] http://www.di.ens.fr/pmvs/

[8] http://ccwu.me/vsfm/

[9] Somogyi, A., Barsi, A., Molnar, B., Lovas, T. (2016): Crowdsourcing based 3D modeling, International Archives of the Photogrammetry, Remote Sensing and Spatial Information Sciences, Volume XLI-B5, pp.587-590

[10] Török, A., Bögöly, Gy., Czinder, B., Görög, P., Kleb, B., Vásárhelyi, B., Lovas, T., Barsi, Á., Molnár, B., Koppányi, Z., Somogyi, J.Á. (2016): Terrestrial laser scanner aided survey and stability analyses of rhyolite tuff cliff faces with potential rock-fall hazards, an example from Hungary, In: Reşat Ulusay; Omer Aydan; Hasan Gerçek;Mehmet Ali Hindistan; Ergün Tuncay (eds.) Rock Mechanics and Rock Engineering: From the Past to the Future: Eurock 2016, pp. 877-881

[11] Kapitany, K., Somogyi, A., Barsi, A. (2016): Inspection of a Medieval Wood Sculpture Using Computer Tomography, International Archives of the Photogrammetry, Remote Sensing and Spatial Information Sciences, Volume XLI-B5, pp.287-291

Teaching Methodology in Higher Education: present and future

Margit Horosz-Gulyás,PhD
Óbuda University, Alba Regia Technical Faculty, Székesfehérvár, Hungary
horoszne.margit@amk.uni-obuda.hu

***Abstract*— This article describe the teaching methodology in Higher Education. The aim of the paper is to display the present methodology. What can we expect in the future? Smart People - Smart University?**

I. INTRODUCTION

In the latest years the role of the universities has been changed. Its judgement, its financial background and also the education in the universities changed and also changing now. What can expect in the future? What change can we expect by the students, the teachers, the methodology, the lessons?

Everybody knows the Bologna Declaration and its effects. The grown students and the permeable education system generated lot of changes. But it is true? In my opinion the most of teachers in higher edication only try to follow these changes. Can we teach with those methods, methodology what worked in the past?

The international tendencies in education show that the traditional teacher-centred education go to student-centred education [1].

High quality and relevant higher education is able to equip students with the knowledge, skills and core transferable competences they need to succeed after graduation, within a high quality learning environment which recognises and supports good teaching.

The reform of higher education depends on the competence and motivation of teachers and researchers, yet staffing levels have often not kept pace with expanding student numbers, putting further pressure on already strained capacities. Better working conditions, including transparent and fair recruitment procedures, better initial and continuing professional development, and better recognition and reward of teaching and research excellence are essential [2].

The aim of the study to show the present methodology and compare that with the further methods. In this digital world it is necessary to recognise and prefer the student-centred education, and also important to develope the best methods (best practices) in higher education.

II. EDUCATIONAL MODELS

The traditional method is to make a course description that we start from the educational material of the course. Teachers decided that in the course, in a semester, what they want to teach, made plans about teaching methods and in the end they appreciated the students knowledges. This approach starts from the knowledge of the teacher, and as valuation it research how students could pick up the curriculum. Course description shows in this case which part of the book/study/other material the teacher will give on the lesson. This approach is called teacher-centred education.

Other model is the student-centred education. This alternative model shows what the students will know finishing a course. This approach is also called as result-based education [3].

III. EDUCATIONAL METHODS

For teacher it is a challenge to coordinate the teaching methods, the techniques of valuation, the criterions of valuation and learning outcomes. But only with this coordination can we help for students to clear the requirements.

Valuation can be formal and summa. Formal valuation is learning-based valuation. This valuation form can help for teacher and also for students that how the students get along with their studies. We use this valuation form usually at the end of the course or during the course. The benchmark of the students can help for the teacher to make good decision what is the adequate direction in teaching. For example: working on the lesson, and after that the student will give instruction and help to achieve the next task. Another example is the oral presentation from certain theme. This can help the student to improve its knowledge, and also improve its skills in communication and organization. Formal valuation is a part of teaching and not part of grading.

Summa valuation is the grading, so finishing a course the students will give a grade. This valuation form show the benchmark of the student in a certain date, and not the whole semester.

The third type of valuation is the continuous valuation, which contain both valuation methods: formal and summa. In deed that means that during a semester there are more summa valuation with grades, but the students give a few feedback from their benchmarks [2].

The different tasks for valuation banter to different learning methods (Table I).

Coordinating the learning outcomes, teaching methods, students work and valuation methods is hard for the

TABLE I.
VALUATION METHODS AND LEARNING METHODS

Valuation methods	Learning methods
Composition, essay: - homework composition - examination essay - exam using materials	memoriters, flash analysis
Objectiv test: - response test - alignment test	strategies
Benchmark valuation: - exercises - oral presentation - poster - interview - critical annotation - project-based learning - work book - case studies, problems - portfolios - small exams - mental maps - Venn-diagram - Small answers	communication, reflex, research, creative skills, information and data mining

teacher, but it can be useful the undermentioned teaching and learning task:

- presentations,
- personal working,
- laboratory,
- field work,
- group working,
- seminars,
- presentation from other students.

An adequate teaching plan can help for the student to learning more efficiently.

Different teaching methods can be grouped:

1. Based on persons
- based on teacher,
- based on student,
- based on both teacher and student.
2. Based on methods
- oral methods,
- modern techniques and methods,
- illustrative methods.
3. Based on pedagogical task
- given new knowledges,
- helping the applications.

As oral method it can be mentioned the presentation which it is in higher education frequently used method on the lessons. Also to this method can be grouped the telling and comments, these can be useful on manual trainings. Dispute is a special oral method, the aim is to improve the mind and communication and also give new informations.

The illustrative methods have two basic form: direct and indirect. Direct is e.g. the experiments, indirect is e.g. watching video.

In modern techniques and methods frequently used the project-based learning. Project-based learning hails from a tradition of pedagogy which asserts that students learn best by experiencing and solving real-world problems. According to researchers, project-based learning essentially involves the following:

- students learning knowledge to tackle realistic problems as they would be solved in the real world,
- increased student control over his or her learning,
- teachers serving as coaches and facilitators of inquiry and reflection,
- students (usually, but not always) working in pairs or groups.

Teachers can create real-world problem-solving situations by designing questions and tasks that correspond to two different frameworks of inquiry-based teaching:

- problem-based learning, which tackles a problem but doesn't necessarily include a student project, and,
- project-based learning, which involves a complex task and some form of student presentation, and/or creating an actual product or artifact.

While project-based learning has been criticized in the past for not being rigorous enough, the following features will greatly improve the chances of a project's success:

1. A realistic problem or project
- aligns with students' skills and interests,
- requires learning clearly defined content and skills (e.g. using rubrics, or exemplars from local professionals and students).
2. Structured group work
- groups of three to four students, with diverse skill levels and interdependent roles,
- team rewards,
- individual accountability, based on student growth.
3. Multi-faceted assessment
- multiple opportunities for students to receive feedback and revise their work (e.g., benchmarks, reflective activities),
- multiple learning outcomes (e.g., problem-solving, content, collaboration),
- presentations that encourage participation and signal social value (e.g. exhibitions, portfolios, performances, reports).
4. Participation in a professional learning network
- collaborating and reflecting upon PBL experiences in the classroom with colleagues,
- courses in inquiry-based teaching methods.

IV. RESEARCH METHOD

The study presents a quantitative research carried out on a sample of 200 students. The age range was between 19 and 26, proportionately from different grades, specialties and gender. The research was done from the term 2013/2014 till the term 2015/2016 at the Obuda University Alba Regia Technical Faculty (earlier University of West Hungary Faculty of Geoinformatics) among the regular students in many courses. The valuation forms were formal and summa and it was continuous. The students statisfaction was also in the research.

The methods was selected from webpage of Tempus Foundation which has huge methodogical swatch (http://www.tka.hu/tudastar_kereso). Sometimes the methods were changed, and also it was developed new methods. Not only teaching, but also valuation methods was used in the research. Also cooperative learning methods has a big literature .

TABLE II.
METHODS IN THE RESEARCH

Course name	Teaching methods
Nature protection and environmental protection	Back to the table Definition bingo Pot game Microstudy Film-culture Board game Reviews Mind mapping
Water management	Back to the table Pot game Definition bingo Microstudy Film-culture Reviews Crosswordpuzzle Amoeba (word or definition) Bluff Project-based learning
Land valuation	Reviews Pot game Group work
Natural resources and environment management	Group work Dispute Film-culture Reviews Cartoon
Land protection and land management	Reviews
Geography of Europe	Board game Cooperative learning
Land valuation cadastre	Mind mapping Group work
Land use and environmental protection	Pot game Microstudy Reviews Film-culture Dispute Cooperative learning
Land use and land valuation	Pot game Microstudy Reviews Film-culture Dispute Cooperative learning

In Table II the methods were summarized.

The background is very important using this methods. We need a good material (coursebook) and a lot of time and effort before the lessons to prepare that. For me it was also very good that sometimes the students give ideas what can be the next method. The cooperation mostly was very good, the success is based on the students. If there motivation was weak it was hard to make interesting the lessons. With ICT technologies the scale of the methods will be wider.

V. RESULTS

During the research the feedbacks were collected from the students. The result was surprising. From 10 students only one said that the task was not good, and from that he could not learn anything. Main difference was by gender. Female students made with pleasure the tasks, unfortunately the female students share in one third part of the whole students. The best practices were by the students:

- project-based learning,
- pot game,
- cooperative learning,
- film-culture.

As a teacher the best practices were:

- dispute,
- project-based learning,
- pot game,
- cooperative learning.

The summa valuation gave very good solution: 63% of the students made the exam with the grade five. Only 10% of the students had unsatisfactory mark.

The formal valuation was also successfully, the students was satisfied with the results and the problem was solved in short period.

As a teacher the application of the methods needs more time and efforts as the teacher-centred approach. Using new methods it is also necessary for the teacher because due to this method we can refresh our knowledge also (lifelong-learning). In my opinion these methods will be more important in the future. The students are changing. The Z generation (and further Alfa-generation) needs interesting teaching methods. E-learning and student-centred education leads to smart university which is one approach in EU strategies [4].

In the future it will be useful to create a web-page about the methods which can be useful in higher education, because the most website does not deal with them.

ACKNOWLEDGMENT

The author declares no conflict of interest.

REFERENCES

[1] D. Boud. R. Cohen and J. Sampson, "Peer Learning in Higher Education: Learning from and with Each Other," Sydney, Australia, 1998, 181 p.

[2] M. Horosz-Gulyás, Several Aspects of Quality in Higher Education. SAMI2016, IEEE 14th International Symposium on Applied Machine Intelligence and Informatics, Herlany, Slovakia, 2016, 333-338 p.

[3] D. Kennedy, "Tanulási eredmények megfogalmazása és azok használata," University of Cork, Nagy-Britannia, 2007, 98 p.

[4] The role of universities in Smart Specialisation Strategies. Report on joint EUA- REGIO/JRC Smart Specialisation Platform expert workshop, 2014, 32 p.

Fault tolerant power supply systems

György Györök *, Bertalan Beszedes **
* Óbuda University/ Alba Regia Technical Faculty, Székesfehérvár, Hungary,
e-mail: gyorok.gyorgy@amk.uni-obuda.hu
** Óbuda University/ Alba Regia Technical Faculty, Székesfehérvár, Hungary,
e-mail: beszedes.bertalan@amk.uni-obuda.hu

***Abstract* — In the case of difficulty accessible data collection system, is important the long-term correct operation, because it is not economical to often service it. For example, a weather monitoring, data collecting and transmission system's elements, which are far from inhabited areas. In this kind of electronic systems need to use more failure-tolerance than our day-to-day life used electronics. In this article, the focus is on the solution of an embedded system, which controls the redundant electronic power supply unit.**

I. INTRODUCTION

A. Theory

Reliability is a predicted number, which is based on collected data of the failures and calculated probability. A reliable system is does not let the system work, in case of some defined type of failure. But a fault-tolerant system, will work even if the system suffers some type of predefined failure. Failures can be single or multiple, based on design. Both in critical (like nuclear power plants) and in non-critical systems (like our example), the handling of fault-tolerance is very similar. Fault-tolerance is implemented into the system, as a combination of hardware and software.

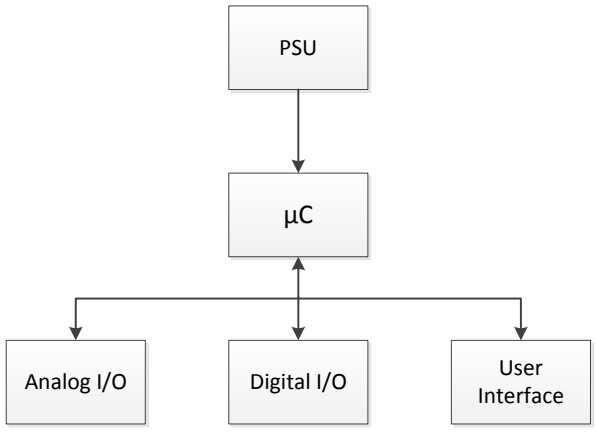

Figure 1. How conventional embedded systems are implemented

In conventional embedded systems, components and peripheries are around the microcontroller, it can be a system on chip (SoC), a printed circuit board (PCB) or separated modules (Fig. 1.). In a fault-tolerant system, the critical components are duplicated, or critical systems components are also can be multiplied. The fault-tolerance system's level is depending of the criticality of the applications. In a basic architecture are designed to handle single faults. Handling multiple faults case increasing reliability, costs and complexity.

In our example consequences can't be that serious if failure happens as an aircraft main controller failure, so we do not need to make redundancy in microcontroller level.

In our realization, we have got two parallel power supply units (PSUs are frequently failing units), and if one of them fails, their pair will take over the role (Fig. 2.). This means, at a time only one is working, and take 100% of the load, the other is waiting or it is currently being under a measurement process. With this redundancy is able to ensure the power supply fault-tolerant nature. This mode is also known as hot-stand-by mode.

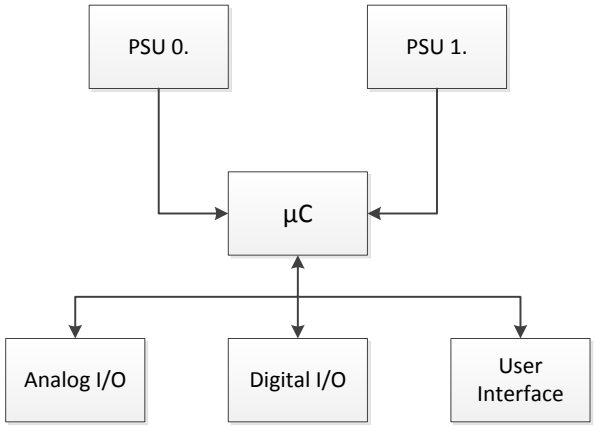

Figure 2. How duplicated PSU based fault-tolerant systems are implemented

Another solution is, when PSUs are sharing the loading current equally. If there is more than two PSU in the system, then they are sharing the load proportionally when one of the PSUs falling out from the operation. The remaining PSUs individual loads are still under 100%. For example, if there is four redundant PSU in the power supply system, and one of them suffers some failure (the monitoring system turns it off), the remaining PSUs are sharing the load equally, so instead of 25% of the loading current, they need to provide 33%. Each PSU are should be capable to provide the full loading current if it is necessary. [1]

B. System design

In redundant PSU fault-tolerant systems there are a few basic points that need to be implemented into the system, such as:

- In hot-stand-by mode or load-sharing mode, the embedded monitoring system should be able to notify the central management system about the actual condition of the PSUs or if there is a failure.
- The monitoring system need to test the PSUs in hot-stand-by mode. It should swap the PSUs periodically or use an external load.
- The power supply system should have the possibility – even in load-sharing mode – to hot-plug-in the individual PSUs, and insure the conditions of smooth running for the main system.

In a fault-tolerant system, with redundant PSUs, there are two type of the controlling system. In the first case there is only one microcontroller, then the main system controlling the main functions (like measuring, logging, communication, etc.) and also handling the power supply system (monitoring, testing and evaluating the PSUs, controlling the switching unit, etc.).

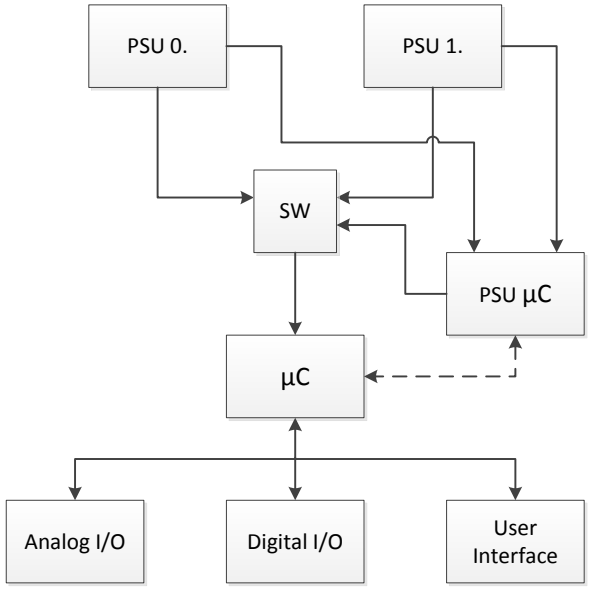

Figure 3. How duplicated PSU based fault-tolerant systems are implemented

Our system is containing duplicated power supply units, and they need to be prepared some basic functions, like measuring effectivity, temperature, etc. In our realization, the main system is do not need to explore, if one of the PSU is suffers some kind of failure, the monitoring system will find it if there is some dysfunction, and notify the main system. The monitoring system is managing the PSUs trough the switching unit. The main system will notify the central management system from the fault trough the applied communication protocol. Using them alternately, to test them time to time. The system has the feature of PSU hot-plug-in to ensures smooth running, and it also ensure uninterrupted running when the monitoring system swap the PSUs by the reason of testing or some kind of PSU failure of when the service personnel changing the PSU modules. The block diagram of the system can be seen in Fig.3.

II. REALISATION

A. Measuring the PSU condition

[2] The most common source of the problem in a power supply, is from some switching or regulating element, typically a MOSFET. It can be a stand-alone component, or a part of an other, more complex component. With power MOSFETs switching can be very fast, resulting in low switching losses, but there are still some losses. The main drawback is $R_{DS(on)}$ and its strong positive temperature coefficient.

$$T_{ep(on)} \approx 6\ldots9\cdot10^{-3}\left[\frac{1}{°C}\right], \qquad (1)$$

where $T_{ep(on)}$ is the temperature coefficient of the epitaxial layer.

The main components of on resistance $R_{DS(on)}$ include the channel, accumulation layer, drift region, and parasitic (metallization, bond wires, and package). The effect of the loading current is really weak for the $R_{DS(on)}$, as Fig.4. shows.

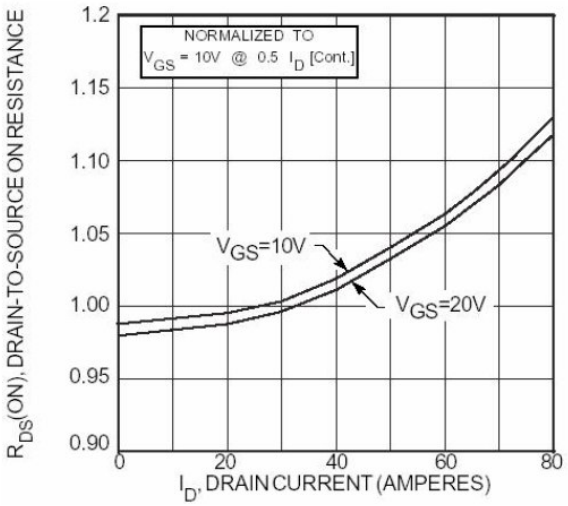

Figure 4. Drain to source on resistance vs. drain current [2]

At the other hand, temperature has a strong impact to the drain-source resistance (Fig.5.). A ΔT temperature difference cause a higher drain-source on resistance:

$$R_{DS(on)} = R_{DS(on)25}\cdot\left(1+\Delta T\cdot T_{ep(on)}\right), \qquad (2)$$

where $R_{DS(on)25}$ is the drain-source on resistance at 25°C.

If the transistor's temperature changes from 25°C to 125°C, the drain-source on resistance approximately doubles. It is able to use for a quick estimation the following correlation:

$$R_{DS(on)125} \approx 2 \cdot R_{DS(on)25}, \quad (3)$$

where $R_{DS(on)125}$ is the drain-source on resistance at 125°C.

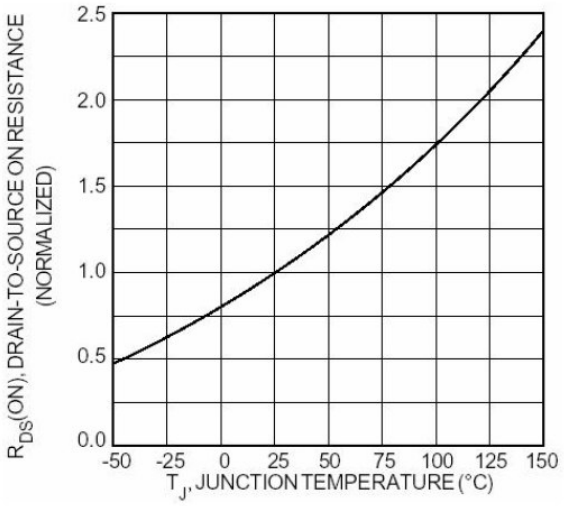

Figure 5. Drain to source on resistance vs. junction temperature [2]

The momentary power loss is depending from the flowing current and the drain-source on resistance (in ohmic range):

$$p(t) = i_D{}^2 \cdot R_{DS(on)}, \quad (4)$$

where $p(t)$ is momentary power loss and $i_D{}^2$ is the momentary drain current.

Because the drain-source on resistance will grows if the layer temperature is higher, the power loss also will grow, the efficiency will be lower.

The positive $R_{DS(on)}$ temperature coefficient is a nice feature when paralleling power MOSFETs because it ensures thermal stability. It does not however ensure even current sharing [3]. What makes MOSFETs easy to use parallelly is their relatively narrow part-to-part parameter distribution. It is advantageous to keep the gate-source voltage at the same level at all of the parallelly connected transistors, then approximately the same current will flow through them. Conversely, it is not recommended for the gates to directly connect each other, because the capacitive type gate inputs and scattered inductance can cause unwanted high-frequency vibrations. In order to avoid vibrations, it is useful to connect serially a small value damping resistors with the gate.

The monitoring system is measuring the input and output power of the PSU, by measuring the voltage and current in the primer and the seconder side of the unit. For these value it calculates the efficiency of the PSU, if this value is under a predefined level, or after multiple measurements says the unit's condition is deteriorating (the efficiency is decreasing more than the allowed slope), the monitoring system is sending an error signal to the main system, and swapping the power supply units.

B. The switching unit

The monitoring system controlling the switching unit to choose one of the PSUs, to supplies power to the main system. The switching unit is containing switching elements. In practice, these are MOSFETs, these are fast and simple to use components.

As any other components MOSFETs also can go out of order. In the first case it can go to short-circuit (it can't be turn off), and at the other hand, it can go to connection-cut (it can't be turn on). Both way can cause some malfunction in the operation of the system.

To increase the fault-tolerance level of the switching unit, it need to be increase the number of the switching components. If there are multiple the number of the MOSFETs, the probability of some type of faulty is much lower.

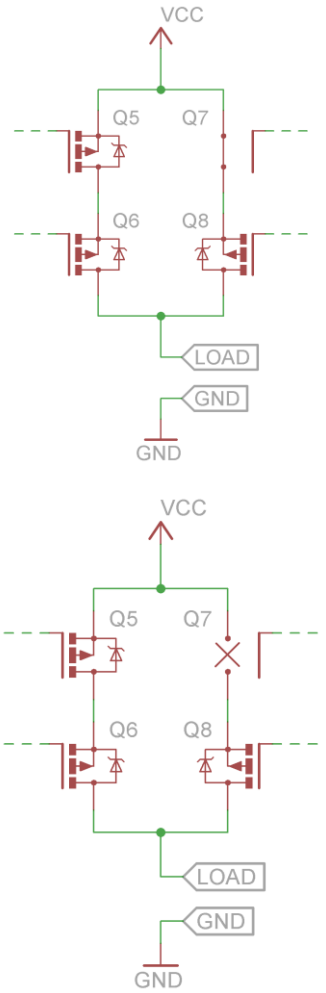

Figure 6. Example for redundant switching components and their fault-tolerance behavior in different type of faults

If there is two serially connected MOSFETs instead of one, and the one of it goes to short-circuit (it does not matter which), then the switching unit is still working properly, because, the other MOSFET can turn on and turn off the line. But, if one of the MOSFETs goes to connection-cut, the line can not be turn on again.

If there is two parallel line, which each are contains two serial MOSFETs, then, if one of the MOSFETs suffers a connection-cut, the other – the parallel – line can take the load, and the switching element still can work properly (see at Fig.6.).

In the switching unit, in one switching element, all of the switching devices (the MOSFETs) are controlled parallel.

When switch-over the PSUs, there is a short period of time, when none of the PSUs are connected to the main system. To avoid blackout, it is need an energy storage device. Practically a capacitor, this allows a smooth switching.

III. A Introduction of Hardware and Software

A. Measuring the PSUs

To determine the goodness of the PSU, is based on calculating the efficiency. If the efficiency drop down, then it is a sign for a future failure (it can cause higher internal resistance for example). To calculate the efficiency, it is need to measure the input and the output power.

In our example we use a DC-DC power supply, and measuring the voltage and the current as well. The voltage measurement is based on a voltage divider, and after a protecting circuit, the microcontroller is measuring it, with an inner ADC periphery. For the current measurement, a hall sensor provides the measured analogue voltage which is proportional to the flow through current. After the measurement of the primer and seconder side, the efficiency is easily calculable.

The monitoring system is carrying out measurements. If the efficiency is dropping under a predefined level, or after compared to the previous measured values and the slope of the efficiency change is too high, the monitoring system will swap the PSUs, and send an error message to the main system, and also the type of the fault.

B. Faults of the PSUs

There is other type of faults that the PSU can suffer, and can be harmful for the main system. The monitoring system is prepared to recognize the next ones (Fig.7.): over current; over and under voltage; voltage fluctuations, voltage ripple, unstable voltage output and no voltage output.

C. The prototype and the program

The modell of the system and the develoopong area can be seen at Fig.8. The monitoring system is implemented to an AVR microcontroller. The program is written a C based programming language.

To setting the parameters of the monitoring system is allowed, it can be set all the measuring parameters and the periodicity of the measures, also can turn on and off the other tile of failure checking, and the error messages. The flowchart of the monitoring program is visible at Fig.9.

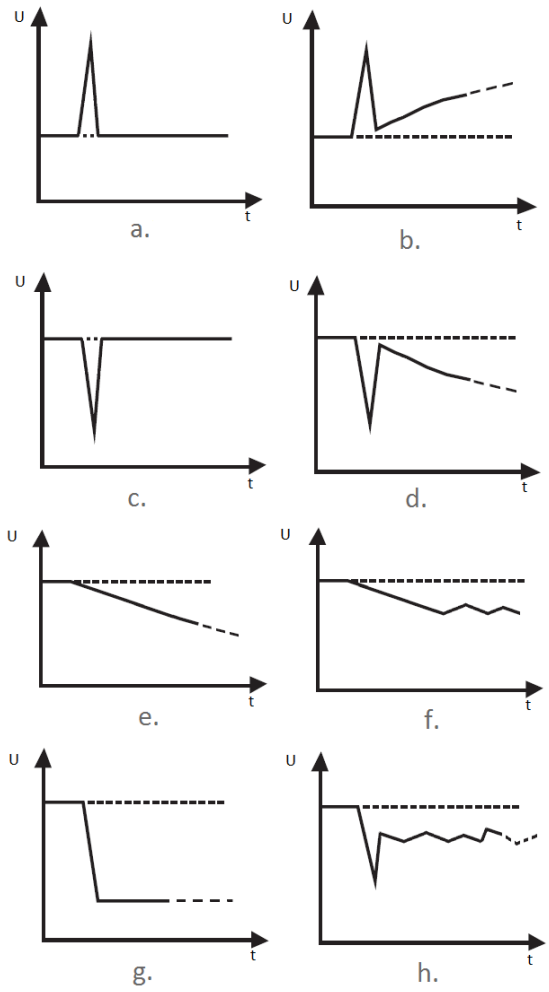

Figure 7. Possible faults of a power supply output:
a.) After a voltage peak, the output voltage returns to normal level;
b.) After a voltage peak, the output voltage stays high level;
c.) After a voltage drop, the output voltage returns to normal level;
d.) After a voltage drop, the output voltage stays low level;
e.) The output voltage continuously decreasing and stays low level;
f.) The output voltage continuously decreasing and gets unstable;
g.) The output voltage after a rapid drop down, stays low level;
h.) The output voltage after a rapid drop down, becomes unstable.

IV. Conclusion

In this paper, after checking the theoretical solutions, we have presented a useful real application. Valuable part of our work is, that we show the system component and programming solutions.

The redundant electronical solutions provides a consistent, reliable operation, by the cooperation of a micro-controller based embedded system. By the mentioned solution, the error-free running time can be increase.

We believe that the developed method can also use in other areas.

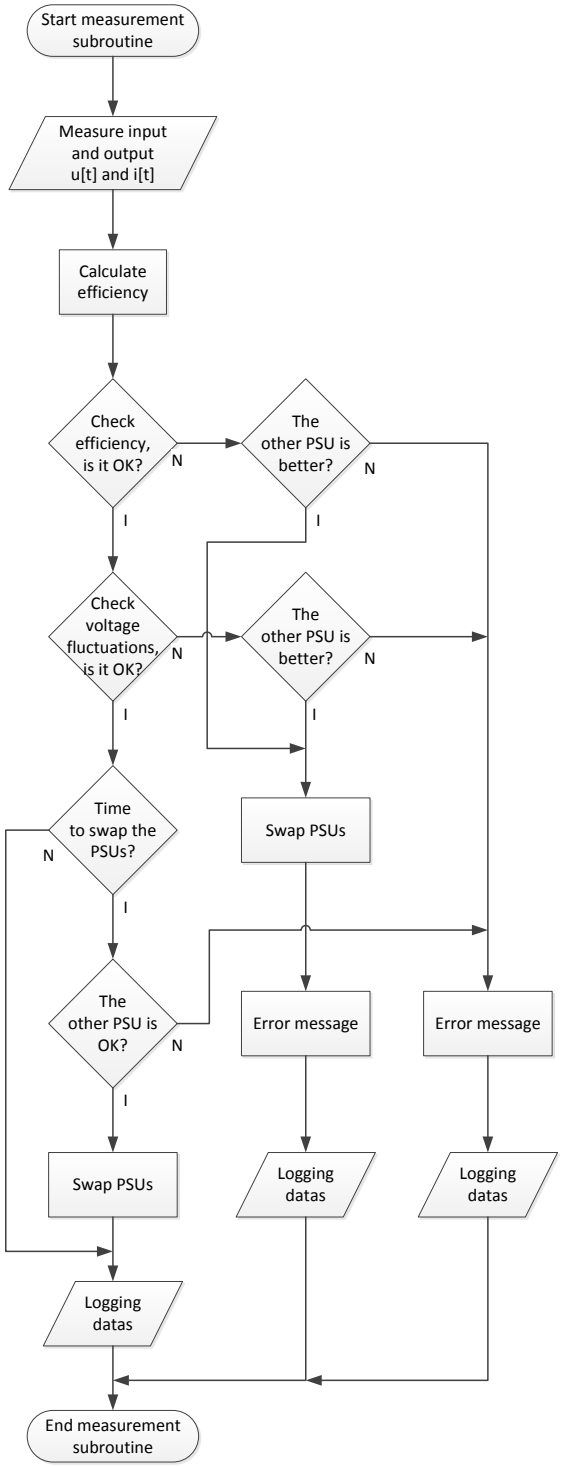

Figure 9. The flowchart of the monitoring program

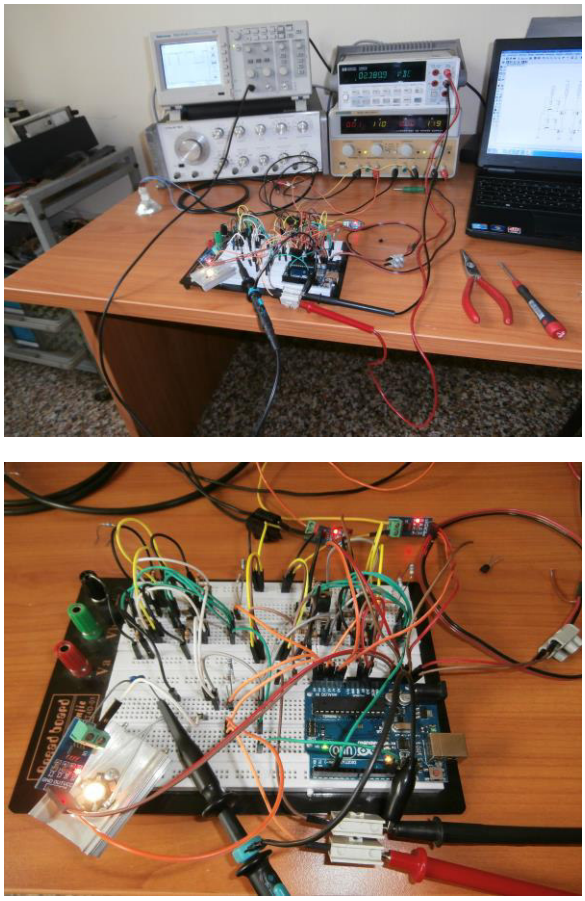

Figure 8. The development area and the model of the circuit

REFERENCES

[1] Power MOSFET Tutorial, Jonathan Dodge, P.E., Advanced Power Technology, Bend, Application Note, APT-0403 Rev B, March 2, 2006

[2] R. Severns, E. Oxner; "Parallel Operation of Power MOSFETs", technical article TA 84-5, Siliconix Inc.

[3] N. Mohan, T. Undeland, W. Robbins; "Power Electronics – Converters Applications, and Design", text book published by Wiley

[4] Gyorok, Gyorgy. Embedded hybrid controller with programmable analog circuit. *Intelligent Engineering Systems (INES), 2010 14th International Conference on*. IEEE, 2010.

[5] Gyorok, Gy. *The FPAA realization of analog robust electronic circuit.* Computational Cybernetics, 2009. ICCC 2009. IEEE International Conference on. IEEE, 2009.

[6] Gy. Györök. A-class amplifier with FPAA as a predictive supply voltage control. Proc. 9th International Symposium of Hungarian Researcherson Computational Intelligence and Informatics (CINTI2008), pages 361–368, November 2008.

[7] Kopják J. Kovács J. *Compering event-driven program models used in embedded systems.* AUTOMOTIVE-ENTWICKLUNGEN UND TECH-NOLOGIEN 2011 (2011): 90-95.

[8] J. Kopják. Dynamic analysis of distributed control network based on event driven software gates. IEEE 11th International Symposium on Intelligent Systems and Informatics, Subotica, Serbia, ISBN: 978-1-4673-4751-8:p. 293–297, 2013.

[9] J. Kopják and J. Kovács. Implementation of event driven software gates for combinational logic networks. IEEE 10th Jubilee International Symposium on Intelligent Systems and Informatics, Subotica, Serbia, ISBN: 978-1-4673-4751-8:p. 299–304, 2012.

[10] Gy. Györök, M. Makó. Configuration of EEG input-unit by electric circuit evolution. Proc. 9th International Conference on

Intelligent Engineering Systems (INES2005), pages 1–7, September 2005.

[11] Gy. Györök, M. Makó, J. Lakner. Combinatorics at electronic circuit realization in FPAA. Acta Polytechnica Hungarica, Journal of Applied Sciences, 6(1):151–160, 2009.

[12] Gy. Györök. The function-controlled input for the IN CIRCUIT equipment. Proc. 8th Intelligent, Engineering Systems Conference(INES2004), pages 443–446, September 2006.

[13] Gy. Györök. Self configuration analog circuit by FPAA. Proc. 4th Slovakien – Hungarien Joint Symposium on Applied Machine Intelligence(SAMI2006), pages 34–37, January 2006.

[14] Gy. Györök. Crossbar network for automatic analog circuit synthesis. Proceedings (Liberios Vokorokos, Ladislav Hluchý, János Fodor szerk.) of the IEEE 12th International Symposium on Applied Machine Intelligence and Informatics (SAMI 2014). IEEE Computational Intelligence Society, Budapest: IEEE Hungary Section, ISBN:978-1-4799-3441-6, pages 263–267, January 2014.

[15] K. Lamár and Veszprémi K. A mikroszámítógépek térnyerése a villamos hajtások szabályozásában. Proceedings of the Kandó Conference 2002, Budapest, Hungary, pages 1–7, January 2002.

[16] K. Lamár and J. Neszveda. Average probability of failure of aperiodically operated devices. Acta Polytechnica Hungarica, 10.(8.):pp. 153–167, 2013.

[17] A. Pilat and J. Klocek. Programmable analog hard real-time controller [programowalny sterownik analogowy]. Przeglad Elektrotechniczny, 89(3 A):38–46, 2013. cited By (since 1996) 0.

[18] J. Tick. User interface redesign based on user behavior analyses. Proc. of ICCC 2003 IEEE International Conference on Computational Cybernetics (ICCC2003), pages 29–31, October 2003.

[19] L. Vokorokos, N. Ádám, and B. Madol. The process control for p-single operators. 19th International Workshop on Robotics in Alpe-Adria-Danube Region, RAAD 2010 - Proceedings, pages 119–123, 2010

Determination of the surface deformation during the eruption of the Sakurajima volcano in February, 2016

Gergely LÁSZLÓ*, Lóránt FÖLDVÁRY*,**
* Óbuda University, Alba Regia Technical Faculty, Institute of Geoinformatics, Székesfehérvár, HUNGARY
** Hungarian Academy of Science, Research Centre for Astronomy and Earth Science, Geodetic and Geophysical Institute, Sopron, HUNGARY
laszlo.gergely@amk.uni-obuda.hu, foldvary.lorant@amk.uni-obuda.hu

***Abstract*—The present study provides an estimate of the vertical movements due to the most recent eruption of the Sakurajima volcano. The motion has been derived by using the InSAR technology; the paper gives an overview of the used data and applied methodology in details aiming to present sufficient information for providing a base for the reproducibility of the results. The observed vertical displacements are found to be reliable consequences of the eruption.**

I. INTRODUCTION

In April 03, 2014 a new era has begun in space-borne geodesy and remote sensing, with the launch of the Sentinel-1A satellite [1] in a joint Copernicus program of European Space Agency (ESA) and European Union (EU). The initial mission plans have contained three Sentinel series (1-3), with three satellite each (A, B, C), but after the first launch, a new satellite (Sentinel-1D) and three more series (4-6) has been added to the mission, which are scheduled to be launch after 2020 [2].

In this paper data produced by Sentinel-1A has been used. The main technical parameters are listed in Table 1 based on [1].

Apogee	693 km
Orbit regime	SSO (Sun-synchronous Orbit)
Inclination	98.18°
Period	98.6 minutes (175 orbit/cycle)
Repeat cycle	12 days
Mission duration	7 years, consumables for 12 years
Mission objectives	atmosphere-, marine- and land-monitoring, climate change, emergency management and security.

Table 1. Sentinel-1A data sheet [1]

Using the state-of-the-art vertical monitoring method, the Synthetic Aperture Radar Interferometry (InSAR) technology [3], a wide range of applications ranging from monitoring vertical displacement of discrete points, through monitoring movements of buildings, to observation of crustal movements on continental scale becomes feasible [4]. The SAR technology is an active remote sensing method [5], and as such, it is independent from the daytime cycle. The satellite radar interferometry is based on comparing one or more radar image. Using the phase values of the images phase differences can be derived, which are then interfered at the steady (i.e. being in no motion) areas. Based on the interferences, an interferogram can be deduced to estimate the amount of vertical movement at the area of interest [6].

II. CASE STUDY: SAKURAJIMA

The subject of this study is the determination of vertical displacements of the surface around the Sakurajima volcano before and after its eruption on 2016-02-05 [7], c.f. Figure 1. The volcano is located on the 3rd largest island of Japan, Kyushu (Figure 2), and is one of the most active volcanoes in Japan, performing several lava eruptions each year. The Sakurajima is a post-caldera volcano belonging to the Aira caldera in the northern half of Kagoshima Bay.The 17 x 23 km caldera has been formed about 22,000 years ago, which has been joined to the Osumi Peninsula during the major explosive and effusive eruption of 1914 [8].

Figure 1. Eruption of the Sakurajima

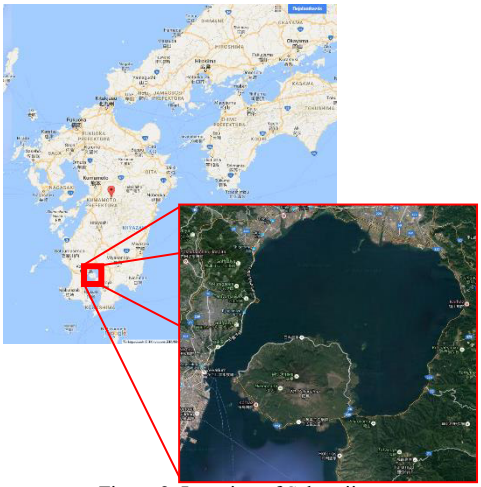

Figure 2. Location of Sakurajima

III. DATA PROCESSING

The data processing has been carried out by using an open-source software provided by the ESA, jointly developed by Brockmann Consult, Array Systems Computing and C-S for processing images of orbiting Sentinel satellites [9]. In this case data from the Sentinel-1A has been used, and most of the processing steps has been carried out with the Sentinel-1 Toolbox of the Sentinel Application Platform (SNAP) [9].

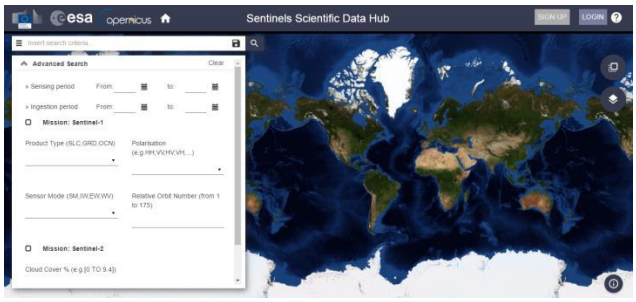

Figure 3. Scientific data hub

Two kind of data is available at the Sentinel Scientific Data Hub site (c.f. Figure 3): the SLC and the GRD. The SLC contains phase and amplitude values, while the GRD contains amplitude only. The present task has been done by using the SLC data as for the InSAR technique phases are the key information.

During the selection of SLC data, it is important to choose files 12 days apart from each other, otherwise the processing will not be possible [10]. The reason of this limitation is that the overlap between the images is only in every 175th full orbit complete [3]. As the most reliable information on vertical deformation can be derived from the vertical-vertical (abbr. VV) polarization [10], it has been set for the download. The time interval has been set between November 2015 and March 2016, and the area has been defined by a user-defined rectangular window. The search criteria are summarized in Table 2, and it has resulted in 7 images. Among them, 6 have been used, at the epochs summarized in Table 3.

Sensing period:	2015/11/01-2016/03/31
Satellite Platform:	S1A_*
Product Type:	SLC
Polarization:	VV
Relative Orbit Number:	163

Table 2. Search parameters

The most of the processing has been performed with the Sentinel-1 Toolbox of the SNAP software, apart from the determination of the vertical deformation map from the interferogram, which can be performed in an independent step with the use of the Statistical-Cost, Network-Flow Algorithm for Phase Unwrapping (SNAPHU) program. The major steps of the processing are as follows:

1. S1 TOPS Coregistration
2. Interferogram formation
3. S1 Tops Deburst
4. Topographic phase removal
5. Goldstein Phase Filtering
6. Phase Unwrapping
    a. Snaphu export
    b. Unwrapping
    c. Snaphu import
7. Phase to Displacement
8. Update Geo Reference
9. Ellipsoid Correction

During the *S1 TOPS Coregistration* step the master and slave images has been set. Every image (ref frame on Figure 4) contains three subsequent *Sub-swath*s (middle white frame on Figure 4), thus another selection has been made to choose that which part is the area should be processed. If necessary, the location can further be narrowed by using the tool *Bursts* (small white frames on Figure 4).

Date	Image filename
2015-11-28	S1A_IW_SLC__1SSV_20151128T211657_20151128T211724_008810_00C921_4D03
2015-12-22	S1A_IW_SLC__1SSV_20151222T211656_20151222T211723_009160_00D2EC_39F8
2016-01-15	S1A_IW_SLC__1SSV_20160115T211655_20160115T211722_009510_00DCEC_EE4A
2016-02-08	S1A_IW_SLC__1SSV_20160208T211654_20160208T211721_009860_00E70E_94CB
2016-03-03	S1A_IW_SLC__1SSV_20160303T211654_20160303T211721_010210_00F131_DF13
2016-03-27	S1A_IW_SLC__1SSV_20160327T211655_20160327T211722_010560_00FB2D_9908

Table 3. Images used during processing

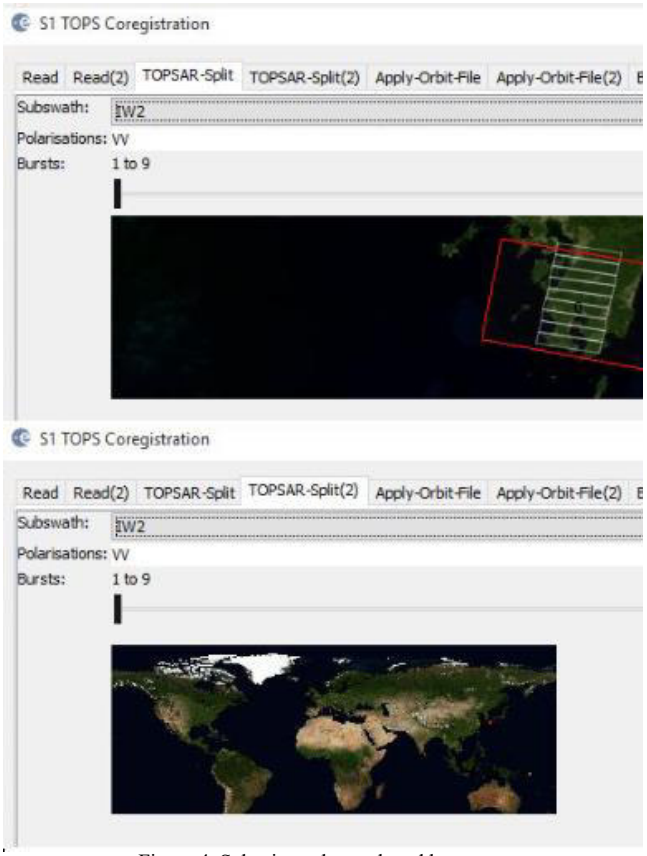

Figure 4. Selecting sub-swath and bursts

The selection shown on Figure 4 for the day 2015-12-22 provides the actual raw image shown on Figure 5, presenting the 9 bursts with interruptions (horizontal black lines) of the phase data (grey colors).

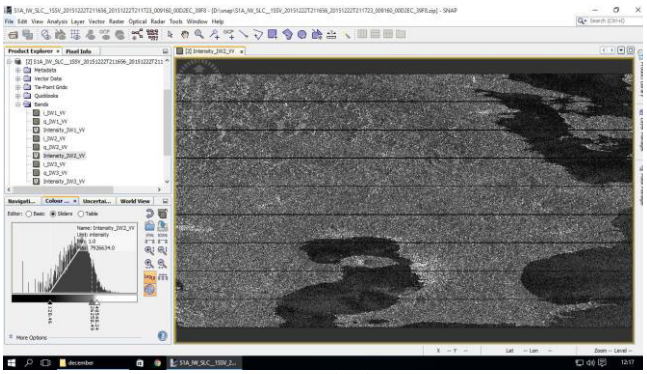
Figure 5. raw image on the day 2015-12-22

At the *Apply-Orbit_File* option *Sentinel Precise* has been set. The last setting here for the Elevation Correction is *Back-Geocoding*, where *SRTM 3Sec* has been chosen.

During the next step, the Interferogram formation, the following corrections are applied [11]:

- $\Delta\phi_{flat}$: phase correction for the Earth curvature (often named as *flat Earth phase*),
- $\Delta\phi_{elevation}$: phase correction due to topography,
- $\Delta\phi_{displacement}$: surface deformation correction,
- $\Delta\phi_{atmosphere}$ phase correction accounting for atmospheric differences,
- $\Delta\phi_{noise}$: phase noise correction generated by temporal change of the scatterers, varying look angle, and volume scattering.

The corrections are simply summed to a correction term, $\Delta\varphi$

$$\Delta\varphi = \Delta\varphi_{flat} + +\Delta\varphi_{displaceent} + \Delta\varphi_{atmosphere} + \Delta\varphi_{noise}$$

where:

$$\Delta\varphi_{flat} = -\frac{4\pi}{\lambda}\frac{B_n s}{R\tan\theta}$$

$$\Delta\varphi_{elevation} = -\frac{\Delta q}{\sin\theta}\cdot\frac{B_n}{R_0}\cdot\frac{4\pi}{\lambda}$$

$$\Delta\varphi_{displaceent} = +\frac{4\pi}{\lambda}d$$

In these equations B_n is the normal baseline, R_0 is the radar-target distance Δq is altitude difference, s is slant range displacement and θ is the radiation incidence angle with respect to the reference. (For the geometrical representation of some of these quantities, see Figure 6.)

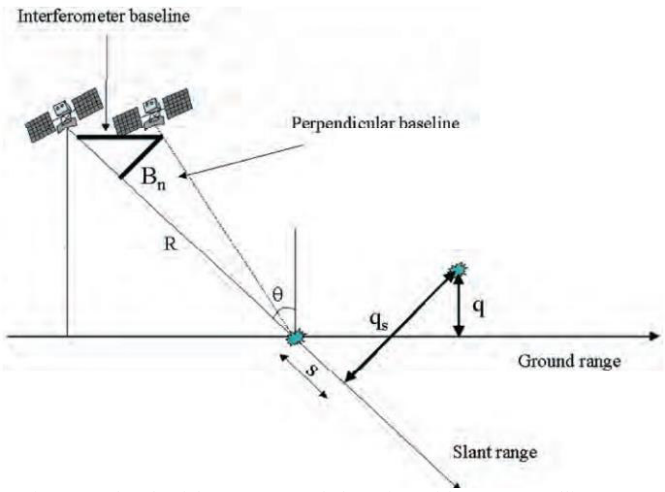

Figure 6. Sketch of the geometry of observing with a SAR satellite for the use of the InSAR technology. [12]

During *S1 Tops Deburst* step, the neighboring stripes are merged into one image, diminishing the bursts appearing on Figure 7.

Topographic phase removal is the subsequent step, which is based on a reference DEM (it can be defined arbitrarily, default setting is SRTM). Based on the DEM and the position of the satellite, the phases are simulated and considered to be a reference phase, which is therefore eliminated (c.f. Figure 7). The colors on Figure 7 are related to different values of phase ranging from 0 (red) to 2π (blue).

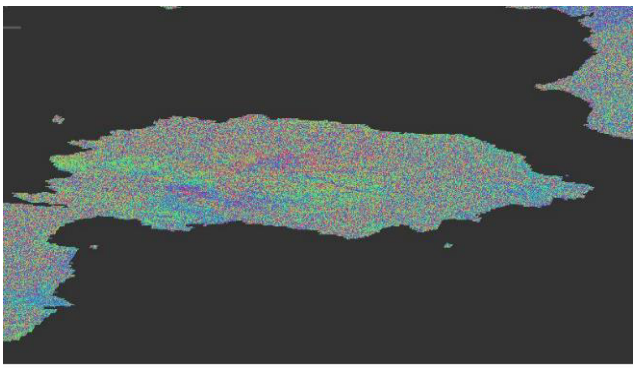

Figure 7. Phases after topographic phase removal (red=0 blue=2π).

The dotty characteristics of Figure 7 are a consequence of loss of coherence. The loss of coherence occurs due to temporal and geometric decorrelations, volume scattering and processing errors. This noisy feature can be reduced by applying *Goldstein Phase Filtering*, resulting on a much smooth image, c.f. Figure 8.

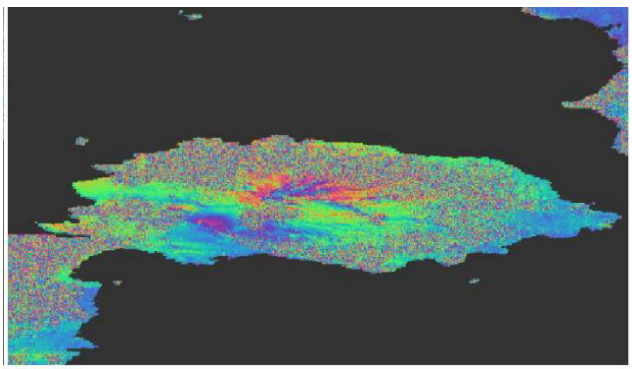

Figure 8. Phases after the Goldstein filter has been applied (red=0 blue=2π).

The interferometric phase on Figure 8 is ambiguous, since it is only known in the interval of 0 to 2π. In order to convert the interferometric phase to the topographic height, the so-called *Phase Unwrapping* should be performed, i.e. the phases must be extracted („unwrapped"). For this step, the images can be processed in a separated software (SNAPHU) and for this, exporting then importing of the date is necessary.

Phase to Displacement is a function to convert phases in radian to vertical displacement in meters.

In order to transform the results into geographical coordinate system, two other function, the *Update Geo Reference* and the *Ellipsoid Correction* should be used. The final results of the vertical deformation are presented on Figure 9 and Figure 10. On Figure 9 the surface deformation between 15 January and 8 February is shown, while Figure 10 display the vertical change between 8 February and 3 March.

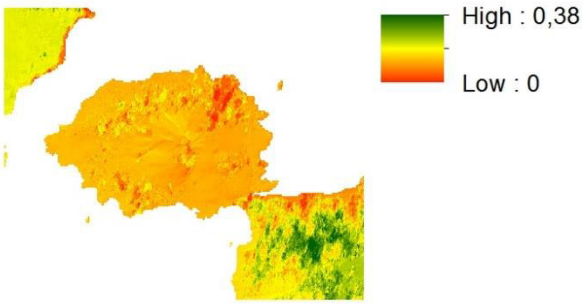

Figure 9. Surface deformation between 15 January, 2016 and 8 February, 2016.

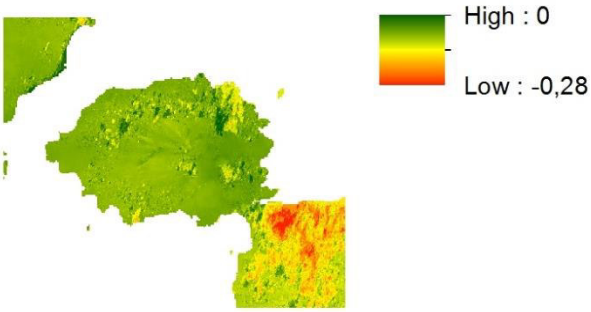

Figure 10. Surface deformation between 8 February, 2016 and 3 March, 2016.

IV. Results

As the eruption has been occurred in 5 February, 2016, Figures 9 and 10 are reliable snapshots of the surface deformations before (Figure 9) and after (Figure 10) of the eruption. In fact, there is a 3-day time lag between the eruption (5 February) and the scan of the middle image (8 February), which leaves sufficient time for near real time relaxations, thus present comparison can be interpreted as long-term relaxations of the ground.

A classical method for monitoring crustal deformation of a volcano in order to predict eruptions is the observation of the slope angle or tilt of the ground in the vicinity of the volcano [13]. Obviously, when the magma pushes the ground upward, the slope of the nearby areas tilts away from the center of uplift. This happens before the eruption. Similarly, when the ground subsides due to

depressurization of the magma chamber, the slope of neighboring areas tilts toward the center of subsidence. The leave of high pressure gases (and some magma) from the magma body definitely results in depressurization of the region. Thus uplift before the eruption and subsidence after the eruption may be expected.

According to Figures 9 and 10, before the eruption the uplift of the curst has reached an approximate average value of *+15 cm*, and the subsidence of the region after the eruption reached the average value of *-7 cm*. This 22 cm change in surface elevation is reliable according to the overall analysis of [14], which has found eruption related surface deformation to be in similar range.

Tilt measurements and increasing seismic activity provides a good base for prediction, but these techniques may provide no information on the eruption-related surface deformations. Measurement of surface deformation of this amount with repeated leveling measurements may be challenging, since the magma chamber is extended far beyond the area of the volcano, so no fix benchmarks in the nearby are available. For the purpose, the InSAR technique was found to be a competent tool.

ACKNOWLEDGMENT

The authors would like to express their gratitude to prof. László Bányai for the valuable support and consultations, and also for providing an access to the processing facility at the Geodetic and Geophysic Institute of MTA CSFK.

REFERENCES

[1] Sentinel-1: ESA's Radar Observatory Mission for Copernicus Operational Services, *S1 Data Sheet*, homepage: http://esamultimedia.esa.int/docs/S1-Data_Sheet.pdf, retrieved 2016-10-18.

[2] ESA, Copernicus: Observing the Earth, homepage: http://www.esa.int/Our_Activities/Observing_the_Earth/Copernicus/Overview3, retrieved 2016-10-18.

[3] L. Bányai, E. Szűcs, J. Kalmár, I. Eperné Pápai, D. Bán, "Az InSAR technológia alapjai és a reflektáló felületek jellemzői", *Geomatikai Közlemények*, vol. XVII, pp. 59-68, 2014.

[4] M. Simons and P. A. Rosen, "Interferometric Synthetic Aperture Radar Geodesy", *Treatise on Geophysics*, vol. 3, pp. 391-446, 2007.

[5] A. Moreira, P. Prats-Iraola, M. Younis, G. Krieger, I. Hajnsek, K.P. Papathanassiou, "A tutorial on synthetic aperture radar". IEEE Geoscience and Remote Sensing Magazine. vol. 1, pp. 6-43, 2013. doi:10.1109/MGRS.2013.2248301

[6] R. F. Hanssen, "Satellite radar interferometry for deformation monitoring: a priori assessment of feasibility and accuracy", International Journal of Applied Earth Observation and Geoinformation, vol. 6, pp. 253–260, 2005.

[7] Sakurajima volcano in Japan erupts: Lava rolls down mountain's slope and smoke billows into sky after eruption in southern Japan, *The Guardian*, Associated Press, 5 February 2016, link: https://www.theguardian.com/world/2016/feb/05/sakurajima-volcano-japan-erupts, retrieved 2016-10-18.

[8] Sakurajima at the Global Volcanism Program, *Smithsonian Institution National Museum of Natural History*, link: http://volcano.si.edu/volcano.cfm?vn=282080, retrieved in 2016-10-18.

[9] Sentinel-1 Toolbox of the Sentinel Application Platform (SNAP), available at the Science Toolbow Exploitation Platform (STEP); link: http://step.esa.int/main/toolboxes/snap/, retrieved 2016-10-18.

[10] L. Bányai: private discussion, 2016.

[11] L. Veci, "Sentinel-1 Stripmap Interferometry: Sentiel-1 Toolbox Interferometry Tutorial", Array Systems Computing Inc., pp. 41, 2015.

[12] K Fletcher (ed.), "InSAR Principles: Guidelines for SAR Interferometry Processing and Interpretation (TM-19, February 2007)", ESA Publications, ESTEC, Postbus 299, 2200 AG Noordwijk, The Netherlands, pp. 48, ISBN: 92-9092-233-8, ISSN: 1013-7076, 2007.

[13] M. Battaglia, P. F. Cervelli and J. R. Murray, "Modeling Crustal Deformation near Active Faults and Volcanic Centers — A Catalog of Deformation Models", Techniques and Methods 13–B1, Chapter 1 of Section B: Modeling of Volcanic Processes, Book 13: Volcanic Monitoring, U.S. Department of the Interior, U.S. Geological Survey, Reston, Virginia, pp. 108, 2013.

[14] J. Biggs, E. Robertson and K. Cashman, "The lateral extent of volcanic interactions during unrest and eruption", Nature Geoscience, vol. 9, pp. 308–311, doi:10.1038/ngeo2658, 2016.

Analysing the pyramid representation in one arc-second SRTM model

G. Nagy*
*Óbuda University, Alba Regia Technical Faculty, Institute of Geoinformatics
nagy.gabor@amk.uni-obuda.hu

***Abstract*—The pyramid representation is an important and popular method in the storage of image data. The lower resolution index images are very useful in displaying the image and several spatial analysis. This paper studies these properties of the pyramid images in the one second resolution SRTM elevation model. In addition to the usual mean-based pyramid representation, I studied the minimum and maximum pyramids.**

***Index Terms*—pyramid representation, DEM, SRTM**

I. Introduction

The pyramid images are a well-known method in the digital image processing. [1], [2] Lower resolution images are created from these original image data, and this images are used in some cases. For example, when an image must be showed in the screen, the program use the pyramid image, which resolution is the nearest to the map resolution in the screen.

The resolution of an image of the pyramid index is the half of the next level of the index. These are $1/2$, $1/4$, $1/8$, ... $1/2^n$ resolution of the original image. The size of the images is $1/4$, $1/16$, $1/64$, ... $1/2^{2n}$ part of the size of the original image. The total size of this pyramid images is the $1/3$ part of the original image.

The pyramid images like index can be used with digital elevation models (DEM) [11], the different resolution DEM grids are used in different cases. The DEM grids are similar to the digital images. Both of these datasets are a two dimensional array of the numbers.

The pyramid index has more kinds depending on the method, that calculates the values of the cells of the derived lower resolution images. The Gaussian pyramid uses Gaussian average, the steerable pyramid uses steerable filter. The Laplacian pyramid is similar to the Gaussian pyramid, but it does not store different images in different levels. These method represented in this article is suitable to compress the image data, instead of the data growth.

II. Pyramid representation with DEM data

The raster (image) data and the DEM grid data are similar in the data storage, because both of them are a two dimensional array, but the georeference of these arrays are different. The raster data contain rectangles, and the DEM data contain nodes of a grid.

The pyramid data even contain rectangles, if the original data contain the nodes of a grid. The rectangles of the first level of the pyramid is based on the 3×3 nodes of the grid (see on the Figure 1.).

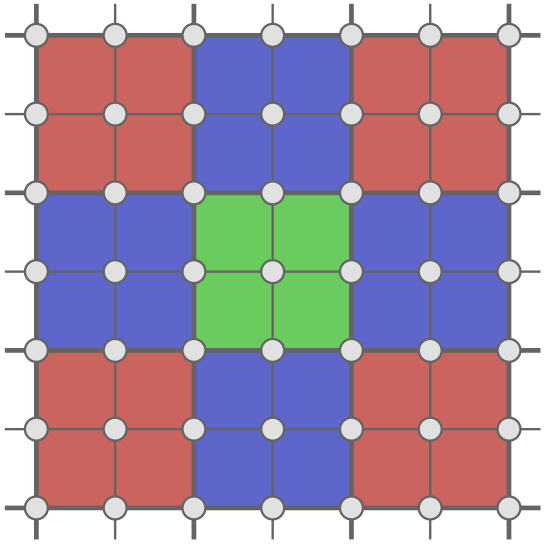

Figure 1. The first level of pyramid, based on a GRID.

The values of the first level pyramid can be calculated with the weights of the Figure 2. The result of this calculation is the average elevation of the area of this 2×2 rectangle (raster) of the grid, which will be one element of the first level pyramid. The other levels of the pyramid will be calculated by simple arithmetic mean. (With 0.25 weight in each raster of the last pyramid.)

The mean of the values of the pyramid rasters are same: the average elevation of the area of the raster. These pyramids are useful to calculate the volume under the elevation surface. This volume under a raster of a pyramid can be calculated by the multiplication the average elevation (the value of the raster) and the area of the raster (the square of the raster resolution, that constant in a pyramid level).

III. Minimum and maximum pyramids

The values of the pyramid rasters can be the minimum or maximum values instead of the average value. The values of this pyramid rasters provides the lower and higher elevation of the area of the raster. These data with the position of the raster assign a bounding box of a part of the elevation surface.

Logically, this inequalities are true:

$$MIN_{UP} \leqq MIN \leqq ELEV \leqq MAX \leqq MAX_{UP}$$

where MIN and MAX are the minimum and maximum values of a raster of the pyramid, the $ELEV$ is the elevation

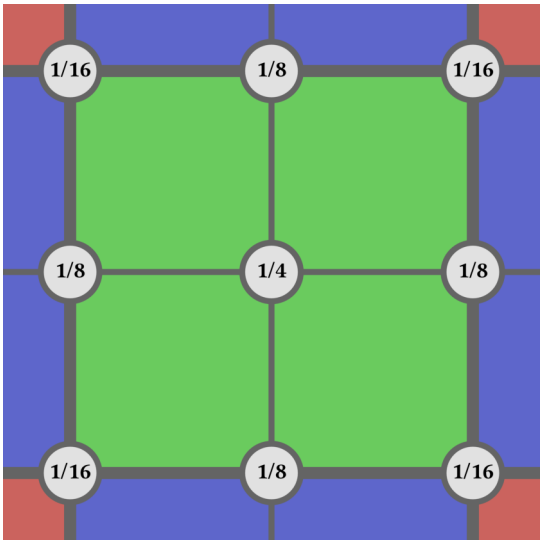

Figure 2. The weights of the first level of the pyramid.

of any point of the DEM surface in the area of the raster, and the MIN_{UP} and MAX_{UP} are the minimum and maximum values of the related raster in the upper level of the pyramid.

The first level of the minimum and maximum pyramids contains the minimum and maximum values of the nine related nodes (see in the Figure 2.) of the grid. The next levels of the pyramid contain the maximum and minimum values of the four related raster of the upper level of the pyramid.

IV. Application of minimum and maximum pyramid data

The minimum and maximum pyramids can be used in viewshed analysis [5], [4], [3], [10]. The classical method of the viewshed analysis checks each elements of the elevation model along the line that joins the viewpoint and the examined point. The number of the steps of this process is proportional to the length of this line, because the number of the examined elements of the elevation model is proportional to the length of the line.

The viewshed analysis can be faster, if the minimum and maximum pyramids are used. One element of a pyramid dataset can decide that a (3 dimensional) line crosses or does not cross the surface of the elevation model in the area of the element. If it can not decide, the process can continue in the lower level of the pyramid recursively.

A line crosses a part of a surface, if any endpoint of the line segment is under the bounding box of the surface's part. (The red lines in the Figure 3.) The line segment is the part of the line, that crosses the horizontal projection of the bounding box. If both of the endpoints of the line segment are over the bounding box, the line does not cross the surface. (The green line in the Figure 3.) The other cases need the test of the bounding boxes of the lower level of the pyramid recursively. (The blue lines in the Figure 3.)

When the program tests recursively the bounding boxes of the lower level pyramid, it does not need check all of the four bounding boxes. The Figure 4. presents some typical layout of the line segments and bounding boxes of the lower level.

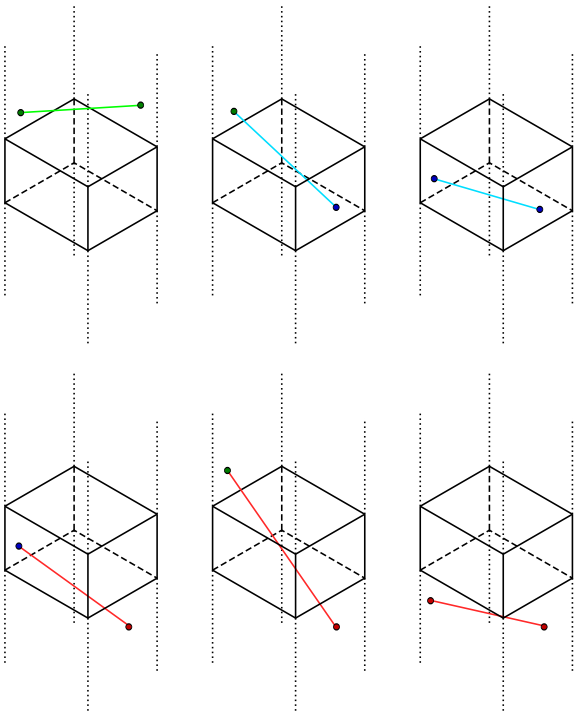

Figure 3. Intersection of a line segment and a bounding box.

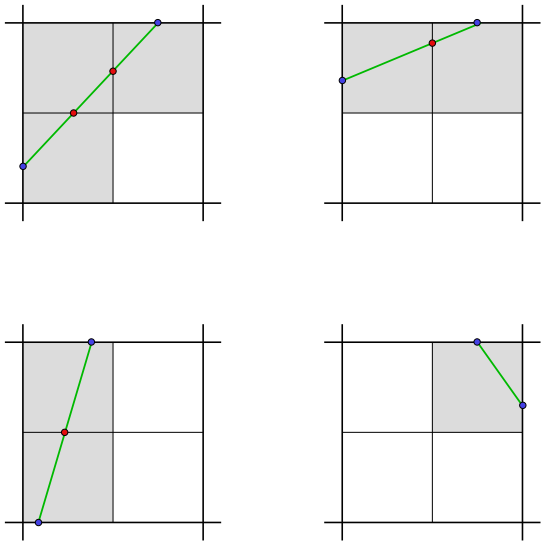

Figure 4. Intersection of a line and the pyramid cells.

V. Study of the one arc-second SRTM dataset

I studied the pyramid data structures with the one arc-second SRTM [6], [7], [9] dataset. This is a global elevation model with around 30 meters (one arc-second) resolution. This dataset was ideal for my research, because it is free and available from different places of the world. I could try the following tests in several type of territories.

I wrote an Python [8] application that reads the SRTM data, and calculate the pyramid data. Another Python applications analyze this pyramid data.

I studied the distribution of the difference between the minimum and the maximum values in different pyramid levels.

I made this analysis in different areas. The areas are in the Table I. My program create the bounding boxes from the pyramid data, and calculate some statistical values of the heights of this bounding boxes (the difference between the minimum and the maximum values). The data from the analysis are in from Table II. to Table VIII.

VI. Conclusion

The pyramid images can be a useful tools in digital elevation models in several spatial analysis. The classical mean-based index is capable of calculate the volume under the surface of the elevation models.

The minimum and maximum pyramids can be used in viewshed analyzes. The recommended method provides the result of a viewshed analysis faster than the program check all elements of the elevation model.

References

[1] Peter Burt and Edward Adelson. The laplacian pyramid as a compact image code. *IEEE Transactions on communications*, 31(4):532–540, 1983.

[2] Trevor Darrell and Kwangyoen Wohn. Pyramid based depth from focus. In *Computer Vision and Pattern Recognition, 1988. Proceedings CVPR'88., Computer Society Conference on*, pages 504–509. IEEE, 1988.

[3] Peter F Fisher. Extending the applicability of viewsheds in landscape planning. *Photogrammetric Engineering and Remote Sensing*, 62(11):1297–1302, 1996.

[4] Leila De Floriani and Paola Magillo. Visibility algorithms on triangulated digital terrain models. *International Journal of Geographical Information Systems*, 8(1):13–41, 1994.

[5] Herman Haverkort, Laura Toma, and Yi Zhuang. Computing visibility on terrains in external memory. *Journal of Experimental Algorithmics (JEA)*, 13:5, 2009.

[6] Andy Jarvis, Hannes Isaak Reuter, Andrew Nelson, Edward Guevara, et al. Hole-filled srtm for the globe version 4. *available from the CGIAR-CSI SRTM 90m Database (http://srtm. csi. cgiar. org)*, 2008.

[7] Ernesto Rodriguez, Charles S Morris, and J Eric Belz. A global assessment of the srtm performance. *Photogrammetric Engineering & Remote Sensing*, 72(3):249–260, 2006.

[8] Guido Van Rossum et al. Python programming language. In *USENIX Annual Technical Conference*, volume 41, 2007.

[9] Jakob J Van Zyl. The shuttle radar topography mission (srtm): a breakthrough in remote sensing of topography. *Acta Astronautica*, 48(5):559–565, 2001.

[10] Jianjun Wang, Gary J Robinson, and Kevin White. Generating viewsheds without using sightlines. *Photogrammetric engineering and remote sensing*, 66(1):87–90, 2000.

[11] Qing Zhu, Deren Li, Yeting Zhang, Zheng Zhong, and Duo Huang. Cybercity gis (ccgis): integration of dems, images, and 3d models. *Photogrammetric engineering and remote sensing*, 68(4):361–368, 2002.

Table I
THE LOCATIONS OF THE STUDY AREAS

short name	min. lon.	min. lat.	max. lon	max. lat.	size
AREA1	18-10-00	47-13-51	18-44-09	47-48-00	2049×2049
AREA2	19-12-00	46-13-51	19-46-09	46-48-00	2049×2049
AREA3	20-10-30	46-15-21	20-44-39	46-49-30	2049×2049
AREA4	18-01-30	46-28-25	18-18-35	46-45-30	1025×1025
AREA5	17-35-30	47-03-25	17-52-35	47-20-30	1025×1025
AREA6	24-02-30	46-13-21	24-36-39	46-47-30	2049×2049
AREA7	15-05-30	47-19-21	15-39-39	47-53-30	2049×2049

Table II
THE DIFFERENCES BETWEEN MINIMUM AND MAXIMUM LEVELS IN AREA1

raster size	2×2	4×4	8×8	16×16	32×32	64×64	128×128
raster count	1049K	262K	65536	16384	4096	1024	256
average	5.11	9.65	17.53	30.46	50.63	82.04	127.74
std. dev	4.87	8.87	15.47	25.53	39.99	60.46	81.92
median	3.0	7.0	12.0	22.0	39.0	65.0	106.5
minimum	0.0	0.0	0.0	0.0	4.0	8.0	12.0
maximum	78.0	110.0	157.0	208.0	305.0	371.0	443.0

Table III
THE DIFFERENCES BETWEEN MINIMUM AND MAXIMUM LEVELS IN AREA2

raster size	2×2	4×4	8×8	16×16	32×32	64×64	128×128
raster count	1049K	262K	65536	16384	4096	1024	256
average	2.41	4.07	6.23	8.9	12.28	16.61	22.31
std. dev	1.41	1.96	2.55	3.18	3.78	4.31	4.53
median	2.0	4.0	6.0	8.0	12.0	16.0	22.0
minimum	0.0	0.0	0.0	0.0	0.0	6.0	12.0
maximum	25.0	28.0	28.0	28.0	28.0	32.0	40.0

Table IV
THE DIFFERENCES BETWEEN MINIMUM AND MAXIMUM LEVELS IN AREA3

raster size	2×2	4×4	8×8	16×16	32×32	64×64	128×128
raster count	1049K	262K	65536	16384	4096	1024	256
average	1.73	2.85	4.21	5.85	7.91	10.65	14.85
std. dev	1.04	1.40	1.82	2.44	3.42	4.67	6.40
median	2.0	3.0	4.0	5.0	7.0	9.0	13.0
minimum	0.0	0.0	0.0	2.0	4.0	5.0	7.0
maximum	27.0	36.0	43.0	46.0	46.0	46.0	46.0

Table V
THE DIFFERENCES BETWEEN MINIMUM AND MAXIMUM LEVELS IN AREA4

raster size	2×2	4×4	8×8	16×16	32×32	64×64	128×128
raster count	262K	65536	16384	4096	1024	256	64
average	3.06	5.58	9.66	16.01	25.66	39.49	59.5
std. dev	2.95	5.17	8.52	13.08	18.84	25.29	35.56
median	2.0	4.0	6.0	11.0	20.0	33.5	50.0
minimum	0.0	0.0	1.0	3.0	6.0	10.0	18.0
maximum	68.0	97.0	103.0	116.0	143.0	143.0	217.0

Table VI
THE DIFFERENCES BETWEEN MINIMUM AND MAXIMUM LEVELS IN AREA5

raster size	2×2	4×4	8×8	16×16	32×32	64×64	128×128
raster count	262K	65536	16384	4096	1024	256	64
average	7.31	13.94	25.56	44.53	73.98	118.77	184.84
std. dev	5.77	10.35	17.65	28.11	41.56	59.98	81.92
median	6.0	11.0	21.0	38.0	66.0	109.0	165.5
minimum	0.0	1.0	2.0	4.0	11.0	24.0	43.0
maximum	57.0	91.0	142.0	196.0	238.0	279.0	394.0

Table VII
THE DIFFERENCES BETWEEN MINIMUM AND MAXIMUM LEVELS IN AREA6

raster size	2×2	4×4	8×8	16×16	32×32	64×64	128×128
raster count	1049K	262K	65536	16384	4096	1024	256
average	8.53	16.50	30.93	54.67	87.93	127.17	167.6
std. dev	5.65	10.34	17.97	28.26	38.56	43.57	38.9
median	8.0	16.0	30.0	55.0	92.0	133.0	168.5
minimum	0.0	0.0	0.0	3.0	5.0	10.0	36.0
maximum	58.0	89.0	130.0	176.0	252.0	265.0	311.0

Table VIII
THE DIFFERENCES BETWEEN MINIMUM AND MAXIMUM LEVELS IN AREA7

raster size	2×2	4×4	8×8	16×16	32×32	64×64	128×128
raster count	1049K	262K	65536	16384	4096	1024	256
average	28.08	54.77	103.51	186.07	311.94	484.55	692.21
std. dev	14.76	26.77	47.12	78.22	120.12	158.34	187.0
median	27.0	53.0	100.0	179.0	300.5	469.0	656.5
minimum	0.0	0.0	0.0	6.0	14.0	78.0	306.0
maximum	263.0	330.0	459.0	650.0	1046.0	1266.0	1483.0

Acoustic Characteristics of Sacral Thracian Sites

Valeria Fol, Györök György*, Tihomir Trifonov**, Alexander Alexiev***, Ivan S. Ivanov****
Institute for Balkan Studies with Centre for Thracian Studies at BAS
* Obuda University, Alba Regia Technical Faculty: 8000 Székesfehérvár, Budai way 45. Hungary
**St. Cyril and St. Methodius University of Veliko Tarnovo, Department of Computer Systems and Technologies and National Military University "Vasil Levski", Department of Communication and Information Systems, Veliko Tarnovo, Bulgaria
***Institute of Mechanics, Bulgarian Academy of Sciences, "Acad. G.Bonchev" Str., bl. 4, Sofia BG-1113, Bulgaria
****National Military University "V. Levski", Dep. of Communication and Information Systems, V. Tarnovo, Bulgaria
E-mail: *gyorok.gyorgy@amk.uni-obuda.hu, tihomirtrifonov@ieee.org*, *al68@abv.bg*, *ivanov_ivan@nvu.bg*

Abstract: **The purpose of this paper is to present initial results for some acoustic characteristics of sacral Thracian objects in Bulgaria, like tombs, sanctuaries etc. Some modern methods of investigating and archaeoacoustic analyzing are used.**

I. Introduction

In Antiquity, lands, which we now call Balkans and Southeast Europe, were populated by numerous tribes with similar lifestyle and culture, forming two main groups - Greeks and Thracians. By the name Thrace old Greeks called the lands north and northeast of them, right down to the Carpathians and of the two rivers Dnieper and Dniester. Herodotus (Hdt. 5.1.3) sets Thracians as the most numerous people after Indian. According to ancient Greek geographer Strabo, Thracian tribes are 22 and under other researchers - they are about 80 similar tribes forming several internal groups with general basic language and tribal dialect. They are the very first human population in these lands, which namely has begun to displace in the central and western parts of Europe from here [1,4,11].

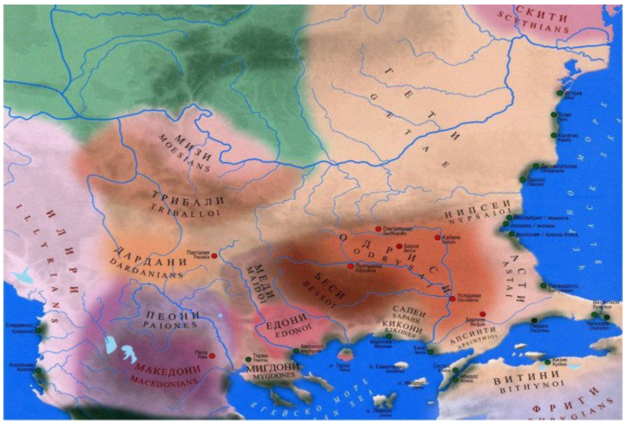

Figure 1. Schema of the Thracian tribes' location. [12]

The ancient peoples who now call Thracians were not slave owners as Greeks.

A team of Bulgarian Academy of Sciences and other research institutions work on project "Thracians - genesis and development of ethnicity, cultural identities, interactions and civilizational heritage of antiquity" funded by the donation of Petar Mandjoukov. The task is investigation of the acoustic characteristics of the interior of archaeological sites and musical instruments from the Neolithic to the late Middle Ages in Bulgarian lands: search for continuity and continuity. The idea of acoustic surveys of Thracian sacred sites is by Dr. Alexandra Fol [2].

The purpose of this paper is to present initial results for some acoustic characteristics of sacral Thracian sites like tombs, sanctuaries etc. Modern archaeoacoustics, precise measurement and computer methods are used. Of the ten surveyed sites, we will concentrate on Sboryanovo Historical and Archeological Reserve and especially on tomb number 13.

II. Sboryanovo Historical and Archeological Reserve

The Sboryanovo Historical and Archeological Reserve is situated in the western part of the Ludogorsko Plateau of Northeast Bulgaria. It is a complex of age-old villages, sanctuaries, and necropolises. The most noteworthy discovery in it is the Sveshtari Tomb, a Thracian king's sanctuary and necropolis. This site was included among the UNESCO World Heritage Sites in 1985.

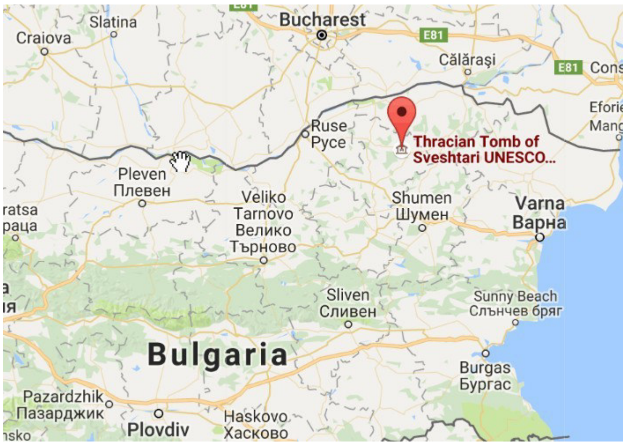

Figure 2. Sboryanovo historical and archeological reserve location.

Mounds 12 and 13 are part of the architectural ensemble of the Sveshtari Tomb under Ginina Mound. They both cover smaller vaulted tombs. They stand out by their symmetrically opening sliding doors, which indicate a specific architectural tradition among the Getae. The tombs in Mounds 12 and 13 date to the end of the 4th – early decades of the 3rd century BC. Only fragmentary remains were found inside: partial human skeletons, sacrificial animals, and other gifts. The tomb under

Mound 12 was destroyed by an earthquake in the early decades of the 3rd century BC [3].

Figure 3. Sboryanovo historical and archeological reserve, the tomb in mound 12 (old photo) [3] .

Figure 4. Sboryanovo historical and archeological reserve, the tomb in mound 12 (actual photo).

Figure 5. Inside mound 13, Archeological reservation Sboryanovo, near to village Sveshtari, Bulgaria

III. SCHEME OF THE TOMB 13 AND INSTRUMENTATION

The scheme of the tomb is obtained by using a laser rangefinder. It is shown on Figure 6,8 and 9.

Experimental set-up includes:

- Pressure-field Microphone Type 4193 Brüel&Kjær, available in Transducer Electronic Data Sheet (TEDS) combinations with the classical Preamplifier Type 2669 with an individual calibration; Dynamic Range: 19 … 162 dB, Sensitivity: 12.5mV/Pa.
- Compact Data Acquisition Unit 3560B Brüel&Kjær, for outdoor use that consist: Dyn-X input modules with a analysis range exceeding 160 dB and automatic detection of front-end hardware and transducers − supports IEEE 1451.4-capable transducers with TEDS (Transducer Electronic Data Sheet); output TCP/IP protocol communication - RJ 45 connector complying with IEEE−802.3100baseX; Multiframe Control option;
- Base software PULSE 12 for CPB (Constant Percentage Band) analysis 2 channels; 5-channel Time Capture; PULSE Bridge to MATLAB®
- MathWorks Software - MatLab&Simulink, toolboxes for FFT and Wavelet analysis.
- Sinusoidal signal and random noise generator 1027, Brüel&Kjær.

Figure 6. Microphone position in camera of mound 13 Archeological reservation Sboryanovo, near to village Sveshtari, Bulgaria

Figure 7. Measurement unit “in situ” in King mound (actual photo).

Through the equipment, mentioned above, typical measurements for architectural acoustics were carried out in mound 13.

IV. SOME RESULTS AND DISCUSSION

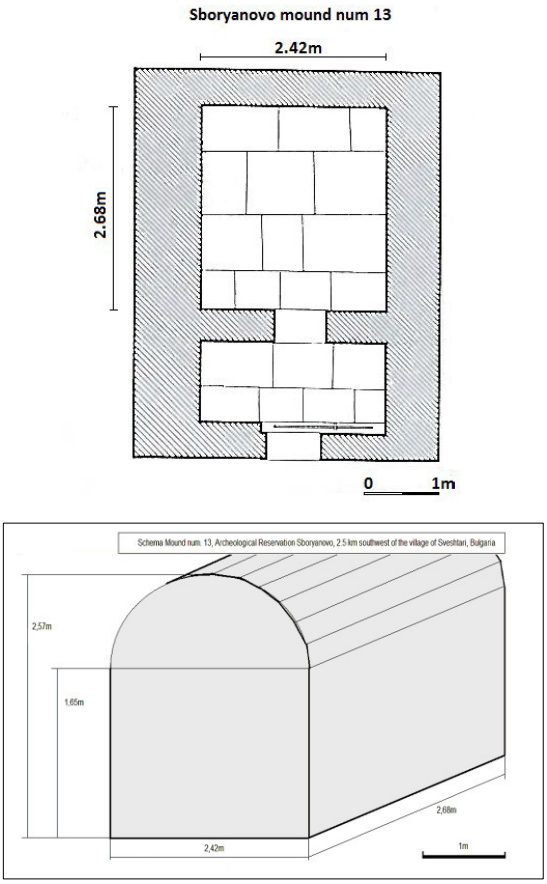

Figure 8. Scheme of the camera of mound 13, archeological reservation Sboryanovo, Bulgaria

It is known, that the acoustics of the room behaves quite uniformly in frequencies above 200 Hz and it is described by its reverberation time RT60 very well. However, in low frequencies (below 200 Hz), the discrete resonances in room will be dominated. [9]
Approximation of the camera by cuboid give us Fig.9.

We can calculate rectangular room first modes,
Length: $l_x = 2.68\text{m}$, Width $l_y = 2.43\text{m}$,
Height $l_z = 2.3\text{m}$

$$f_i = \frac{v}{2}\sqrt{\frac{n^2}{l_x^2} + \frac{p^2}{l_y^2} + \frac{q^2}{l_z^2}}\,.$$

num	n	p	q	Mode	Frequency Hz
1	1	0	0	Axial	64,3
2	0	1	0	Axial	71,2
3	0	0	1	Axial	74,9
4	1	1	0	Tangential	95,9
5	1	0	1	Tangential	98,7
6	0	1	1	Tangential	103,3
7	1	1	1	Oblique	121,7

No modal boost: 1Hz to 64Hz.
Room modes dominated 64Hz to 176Hz.
Diffraction and diffusion dominated 176Hz to 704Hz.
Specular reflections and ray acoustics prevail: 704Hz to 20000 Hz, see [10].

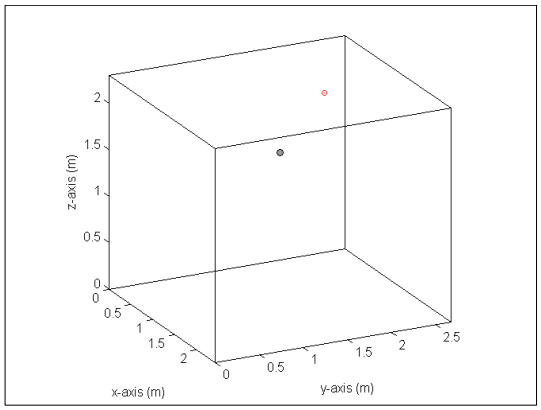

Figure 9. The microphone is on the center of the camera. The location of the source can be seen too.

First we estimate the reverberation time RT60 of the camera by impulse measurement techniques. The pistol shot and balloon boom were made for obtaining the impulse response of a camera. The signals are collected by microphone 4193 Brüel&Kjær and PULSE data acquisition unit 3560B, [6]. Sample frequency $Fs = 2^{16}$ samples per sec. On Fig.10 it can be seen, that the RT60 is about 0.56sec.

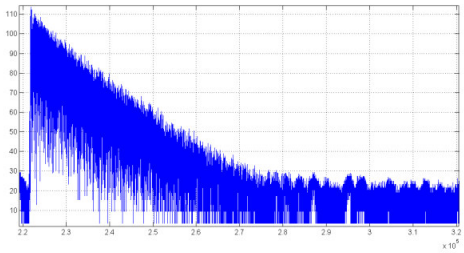

Figure 10. Signal pistol shot decay waveform (microphone in the centre of camera), RT60 is about 0.56sec, frequency of simples is 65536Hz

If we considered that sound velocity $v \approx 343m/s$, (the temperature about 20deg Cels. or 68deg Far.), and the sample frequency Fs is 65536Hz, then the one sample is equal to 5.23E-3 meter, or 5.23mm.

The scalograms (Continuous Wavelet Transforms) are applicable to estimation of impulse responses [5,7,8].

The signal's waveform in time and scalogram (Continuous Wavelet Transform - CWT, Daubechies wavelets) are illustrated on Fig. 11.
The zoomed in time first parts of the same signal waveform and its scalogram are shown on the Fig. 12 and 13.

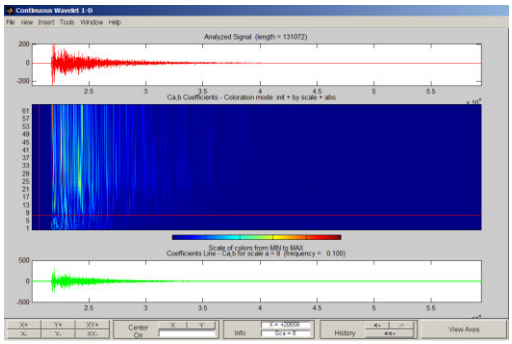

Figure 11. The shot waveform in time and its scalogram. The signal is collected by microphone 4193 Brüel&Kjær and PULSE data acquisition unit 3560B.

From the CWT, shown on Fig. 12, it can be seen the structure of maxima for the first reflections. In fact, these are the first 12 milliseconds, or 766 samples (or 4.01 meters).

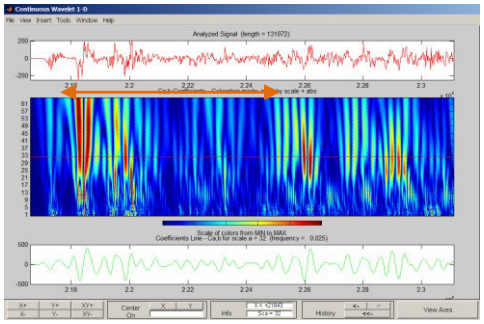

Figure 12. Scalogram of a shot waveform first 12 milliseconds, 766samples (or 4.01meters)

The structure of the first 3.8 milliseconds of the shot waveform can be seen on Fig. 13.

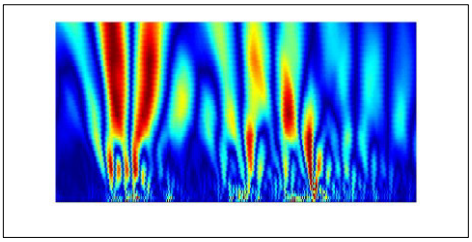

Figure 13. Scalogram of the shot waveform - first 250 samples or about 3.8 ms (or 1.31m).

V. CONCLUSIONS AND FUTURE WORKS

The initial and partial processing of the results allows the following conclusion:

- Almost certainly, in the chambers of Thracian mounds were performed rituals that were accompanied by music and speech.
- Obtained modes in the range of 64 to 176 Hertz allow us to assume that the voices were mostly male voices.

In the future, the authors plan to analyze specific resonances in the sonic and in the infrasonic ranges in this and in the other Thracian sacral sites. The results will be useful in archeology and archaeoacoustics.

In a very short time, the authors will conduct the experiment of recording of ancient music, performed by significant Bulgarian musicians by models of typical ancient Thracian musical instruments like lira, guitar, ancient flute etc.

REFERENCES

[1] Alexander Fol, Studies on the Greek Sources for Ancient Thrace. VII. Conon: „Stories", In: Annual Edition of Sofia University "Kliment Ohridski", 1983

[2] Alexandra Fol, Thracian Architecture – a Syncretistic Presentation and Tangible Realization of Musica Universalis?, Problems and Investigation of Thracian Culture, Vol. IV, pp.127-134, Irita, Kazanlak, 2009, ISSN 1312-8256

[3] Christoskov, L., D. Gergova, V. Rizzo. Traces of Seismic Effect on Archaeological Sites in Bulgaria. In: Terremoti et Civilta Abitative. Roma, ottobre 1993, Annali Geofisici, 1994, online [http://www.annalsofgeophysics.eu/index.php/annals/article/view/4078/4145]

[4] Alexander Fol, Thracian Orphism, St.Kliment University Press, Sofia, 1986, in Bulgarian

[5] Dimkov G., T. Trifonov, I. Simeonov „Improving the visualization of scalograms by means of transformation in the complex planel, *Proceedings of the Forty Second Spring Conference, of the Union of Bulgarian Mathematicians,* Borovetz, April 2–6, 2013, p.218. [http://www.math.bas.bg/smb/2013_PK/tom_2013/pdf/218-221.pdf]

[6] Trifonov T. and Ivanov I.S. Application of modern computer methods for acoustic phenomena investigation, *10th International Symposium on Applied Informatics and Related Areas , AIS-2015*, Óbuda University, Székesfehérvár, Hungary, 11 Nov. 2015.

[7] Trifonov T., I. Simeonov, R. Dzhakov „Features of time-frequency analysis visualization of large dynamic range signals", *XLVII International Scientific Conference on Information, Communication and Energy Systems and Technologies (ICEST 2012)*, Veliko Tarnovo, June 2012, pp. 155-158

[8] The Bell Project-Research and Identification of Valuable Bells of the Historic and Culture Heritage of Bulgaria and Development of Audio and Video Archive with Advanced Technologies, online [http://www.math.bas.bg/bells/belleng.html]

[9] Siegfried Linkwitz, Investigation of Sound Quality Differences between Monopolar and Dipolar Woofers in Small Rooms, 105th AES Convention, San Francisco, 1998, Preprint 4786 online [http://www.linkwitzlab.com/AES'98/aes-98.htm]

[10] A. Melcher, Amroc - the room mode calculator, Institut für Musikwissenschaft der Universität Wien, online [http://amroc.andymel.eu/java/]

[11] Alexander Fol, Todor Spiridonov. Historical Geography of the Thracian tribes to III century BC and Atlas. Publishing House of the Bulgarian Academy of Sciences, Sofia, 1983.

[12] Alexander Fol, Valeria Fol, The Thracians,TangraTanNakRa Publishing House, Sofia, 2005, p. 32.

The English classroom as a social site for negotiating cultural identity

A pinch of Oman

Marianna Machata

Alba Regia Technical Faculty, University of Obuda, Székesfehérvár, Hungary

machata.marianna@amk.uni-obuda.hu

Abstract - The present paper reveals the findings of the author's ethnographic research she conducted into intercultural communication in the circle of her own students in the duration of her two-year- long teaching period in Oman. The study is aimed at understanding orientations to interculturalism focusing on mediating culture-specific features, communicative intent and emotional stances in the English classroom settings at an Omani university where the teacher is Hungarian and the students are Omani. The first languages (L1) of the participants are Hungarian (teacher) and Arabic (students), English, a second language (L2) for all of them is used as a tool of communication. The discourse-analytic approach to documentation and analysis of language-related episodes reveal the evolution of the participants' acceptance of the shared interpretation of crosscultural awareness and sensitivity. Free and spontaneous interactional exchanges exemplify how the students organize, regulate and negotiate their own and their teacher's conduct and language use. When analysing the participants' cultural behaviour, patterns are identified pertaining to cultural identity as reflected in various tranformations, preferences, motivations and group affiliations.

I. Introduction

The longitudinal participant observation conducted in my English classroom provided a close insight and a better understanding of the process of interculturation. I investigate the phenomenon in terms of shared attitudes and values. The classroom itself provided a fruitful arena for investigating the group members' attitudes, norms, beliefs, values as expressed by the accepted behaviour of the members, including, of course, their language behaviour.

II. Discussion -- Cultures in contact

Analysing my dataset I witnessed how socially and culturally determined features are reflected and communicated in the way members of the classroom use language, for example, what they choose to say and how they say it. Also, I learned that some words, acts and behaviours may be used in certain circumstances and not in others, that certain topics, behaviours which have cultural connotations are considered profane if used outside the respective culture.(Al-Husseini, 2007) Below I give an overview of how culture is communicated and negotiated in interactions in terms of the participants'communicative intent by grouping the data according to certain categories.

1. Communicating shared values

When negotiating culture-specific features and cultural identity it was amazing for me to percieve that classroom discussions created a solid foundation for approximating cultures, and gave an opportunity to consider so far unknown aspects of interculturalism. (Gafaranga,2012) Similarly, the

classroom was the place where I could witness manifestations of a certain acculturation process and that of the assimilating efforts in both of us. Our talk-in-interactions gave evidence that the teacher and the students representing two distant cultures exhibited shared understanding and interpretations of general higher-order human values and are equally committed to approximating and accommodating to the locally established norms. I interpreted manifestations of allignment efforts and alliance formulation with the respective foreign community as the sign of a strong and conscious group affiliation effort.(Baker, 2006; Pavlenko, 2006) The examples below are to illustrate my conclusion.

'Teacher put on those clothes with the colours of Hungary, you know, the Omani colours are the same.'

'I bought the petticoat because I want to look like you. You put on an abaya, why can't I look like a European?'

'Eid in Oman is something like your fir tree decoration elebration'

'At home we wear clothes like you. Nefsztusej, teacher.'

'For our national holiday you need henna. On this occasion Omani women must wear it. Then you look real Omani'

'Do you cook pig?' But eats rubbish. Ok, no worries, teacher, we love you anyway.'

'Do you go to school when it snows?' 'Do you go out in winter?'

For them rarely experienced heavy rains mean severe weather conditions when schools are closed and people stay at home having roads blocked by floods. As a consequence, being determined by their cultural esperience they assume, we have the same experience in our culture.

'Miss, His Majesty Sultan Qaboos gave happiness to Omani people. What's the name of your leader who did so much good to the people in your country?'

Discussions of political and economic issues were rare in the classroom and generally in the circle of local people for the simple reason that they are not interested in topics of such nature. However, once such topics emerged they expected a straightforward and shortcut answer.

My answer emphasizing that the leader of a country either elected or inherited should be committed to their nation's progress fully satisfied their expectations and was totally approved, at the same time it elicited my students' remark as follows:

'Then teacher, you think like an Omani.'

In the beginning I interpreted their directness and straightforwardness as a rude and impolite attitude, which greatly contributed to the cultural shock I overcame, later, however, with immersing in the new culture, I realized, it was a culture-specific phenomenon, which was primarily attributed to their insufficient language competence. Nevertheless, I was expected to answer all their questions even though some of them were utterly challenging and embarrassing. The utterance below exemplifies such a case.

'Teacher, would you like to live in Oman for the rest of your life?'

The utterances above give evidence that when talking about cultural specificities, they made definite attempts to shorten the distance and and soften the differences between our two cultures by

emphasizing similarities simply to show their emotional attachment.

2.Constituting locally valued competences and identites – Socializing into local norms of conduct (Cekaite & Björk-Willén, 2012)

Langauge related episodes and spontaneous comments highlighted the normative preference for correct and relevant language use and emphasize the appropriateness of the relevant behaviour The utterances below show how my students discipline me.

'Teacher, don't hurry, we always walk slowly.'

'Teacher, collect the prayer rug from your chair to make sure no one sits on it'

'Teacher, you mustn't mark him absent, he went to pray.'

The English classroom revealed manifestations of my students' dynamic and transforming identity, illustrations of how they regulate, identifie and redefine themselves in the cultural group depending on their and their teacher's personal needs and interests. (Dörnyei, 2005) The English language served as a strategic tool to liberate their thoughts and to lower inhibitions.

While analysing the data I collected during my immersion teaching practice I identified a couple of examples that spontaneous classroom reactions between me and my students reflect the reciprocal character of communication where the interlocutors share and exchange values and ideas, organize, regulate, control and discuss the appropratiVeness of each other's behaviour and language use.

'Sorry teacher, I am late, because…'

'Don't touch her hair, it's rude in her country.'

'Give it a personal touch. Be confident'

The utterances above give evidence of my students' accommodation to my cultural expectations.

3. Accomodating to the established language use rules

1.Regulations in terms of the appropriate language use in the English classroom was a recurring element. We stated that using Arabic, a languge that is not shared by each member of the group can have a bad impression of intentional exclusion of someone even though it is originally meant to signal privacy and alliance.

Their recurrent switch to Arabic needed constant regulation and disciplining in the classroom. To make them feel how rude, insulting and offensive their use of Arabic might be, all of a sudden, with no transition, I started to speak Hungarian as a respond to their inappropriateness, which had a real chilling effect. Having percieved the intentionality behind my speaking in Hungarian, they stopped talking in their own language. At the same time, such embarrassing cases gave a good opportunity for me to allocate a couple of minutes to discuss culture-related issues. We grounded the rules to be obeyed in our culturally diverse environment and stated the importance of mutual crosscultural respect. Such discussions proved to be very effective and changed their attitude. We stated that the relevance of appropriate language is part of the local norms and it was a recurring topic of discussions.

4. Easing tension - Injecting humour

'Injecting humour' termed by Baker (2006) was used not simply for self-serving entertainment, my students usually operated it as an effective communication strategy. Switches to Arabic were frequently utilized tools to control power relationships in a discourse event and generate the

expected discourse behaviour, laughter, amazement, embarrassement in the interlocutor.

'Bidun warqa, teacher'(Without paper)

'You want to learn Arabic? Why don't you take notes? You will forget it.'

'She is taking a photo of it, teacher. Do you remember how it is in Arabic?'

Their emphatic and provocative repairs and requests are indexical of their authoritative position and of their entitlement to know and teach the correct use as persons who are more skilled in Arabic. Their remarks above appeared to be an effective tool to develop a counter-discourse with the aim to counterbalance their inequitable subject position in an embarrassing situation, e.g. when they failed to submittheir homework. (Norton, 2000) The comments with reference to my Arabic knowledge and learning style released them and put them in the 'in-know' position. In addition, it also gave them an opportuniy to abandon an embarrassing topic, win time and also divert my thoughts from the original curriculum. Provoking me for my mistakes and making it instances of a humorous moment was frequently operated by them.

They knew that I was eager to learn Arabic, thus they regularly checked out and monitored my progress. Several times when I failed to translate an English expression asked by them into Arabic, they echoed my comments I made in case of their failure and reproached me for using notes as cheating attempts with reference to my words that the curriculum should be reproduced by heart without using notes.

Inserting humour and bringing about humorous effects proved to be an effective strategic tool to defend themselves and to win attention. My reactions, my relevant discourse behaviour, for example, laughters, smile on my face signalled for them that their humorous act hit the target. From the way I responded they concluded that they can redefine their position in the classroom, which gave them the opportunity to control the situation and also enhanced the stylistic effectiveness and intensity of their messages, as a consequence, they took advantage of such situations.

The switch to Arabic in the utterance below was meant to ease tension and embarrassment felt over not fulfilling responsibilities and expectations, also was well-placed to conciliate and soften me.

The utterance *'Szubri teacher, szubri!' ('Wait, teacher')* with the relevant hand movement as a referential sign: shaking one fist in an upright position holding the tips of their three fingers (thumb, index and middle) together tight.

When talking about cultural specificities, they made definite attempts to shorten and even eliminate the distance between our cultures by overemphasizing certain features and disguise differencies.

5. Directness in communicating cultural features

I percieved the directness in their behaviour and language use as wierd, insulting and inappropriate at the start, though with the time proceeding I realized that was simply a manifestation of their cultural identity, which must not be considered as an untoward attitude, for the simple reason that they were attributed to their insufficient language competence. Still such manifestations of cultural identity evoked commentary and became the subject of discussions frequently because some of their movements and body postures made me feel uncomfortable. After a while I did not handle those attitudes as a trouble source and I did not interpret them as hostile and disregarding behaviour.

'Come, teacher!', Szubri,{wait} teacher!, Cold, AC, teacher' with the accompanying handwave first interpreted by me as disregarding and offensive, which often placed me in an inequitable subsect position. Feeling discomfort, from time to time, I signalled them the inappropriateness of the move stating that in my cultural view and understanding such moves make a bad impression and have a negative connotation.

Similarly, emphasizing certain elements of verbal and non-verbal communication as prerequisites and key factors of successful communication astonished and scared them being constituting distinctions between our two cultures. Facing the problemacity of cultural differences was a frequently experienced phenomenon. When discussing presentation techniques and the requirements of oral performance I talked about the importance of an impressive and confident presentation in public and demonstrated what I meant in front of the class, their facial expression reflected enthusiasm and approval. However, when I asked them to do it in practice, rehearse those techniques and demonstrate what was discussed, they only giggled and refused to stand up and act out in front of the class. It took a while to persuade them to follow my instructions and exhibit the proper body and verbal language. In the beginning I instructed them how to deliver a talk in order to advance communication with reference to the tiniest details, such as: chin up, open lips, speak articulated and in high-voice, let your personality shine through the performance, give the presentation a personal touch, keep eye-contact and inject humour. First, they, especially the girls, found such a behaviour bizarre and profane. However, after a while, when they realized, they won attention and appreciation by displaying self-confidence, they started to accommodate. They were able to act impressively on the stage, in additon, they took upright pride of their success and during peer assessment sessions they were eager to evaluate and criticize each other's performance.

Although I experienced high-level of cooperation and tolerance in their attitude, their rule and deadline ignorance and negligence were frequent trouble sources. Lateness, absenteesm were recurrent phenomena. To avoid conflicts and make repair without insulting them, in a respective way, I decided to ground classroom rules recurrently at the beginning of each classroom session. We started every class with listing the rules. I invited my students to name the rules to be obeyed one by one. As a response to my request they echoed all our classroom rules, such as: Phones are off, Don't be late, once you are, say why, Respect: I listen to you, you listen to me, Be confident, Speak clearly, Don't be angry, Be honest.

Establishing our own inner local rules, framing our social interactions and local norms, verbalizing our preference of the appropriate conduct and language use have greatly contributed to strong group affiliation. Also we established our vernacular style and manner, and forged a sense of belonging between us, which we experienced as a kind of alliance and privacy.

III. Conclusion

Undoubtedly, English served as a bridge to reveal cultural norms and shade meanings, the English classroom created a social site for intercultural communication to facilitate our knowing more about each other. Interpersonal interactions, long-term coexistence, loose conversations greatly contributed to handle taboos, to feel comfortable enough to discuss things without limitations and restrictions. The English classroom created favourable conditions for intercultural understanding for the simple reason that utterances, meanings conveyed in English were perceived as

less offensive and troubling for the cospeakers. In addition, long-term coexistence created a high-level of confidence, friendly rapport, loose conversations, which established a solid foundation for exchanging ideas, views and values. Nevertheless, we experienced that norms of the indigenious culture will always shine through.

References

{1} Cekaite, A., & Björk-Willén, P. 'Peer group interactions in multilingual educational settings: Co-constructing social order and norms for language use.' *International Journal of Bilingualism* 17(2) 174-188. 2012.

{2} Baker, C. '*Foundations of bilingual education and bilingualism.'* 4th ed. Clevedon: Multilingual Matters. 2006.

{3} Dörnyei, Z. '*The psychology of the language learner.'* London: Lawrence Erlbaum. 2005.

{4} Duff, P. 'Research approaches in applied linguistics.' In R.B. Kaplan (Ed.), *The Oxford handbook of applied linguistics* (pp. 13-23). Oxford: Oxford University Press. 2002.

{5} Gafaranga, J.,) 'Language alternation and conversational repair in bilingual in bilingual conversation.' *International journal of bilingualism.* 16(4) 501-527 SAGE. 2012.

{6} Hasim Aliwey Mohammed Al-Husseini: 'Euphemism in English and Arabic.' 2007

{7} Norton, B. '*Identity and language learning: Gender, ethnicity, and educational change.'* Edinburgh Gate: Pearson Education. 2000.

{8} Pavlenko, A. '*Emotions and bilingualism.'* Cambridge: Cambridge University Press. 2006.

Pre-processing Techniques for Hungarian Handwriting Recognition

Gaye Ediboğlu Bartos*, Éva Hajnal**
* Anadolu University/Department of Computer Engineering, Eskişehir, Turkey
* Bilecik Şeyh Edebali University/Department of Computer Engineering, Bilecik, Turkey
** Óbuda University Alba Regia Technical Faculty, Székesfehérvár, Hungary
gayeediboglu@anadolu.edu.tr, gaye.ediboglu@bilecik.edu.tr
hajnal.eva@amk.uni-obuda.hu

***Abstract*— The technology for offline handwriting recognition has reached a very successful level for Latin character recognition for discretely written characters. However, there are still issues for recognising cursive handwritings. In addition to that, there are only a few studies conducted for Hungarian handwriting recognition. Recognition of Hungarian handwritten texts is challenging for various reasons such as the tradition of using cursive handwriting and letters with punctuation. It is known that pre-processing phase is essential for a successful recognition and the outcomes of the pre-processing phase determine the accuracy of the recognition. This paper provides the most suitable pre-processing techniques for offline Hungarian handwriting recognition. All the methods applied are provided with the results and the most suitable methods are highlighted.**

I. INTRODUCTION

Optical Character Recognition (OCR) is conversion of scanned images of machine printed or handwritten text, numerals, letters and symbols into a computer processable format such as ASCII without any human intervention. There are two types of OCR namely online and offline recognition. In online recognition, the characters are recognised as they are drawn. Furthermore, the order of strokes are available and successive points are represented as a function of time [1][2]. On the other hand, in offline recognition optical recognition is performed after the writing or printing has been completed. In other words, its input is an image or a scanned document [3].

An OCR system consists of several components. Fig. 1 shows the components in a typical OCR system. As can be seen from the Fig. 1, firstly the document is scanned through an optical scanner. Secondly the crucial pre-processing phase is applied. Pre-processing is critical for an OCR system since the outcomes of this step are going to be recognized in the next step. Generally in the pre-processing phase binarization, noise removal, normalization, feature extraction and segmentation are performed. Finally in classification step, the recognition is performed. In addition to those steps, an extra post-processing phase could be adopted in which verification is performed in order to improve the accuracy rate.

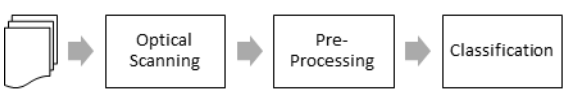

Figure 1 Components of a typical OCR system

This paper presents pre-processing techniques that applies to offline Hungarian handwriting recognition. Hungarian handwriting recognition is challenging for various reasons. The next section provides the properties of Hungarian handwriting with reference to why it is challenging. In the following sections pre-processing techniques that have been tested are explained and the results are provided. Finally the conclusion is presented in the final section.

A. *Properties of Hungarian Handwriting*

Hungarian language consists of 44 letters (Fig. 1). Some Hungarian letters are the same as English letters however other letters have punctuation and some consist of more than one character. These letters of the language generate a challenge for recognition purpose such as avoid removal of the punctuation at the noise removal phase.

Another challenge in recognising Hungarian handwriting is that in Hungary there is a tradition of using cursive scripts. Cursive character of the handwriting brings about the challenge to the segmentation phase. Tappert defines five difficulty levels for handwritten characters which are namely boxed discrete characters, spaced discrete characters, run-on (touching or overlapping) discretely written characters, pure cursive handwriting, and mixed cursive and discrete characters (Fig. 3) [4]. In our data sample, most of the handwritings belong to the most difficult categories which are pure cursive handwriting, and mixed cursive and discrete characters. Therefore, Hungarian handwriting recognition is very challenging compare to other Latin handwritings. Additionally, there are not many studies conducted for the purpose of Hungarian handwriting recognition.

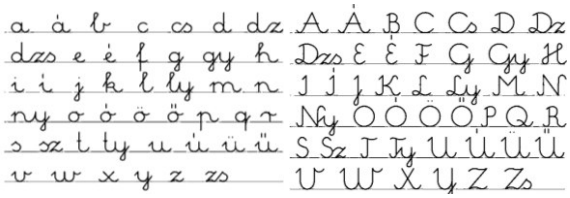

Figure 2 Hungarian Alphabet

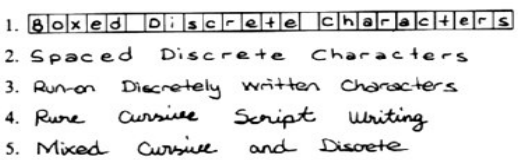

Figure 3 Five stages of handwritten word recognition problem

II. PRE-PROCESSING

Raw data must be pre-processed in order to make it more suitable and useful. This process establishes the path between handwriting and recognition. The pre-processing for offline handwriting recognition consists of many steps which usually include binarization, noise removal, normalisation, skew correction, slant removal and segmentation. According to different needs, different steps may be included or excluded.

Our data sample was created by scanning handwritten papers in 300 dpi and storing them in grayscale image in png format. Then below mentioned pre-processing methods were applied respectively in the MATLAB 8.3 environment.

A. Binarization (Thresholding)

Image binarization is used in order to convert a gray-scale handwritten image into a binary image. This process also helps to reduce the size of the image and therefore speed the image processing up. There are two types of thresholds namely global and local (adaptive) thresholds [5]. In global thresholding, one threshold is used for the entire document. There are several techniques in the literature for picking the optimal threshold for example Otsu's thresholding technique is amongst the most popular ones [6]. On the other hand, local thresholding uses different threshold values for each pixel according to the local area information [7].

For our work we tried two different global thresholding methods. Firstly, the threshold value was given manually by looking at the histogram of the image. Then, Otsu's Global Thresholding was adopted [6]. As can be seen from the Fig. 4, there was not a visible difference in the results and the results were both good therefore no more methods were applied. It is worth pointing out that, no prior normalization was applied to the image. However, after applying the same noise removal techniques, it became visible that Otsu's thresholding gave better results. Therefore, Otsu's thresholding was adopted for the later processes.

(a)

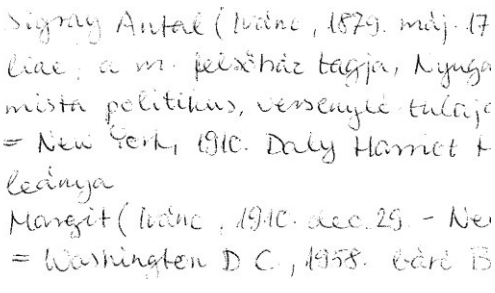

(b) (c)

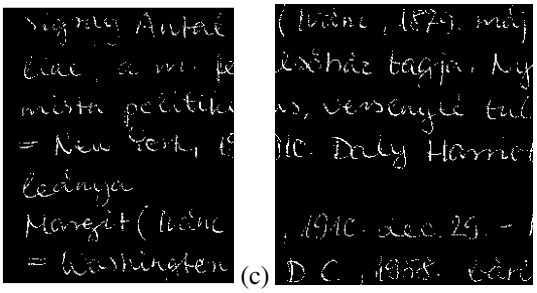

Figure 4 Global Thresholding Applied to the Image: (a) original image, (b) manual thresholding, (c) Otsu's Thresholding

B. Skew Correction and Slant Removal

Skew correction is used when the document needs to be aligned with the coordinate system. Inaccuracies in the scanning process and the style of handwriting may result in tilted or curved lines within the image. Most popular approaches for skew correction includes correlation, projection and Hough transform [8], [9].

The slant of handwritten texts varies from person to person. Several methods are proposed for slant removal purpose. Examples of popular techniques are calculation of the average angle of near-vertical elements and Bozinovic- Shriari Method (BSM) [10], [11].

The data used for the study did not include a significant amount of skewed lines or slanted words. Therefore, this step was skipped in this study.

C. Noise Removal

The quality of the document is going to be improved by using noise reduction methods such as filtering and morphological operations (erosion, dilation etc.). Normalization also provides a tremendous reduction in data size by thinning and extracts the shape information of the characters [9], [12].

Most popular techniques for noise removal include filtering and morphological operations. Filters are usually aimed at smoothing, sharpening, thresholding, removing background and adjusting contrast [13]. Commonly used filters for noise removal include linear filtering, median filter, adapting filtering and averaging filter. As for the morphological operations, they replace the convolution operation by the logical operations. There are numerous morphological operations designed for noise removal such as thickening and thinning the characters; connecting the broken strokes and decomposing the connected strokes[10], [13].

In our work, standard MATLAB morphological operations were applied to the binary image. Firstly, the holes were filled by using 'imfill' operation. Subsequently, 'dilate' operation was adopted for thickening the characters. One point to worth mentioning is the result of performing a 'dilate' operation after applying an 'erode' operation was better than a merely 'dilate' operation. Hence, 'dilate' was performed after an 'erode' operation. Finally, a 'thin' operation was performed for thinning.

Median filtering and adapting filtering were applied to the image. However, the results were not satisfying since the noise in the image is not a real white noise or black and white noise. The filters removed the punctuation while removing the noise. Therefore, no filters were adopted. Instead, 'bwareaopen' was used to remove small noise from the image. The image after noise removal can be seen in Fig. 5.

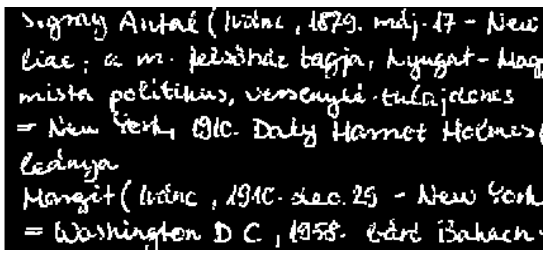

Figure 5 Binary Image After Morphological Operations

Hungarian is a very challenging language for noise removal. The reason is that many letters contain punctuation and those punctuation marks are hard to discern with noise and they are highly likely to be removed at the noise removal phase.

D. Segmentation

Segmentation step is considered as the most crucial step for character recognition considering that the success of the recognition highly depends on a successfully segmented image[14], [15].

Since the input of the system is an image, segmentation is applied for multiple purposes. Firstly, line segmentation should be applied in order to divide the lines. Secondly word segmentation is adopted to extract words from each line. Finally character segmentation is performed.

1) Line Segmentation

In our study, in order to perform line segmentation different methods have been applied such as smearing, Hough Transform (HT), Watershed Transform (WT) and Horizontal Projection. WT did not perform well since it tried to segment not only lines but also words and individual characters at the same time. The image is segmented into many regions which are not necessarily meaningful. In order to overcome this, WT was applied to a smeared image in which regions are more apparent. In order to perform the smoothing with smearing, run length smoothing algorithm was applied to the image. This algorithm smears consecutive white pixels along the horizontal direction [16]. WT was tried on different smearing levels. However, the results were not satisfactory to be adopted in our system. The results of the WT can be seen in the Fig. 6.

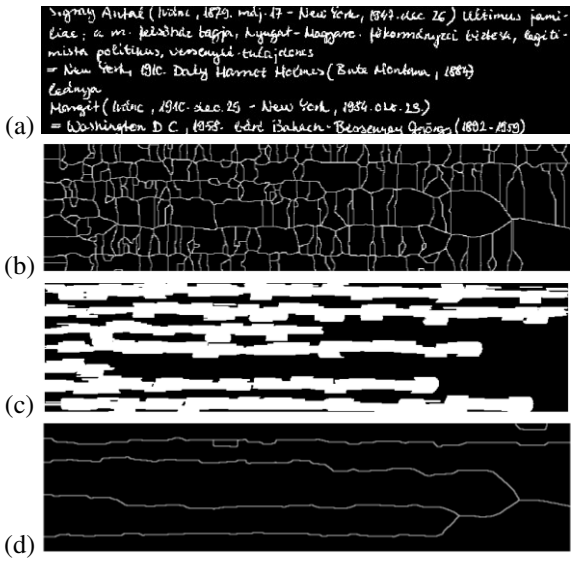

Figure 6 Segmentation with Watershed Transform: (a) original image, (b) segmentation of the original image with watershed transform, (c) smeared image, (d) segmentation of smeared original image with watershed transform

As another widespread method for several years, HT was applied to the image in order to find and then segment the lines [17], [18]. In contrary to WT, HT performed well for cursive handwritings. The results can be seen in Fig. 7. The green lines show the detected lines.

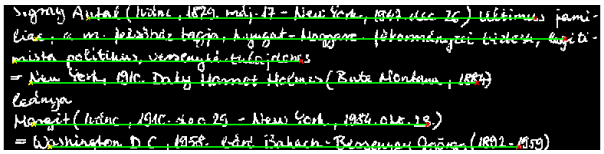

Figure 7 Line Detection with Hough Transform

Finally, Horizontal Histogram Projection was adopted for Hungarian Handwriting Recognition purpose. This method is generally used for character, word and line segmentation [19]–[21]. Horizontal Projection provides the histogram of the sum of the black or white pixels. It can be seen from the Fig. 8, the histograms clearly indicate where a line ends and another one starts in both images.

A threshold value can be used separate the lines. However, any set threshold value might led to cutting the tails of the words since there are overlaps between the lines caused by the tails of the letters. Instead a very effective and simple method was adopted. As can be seen from the Fig. 9, after smoothing the histogram, finding the regional minima gives a great result for segmentation. The first histogram (a) is the histogram of the number of white pixels in each row and the second histogram (b) is the smoothened histogram a, by using 'smooth' operator. The last one (c) is the histogram of the regional minimas. In MATLAB, 'imregionalmin' sets the regional minimas into 1 where and the rest into 0. This provides a straightforward way for finding the pixel where the lines should be separated.

Figure 8 Horizontal Histogram Projection of the Images: (a) projection of the original image, (b) projection of the smoothened image

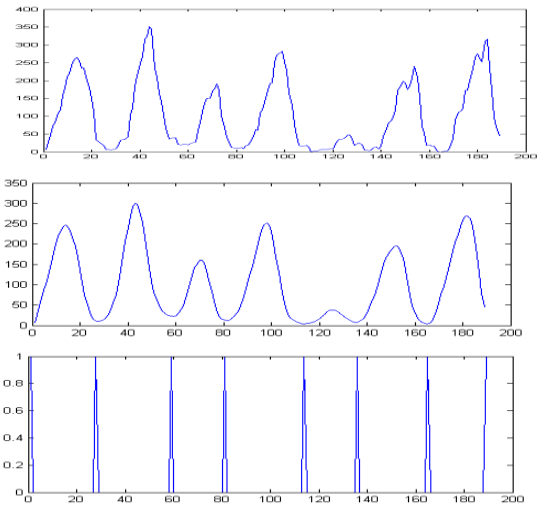

Figure 9 Histograms of the lines: (a) histogram of the number of white pixels, (b) smoothened Histogram (a), (c) histogram of regional minimas

2) Word Segmentation

Similarly to the line segmentation, a vertical projection method can be applied for word segmentation. When it comes to word segmentation phase, the challenges caused by the cursive handwriting starts to appear. As can be seen from the Fig. 10, vertical projection of an ordinary line would have zero pixel count at gaps between the words and within the words. In other words, any section of the line where there is not ink would be zero pixels at the vertical projection.

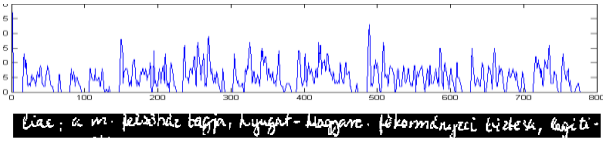

Figure 10 Vertical Projection of a Line

In order to overcome the challenge, the length of the consecutive zero pixels were taken into consideration. For this purpose, mean of five smallest consecutive zero counts was set as the threshold. As an alternative threshold, a set 7 pixels also gave very similar result. Subsequently to this process, the words were segmented. A point worth mentioning is by segmenting the words this way; punctuation marks and parenthesis are also segmented. However, elimination of those at this stage would be more convenient than trying to eliminate those at the recognition phase. Therefore, another threshold was adopted in order to ignore segments including the punctuation marks which are smaller than the threshold. An example histogram of a line containing punctuation mark and another histogram for a word containing a gap within the word can be seen in Fig. 11.

Figure 11 Examples of histograms of the words and punctuation marks: (a) an example histogram and a n image for punctuation marks, (b) an example for a word containing gap within the letters

3) Character Segmentation

Several methods for character segmentation have been adopted over years. It is possible to group those into two categories as explicit segmentation and implicit segmentation [22]. Explicit Segmentation refers to partition of the word into individual characters. Then, the recognition is performed according to the results of segmentation. Therefore, the accuracy of the segmentation is very important for a successful recognition. Implicit Segmentation on the other hand tries to match any input over the image with its alphabet. It basically searches all possible locations across the whole word signal [23]. The recognition is performed at the same time with segmentation.

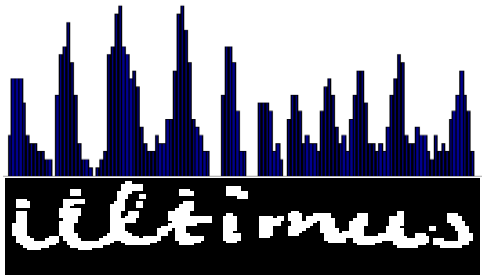

Figure 12 Vertical projection of a Word

In our work, explicit segmentation was adopted. Vertical Projection of the words was calculated and the individual characters were segmented according to the low pixel count at the point. However, when it comes to letters, a low number of pixels at a certain vertical line do not necessarily indicate a connection between letters. As can be seen from Fig. 12, it may also be the letter itself.

In order to distinguish between letters and the connecting lines, another measure was adopted before segmenting according to the threshold. The threshold is the centre line which is acquired by the horizontal projection of the word. And the line containing the highest pixel run is considered as the centre line [5]. If the pixel count is below threshold at a certain vertical line, then location of the white pixels are checked. If they belong to the upper part of the image, then there is no segmentation. On the other hand, if the white pixels are below or over the centre line then the segmentation is performed. This way, letters having low pixel count at their top are segmented correctly (h, m, n, r, t). Another addition to the algorithm is about the very last pixels. The algorithm ignores the low number of pixels in the very end of the image, in order to avoid segmentation of the ends of the letters into several pieces.

4) Evaluation of the Segmentation

Segmentation accuracy indicates how precise the prediction of the segmented image is. However, accuracy alone cannot be relied on in judging the performance of the given segmentation [24]. That is where the application of a confusion matrix can help. By setting the predicted segmentation against the true segmentation, not only the overall loss can be calculated, but the cost of different types of segmentation errors are also revealed by each cell of the matrix [25]. Table 1 shows the confusion matrix. In the table below, 'a' is the number of correct negative predictions, and 'b' shows the number of incorrect positive predictions, while in the following row 'c' is the number of incorrect negative predictions, and 'd' indicates the number of correct positive predictions [26].

TABLE I
CONFUSION MATRIX

		Predicted	
		Negative	*Positive*
Actual	*Negative*	a	b
	Positive	c	d

We adopted four measures for evaluation namely accuracy, precision, recall and f measure. Table II, represents those results of the line segmentation, word segmentation and character segmentation methods adopted. Line segmentation method worked very well with the data set. The accuracy for line segmentation is 96% for projection of histogram method. As can be seen in the Table II, HT and WT did not perform as well as the projection of histogram method.

TABLE II
RESULTS

	Line			Word	Character
Method	Projection of Histogram	HT	WT	Projection of Histogram	Projection of Histogram
Accuracy (%)	96	79	38	85	78
Precision	0,97	0,85	0,43	0,90	0,78
Recall	0,99	0,91	0,55	0,90	1
F-measure	0,98	0,88	0,55	0,90	0,88

In case of word segmentation, the accuracy was only 85% with 0,9 precision, recall and f measure value. Words written very close to each other created the biggest miss-segmented words group. This challenge comes with cursive handwriting. In the future, other methods will be adopted in order to overcome this issue. Finally, character segmentation phase was completed and the accuracy rate was only 78%. The method adopted did not perform very well on cursive handwritings. However, after modification certain difficulties were overcome. Segmentation of individual characters in cursive script is still problematic when it comes to real life documents with low quality. In the future, different methods are going to be employed for character segmentation purpose.

III. CONCLUSION

Pre-processing is a crucial step for Optical Character Recognition. At the same time, it is also very challenging especially in offline recognition since the quality of the input cannot be controlled. Recognition of real life documents is different from the ready databases as they can be in any form. Our data set was obtained by scanning handwritten lecture notes in Hungarian. The handwritings in the data set were all cursive or mixed cursive and discrete which are the most difficult handwritings for recognition [4].

In this paper, we proposed pre-processing techniques for Hungarian handwritings. The proposed method is also applicable to other languages with Latin characters. After completion of the binarization and noise removal, the images of pages were segmented into lines, words and finally characters respectively. The results were satisfying for line segmentation and word segmentation. However, character segmentation accuracy was lower than ideal.

The expected accuracy for character segmentation is very high since the accuracy of the recognition is highly dependent upon that. It is hard to compare the results of this work with others because different data sets were employed. In addition to this, there are not many research conducted for Hungarian Handwriting recognition. However, the results of the current work are going to be compared with the results of the future works.

IV. FUTURE WORK

Looking at the results, implementation of other word and character segmentation techniques seems to be beneficial. Alternatively, implicit segmentation methods can also be adopted for the same data set. Additionally, skew correction and slant removal phase was skipped due to a very little amount of skewed lines and slanted words in this data set. Therefore, those were ignored. However, in the future work, worse handwritings are going to be recognized. Hence, skew correction and slant removal phase is estimated to be included in the future work.

Subsequent to this study, a recognition step is going to be completed by using different techniques. After the completion of the recognition of Hungarian handwritings, more challenging Hungarian handwritings are going to be tested. If necessary, the methods are going to be chanced according to the needs of the new handwritings. As a result, a common recognition system for Hungarian handwriting will be provided.

REFERENCES

[1] J. Pena, S. Letourneau, and F. Famili, “Application of Rough Sets Algorithms to Prediction of Aircraft Component Failure,” in *Advances in Intelligent Data Analys*, no. i, 1999, pp. 473–484.

[2] R. Plamondon and S. N. Srihari, “On-Line and Off-Line Handwriting Recognition : A Comprehensive Survey,” *IEEE Trans. Pattern Anal. Mach. Intell.*, vol. 22, no. 1, pp. 63–84, 2000.

[3] P. K. Charles, V. Harish, M. Swathi, and C. H. Deepthi, “A Review on the Various Techniques used for Optical Character Recognition,” *Int. J. Eng. Res. Appl.*, vol. 2, no. 1, pp. 659–662, 2012.

[4] C. C. Tappert, “Adaptive on-line handwriting recognition,” in *7th International Conference on Pattern Recognition*, 1984, pp. 1004–1007.

[5] N. Arica and F. T. Yarman-Vural, “Optical character recognition for cursive handwriting,” *IEEE Trans. Pattern Anal. Mach. Intell.*, vol. 24, no. 6, pp. 801–813, 2002.

[6] N. Otsu, “A Threshold Selection Method from Gray-Level Histograms,” *IEEE Trans. Syst. Man, Cybern.*, vol. 9, pp. 62–66, 1979.

[7] P. K. Sahoo, S. Soltani, and A. K. C. Wong, “A Survey of Thresholding Techniques *,” *Comput. Vision, Graph. Image Process.*, vol. 41, no. 2, pp. 233–260, 1988.

[8] N. Priyanka, S. Pal, and R. Mandal, “Line and Word Segmentation Approach for Printed Documents,” in *IJCA Special Issue on Recent Trends in Image Processing and*

Pattern Recognition-RTIPPR, 2010, pp. 30–36.

[9] B. Mağden and S. Telçeken, "Probabilistic Rough Sets in Turkish Optical Character Recognition," in *6th World Conference on Soft Computing*, 2016.

[10] R. K. Nath and M. Rastogi, "Improving Various Off-line Techniques used for Handwritten Character Recognition : a Review," *Int. J. Comput. Appl.*, vol. 49, no. 18, pp. 11–17, 2012.

[11] R. M. Bozinovic and S. N. Srihari, "Off-line cursive word recognition," *IEEE Trans. Pattern Anal. Mach. Intell.*, vol. 11, no. 1, pp. 68–83, 1989.

[12] R. J. Rodrigues, A. Carlos, and G. Thom, "Cursive character recognition – a character segmentation method using projection profile-based technique," in *The 4th World Multiconference on Systemics, Cybernetics and Informatics SCI 2000 and The 6th International Conference on Information Systems, Analysis and Synthesis ISAS*, 2000.

[13] S. Mo and J. Mathews, "Adaptive, quadratic preprocessing of document images for binarization," *IEEE Trans. image Process.*, vol. 7, no. 7, pp. 992–999, 1998.

[14] B. Verma and M. Blumenstein, "Fusion of Segmentation Strategies for Off-Line Cursive Handwriting Recognition," in *Pattern Recognition Technologies and Applications: Recent Advances*, New York: Information Science Reference, 2008, pp. 1–16.

[15] A. R. Khan and M. Zulkifli, "A Simple Segmentation Approach for Unconstrained Cursive Handwritten Words in Conjunction with the Neural Network," *Int. J. Image Process.*, vol. 2, no. 3, pp. 29–35, 2008.

[16] K. Y. Wong, R. G. Casey, and F. M. Wahl, "Document analysis system," *IBM J. Res. Dev.*, vol. 26, no. 6, p. 647–656., 1982.

[17] D. H. Ballard, "Generalizing the Hough transform to detect arbitrary shapes," *Pattern Recognit.*, vol. 13, no. 2, p. 111–122., 1981.

[18] R. O. Duda and P. E. Hart, "Use of the Hough transformation to detect lines and curves in pictures.," *Commun. ACM*, vol. 15, no. 1, pp. 11–15, 1972.

[19] M. H. Glauberman, "Character recognition for business machines," *Character Recognit. Bus. Mach. Electron.*, vol. 29, no. 2, pp. 132–136, 1956.

[20] R. Kasturi, *Image analysis applications.*, 24th ed. CRC Press, 1990.

[21] O. D. Trier, A. K. Jain, and T. Taxt, "Feature extraction methods for character recognition - A survey," *Pattern Recognit.*, vol. 29, no. 4, pp. 641–662, 1996.

[22] A. Choudhary, "A Review of Various Character Segmentation Techniques," vol. 4, no. 6, pp. 559–564, 2014.

[23] C. Viard-gaudin and É. Caillault, "Using Segmentation Constraints in an Implicit Segmentation Scheme for On-line Word Recognition," in *Tenth International Workshop on Frontiers in Handwriting Recognition*, 2006.

[24] N. Xue, "Chinese word segmentation as character tagging," *Comput. Linguist. Chinese Lang. Process.*, vol. 8, no. 1, pp. 29–48, 2003.

[25] D. Hand, H. Mannila, and P. Smyth, *Principles of Data Mining*. MIT Press, 2001.

[26] "Confusion Matrix." [Online]. Available: http://www2.cs.uregina.ca/~dbd/cs831/notes/confusion_matrix/confusion_matrix.html. [Accessed: 07-Sep-2016].

Aerial Triangulation Test Project with UAS Technology

Tamas Jancso - Peter Udvardy

Institute of Geoinformatics, Alba Regia Technical Faculty, Óbuda University
Pirosalma u. 1-3, Székesfehérvár, H-8000, Hungary
jancso.tamas@amk.uni-obuda.hu
udvardy.peter@amk.uni-obuda.hu

***Abstract*— the paper deals with the optimization of the aerial triangulation based on UAS images. The images were taken with a DJI Phantom 3 Advanced quadrocopter and they were measured in Photomod UAS Lite ver. 6. The bundle adjustment was carried out twice, first in Photomod Solver and later in BINGO ver. 6.8. During the adjustment 14 ground control points were used and 34 points were calculated as new points. Using these new points we could compare the coordinates to the coordinates received from the high-precision field surveying measurements. From the coordinate differences the calculated RMS errors of horizontal coordinates are below the pixel size on the ground horizontally and vertically as well. The final results showed us that a non-metric camera at low flight height with a quadrocopter can be used effectively and accurately at aerial surveys of relatively small areas.**

***Keywords*— UAS, aerial triangulation, bundle adjustment, error assessment**

I. Introduction

For testing, some large scale aerial photos were used taken at a relative height of 116 m. The test field was marked with 49 signs distributed by a grid. The images were taken with a DJI Phantom 3 Advanced quadrocopter having a 12 Mpixel camera and they were measured in Photomod UAS Lite ver. 6. and the bundle block adjustment of 16 images was done initially in Photomod. After checking the residuals and RMS values a second bundle adjustment was carried out in BINGO ver. 6.8. During the final block adjustment the camera calibration and the systematic image distortion compensation was calculated as well. During the adjustment 14 ground control points were used and 34 points were calculated as new points. Using these new points we could compare the coordinates to the coordinates received from the high-precision field surveying measurements. From the coordinate differences the calculated RMS errors of horizontal coordinates are around 2 centimeters and the RMS error of vertical coordinates is 3.2 centimeters. The pixel size on the ground was 5 cm, which means the RMS errors corresponds to 0.4 pixel in X, Y and to 0.6 pixels vertically.

II. Test Area

For testing, we used an area of 200x200 m near Szekesfehervar close to village Iszakszentgyorgy. The size of the point marks was 50x50 centimetres (see Fig. 1 and Fig. 2). On Fg 1 the control points are indicated with red circles.

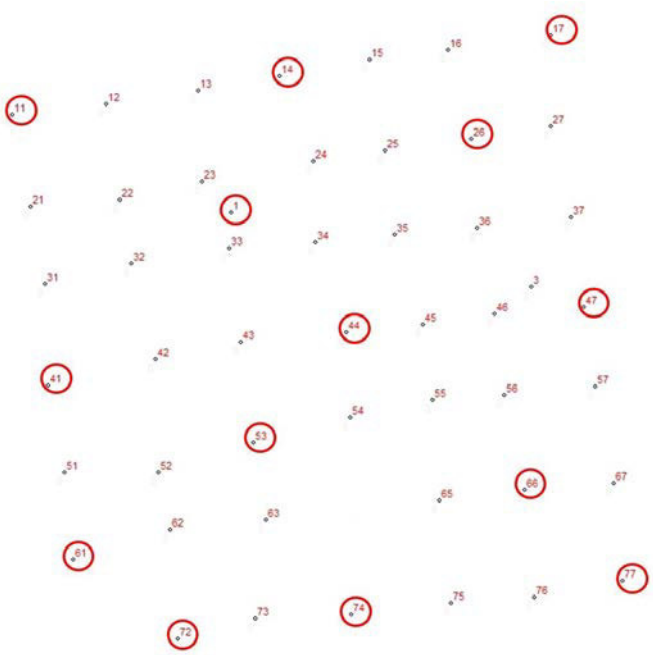

Fig. 1 Coordinate system for relative orientation

Fig. 2 Point mark on the test area

III. 3. Phantom DJI 3 Advanced

The DJI (official name is Dà-Jiāng Innovations Science and Technology Co., Ltd) company manufactures unmanned aerial vehicles for aerial photography and for video purposes. The company headquarter is located in the industrial heart of

China in Shenzen. One of the leading economic journal of the world chose DJI for the leading company of civil drone industry in 2015. One of the most popular product of the company is the Phantom series quadcopters.

A. Technical Data

Our Faculty has a DJI Phantom 3 Advanced aircraft (Fig. 3.). This UAV is available from the middle of 2015 and has more new features e.g. safer indoor use. The whole equipment is 1280 grams and its maximum ascend speed is 5 km/h and maximum horizontal speed is around 45 km/h. The UAV is equipped with GPS/Glonass receiver and has a precise 3 axis gimbal for good performance. The maximum operating range is more than 2 kilometres and the 4480 mAh LiPo battery operates for 22 minutes per charges.

Autopilot and 'GO HOME' function is available at any time or at less than 20 percent battery operation time. During flight an almost real time video (latency is 220 ms) is available thanks to DJI's Lightbridge technology.

The on board camera is a Sony EXMOR 1/2.3" camera which has 12.4 million effective pixels (the total pixels are 12.76 millions). The lens has a FOV of 94° with 20 mm focal length (35 mm format equivalent) and with f/2.8. The ISO range is 100-3200 for video recording and 100-1600 for photos. The shutter speed varies between 8 and 1/8000 seconds.

A new technology helps to fly safe indoor as the UAV is equipped with ultrasound sensors. The still photography modes contains single shot, burst shooting (3/5/7 shots), auto exposure and time lapse. The video mode contains 2.7K, FHD and HD.

The DJI GO application is available for IOS and Android. We use this device with Samsung Galaxy3 8" tablet.

Fig. 3 DJI Phantom 3 Advanced UAS (source: DJI.com)

B. Mission Planning

The images were taken on September 7, 2016. We managed to get 16 images organized in 4 strips with relative flight height of 116 m and with the following image numbers (see also Fig. 4):

Strip 1: 14, 15, 16, 17;
Strip 2: 18, 19, 20, 21;
Strip 3: 22, 23, 24, 25;
Strip 4r: 26, 27, 28, 29.

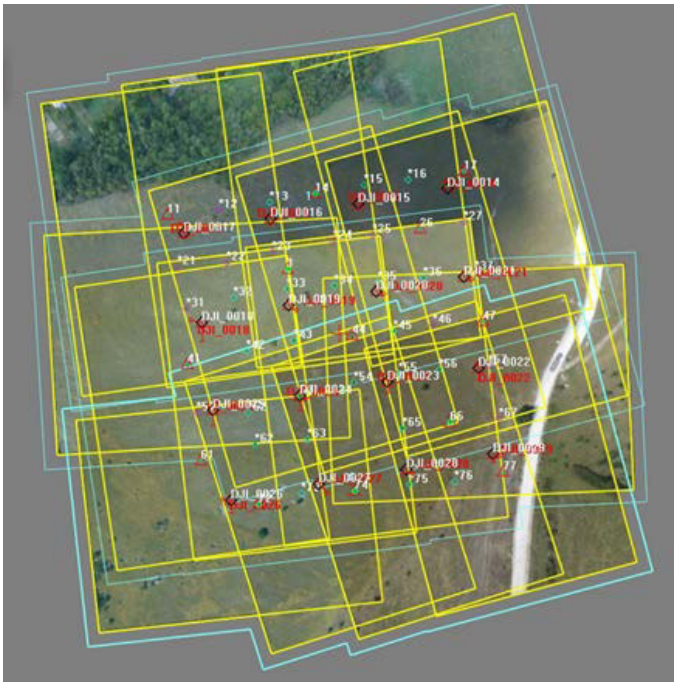

Fig. 4 Block of images

We carried out the flight in autopilot mode using the UgCS (Universal Ground Control Station) software application. In UgCS we managed to setup a 70 % overlap between the images and 60% overlap between the strips (Fig. 5). The whole autopilot flight procedure had the following steps:

1. Plan the flight in desktop application.
2. Go to the test area.
2. Switch on the remote controller and then the drone.
3. Connect the remote controller and the tablet by wire.
4. Switch on the tablet and start the UgCS application.
5. Join the tablet and the laptop into the same Wi-Fi network.
6. Launch the UgCS application on the laptop and wait for recognition of the drone.
7. Switch to "P" mode the remote controller and take off (approximately at 1m height) and then switch to "F" mode.
8. Choose the flight plan and upload it to the tablet.
9. Launch the "Auto Mode".
10. At the end of the mission: "Return Home".

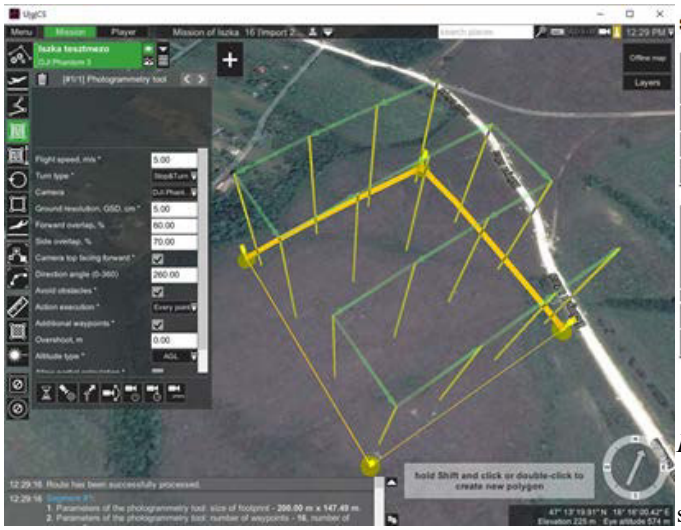

Fig. 5 Mission planning in UgCS

IV. 4. AERIAL TRIANGULATION

C. *Orientation and Measurement in Photomod*

After pre-processing and improving the bright and contrast on images we started the orientation process of 11 images in Photomod UAS Lite v6. [2]. The interior orientation meant simply to key in the camera parameters.

The next step was to measure the ground control points (GCPs) and new points on each stereo-pair (Fig 5).

After the measurement of all points we could initiate the relative orientation for the block and checking the vertical parallaxes on each stereo-pair and triplets we managed to prepare the whole block for the aerial triangulation (Fig. 6).

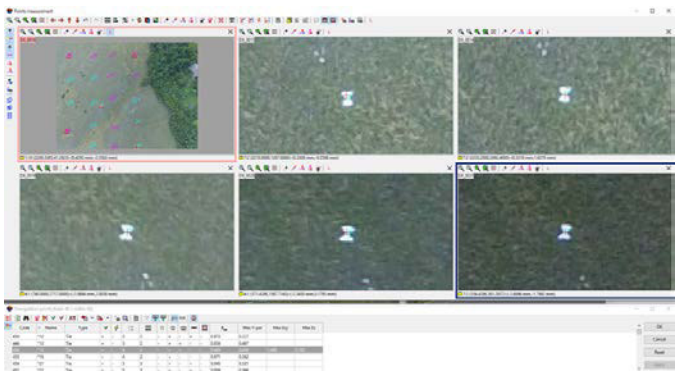

Fig. 5 Measuring of control and tie points

Strip: 1

	Stereopair	Number of points	Vertical parallax, pix.			Discrepancy of kappa angle, gon	Distribution uniformity	
			RMS	Mean abs.	Max			
*	DJI_0017—DJI_0016	10	0.213	0.187	0.395	-0.340741	Non-uniform	+ -
*	DJI_0016—DJI_0015	12	0.412	0.362	0.766	0.692129	Non-uniform	+ -
*	DJI_0015—DJI_0014	8	0.435	0.354	0.833	-2.047492	Non-uniform	+ -

	Triplet	Number of points	Tie residuals, pix.					
			RMS		Mean abs.		Max	
			E_{xy}	E_z	E_{xy}	E_z	E_{xy}	E_z
*	DJI_0017—DJI_0016—DJI_0015	2	0.224	0.674	0.224	0.672	0.243	0.710
*	DJI_0016—DJI_0015—DJI_0014	3	0.236	1.093	0.223	1.022	0.329	1.567

Fig. 6 Relative orientation results for the sirst strip

D. *Aerial triangulation*

Finishing the measurement we could build the block scheme and we could start the block adjustment procedure in Photomod Solver [3], (Fig. 7.).

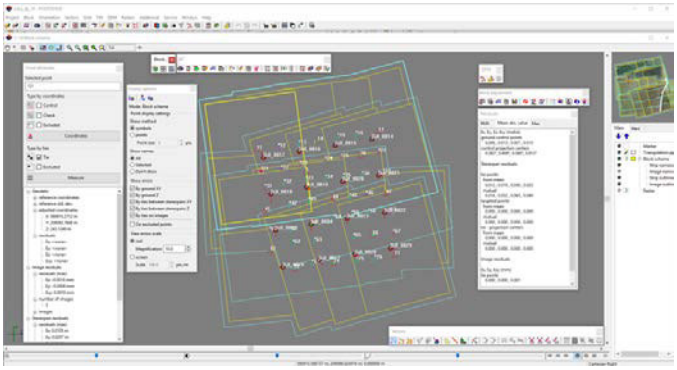

Fig. 7 Results in Photomode Solver

In order to have better results we decided to repeat the bundle block adjustment using the BINGO v6.8 software. The initial values of the exterior orientation elements were taken from Photomod Solver, so we expected only small corrections. Before running the BINGO we decided to add the camera calibration process to the adjustment and referring to the BINGO manual [1], we added 17 additional parameters to correct the systematic image errors. The final report of results is shown on Fig. 8. The sigma0 is 0.79 microns, which is acceptable. Since the adjustment procedure is optimised to the ground control points, the RMS errors of GCPs are extremely good, in X, Y it is only 3 mm and in Z it is 1 mm.

On Fig. 9 we can observe the distribution of error ellipses on new points printed out from the Bingo error assessment module.

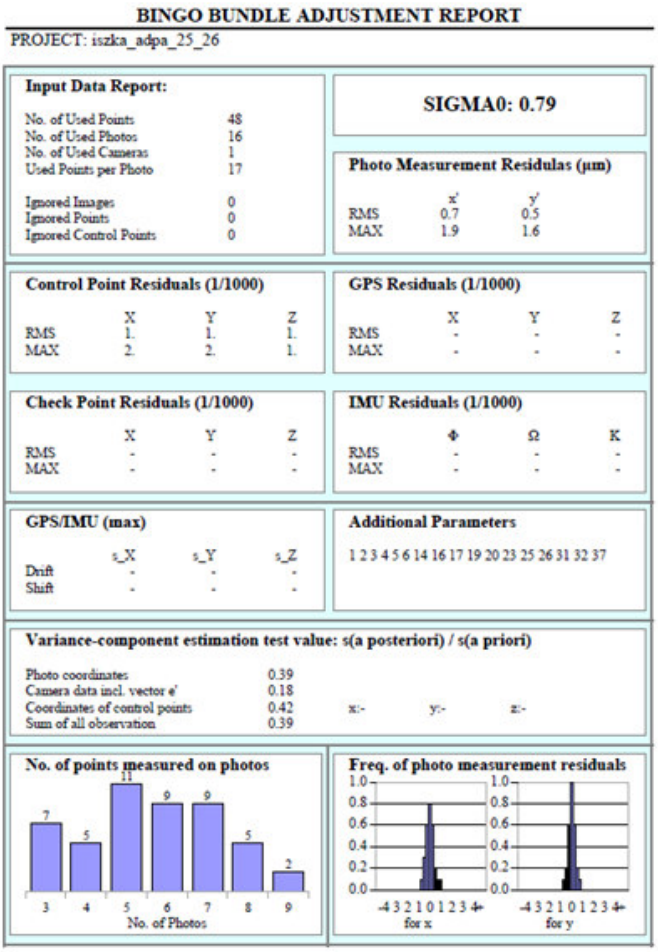

BINGO BUNDLE ADJUSTMENT REPORT

PROJECT: iszka_adpa_25_26

Input Data Report:

No. of Used Points	48
No. of Used Photos	16
No. of Used Cameras	1
Used Points per Photo	17
Ignored Images	0
Ignored Points	0
Ignored Control Points	0

SIGMA0: 0.79

Photo Measurement Residulas (µm)

	x'	y'
RMS	0.7	0.5
MAX	1.9	1.6

Control Point Residuals (1/1000)

	X	Y	Z
RMS	1.	1.	1.
MAX	2.	2.	1.

GPS Residuals (1/1000)

	X	Y	Z
RMS	-	-	-
MAX	-	-	-

Check Point Residuals (1/1000)

	X	Y	Z
RMS	-	-	-
MAX	-	-	-

IMU Residuals (1/1000)

	Φ	Ω	K
RMS	-	-	-
MAX	-	-	-

GPS/IMU (max)

	s_X	s_Y	s_Z
Drift	-	-	-
Shift	-	-	-

Additional Parameters

1 2 3 4 5 6 14 16 17 19 20 23 25 26 31 32 37

Variance-component estimation test value: s(a posteriori) / s(a priori)

Photo coordinates	0.39		
Camera data incl. vector e'	0.18		
Coordinates of control points	0.42	x:-	y:- z:-
Sum of all observation	0.39		

No. of points measured on photos

Freq. of photo measurement residuals

Fig. 8 BINGO adjustment report page

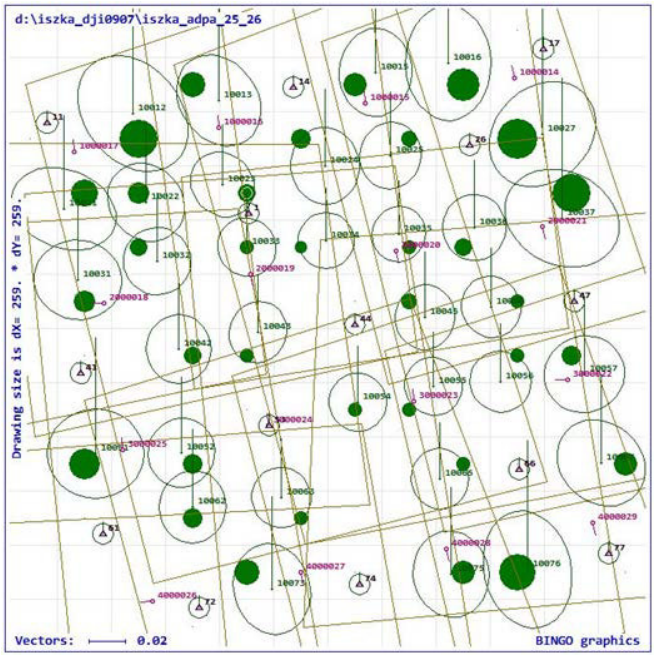

Fig. 8 Error ellipses on new points

V. Conclusions

As a summary we can say that the field resolution of the images was 5 centimetres and after the adjustment the horizontal error was 2 centimetres. We can say that the UgCS software is a user friendly and freeware application and it can be used easily for planning and executing of aerial surveying missions. During the geotagging of the pictures the „yaw," „pitch" and „roll" values were logged, but these values should be interpreted with much care.

References

[1] Kruck, E. – Bingo 6.6 Manual, Bundle Adjustment for Engineering Applications, A Program System for Close Range Photogrammetry and Aerial Triangulation Including Three-Dimensional Geodetic Network Adjustment, Aalen, , pp. 156, 2014

[2] Racurs – User Guide - Processing of UAV Data ver. 5.3., pp. 22, Moscow, 2014

[3] Racurs – User's manual of Photomod Solver 4.4., pp. 75, Moscow, 2008

Using geoinformatics tools in archeology

V. Balázsik* and Z. Tóth*
Institute of Geoinformatics, Alba Regia Technical Faculty, Óbuda University
Pirosalma u. 1-3, Székesfehérvár, H-8000, Hungary
balazsik.valeria@amk.uni-obuda.hu, toth.zoltan@amk.uni-obuda.hu

The technological advancements in data sourcing and processing techniques gives entirely new possibilities in the field of archeology. These range from quarry discovery to 3D modeling of artifacts. Introducing new technologies holds several advantages, such as improving the effectiveness of quarry discovery, shortening the time required for the excavation, more detailed and more accurate data sourcing and processing methods, usage of complex databases, which can directly lead to more detailed analytical approaches, and last, but equally importantly, the 3d modeling and visualization of artifacts and analysis results.

I. DISCOVERY OF EXCAVATION SITES

Using aerial photographs is a well known technique used to find excavation sites. The different types of vegetation, unusually regular shapes in plant life, and at the end of winter season, the snow melting patterns can indicate remains of manmade structures. These discovery methods have been extended with the following approaches:

Parallel to taking aerial photographs, taking high resolution laser mapping images of the surface *(LIDAR)* is also available. These dataset can contain up to 8-10 data points -or more- for every square meter, taken from 1000-1200 meters in the air with an approximately 0.15m absolute elevation precision. The relative precision can be much higher, and a result, the difference between the ground surface and artifacts can be as low as ~2-3 centimeters. This means that it can not only visualize data and information that's practically invisible to the human eye, but also give us the opportunity to look at the current advancement state of the plantation. Thus, the discovery of hill and earth forts through the usage of detailed and accurate surface models is much more effective, especially since there's no historical written material regarding the building of these structures, only this sort of representation can visualize their existence.

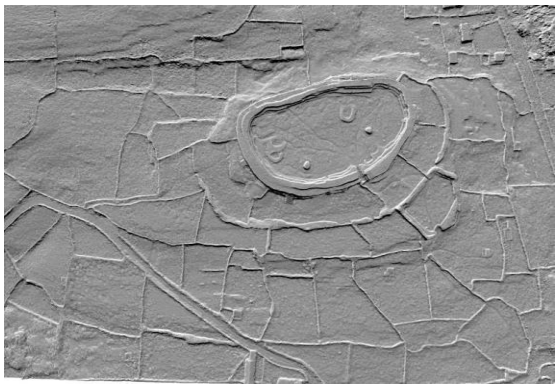

Figure 1. Surface model calculated from LIDAR imagery [1]

Walls and other remains within the soil can alter groundwater levels and generally the water percentage of the soil, which results in different plantation development and advancement levels. If the recording and the analysis is made within the spectrum that can be used to detect the smallest variance, then we can use image processing, namely spectral distribution analysis to find possible excavation sites. Figure 2. shows a site on an infrared snapshot. The sub-soil lines of buildings is much more apparent compared to the original aerial imagery.

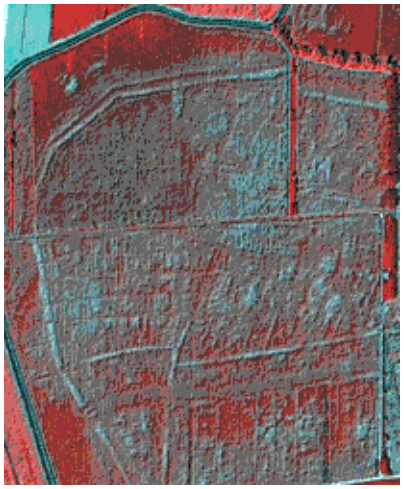

Figure 2. Excavation site on an infrared image [2]

High resolution and high precision surface models can be also reached by using unmanned aerial vehicle *(UAV)* discovery flights. By only using amateur photography equipment, we can record images up to 1-2cm precision level, while flying low altitude, given ideal conditions. By applying it on a smaller surface area, repeating the process 8 to 10 times, the processing software can produce imagery that matches the precision and resolution of the original recordings. The end result is normally a surface mesh of the ground surface. The advantage of the UAV data sourcing is that it can be used on territory that's complicated to access or not accessible at al.

Among the various geophysical methods *(magnetometer, soil resistivity, seismic)*, we used radar technique in our exploration practice. The basic principle of its mechanism that electromagnetic radiation entering the soil is reflected from strata with different dielectric constant. The result is more unambiguous and nicer in non-urban areas where there are no interfering objects such as underground utility lines. It is less efficient to use in densely built urban environment, since the signal is reflected not only from underground lines but also from debris and rocks, and it is difficult to filter the data of archaeological value from the “noisy” image.

Figure 3. shows an earth fort detected by ground penetrating radar by the evaluation of our own survey [3], representing the sections on a satellite image. Remains of medieval buildings can be observed in the central area. The homogeneous appearance of the buildings of the earth fort on the radar image is due to the fact that no human activity - other than agriculture - was carried out over the past centuries which could have deleted the effects of the methodology applied in the construction of the earth fort. Therefore, these phenomena can be easily detected even at present.

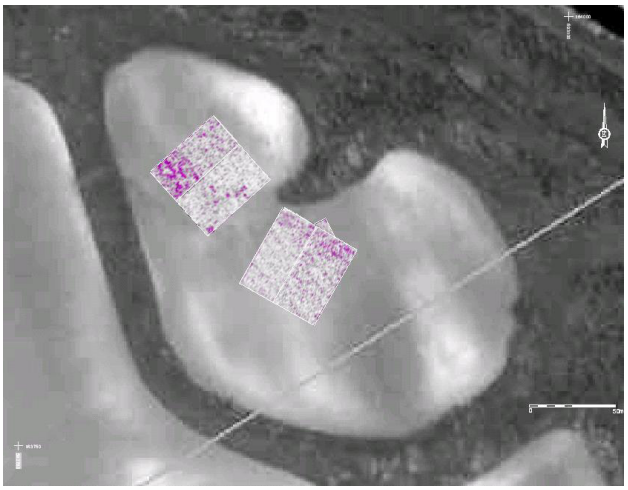

Figure *3*. Earth fort explored by ground penetrating radar near Szabadhídvég [3]

Underwater imaging is not a new technique in archaeology but it has to be mentioned for the sake of completeness. In this field as well, the spectral sensitivity and the geometric resolution of imaging systems have increased in the recent past which yields greater accuracy after processing.

II. SURVEY AND DOCUMENTATION OF ARTIFACTS

"Act No. LXIV of 2001 on the Protection of Cultural Heritage (hereinafter: Act on Heritage Protection) contains the main terms regarding the conservation of archaeological relics.

The protection of archaeological heritage involves the discovery, evaluation, documentation, registration, conservation of the archaeological heritage and the establishment of protection on archaeological sites [Act LXIV of 2001, Section 7, Item 7/A "[4]

Archaeological artifacts discovered underground or below some structure and the circumstances of their discovery were traditionally recorded with geodetic measurements, scaled drawings and paper-based, later digital images over a long period of time. New data acquisition and processing techniques – partly due to the geodesists participating in the surveys, partly due to the appearance of the new generation of archaeologists – are beginning to spread within the discipline. This considerably decreases the time necessary for the exact surveying and documentation of artifacts. These economic and other advantages – e.g. less field days, time schedule of constructions – are benefits not only for archaeologists but in many cases also for other, affected disciplines, such as road construction and utility services. In the case of a survey in residential area, these benefits are experienced by the residents as well who have to face the inconveniences resulting from the closure of public areas for a shorter period of time.

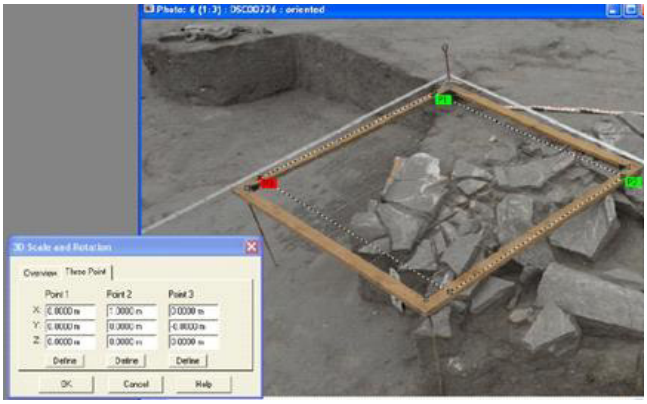

Figure 4. Conventional documentation of an archeological survey in the planned trajectory of the M6 motorway, Baracs, 2009. [5]

Apart from economic advantages, it is very important for archaeologists that the quantitative and qualitative properties of recorded data improved by orders of magnitude due to digital data registration and modern technologies in geoinformatics.

Advantages of technologies in geoinformatics:

- site survey without its "disturbance/damage"
- greater accuracy during surveys,
- more detailed artifact recording,
- options for 3D modelling,
- shared database with data form other sources
- option for complex analysis (geographical information software)
- various visualization options
- options for subsequent data acquisition

It has to be noted that the spread of technologies was also facilitated by the fact that these days the images recorded with so-called amateur cameras are also suitable for processing, and some user software can be downloaded for free.

Below we present a few examples where geoinformatics technologies were applied in archaeological surveys and documentations.

- **ground laser scanner**

When surveying with the ground laser scanner, the laser beam emitted from the instrument and reflected from the surface of the surveyed object determines the exact place of reflection. Before the measurement we can set the point density to be obtained on the surface of the scanned object. Generally, the details of terrain objects can only be surveyed from several positions, partly due to the dimensions of the objects but in some cases also because of the dead angle of measurement of the laser scanner. The results of each scanning can be integrated which also enables the merging of internal and external scanned point clouds of buildings or building remnants. Based on these, we can prepare the section views of the object. Likewise, the point clouds produced from aerial and ground laser scanning can be also handled together. The latter solution is suitable for building a 3D city model which does not only provide a spatial view but the shared point cloud enables high accuracy data can be searched, sections can be plotted, such as the structure gauges of roads bounded by trees. Figure 5. shows the presentation of point clouds produced by the external and internal scanning of the medieval Anna Chapel.

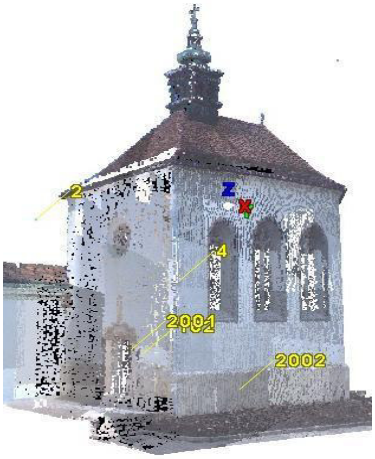

Figure 5. External point clouds of the Anna Chapel in Székesfehérvár [6]

Simultaneously with laser scanning, pictures were taken of the surveyed object. Their colors can be linked with the detected points which gives a colored point cloud. With sufficient point density, the scanned object can be viewed as a continuous model appearing in original colors, being able to distinguish fine details and exact coordinates can be read. In the archaeological use of the survey technology, it can be also highlighted that the spectral values linked to the points can serve as further information.

- **UAV, photogrammetry**

Digital images taken by unmanned aerial vehicles can be used for the composition of orthophoto tile image and the surface model of excavation areas. The sensor fitted to the aerial vehicle (UAV) - most commonly a high resolution ordinary camera - can take pictures of 1-2 cm resolution due to the low flying level. Due to repeated overlapping, high accuracy data can be obtained even after processing. Under favourable circumstances, data accuracy is close to, or may even reach the on-site resolution value of original images. The accuracy of fitting to the national projection system used by archaeologists is affected by the determination method of points used for fitting. Fitting points can be determined with a measuring station in such a way that measurements are carried out for known reference points but these can be determined by GNSS technology as well.

Figure 6. Kopter type UAV

Figure 7. and 8. shows the works of the excavation carried out in the historical centre of Székesfehérvár and the orthophoto tile image presenting the developed area. The image, free of distortion, shows wall remains from different ages. These can be compared with the previously explored and documented, nearby wall remains in a joint database with geographical information tools. The results obtained by the analysis may be included in the arguments of a dispute of decades, as to whether existed a royal castle/palace in the vicinity of Grand Prince Géza's four-wing church, that is to say, near today's Basilica. (Fejér Megyei Hírlap, 1 October 2016)

Figure 7. Development of the church of Grand Prince Géza

Figure 8. Orthophoto tile image of the development area

In the dispute of archaeologists and historians, the possibility of visualization cannot be negligible. Whereas historians place a greater emphasis on occurrences in historic documents, archaeologist consider the discovered artifacts as more significant. A 3D visualization may move both theories to either accept or reject the other hypothesis.

Unmanned aerial vehicles, commonly known as drones, can be purchased at an affordable price. The expectations regarding the cameras on the drones are not as strict as for the professional photogrammetry survey cameras. As such, digital cameras providing good optical quality images can also have a role in this technology which is applied in an increasing range of areas. Since these tools collect such a large amount of data from the area of archaeological surveys which could have only been gathered with several weeks of field work in the conventional documentation previously applied in archaeology, their purchase price returns soon, even several times. Developers offer several software for the processing of images and their use is now easier to learn This explains why they spread so fast.

Figure 9. Wall remains outlined based on the visual interpretation of the orthophoto

The polygons delimiting the wall remains are classified based on the archaeological dating according to the time of their origin, into different layers. The development has been completed, the excavation area has been backfilled, the public area serves for its original function. Detailed documentation and the joint database enables comparison with the previously explored and also backfilled wall remains, as well as the analysis of the presumed relationship between them.

- **Close-range photogrammetry**

  These days not only the images taken by photogrammetry cameras are suitable for evaluation but also the good quality, overlapping digital images taken by ordinary cameras can be used for preparing the proportional, 3D model of objects and the discovered artifacts. We can fit image details to the surfaces of the space model by which we can achieve the photo-realistic visualization of the object. The model can be scaled afterwards and it can be transformed in the field system by using points of known coordinates. The newer versions of the software determine the object points by bearing based on the homologous radii of overlapping images and automatically generate a high-density point cloud.

Figure 10. 3D model of a dish [6]

III. ESTABLISHMENT OF DATABASES, ANALYSIS AND VISUALIZATION OPTIONS

All presented data acquisition and documentation procedures enable the generation of spatial, digital products which can be raster and vector data as well. The software applied during data processing enable the conversion of different data formats by which the data obtained as a result of various technologies can be integrated in a joint database. Geographical information software can handle various data together, enable searching with logical conditions, filtering and analysis. Data organized in layers in a practical way – e.g. according to their time of origin – can be visualized in arbitrary combinations, therefore they provide opportunity to examine the relationships among them. Previously this was possible only with visual interpretation and the manual redrawing of different thematic archaeological maps. There are various ways for the visualization of results obtained by the analyses. Different plans, sections can be prepared but it is also

possible to read spatial models and transform the into another system.

During the preparation of urban development plans, care must be taken of the presumed archaeological sites, the protection and unearthing of valuable artifacts. The legend of Figure 11 and its legend shows that the historical city wall was partly developed in the centre of Székesfehérvár but there are also presumed sections of the wall. The medieval city walls have to be made visible after development. Geoinformatics technologies can be applied both for development and making the walls visible. A well established archaeological database can be used as a source of information when preparing urban development plans, the formation of local construction regulations and the control of their observation.

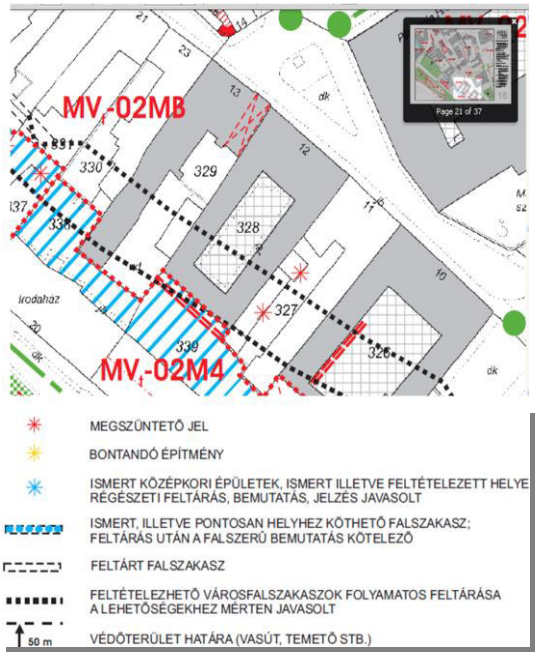

Figure 11. Detail of the development plan of Székesfehérvár and its legend

The presented examples clearly show that modern data acquisition methods, data processing technologies and 3D modelling options can be used in various ways in archaeological operations. These make the survey of archaeological sites more successful, they provide more efficient, more accurate and more detailed documentation. These enable subsequent data acquisition after the backfilling of the site. Digital databases with practical structure and geographical information software enable complex analyses. The spatial and temporal relationship of remains developed in different periods can be examined. The spatial visualization of models can bring history closer to the broader audience.

IV. SUMMARY

Although some of the measuring equipment used in geoinformatics technologies, such as the laser scanner are rather expensive but the data acquisition carried out by them is more efficient, more detailed and more accurate. Therefore, with sufficient utilisation, their purchase price or the costs of the measurements carried out with them, result in a relatively quick return. Among the modern tools used in archaeological surveys, UAVs are affordable nowadays, they can provide the expected measurement accuracy for the documentation of artifacts. The data gathered by this technology also enables quick plotting of plane projections, sections and the spectacular 3D visualization of artifacts and their environment.

REFERENCES

[1] http://aerialarchaeology.blogspot.hu/2015/08/dun-chonchuir-inis-meain.html

[2] http://archive.archaeology.org/0911/trenches/roman_venice.html

[3] Cs. Szőllősy, K. Pokrovenszki, Z. Tóth “Szabadhídvég Pusztavár roncsolásmentes műszeres felmérése” in Gesta XII. 2013, pp. 20–29.

[4] https://epitesijog.hu/fooldal/1310-a-regeszeti-lelohely

[5] K. Farkas: Thesis work, 2009, V. Balázsik

[6] Z. Tóth “Távérzékelési és geofizikai módszerek az objektum és tárgyrekonstrukcióban” Fiatal középkoros régészek konferenciája, 2014,

Simulation of Electro-physical Characteristics of the Bulk Material in the Electric Field of Capacitive sensors

A. Kadyroldina** and A. Arinova*

* D. Serikbayev East Kazakhstan State Technical University/Department of Information Technology and Business, Ust-Kamenogorsk, Kazakhstan

** National Research Tomsk Polytechnic University/ Institute of High Technology Physics, Tomsk, Russia

akadyroldina@gmail.com

ab.arinova1190@gmail.ru

***Abstract*— The present article covers mathematical and computer simulation of behavior of the bulk material with varying particle composition in relation to development of capacitive humidity sensors, which uses wide band of electrical field where a sample of the mentioned bulk material is put during measurements and researches. The developed model of electrical and physical properties of the bulk material is used to receive frequency and humidity characteristics of a matter consisting of particles of two different sizes. There was also a program developed to calculate and visualize frequency and humidity properties, which allows entering different sizes of two particles and changing qualitative characteristics of these materials. Results presented in the article helps to construct multiparameter humidity sensors and improve accuracy of measurements received with their use.**

I. INTRODUCTION

Most mathematical bulk material models have such a weak point as that they are not able to obtain frequency and humidity properties of bulk materials with varying particle sizes [1].

In general, a problem of modeling of electrical and physical properties of bulk materials reduces to finding of integral values of the total electrical conductivity of a bulk material sample. A structure consisting of two particles with different geometrical dimensions should be taken from the bulk material sample in order to mathematically describe the whole sample. Such a structure is called the basic or elementary structure of the bulk material. We assume that the whole volume of the bulk material consists of such basic particles. Thus, properties of the whole volume of the bulk material can be inferred when examining characteristics of an individual particle. Since such characteristics are applied to an individual particle they are conventionally called as differential parameters. Specific electrical resistance, specific conductivity, relative permittivity, microhardness, density, heat capacity and other parameters could be investigated. Parameters of the bulk material investigated in the electric field of a capacitive sensor are relative permittivity ε or dielectric loss tangent tgδ. Their volumes depend on bulk material properties such as particle composition, particle nature, moisture content in the bulk material and others [2].

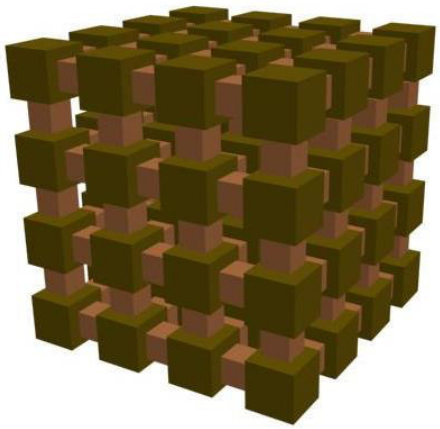

Figure 1. Proposed variant of particle packing of the bulk material consisting of particles with two different sizes (each particle having its own nature)

When developing a mathematical model of bulk material behavior in the frequency spectrum of the electrical field the real chaotic structure is replaced by an adequate ordered structure. Analytical forms are obtained for such simplified structure and used to receive frequency and humidity characteristics of the material under examination in the required frequency range [3].

II. IDEALIZATION OF THE FORM AND PACKING OF BULK MATERIAL PARTICLES

We assume that the bulk material under examination consists of two types of cube-shaped particles packed as shown in Figure 1.

Let us consider an idealized structure of the bulk material packed in the manner shown in Figure 2 in one of the orthogonal planes. In order to develop a mathematical model of the bulk material we hypothesize the following facts:

- the bulk material is heterogeneous and two-component;
- Particles 1 and 2 are respectively the first and the second cube-shaped components and have different sizes;
- the particle is evenly moistened;
- packing of particles in relation to each other and the electric field vector *E* is shown in Figure 2;

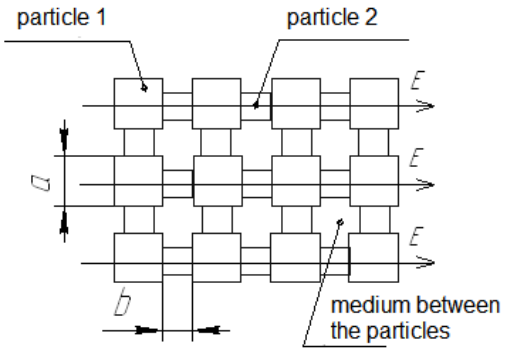

Figure 2. Idealized bulk material structure with cubic packing presented in one of the coordinate planes

- there is some space between particles having the medium with its electrical and physical properties, and porosity of the bulk material structure is determined by a

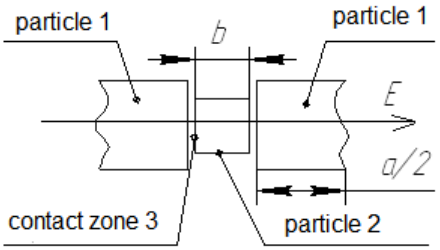

Figure 3. System consisting of two particles

ratio of geometrical dimensions of particles;

- surfaces of particles in the direction of the electric field vector are equipotential;

- current lines in particles are parallel to the electric field vector *E* and are equally distributed in particles.

The bulk material structure in Figure 2 has two cube-shaped particles, where a and b are edge dimensions of such particles, wherein $a \geq b$ and $a = k \cdot b$. Space between bulk material particles is filled with certain medium. The bulk material under examination is capillary-porous body.

In order to receive differential parameters of the bulk material we choose a section in the volume of the bulk material, which consists of two particles and contact zones. Such a system consisting of two particles is shown in Figure 3.

The Particle 2 is presented in the system as an entire cube with b edge. The Particle 1 is divided into two equal halves with $a/2$ edge in the direction of the electric field vector *E*. Such representation of two particles system allows considering conductivity of particles and contact zones between particles. Change of a and b sizes results in change of the bulk material particle composition.

III. Calculation of Conductivity of the Two-Particle System

We divide the two-particle system into different zones, where active and reactive components of the system conductivity are found using simple methods.

Let us call the zones 1 and 2 in Figure 3 as conduction areas of the Particles 1 and 2, and the zone 3 as the contact area. In this respect we also consider two halves of the zone 1 as the whole zone 1.

We represent the two-particle system as a series connection in the direction of the vector *E*. In order to take into account different polarization states of the bulk material, each part of the connection is represented as active resistance *R* and capacity *C* on zero and infinite frequency. For fast and slow polarization processes we assume parallel and sequential substitutional connections respectively [4]. Equivalent substitutional connection of the two-particle system is shown in Figure 4.

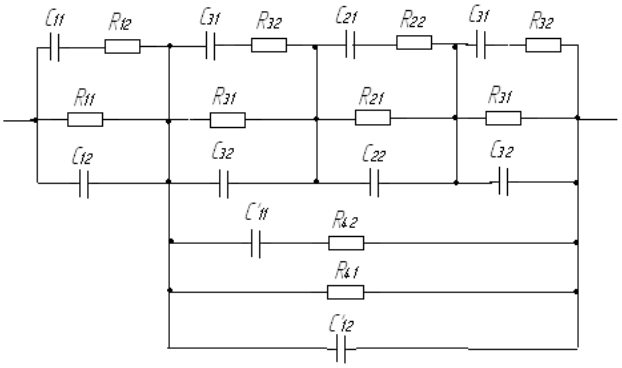

Figure 4. Equivalent substitutional connection of the two-particle system without regard to the effect of inductivities

The following symbols have meanings as follows in Figure 4:

R_{11}, R_{21}, R_{31} and R_{41} respectively mean active resistance of zones 1, 2 Contact Zone 3 and the medium to direct current;

C_{11}, C_{21}, C_{31} and C_{11}' respectively mean additional capacity between proper surfaces of the Zone 1, Zone 2, Contact Zone 3 and between surfaces of different Particles 1 with the deduction of capacity of the Contact Zone 3 under direct current and in the direction of the vector *E*;

R_{12}, R_{22}, R_{32} and R_{42} respectively mean additional active resistance of Zones 1 and 2, Contact Zone and medium on infinite frequency;

$C_{12}, C_{22}, C_{12}', C_{32}$ respectively mean capacity in the direction of the vector *E* between surfaces of the Particle 1, Particle 2, areas of the different Particles 1 with the deduction of the Contact Zone 3, and the Contact Zone 3 on infinite great frequency of alternate current.

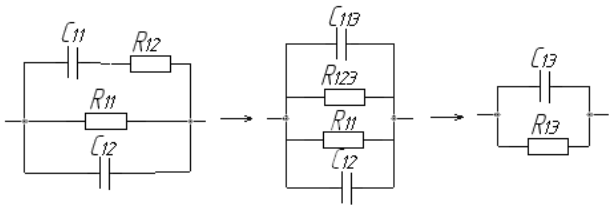

Figure 5. Sequence of conversion of the substituional connection of the Particle 1

The scheme in Figure 4 is simplified with use of formulas of active and reactive resistance when conversing series R and C connection into parallel collection and vice versa [4]. Conversions are carried out sequentially for each part of the substitutional connection (Figures 5, 6 and 7).

$$R_{12э} = R_{12}\left[1+\frac{1}{(\omega C_{11}R_{12})^2}\right]$$

$$C_{11э} = \frac{C_{11}}{1+(\omega C_{11}R_{12})^2}$$

$$R_{1э} = \frac{R_{12э}R_{11}}{R_{12э}+R_{11}} = \frac{R_{11}R_{12}\left[1+\frac{1}{(\omega C_{11}R_{12})^2}\right]}{R_{11}R_{12}\left[1+\frac{1}{(\omega C_{11}R_{12})^2}\right]}$$

$$C_{1э} = C_{11э}+C_{12} = \frac{C_{11}}{1+(\omega C_{11}R_{12})^2}+C_{12}$$

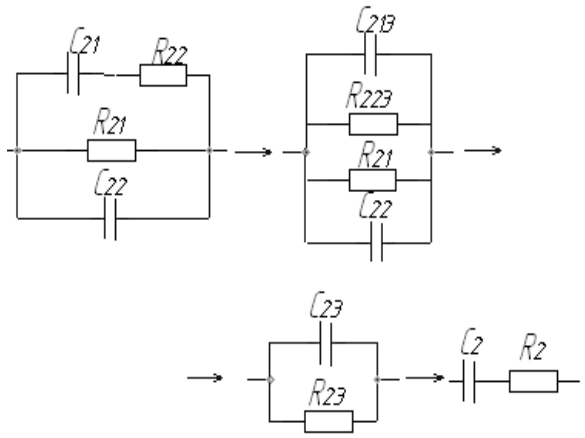

Figure 6. Sequence of conversion of the substitutional connection of the Particle 2 and substitutional connection of the Contact Zone 3

$$R_{22э} = R_{22}\left[1+\frac{1}{(\omega C_{21}R_{22})^2}\right]$$

$$C_{21э} = \frac{C_{21}}{1+(\omega C_{21}R_{22})^2}$$

$$R_{2э} = \frac{R_{22э}R_{21}}{R_{22э}+R_{21}} = \frac{R_{21}R_{22}\left[1+\frac{1}{(\omega C_{21}R_{22})^2}\right]}{R_{21}R_{22}\left[1+\frac{1}{(\omega C_{21}R_{22})^2}\right]}$$

$$C_{2э} = C_{21э}+C_{22} = \frac{C_{21}}{1+(\omega C_{21}R_{22})^2}+C_{22}$$

$$R_2 = R_{2э}\frac{1}{1+(\omega C_{2э}R_{2э})^2} = \frac{R_{21}R_{22}\left[1+\frac{1}{(\omega C_{21}R_{22})^2}\right]}{R_{21}R_{22}\left[1+\frac{1}{(\omega C_{21}R_{22})^2}\right]}\times$$

$$\times\frac{1}{1+\left[\omega\left(\frac{C_{21}}{1+(\omega C_{21}R_{22})^2}+C_{22}\right)\frac{R_{21}R_{22}\left[1+\frac{1}{(\omega C_{21}R_{22})^2}\right]}{R_{21}R_{22}\left[1+\frac{1}{(\omega C_{21}R_{12})^2}\right]}\right]^2}$$

$$C_2 = C_{2э}\left(1+\frac{1}{(\omega C_{21э}R_{21э})^2}\right) = \left[\frac{C_{21}}{1+(\omega C_{21}R_{22})^2}+C_{22}\right]\times$$

$$\times\left(1+\frac{1}{\left(\omega\left(\frac{C_{21}}{1+(\omega C_{21}R_{22})^2}+C_{22}\right)\cdot\frac{R_{21}R_{22}\left[1+\frac{1}{(\omega C_{21}R_{22})^2}\right]}{R_{21}R_{22}\left[1+\frac{1}{(\omega C_{21}R_{22})^2}\right]}\right)^2}\right)$$

For the Contact Zone:

$$R_{32э} = R_{32}\left[1+\frac{1}{(\omega C_{31}R_{32})^2}\right]$$

$$C_{31э} = \frac{C_{31}}{1+(\omega C_{31}R_{32})^2}$$

$$R_{3э} = \frac{R_{32э}R_{31}}{R_{32э}+R_{31}} = \frac{R_{31}R_{32}\left[1+\frac{1}{(\omega C_{31}R_{32})^2}\right]}{R_{31}R_{32}\left[1+\frac{1}{(\omega C_{31}R_{32})^2}\right]}$$

$$C_{3э} = C_{31э}+C_{32} = \frac{C_{31}}{1+(\omega C_{31}R_{32})^2}+C_{32}$$

$$R_3 = R_{3э}\frac{1}{1+(\omega C_{3э}R_{3э})^2} = \frac{R_{31}R_{32}\left[1+\frac{1}{(\omega C_{31}R_{32})^2}\right]}{R_{31}R_{32}\left[1+\frac{1}{(\omega C_{31}R_{32})^2}\right]}\times$$

$$\times \frac{1}{1+\left[\omega\left(\frac{C_{31}}{1+\left(\omega C_{31}R_{32}\right)^2}+C_{32}\right)\frac{R_{31}R_{32}\left[1+\frac{1}{\left(\omega C_{31}R_{32}\right)^2}\right]}{R_{31}R_{32}\left[1+\frac{1}{\left(\omega C_{31}R_{32}\right)^2}\right]}\right]^2}$$

$$C_3 = C_{3\text{э}}\left(1+\frac{1}{\left(\omega C_{3\text{э}}R_{3\text{э}}\right)^2}\right) = \left[\frac{C_{31}}{1+\left(\omega C_{31}R_{32}\right)^2}+C_{32}\right]\times$$

$$\times\left[1+\frac{1}{\left(\omega\left(\frac{C_{31}}{1+\left(\omega C_{31}R_{32}\right)^2}+C_{32}\right)\cdot\frac{R_{31}R_{32}\left[1+\frac{1}{\left(\omega C_{31}R_{32}\right)^2}\right]}{R_{31}R_{32}\left[1+\frac{1}{\left(\omega C_{31}R_{32}\right)^2}\right]}\right)^2}\right].$$

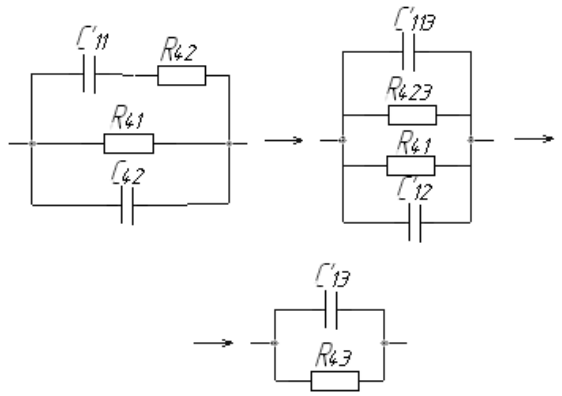

Figure 7. Sequence of the conversion of the substitutional connection of themedium

$$R_{42\text{э}} = R_{42}\left[1+\frac{1}{\left(\omega C'_{11}R_{42}\right)^2}\right]$$

$$C'_{11\text{э}} = \frac{C'_{11}}{1+\left(\omega C'_{11}R_{42}\right)^2}$$

$$R_{4\text{э}} = \frac{R_{42\text{э}}R_{41}}{R_{42\text{э}}+R_{41}} = \frac{R_{41}R_{42}\left[1+\frac{1}{\left(\omega C'_{11}R_{42}\right)^2}\right]}{R_{41}R_{42}\left[1+\frac{1}{\left(\omega C'_{11}R_{42}\right)^2}\right]}$$

$$C'_{1\text{э}} = C'_{11\text{э}}+C'_{12} = \frac{C'_{11}}{1+\left(\omega C'_{11}R_{42}\right)^2}+C'_{12}$$

Taking into account all conversions, scheme shown in Figure 4 takes the form shown in Figure 8.

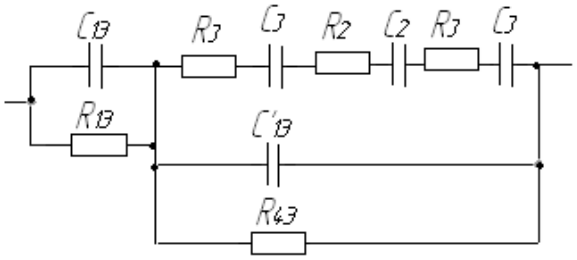

Figure 8. Substitutional connection of the two-particle system with the consideration of intermediate conversions

Further conversion of the substitutional connection is shown in Figure 9. Parameters of the scheme are calculated according to the formulas given below.

$$R'_{\text{э}} = 2R_3 + R_2$$

$$C'_{\text{э}} = \frac{2C_2 \cdot C_3}{2C_2 + C_3}$$

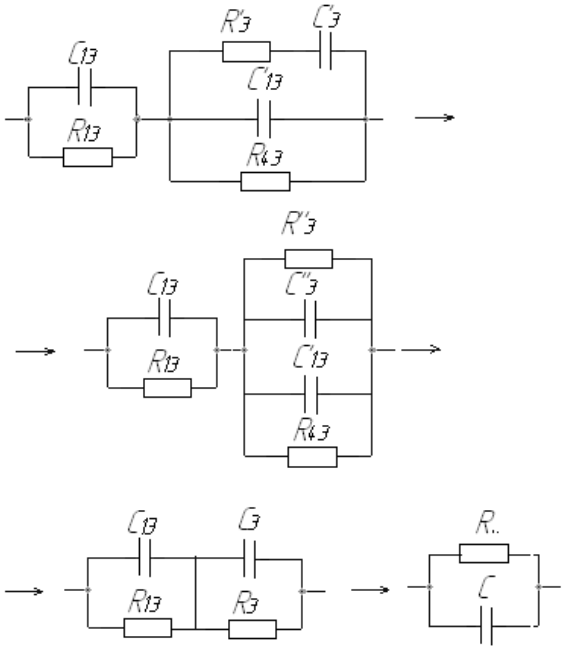

Figure 9. Subsitutional connection of the two-particle system with the consideration of intermediate conversions

$$R''_{\text{э}} = R'_{\text{э}}\left[1+\frac{1}{\left(\omega C'_{\text{э}}R'_{\text{э}}\right)^2}\right]$$

$$C''_{\text{э}} = \frac{C'_{\text{э}}}{1+\left(\omega C'_{\text{э}}R'_{\text{э}}\right)^2}$$

$$C_Э = \frac{C'_Э}{1+\left(\omega C'_Э R'_Э\right)^2} + C'_{1Э} \quad (1)$$

$$R_Э = \frac{R_{4Э} \cdot R'_Э\left[1+\frac{1}{\left(\omega C'_Э R'_Э\right)^2}\right]}{R_{4Э} + R'_Э\left[1+\frac{1}{\left(\omega C'_Э R'_Э\right)^2}\right]} \quad (2)$$

For cubic packing of the bulk material shown in Figure 1, conductivity along any of the x, y, z axes equals to a sum of conductivities of individual chains parallel to a respective axis; and resistance of each of the chains is equal to a sum of resistance of individual particles [3]. If the electric field vector *E* is collinear to any of the reference axes, components of total conductivity of the cubic volume of the bulk material with number of particles on each side equaling *n* is equal to components of conductivity along the corresponding axis:

$$C_M = nC \;; \qquad \gamma_M = \frac{n}{R},$$

where *C* means capacity of the two-particle system (1), *R* means resistance of the two-particle system (2).

Substituting *C* and *R* we obtain the following formulas:

$$C_M = \frac{n \cdot \left(R_{1Э}^2 C_{1Э} + C_Э R_Э{}^2 + \left(\omega R_{1Э} R_Э\right)^2 \cdot C_{1Э} C_Э \left(C_{1Э} + C_Э\right)\right)}{\left(R_{1Э} + R_Э\right)^2 + \left[\omega R_{1Э} R_Э \left(C_{1Э} + C_Э\right)\right]^2}$$

$$\gamma_M = \frac{n \cdot \left(R_{1Э} + R_Э + \omega^2 R_{1Э} R_Э \left(R_{1Э} C^2{}_{1Э} + R_Э C_Э{}^2\right)\right)}{\left(R_{1Э} + R_Э\right)^2 + \left[\omega R_{1Э} R_Э \left(C_{1Э} + C_Э\right)\right]^2}$$

If particles are cubic packed, value of the total conductivity of the bulk material does not depend on the direction of the electric field. Based on the mathematical model of the bulk material behavior, we could find dependence of the dielectric loss tangent of the finite volume of the bulk material on frequency change of the applied electric field, where this volume of the material is put.

$$tg\delta_M = \frac{1}{\omega \cdot n^2 \cdot R_M C_M},$$

where resistance of the cubic volume of the bulk material on the relevant axis is calculated according to the following formula:

$$R_M = \frac{1}{\gamma_M}$$

The present mathematical model has distinctive features as follows: firstly, it analytically describes behavior of the two-component bulk material in the electric field; and secondly, it takes into account particle size composition of the bulk material. Abovementioned features make it possible to improve applicability of the mathematical model to analysis of bulk materials with different component and particle size compositions.

Analytical frequency and humidity characteristics of the bulk material found with the use of the present mathematical model could be considered as basis for selection of the optimal frequency of humidity sensors, and for mathematical description of behavior of capacity sensors in the electric field of measuring circuit of a signal converter to a signal convenient for further processing.

IV. Program of Visualization of Frequency Characteristics of the Bulk Material

Need in development of a program for calculation and visualization of calculation results originates from the fact that MathCad 8 computer-aided design system has no option for enlargement of the frequency range of the applied voltage over 1 MHz. Whilst the required variation frequency range is determined by need in stressing of a volume of the bulk material in a capacity cell of the sensor by changing of the voltage frequency over 1 MHz.

There was a software tool developed in the Microsoft Visual Studio [5] environment with options as presented below.

1) Updatability of input data, such as:

a) particle size:

a – edge length of the cube-shaped Particle 1, m;

k – ratio of dimensions of the cube-shaped Particle 1 and cube-shaped Particle 2.

Frequency change range in increments of subintervals equaling to W:=(w1,w2,w3):

w1 – voltage frequency variation range increment;

w2 – lower limit of the voltage frequency range;

w3 – upper limit of the voltage frequency range.

The following constant is used:

e – electric constant, 8,85 10^{-12}, Fm^{-1}.

b) electrical and physical properties of the particles, such as:

b – dielectric permittivity of the Particles 1 and 2 under direct current;

c – dielectric permittivity of the Particles 1 and 2 on infinite frequency;

d – specific resistance of the Particles 1 and 2 under direct current;

f – specific resistance of the Particle 1 and 2 material on infinite frequency;

p – specific resistance of the Contact Zone under direct current;

q – specific resistance of the Contact Zone on infinite frequency;

g – dielectric permittivity of the medium under direct current;

h – dielectric permittivity of the medium on infinite frequency.

Electrical and physical parameters of the medium, such as:

l – specific conductivity of the medium under direct current;

m – specific conductivity of the medium on infinite frequency.

Other data such as:

n – number of Contact Zones of the Particle 1 and 2;

j – radius of the Contact Zone, m..

2) Wide variation range of the voltage frequency.

3) Ability to improve the software tool in connection with changes in requirements to the process of calculation and visualization of results.

Data for experimental calculations were taken from [1] taking into account the varying particle loose medium (Figure 1).

Work with the application (Figure 10) is carried out sequentially as described below:

1) data are input or default data are loaded ("Default" («Умолчание») button);

2) any change of data requires acceptance of such changes ("Accept" («Принять») button);

3) activity and calculation results in real time could be reviewed at the "Terminal" («Терминал») tab;

4) having results of calculations different tabs could be used. "FW Results Array" («Массив результатов FW») represents a list of results of the "Calculation 1" («Расчет-1») function, shows calculations of all the variables for the present FW, pointwise calculations. "W Results Array" («Массив результатов W») represents array of calculations in accordance with the given frequency W(w1,w2,w3), execution of a group of 33 functions, which are located on the tools menu for each W value. Calculation results are presented on the tab called "W Results Array" («Массив результатов W»). The "W Results Array" («Массив результатов W») tab shows first 500 lines of the array with 33 values of variables in order to optimize the process time needed for data output. It supports viewing of any number of lines in the capacity of the array part.

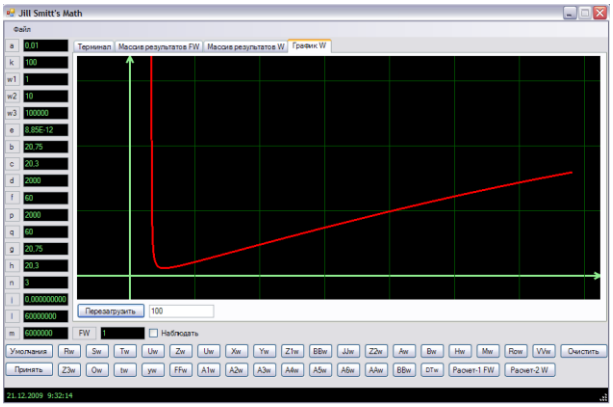

Figure 10. Visualization window of the program of calculation of the dielectric loss tangent of the finite volume of the bulk material on the sensor voltage frequency

5) calculating panel allows calculating separate functions or running one of the two automatic functions called "Calculation-1" and "Calculation-2" («Расчет-1» and «Расчет-2») for FW and W respectively.

THE RESULTS OF THE RESEARCH

We developed a mathematical model of behavior of finite volume of the two-component bulk material with varying particle size composition in the alternate electric field of the capacity sensor [6], which allows calculating dependence of the dielectric loss tangent on frequency of alternate field of the capacity sensor.

There was a program developed to calculate and visualize calculation results and dielectric loss tangent dependence on frequency of alternate field of the capacity sensor in the Microsoft Visual Studio environment, which has an ability to change source data.

REFERENCES

[1] Dubrov N.S. Mnogoparametricheskie vlagomery dlya sypuchih materialov / N.S. Dubrov, E.S. Krichevskij, B.I. Nevzlin. – M.: Mashinostroenie, 1980, p. 144.

[2] Krichevskij E.S. Kontrol' vlazhnosti tverdyh i sypuchih materialov/ E.S. Krichevskij, A.G. Volchenko, S.S. Galushkin; Pod.red. E.S. Krichevskogo. – M.: Energoatomizdat, 1987, p. 136.

[3] Arinova N.V., SHadrin G.K., Muzdybaeva SH.A. Matematicheskaya model' ocenki ehlektrofizicheskih parametrov sypuchih materialov //Perspektivnye tekhnologii, oborudovanie i analiticheskie sistemy dlya materialovedeniya i nanomaterialov: Mezhdunarodnaya Kazahstansko-Rossijsko-YAponskaya konferenciya. – Ust'-Kamenogorsk, 2008, pp. 646-654.

[4] Atabekov G.I. Osnovy teorii cepi. Uchebnik dlya vuzov. M., «Energiya», 1969, p. 424.

[5] SHevyakova D.A., Stepanov A.M., Karpov R.G. Samouchitel' Visual Basic 2005/ Pod obshchej redakciej A.F. Tihonova. – SPb.: BHV-Piterburg, 2007, p. 567.

[6] Arinova N.V., SHadrin G.K., Muzdybaeva SH.A. Nauchnye aspekty postroeniya izmeritel'nyh preobrazovatelej promyshlennyh vlagomerov sypuchih materialov //Rol' universitetov v formirovanii innovacionnoj ehkonomiki: Mezhdunarodnaya nauchno-tekhnicheskaya konferenciya. – Ust'-Kamenogorsk, 2008, pp. 7-10.

The control system of energy efficiency of the LED lighting

A.Baklanov*, V.Sayun**, E.Grigoryev**
* D.Serikbayev East Kazakhstan State Technical University/ Faculty of Information Technology and Business Engineering, Ust-Kamenogorsk, Kazakhstan
** Tomsk State University of Control Systems and Radioelectronics/ Faculty of Electronic Engineering, Russia
ABaklanov@ektu.kz, svm@ie.tusur.ru

***Abstract* – The article considers the modern state energy consumption in Kazakhstan and Russia, an analysis of the prospects for the introduction of energy efficiency LED lighting technology. The paper presents LED lighting control system based on programmable counters and an information system for monitoring energy consumption. Designed LED lighting system has been introduced in the educational building of the University. A comparative analysis of the two lighting technology - LED lighting and compact fluorescent lamps.**

I. Introduction

The problem of rational use of energy the conditions of limited resources and the growth of consumption is one of the most important for the world community, and its decision to become a strategic priority for many countries. Prolonged global economic crisis, increase in prices of natural energy resources, environmental issues, emissions reduction of harmful substances and greenhouse gases into the atmosphere dictate the need to address energy conservation and efficiency.

Energy costs are rising in proportion to the needs of the world's population and is predicted doubling of electricity demand by 2025 [1]. The introduction of modern technologies ensuring efficient use of energy resources will avoid the electricity deficit.

Lighting is among the directions with great potential for energy savings. On lighting consumed 110 billion kW/h in Russia and almost 10 billion kW/h in Kazakhstan annually. The total potential for reducing energy consumption is estimated at 40% for Russia and 30% for Kazakhstan [2, 3]. In this regard, one of the priorities to reduce energy consumption is to reduce energy consumption for lighting.

Modern LED lighting systems allow for energy savings in relation to the lighting systems that use halogen and fluorescent lamps.

II. Current status and analysis of energy consumption of Kazakhstan

Efficient energy consumption provides 40% of the contribution to the reduction of fossil fuel consumption, which is equivalent to 106 billion euro savings per year on a global scale. From an environmental point of view this corresponds to a reduction of carbon dioxide emissions by 555 million tons per year, an annual saving of 2 terawatts of electricity, saving 1.5 billion barrels of oil [4]. The energy consumption for lighting is responsible for 6-8% of greenhouse gas emissions [5].

According to the International Energy Agency (IEA), 20% of global electricity production is consumed on the network electric lighting. Consumption of total energy produced in the World by sector is shown in Fig. 1.

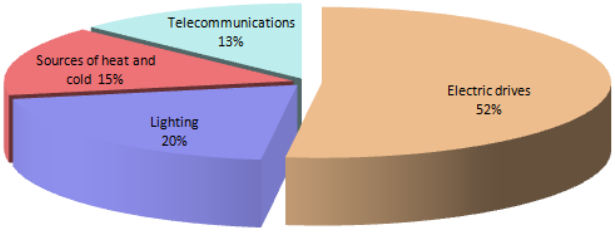

Figure 1. Consumption of electricity generated in the world [6]

Artificial lighting is 12-14% of total energy consumption for Kazakhstan [7]. This indicator is an average of 13-15% for Russia [8].

Energy consumption data by economic sectors Kazakhstan indicate that a major consumer of electricity is industry to 70%. Industrial facilities spend on illumination of 10% of the total electricity consumption. Second place for the consumption of electric energy takes the housing and communal services - 12.5%. An average statistical electricity consumption branch of the economy is shown in Fig. 2.

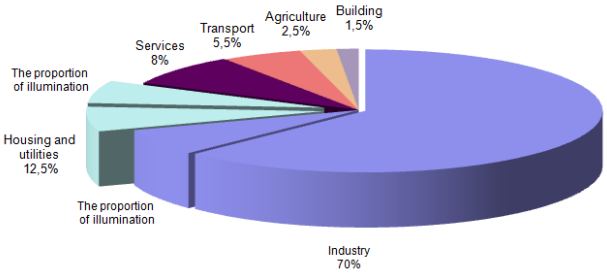

Figure 2. Average statistical electricity consumption branches of the economy in Kazakhstan [9]

The proportion of electricity consumption by lighting in public and residential buildings is 40% -60%, which is 2-3 times higher than in Europe [10].

Analysis carried out by the IEA of economic development and energy efficiency of existing trends in the world allowed to predict the increase in demand for artificial lighting by 60% over the next 20 years. Without improvement of technology and the implementation of energy efficiency policies such rates of increase of electricity production will lead to an increase in energy consumption, most of which are non-renewable and environmental degradation associated with the increase in hydrocarbon fuel emissions.

Thus the task of improving the efficiency of lighting becomes relevant. In general, this will positively affect the country's energy balance and global climate processes (reduction of greenhouse gas emissions)

Introduction of modern energy-saving technologies is possible only through the establishment of new standards for artificial lighting therefore many countries have a systematic policy to develop such standards. For example, in the United States entered into force on regulatory act, which establishes a complete rejection of inefficient light sources with 2014, in this case the costs will be reduced by more than 20 billion dollars. The European Union banned the sale of incandescent light bulbs 100W in September 2009, and all the light bulbs in 2012.

Not only North America and the EU declared the adoption of measures aimed at energy conservation and promoting the use of energy-saving light sources. New legislation in the field of energy efficiency, including the phasing out of incandescent lamps operates in Australia, New Zealand, Russia, Japan, South Korea, Brazil, Argentina and other countries.

Kazakhstan is also moving in this direction. However, it may be noted that the replacement of a very small amount undergoes light points in different segments and lamps only, but not the full lighting system. However, a complete replacement of obsolete lighting in homes, offices, shopping squares and streets can lead to 57-80% energy savings with a return on investment in the period from 2 to 5 years [1].

46 countries, including Kazakhstan and Russia, approved the program stimulating energy savings, as well as the transition to energy-efficient lighting technology. Implementation of the lighting market transformation program allowed to change structure of consumption lamps in favor of energy efficient luminaries in Kazakhstan.

Substantial savings of lighting can be achieved through the use of new semiconductor light sources. The main element of the semiconductor lighting is light-emitting diode (LED). LEDs have high technical and economic parameters (high luminous efficiency, long lifetime, high reliability, easy maintenance, economic efficiency), have a wide range of colors, configurations and capacities.

Solid-state lighting has advantages under application conditions: environmentally friendly, a higher mechanical strength and vibration resistance, in the emitted light is not harmful ultraviolet radiation and stroboscopic effect, inertia with lamps turned on and working at a lower temperature. Of special note is the ability controlling the luminous flux of the LED of a wide frequency band. It is because of these qualities, the LED semiconductor lighting is one of the promising directions of development of lighting.

Segment LED lamps will grow from 170 thousand pieces in 2013 to 10 million pieces in 2018, and in monetary terms from 2.2 million in 2013 to 42 million USD in 2018 (Fig. 3). The growth market of lamps in 2016 will be due to increased consumption of the LED lamps in the professional segment, especially in offices, retail outlets, hotel and restaurant businesses.

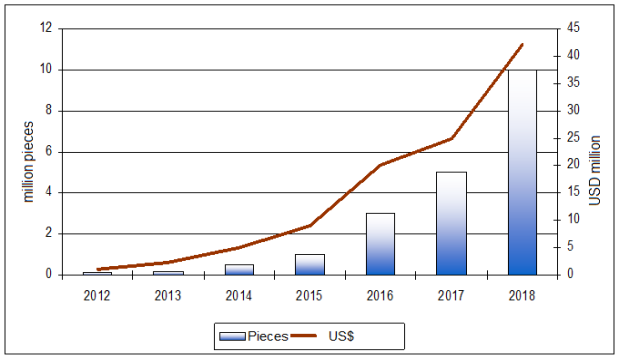

Figure 3. The forecast of LED lamps in Kazakhstan [11]

This increase is explained by a decrease in production costs, and, as a consequence, the price of LED lamps to a level where the total cost of ownership of this type of lamp is more attractive than the total cost of ownership of other types of energy-efficient lamps. The retail price of this type of lamps will be $ 6.57 in 2016 and $ 4.20 per share in 2018 (Fig. 4).

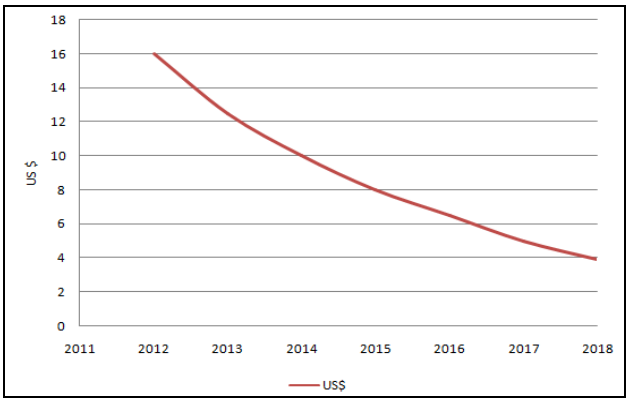

Figure 4. The forecast cost of LED lamps in Kazakhstan [11]

The ban on the production and sale of incandescent lamps 25 W and above will result in a massive shift to the first use of compact fluorescent light bulbs, and then the LED lamps. The total energy savings for the period from 2013 to 2018 will 3011 MW (Fig. 5).

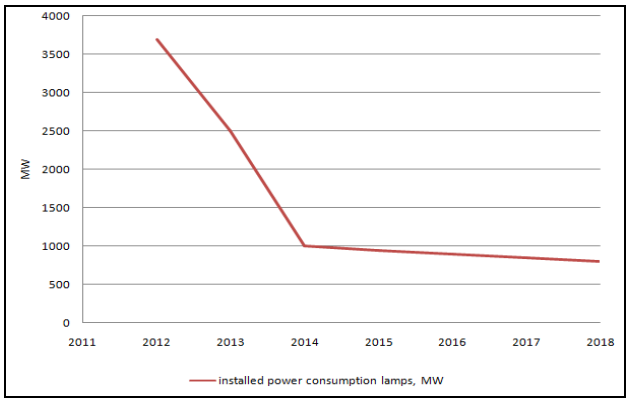

Figure 5. Reduction of installed capacity from 2013 to 2018 [11]

It is impossible not to mention one more aspect of the energy savings associated with the use of LED lamps. Their work is easily programmed and controlled to optimize lighting, adjusting its intensity. This quality extends the functionality of of lighting devices, offers the prospect of creating an ergonomic variable light environment, in contrast to today - uncontrolled and static.

2 THE AUTOMATED CONTROL SYSTEM OF LED LIGHTING

There are two directions of technological development in the field of electric lighting. The first is to improve the light-emitting components and designs lighting equipment: an increase the light output of the light source, reduction of power density; improving lighting and energy characteristics. The second trend involves the development of methods and modes of operation of lighting products: optimizing the placement of lamps depending on the purpose of visual tasks; efficient use of natural light with view of the diurnal cycle, seasonal and climatic region; implementation of lighting control systems.

The automated control system of the LED lighting was developed in East Kazakhstan State Technical University [12]. Field experiments were conducted to analyze the energy efficiency this system lighting. We measured the power consumption of lighting recreations two floors academic building.

Schematically floor with lighting fixtures and automated control system is shown in Fig. 6.

On one floor used daylight fluorescent lamps, and on another floor LED lamps which operate in two modes: normal mode without a control system and with use automated control system. In addition, motion sensors and light sensor was installed which allowed to implement the various scenarios of the lighting system in all floors. On the second floor of the fluorescent lamps were installed with a total light output equal light output of LED lamps of the first floor.

For each segment were installed electronic meters «Mercury 230» to pass data to the PC for the comparative analysis of the efficiency of the lighting technology.

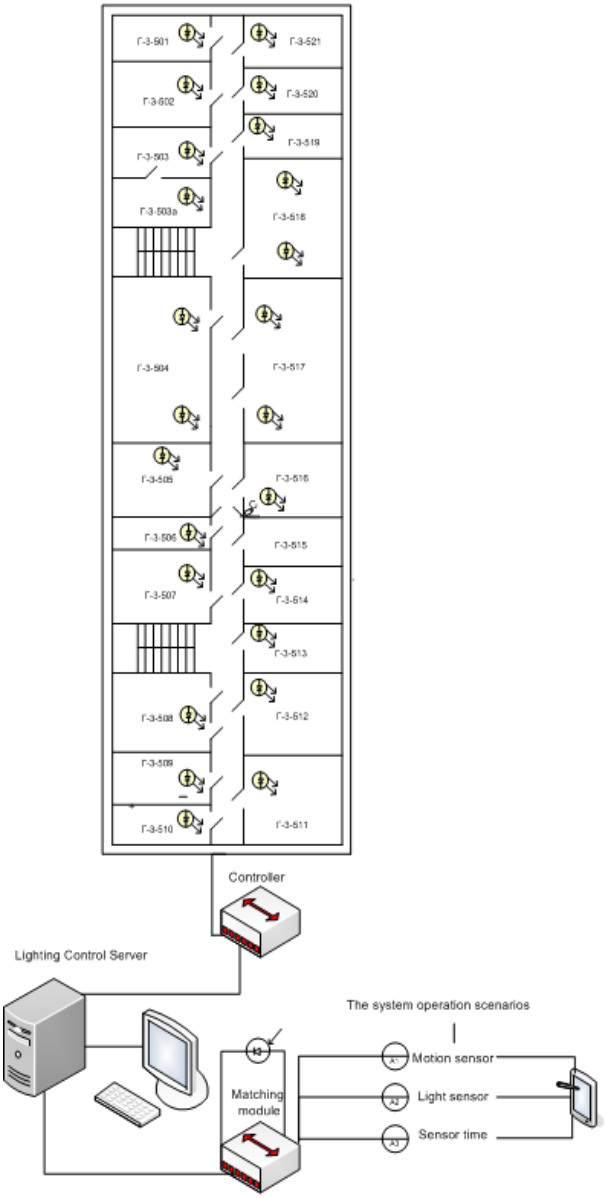

Figure 6. Scheme of automation and accommodation of LED lamps

Connection diagram counters to a computer is shown in Fig. 7.

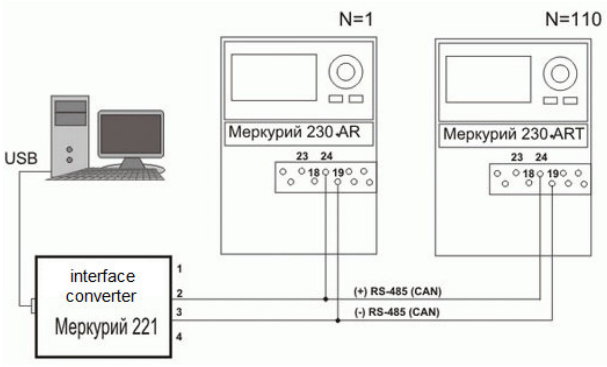

Figure 7. The connection diagram counters «Меркурий-230» to the computer

Data transmission takes place the RS-485 standard with using the interface converter which is designed to convert the USB interface CAN/RS-232/RS-485. After installing the USB driver interface converter is defined as a virtual COM-port. All interface converter terminals are galvanically isolated from the USB interface of the computer.

For visual monitoring of electricity consumption the interface was developed, showing graphs and histograms of energy efficiency both floors (Fig. 8).

Figure 8. Appearance of the connection meters with monitor

Information coming from the counters, transmitted to the server and stored in a database. This allowed for the study of energy efficiency LED lighting system automated.

3 Evaluation of LED lighting system

The developed application provides information on electric power consumption and efficiency of lighting systems. The data is displayed on the monitor and recorded in the database (Fig. 9).

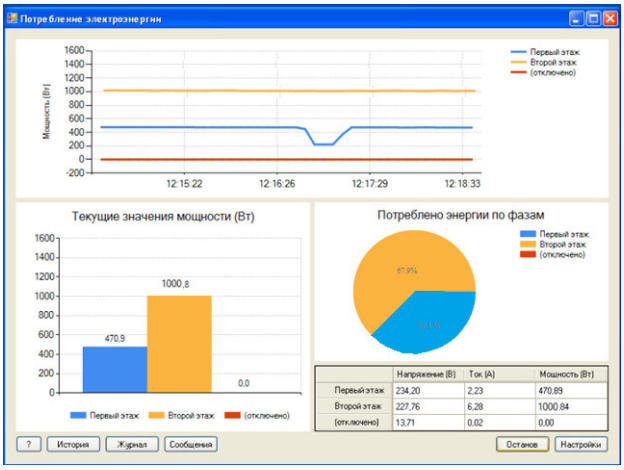

Figure 9. Interface of the power consumption control

The working field of the interface is divided into three parts. Electric power consumption is displayed at the top in real-time. The current time is plotted on the horizontal (in this case 12 hours 15 minutes). It can be seen that the energy consumption of the second floor is 1000W, and the consumption of the first floor with an automated LED lighting system is 470W. The graph shows a sharp decrease in power. This is a demonstration of the system performance (briefly off the light on the first floor at 12 o'clock 17 minutes).

In the bottom of the interface shows a histogram of power consumption. These histograms show the exact power consumption of the first and second floor, as well as the percentage of energy consumption on the floors. The values shown on the chart are average for a long time of full-scale tests (within 5 months).

On the basis of the obtained information on the power consumption of the lighting systems of the two floors have been calculated annual energy costs (Fig. 10).

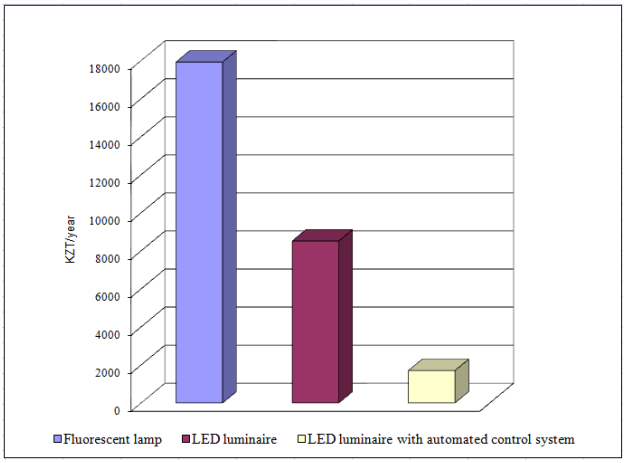

Figure 10. Chart of energy costs of the lighting systems

LED lights do not require operating costs (disposing, purchase consumables). Fluorescent lamps require constant maintenance. Cost of which is increasing by about 15% per year. Also, fluorescent lamps require a dispose that more increases maintenance costs by 5%.

Total costs with operational costs for a single lamp «Armstrong» in different segments are shown in Fig. 11.

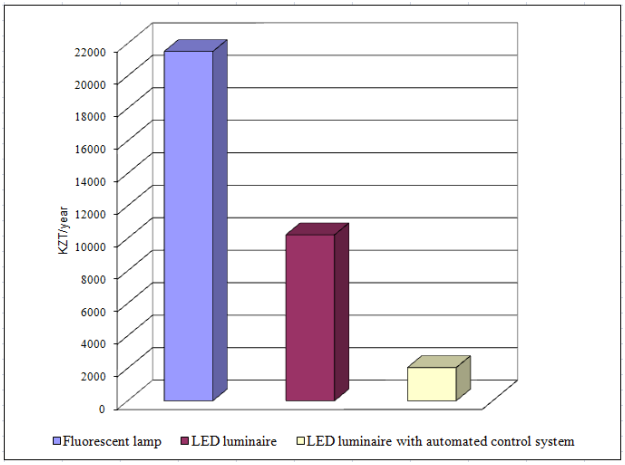

Figure 11. Chart total costs of exploitation of the lighting systems

On the basis of this data is visible to real savings the energy costs and savings of the total operating costs of LED lighting systems. Thus, in operating mode of the system LED lighting compared to fluorescent lamps energy savings is 91% with a motion sensor and 52% without.

CONCLUSION

The article presents the results of the implementation of the automated control system of LED lighting. Field tests showed the stability of the developed system.

The installed system of the control and monitoring allows us to calculate the energy efficiency of the LED lighting devices. It is demonstrated that the use of automated control system of the LED lighting saves energy almost 10-12 times as compared with currently available illumination based on fluorescent lamps.

Also, field measurements showed that the LED lighting fixtures allow you to save the electricity by 2-3 times, even without the use of automated systems.

REFERENCES

[1] Applied marketing research in the priority sectors of the economy, Almaty, 2014, 47p.

[2] Press release of the Ministry of Energy of the Russian Federation of 05.13.2015. URL: http: // http://minenergo.gov.ru/node/2673.

[3] E.Abdrakhmanov. *Development of energy-saving activities in Kazakhstan*, Vestnik of Almaty University of Energy and Communications, 2013, vol.3(22), pp. 16-25.

[4] International Energy Agency. *Light's Labour's lost. Policies for Energy-efficient Lighting*, OECD/IEA, 2006, 516 p.

[5] R.Provoost, M.Goetzeler. *A global transition to efficient lighting*. COP 16 United Nations Climate Change Conference Cancun, Mexico, 2010, pp. 84-85.

[6] A.Starostin, V.Sushkov, A.Mikryukov. *Development of semiconductor lighting*, Solid-state lighting, 2014, vol.2, pp. 8-10.

[7] A.Babko, S.Inyutin. *Energy audits and light in buildings and street lighting*, Astana, 2014, 174 p.

[8] V.Dadonov, A.Bondar. *Analysis of the development and contemporary state lighting market*, Engineering Journal: Science and Innovation, 2014, vol. 5(29), pp. 21-34.

[9] Resolution of the Government of the Republic of Kazakhstan. *On approval of the Program "Energy Saving* - 2020", 2013.

[10] Kang H., Sung J., Park S., Kang H., Choi J., Kang T. Automatic Lighting Control System and Architecture Using Ambient Light Sensor // The Tenth International Conference on Systems. – Barcelona, 2015. – pp. 44-45.

[11] Analysis of the status and prospects of the market of lighting products in the member states of the Eurasian Economic Union, Lighting Business Consulting, 2015, 82 p.

[12] A.Baklanov, D.Titov, S.Grigoryeva. *The practical realization of robustness for LED lighting control systems*. 11th International Forum on Strategic Technology (IFOST 2016), Novosibirsk, Russia, 2016, vol.2, pp.52-56.

Raised Graduation Information Technology Solutions for the Visual Interface

László Gugolya*
*Óbuda University AMK, Székesfehérvár, Hungary
gugolya.laszlo@amk.uni-obuda.hu

***Abstract*— In Hungary, the information technology subject teaching scarce resources to cultivate. The number of contact lessens are low, so teachers should think about a solution by which, home practicing is prioritized. The active programming tasks usually highly motivate students. Responsible teachers must teach students the basics of informatics. This way students will recognize if they are interested in information technology. Currently, the graduation information technology system of general education subjects requires deep comprehensive knowledge of programming. Comprehensive test exercises are being developed in such a way that a wide variety of programming languages can be applied for finding the solution. This principle leads to a situation where the tasks are basically console applications, which in today's world do not represent a strong motivation for the majority of students. According to the facts mentioned before, we examined whether it is worth teaching visual programming in high school graduation for some particular tasks.**

I. INTRODUCTION

For several years, I have been participating in the implementation of advanced information technology exams. The participatory element was diverse as well as an organizer, as an examiner, oral teacher involved in the process.

The final graduation system had been introduced in 2005, was an important point in the programming part of the release .Tasks are basically accomplished by applying elementary programming theorems and usually completed by text file handling. Solving the problems you can use multiple programming languages, which you selected. The list of programming languages is constantly changing. Because of the changes and differences in language tasks are developed in such a way that the console interface: they should be solved without any input controls.

Several arguments can be made either against or pro console application. To tell the truth, the console application motivational point of view is not the best choice. The question is therefore raised: what kind of results should be reached in teaching visual interfaces. What are the disadvantages, what are the benefits if the problems are solved by choosing visual programming methods and tools. This topics is being discussed in the followings.

A. Opportunities

The option of choosing programming languages changed from year to year, but not fundamentally. The most significant change is the disappearance of Borland's products from the list. This fact, however, does not affect teaching Pascal due to the appearance of Lazarus. In the case of C ++, however, the only choice is Visual Studio C ++ (Visual programming point of view). In Linux environment, Eclipse is used instead of NetBeans. In the case of C++ programming language we use QtCreator.

The list shows that the visual interface when creating the Lazarus / Pascal, Java (NetBeans / Eclipse), Visual Studio (C / C ++, Basic, C #) selection is possible. The possible systems are shown in the figures below.

FreePascal 2.6.4
FreePascal 2.6.4 + Geany 1.25
Lazarus 1.4.2 (fpc 2.6.4)
Code::Blocks 13.12 MinGW/GCC (4.8.1)
MinGW/TDM-GCC 4.8.1 + Geany 1.25
Python 3.4.3 + IDLE (Python GUI)
MS Visual Studio 2013 Express for Windows Desktop (Visual Basic, Visual C#, Visual C++)
JAVA SE – NetBeans 8.0.2, JDK 8

Figure 1. MS Windows systems, radio programming environments (2016)

II. CASE STUDY

A. Official solutions with visual tools

The exam took place 17 to 32 have a formal arrangement pascal or derivatives language was issued. There are two solutions for Visual Basic, C # solution for five and eight were between C ++ solution.

It is located between an official of the solutions, which have been among the visual interface. Between the first two series of tasks we find written in Delphi solution, and then after a long pause in 2012 by Lazarus (Delphi clone) was the official sample solution. These solutions can also be seen how could allow the visual interface.

When you open and save dialogs when files are used so that you can avoid common errors in file open. The task

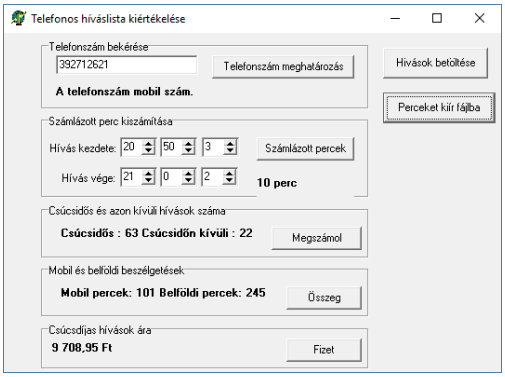

Figure 2. Official Solution - February 2006 (Delphi)

management with a list of phone calls show that the subpoenas sought to be made more user-friendly. This SpinEdit were used for the appropriate restrictions. In this case, the DateTimePicker also a good choice, it also allows a controlled input. The other task has seen limited use, because the tasks are executed by pressing buttons, and the results appear in-TLabel.

For color images exercises in autumn 2012 in the screenshot shows the order of the task. It is also seen that here were used to solve particular tasks buttons. The Open, Save dialog windows are also resolved. The results of the multi-line text component (TMemo) appear. Request for information on the limited to simple text input.

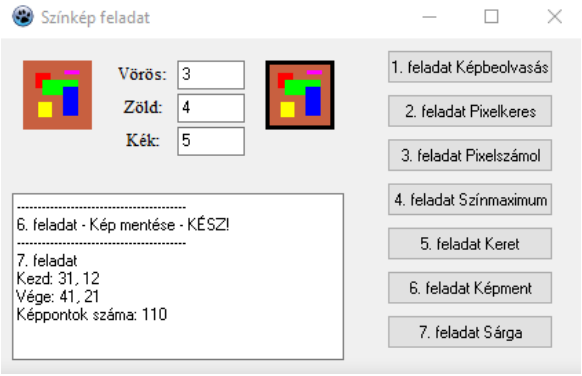

Figure 3. Official Solution - October 2012 (Lazarus)

You can see that in the event of a formal solutions are also displayed on the visual interface. It is quite one-sided, because only with the great Hungarian tradition Pascal family of solutions can be found. Also, check out other options as well, and also to consider whether it still lies in whether other options for Pascal/Lazarus.

B. Lazarus/Free Pascal (Delphi)

Unlike other language in the Pascal language difficulties managing a dynamic array[4]. The problem solving this is not necessary, because it would always provide the maximum number of elements, but understandably convenient programming data to the list-like structure. This can be overcome by using the indicators, but experience shows that this understanding of time-consuming for students. If simple. say consisting of text data list, you need to be a TComboBox or TListBox replace elements of a dynamic list. Here, the elements are stored in the Items property of which TStringList[1]. Thus, it is no use visual interface. A good example is the May 2015 maturity and a foreign language (Latin dance)

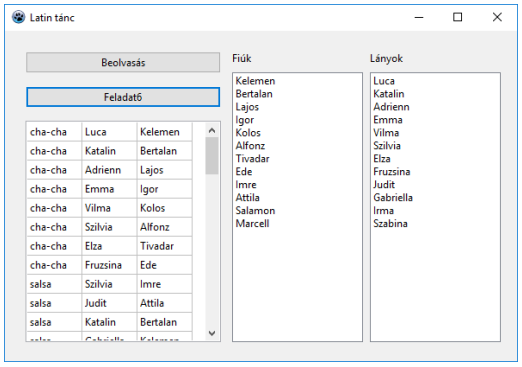

Figure 4. Latin Dances – TStringGrid and TListBox

exercises. In the sixth task I had to collect the girls and the boys' list. The listbox handling is easy to do.

```
for  i := 0 to Length(Adat)-1 do
begin
  if lbxFiu.Items.IndexOf(Adat[i].fiu)=-1
   then lbxFiu.Items.Add(Adat[i].fiu);
end;
lbxFiu.Items.SaveToFile('.\\szerepek.txt');
```

This example demonstrates that you can easily save file, although it is true that it is not formatted export permits. In such cases, the conventional iterative design portfolio.

In another example, an overview of the stock is being scanned. This should be the exercises in autumn 2007, where you had to process the results of a major football championship track. Needed to store data structure is as follows.

```
type
     TEgyMeccs = record
        Fordulo : Byte;
        hGol, vGol : Byte;
        hfGol, vfGol : Byte;
        Hazai, Vendeg : String[20];
      end;
      TMeccsTomb = array of TEgyMeccs;
var
      Meccs : TMeccsTomb;
```

The length of the array used to store the results of the scan is determined (setLength). Here, too, it used a dynamic list. You can upload a file directly. In this example, the data displayed in a Grid. The filling can be done directly using TStringList[2] per line. The data records disassembling the appropriate fields in the Pascal "new" elements of language (delimiter) is possible.

```
var TextFile, sor : TStringList;
  i :integer;
begin
  TextFile := TStringList.Create;
  TextFile.LoadFromFile('.\\meccs.txt');
  Sor := TStringList.Create;
  sgrdAdatok.RowCount := TextFile.Count;
  SetLength(Meccs,TextFile.Count);
  for i := 1 to TextFile.Count-1 do
  begin
    Sor.Clear;
    Sor.StrictDelimiter:=true;
    Sor.Delimiter:=' ';
    Sor.DelimitedText:= TextFile[i];
    sgrdAdatok.Rows[i] := Sor;
    with Meccs[i] do
    begin
      Fordulo:= StrToInt(Sor[0]);
      hGol:= StrToInt(Sor[1]);
      vGol:= StrToInt(Sor[2]);
      hfGol:=StrToInt(Sor[3]);
      vfGol:= StrToInt(Sor[4]);
      Hazai:= Sor[5];
      Vendeg:= Sor[6];
    end;
  end;
end;
```

TListBox in the display, chasing solution is useful in the task 7, where the number of results occurring had to be determined (indexOf, Add). The handling of files (save,

load) can be easily solved by using dialog windows and grid.

```
1. //TOpenDialog
2. if Open.Execute then
3.   begin
4. grd.LoadFromCSVFile(Open.FileName,' ',false)
5.     grd.DeleteRow(1);
6.   end;
7. //TSaveDialog
8. if Save.Execute then
9. grd.SaveToCSVFile(Save.FileName,' ',false);
```

C. *Netbeans/Java*

Java visual editor interface provides the least help. Under MS Windows optional NetBeans provides more opportunities than WindowBuilder under Eclipse. Let's look at the previous "soccer" task. First, we are prepared to class, which allows you to store can be a dynamic array (ArrayList)[7].

```
1. public class Meccs {
2.   private int fordulo;
3.   private int hazaiVege;
4.   private int vendegVege;
5.   private int hazaiFelido;
6.   private int vendegFelido;
7.   private String hazaiNeve;
8.   private String vendegNeve;
9.
10.    Meccs(String sorMeccs){
11.    String [] data=sorMeccs.split(" ");
12.    fordulo=Integer.parseInt(data[0]);
13.    hazaiVege=Integer.parseInt(data[1]);
14.    vendegVege=Integer.parseInt(data[2]);
15.    hazaiFelido=Integer.parseInt(data[3]);
16.    vendegFelido=Integer.parseInt(data[4]);
17.    hazaiNeve= data[5];
18.    vendegNeve= data[6];
19.    }
20.    }
```

A few clicks prepared from the get / set methods for the data fields. The data were also done in a table (JTable) imaging help. NetBeans provides an opportunity for entering properties.

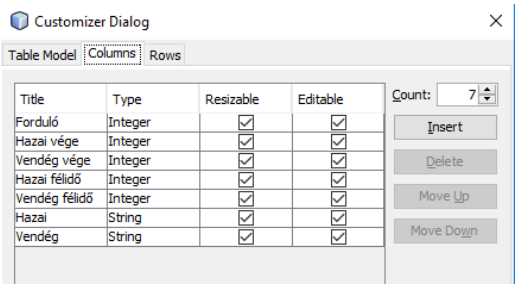

Figure 5. JTable edit - NetBeans

Then the scan result.

```
1. be = new BufferedReader(
            new FileReader("meccs.txt"));
2. String line;
3. line = be.readLine();
4. while((line = be.readLine()) != null){
5.    t.addRow(line.split(" "));
6.    mind.add(new Meccs(line));
7. }
8. be.close();
```

Like Lazarus to use subpoenas to the controlled JCombobox or JSpinner. The date is difficult deems visual equipment. The JSpinner be used for this, but this is cumbersome compared to other devices. So far, the images on screen.

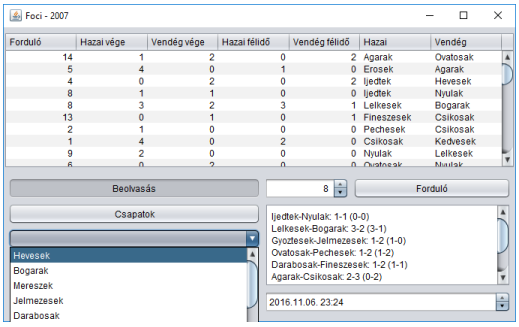

Figure 6. JTable - NetBeans

D. *Visual Studio – C#*

The graduation-use visual interfaces are a great solution for MS Visual Studio. Here you can choose from several languages the candidate. The visual elements of the language in terms of secondary consideration. Currently, the high school in the C # language taught in information technology teachers, so we can consider it. controls used in the other two instruments are available here as well[5]. The Java with the opposite is also possible to specify in structure (struct)[6], so as to avoid the introduction of the class as well. The user-friendly data entry can be easily achieved using the available components. The numbers are easy to use to request the NumericUpDown. The list for treatment, prompted the ListBox, ComboBox. Display the data in a TextBox, Label used. The date, time by asking, for managing the MonthCalendar, DateTimePicker. Data scan and display the DataGrigView, OpenFileDialog, SaveFileDialog use.

The suggests that the previous visual elements are preferred in certain cases. But it is worth to consider whether, overall, all problem what we experience. So let's look at an example of the recent series of problems.

E. *Current graduation exercises – C#*

The exercises associated with a small company call center[4]. The exact exercises found in the www.oktatas.hu side. Here are just highlight the essential parts. In solving the problems of the keys used, these may be selected from the menu instead of treatment. The solution, the official solution we used with minor changes. The official solution for C ++ have contributed. The solution is based on our screenshot below.

The first problem was to create a function which later

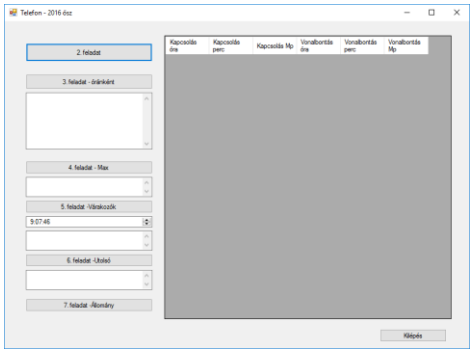

Figure 7. October 2016 graduation – MS Visual Studio

had to be used. So it did not require visuals.

The second problem is to read the text file. The scan time to avoid errors in the OpenFileDialogot used, consisting of data structure read the information. The scan data DataGridView visualized. The Grid and OpenFileDialog properties customized to fit the job.

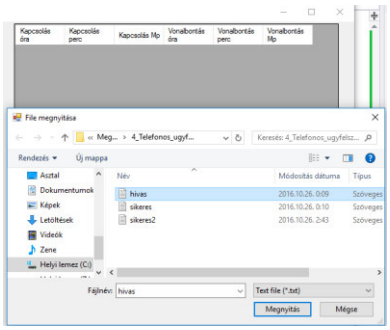

Figure 8. 2. problem – MS Visual Studio

During the third problem to be defined, where the number of outputs per hour calls. Here is a multiline TextBox was used on the dump that we comply with the description.

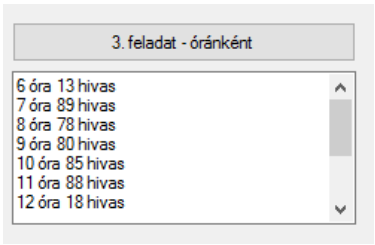

Figure 9. 3. problem – MS Visual Studio

The fourth problem is to determine the longest call has been made. The task of simplifying asked since it was sufficient to show one match.

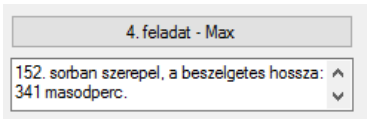

Figure 10. 4. problem – MS Visual Studio

The fifth problem was a time in requesting the task of working hours, and this had to do a search. Here, the visual prompted nice body could help to customize the DateTimePicker. The result is displayed formatted (String.Format) TextBox also-ran solved.

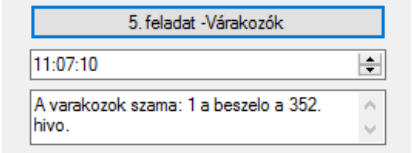

Figure 11. 5. problem – MS Visual Studio

The sixth problem was to define the last details of the conversation. Here again, it was enough to dump a formatted text box.

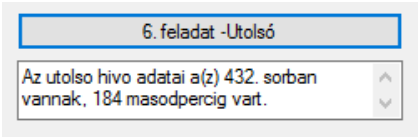

Figure 12. 6. problem – MS Visual Studio

The seventh problem was to make stock, whatever it was the list of successful calls in that format. It's SaveFileDialog was used to correct for the job property settings.

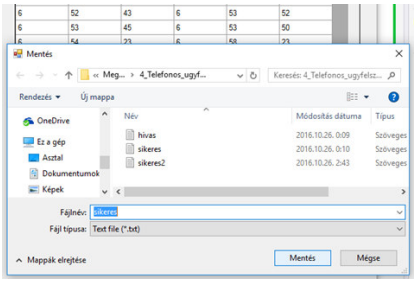

Figure 13. 7. problem – MS Visual Studio

As a conclusion, we found the followings for the case of the comprehensive exams in October 2016. Applying visual interfaces helped students only in one problem for input requests and file handling.

SUMMARY

During preparing this series of problems we got to the conclusion that applying visual programming interface does not support the solution very much. Just a few problems are simplified due to the easier input request, but this control is not part of maturity, so it is also an "excess benefit". Based on our experience in teaching visual interfaces it takes extra time to learn in the current conditions of education. Based on the experience of advanced programming education curriculum it takes two hours a week the school year, when the console interface is taught. Learning visual interfaces need at least three hours a week.

The visual interface teaching is definitely an advantage in the future to help students getting much more motivated towards using a more modern programming interface. They are commonly making more experiments and programming at home. Object-based thinking is being developed, which is also useful when dealing with information technology students in the future.

REFERENCES

[1] http://www.freepascal.org/docs-html/rtl/classes/tstringlist.html.

[2] http://wiki.freepascal.org/TStringList-TStrings_Tutorial.

[3] http://www.oktatas.hu/kozneveles/erettsegi/feladatsorok/emelt_szint_2016osz

[4] Benkő Tiborné - Tóth Bertalan, *Együtt könnyebb a programozás - Free Pascal,* Conputerbooks, 2010.

[5] Benkő Tiborné - Tóth Bertalan, *Együtt könnyebb a programozás – C#,* Conputerbooks, 2011.

[6] Reiter István, *C# programozás lépésről lépésre,* Jedlik Oktatási Studio Kft., 2016

[7] Végh Csaba, Dr, Juhász István, *Java-start!* Logos Kiadó, 2000

,

SUPPORTED THROUGH THE NEW NATIONAL EXCELLENCE PROGRAM OF THE MINISTRY OF HUMAN CAPACITIES

Finding pairs in mathematical games

Borbély József

Óbudai Egyetem, Székesfehérvár, Hungary

borbely.jozsef@amk.uni-obuda.hu

Abstract— **In this paper we will present some two-personal mathematical games. The problems will be taken from mathematical competitions and we will give a winning strategy for special cases in every game presented below. Some of the problems were invented by the author.**

I. INTRODUCTION

In this paper we will present some abstract strategy games, where no chance is involved. In all of the investigated games we will use some "pairing principle", i.e. we will establish disjoint pairsto describe how one can win the game.

The tools used to solve these problems are totally elementary, but one needs to have a good idea to find the winning strategy (or to find out which player has a winning strategy). The problems were posed in mathematical competitions like Nemzetközi Magyar Matematikaverseny (NMMV), Országos középiskolai tanulmányi verseny (OKTV), or the Tournament of the Towns (TT).

Let us begin with a theorem that will ensure the determinancy of our games (see [1]):

Theorem 1 (Zermelo, 1912) *In any combinatorial game, at least one of the players has a non-losing strategy.*

Theorem 1 is called the fundamental theorem of combinatorial games. Using this theorem, we always can

be sure that in the investigated game one of the players has a winning strategy.

We will call the players in all of the games "first player" and "second player". The "first player" will be tha player who makes the first step in the game.

II. FINDING PAIRS

The following is a generalization of a problem posed in the OKTV competititon in 2014 (the proposer was Borbély).

Game 1: *Two players alternately delete a number from the set {1,2,..., n} until two numbers remain. If the sum of the two remaining numbers is a square number, then the second player wins, otherwise the first player wins.*

We will prove the following result:

Theorem 2: *If n is divisible by 8, then in Game 1 the second player has a winning strategy.*

Proof:

We will prove by induction on k, that the elements of the set {1,2,..., 8k} can be ordered into pairs in such a way that the sum of the numbers in every pair equals a square number.

Note that this would imply the result of the theorem, because player two has the possibility to erase in each of his step the number, that was the pair of the number deleted by player one in the previous step.

For k=1 the statement holds, because the pairs (1,8), (2,7), (3,6), (4,5) correspond to the conditions.

Let us assume that we proved the statement for 1,2,...,k-1. We will prove the statement for k, too. Let s be the smallest odd square number greater then 8k (where $k \geq 2$). We will show that $s<16k$.

Let s be s=$(2m+1)^2$=$4m^2$+4m+1.

Note that if k≥2, then m≥3. If m≥ 3, then we have the estimates

$$\frac{s}{8k}=\frac{4m^2+4m+1}{8k}<\frac{4m^2+4m+1}{4m^2-4m+1}=1+$$

$$+\frac{8m}{4m^2-4m+1}\leq 1+\frac{(4m-4)m}{4m^2-4m+1}<1+1=2,$$

which implies the inequality s<16k.

It is easy to see that (s-1) is divisible by 8, thus we can make pairs in the following way:

(8k, s-8k), (8k-1, s-8k+1),..., $(\frac{s-1}{2},\frac{s+1}{2})$. In these pairs the sum of the numbers is a square (namely the number s). The number (s-8k-1) is divisible by 8, thus by the induction hypothesis we can make pairs from the elements of the set {1,2,...,s-8k-1} in the appropriate way. So our proof is complete, we proved the required result.

Remark: it is an open question which of the two players has a winning strategy if n is not divisible by 8.

The following is a generalization of a problem posed in the NMMV competititon in 2012 (the proposer was Borbély)

Game 2: *n andk are fixed positive integers. Two players alternately delete a number from the set {1,2,..., n} until two numbers remain. If the absolute value of the difference of the two remaining numbers is a prime number greater than k, then the second player wins, otherwise the first player wins.*

We will prove the following result:

Theorem 3: *If n is even,* $\frac{n}{2}$ *is a composite number, q is the greatest prime number not exceeding* $\frac{n}{2}$ *- 1 , and* $q+\frac{n}{2}$ *is also a prime number, then in Game 2 the second player has a winning strategy iff k≤q-1 .*

Proof:

1. If k≥q, then the first player can play in such a way that he always deletes the greatest number that was not

deleted. If he plays so, then the absolute value of the difference of the two remaining numbers cannot exceed $\frac{n}{2}$, thus (by the definition of q) cannot be a prime number greater than q.

2. Now assume that k≤q-1.

We will order the elements of the set {1,2,...,n} into disjoint pairs in such a way that the absolute value of the differences for every pair is a prime number. That implies that in this case the second player has a winning strategy, because player two has the possibility to erase in each of his step the number, that was the pair of the number deleted by player one in the previous step. Let us make the pairs in the following way:

First we establish the pairs

(1, q+$\frac{n}{2}$ +1), (2, q+$\frac{n}{2}$ +2),...,$(\frac{n}{2}-q,n)$, then we establish

the pairs

$(\frac{n}{2}-q+1,\frac{n}{2}+1)$, $(\frac{n}{2}-q+2,\ \frac{n}{2}+2)$, ..., $(\frac{n}{2}$, $\frac{n}{2}+$

$+q)$.

In our construction in the first group the difference is always q+$\frac{n}{2}$, which is by our assumption a prime number. In the second group the difference is always q. The pairs are disjoint, thus we proved the desired result.

Remark: it is an open question which of the two players has winning strategy if n and k have other number theoretical properties.

The following is a generalization of a problem posed in the OKTV competition in 2005:

Game 3: *Let n be a fixed positive integer. Two player write alternately numbers on the board. Player one writes down the number 1. Then in each turn the following player writes down a number that is a sum or a product of two already written numbers, but he cannot write down numbers that are already on the board and he cannot write down a number greater than n. The player who writes down the number n wins the game.*

We will prove the following result:

Theorem 4: *If n is an odd prime number, then in Game 3 player one has a winning strategy.*

Proof:

Note that if n is a prime number, then the number n can be generated only by addition.

Let us order the elements of the set {1,2,...,n} into disjoint pairs with the exception of the element n:

(1, n-1), (2, n-2),..., $(\frac{n-1}{2}, \frac{n+1}{2})$.

Let player one play in the following way: after each step of player two he shall write down the least positive integer x such that neither x nor n-x were written down. If he always can do that, then he wins the game because n is odd. Thus we have only to prove that player one can use this strategy throughout the whole game.

We prove this by induction on the number of the steps. In the first step he can use this strategy (he writes down the number 1). Let k≥2 and let us assume that player one was able to apply his strategy. Let us assume, that each of the players made k steps, and it is player one's turn. Let x be the least positive integer such that neither x nor n-x were written down (if no such x exists, then player ine can write down the number n).

x≤2k+1, because in the set {1,2,...,2k+1} there must be a number y such that neither y nor n-y were written down (2k numbers were written down). By the strategy of player one, he chose all his k numbers from the set {1,2,...x-1}. Player two had to choose as his first step the number 2, thus at least k+1 elements of the set {1,2,...x-1} are already written on the board. That means that player one can establish the number x by addition, because x≤2k+1.

Thus player one has a winning strategy.

Remark: one can similarly show that if n is the double of a prime number, then player two has a winning strategy. But generally it is an open question which of the two players has a winning strategy.

Finally we present two games from the reputed competition Tournament of the Towns, and we will show that the two games have a common root.

The following game was presented in the TT competititon in 1987:

Game 4: *The game is played on an 8*8 chessboard. Player one places a knight on the board. Then each player in turn moves the knight, but cannot place it on a square where it has been before. The player who cannot make a move looses.*

The following game was presented at the TT competititon in 2009:

Game 5: *Player one and player two visit Archipelago with 2009 islands. Some pairs of islands are conneceted by boots which run both ways. The folllowing game is played:*

Player one chooses the first island where they arrive by plane. Then player two chooses the next island they will visit. Thereafter, the two take turns choosing an island which they not have yet visited. When they arrive at an island which is connected only to islands they had already visited, whoever's turn to choose next would be the looser.

And now we will show the connection between Game 4 and Game 5. The problems will be reformulated in the language of graphs.

Game 6: *Player one and player two alternately select distinct vertices v_1, v_2,... of a graph in such a way that v_i and v_{i+1} always must be adjacent vertices. The last player able to choose a vertex wins the game.*

We will exactly determine when player one and when player two in Game 6 has a winning strategy. Using our result we can easily determine which of the players has a winning strategy in Game 4 and game 5.

Theorem 5: *In Game 6 player two has a winning strategy iff the graph they use for the game has a perfect matching.*

Proof:

If the graph has a perfect matching, then player two clearly has a winning strategy: he can always choose the pair of the vertex chosen by player one, and thus cannot loose the game.

If in the graph there are not any perfect matchings, then let M be a maximal matching in the graph. Player one begins with a vertex that is not covered by M. Then player two has to choose a vertex covered by M (because M was maximal). In his next turn, player one chooses the pair of the vertex chosen by player two.

We will show that player one can continue the game in such a way. More exactlx, we state that player two cannot choose a vertex not covered by M.

Namely, if in any of his steps player two would be able to choose a vertex not covered by M, then let us consider the tour already made by the players. In the tour they used an odd number of edges, that were alternately not in M and in M (in this order). Thus changing the rules of the edges in this tour we could find a matching greater than M, which is impossible.

Thus player two can only choose vertices covered by M and player one has a winning strategy.

Remark: using the result of Theorem 5, it is easy to see that in Game 5 the first player has a winning strategy. In Game 4 one can find a proper pairing which shows that here the second player has winning strategy (see [2]).

ACKNOWLEDGMENT

The author wants to express his gratitude towards the Hungarian Ministry of the Human Capacities and the Óbudai Egyetem for having generously granted the research work.

REFERENCES

[1] E. Mendelson, *Introducing Game Theory and its Applications, Discrete Mathematics and its Applications, 2016*

[2] P.J. Taylor (editor), *Tournament of the Towns 1984-1989, Australian International Centre for Mathematics Enrichment, 1992*

SUPPORTED THROUGH THE NEW NATIONAL EXCELLENCE PROGRAM OF THE MINISTRY OF HUMAN CAPACITIES

Counting graphs

Borbély József, Csala-Takács Éva

Óbudai Egyetem, Székesfehérvár, Hungary

borbely.jozsef@amk.uni-obuda.hu

csala.takacs@amk.uni-obuda.hu

Abstract— **In this paper we will present some problems which show the connection between algebraic formulas and combinatorial principles. Each problem is based on the idea counting the number of special graphs or subgraphs.**

I. INTRODUCTION

Using combinatorial arguments to prove algebraic identities is an effective method. In this paper we will solve some problems in which both algebraic and combinatorial methods are involved. We will see that the ideas we use are very general.

Our methods are elementary but one can have benefits from the ideas presented below. We tried to search problems on which we have worked.

The first theorem is a result of Borbély, the proof of the third theorem presented in the paper was given by Borbély and deviates from the official one. With similar approaches one could prove other formulas of this type..

II. THE THEOREMS

As warming-up we prove the following theorem, which was a problem in the OKTV in 2013, proposed by Borbély.

Theorem 1: *For ever positive integer n, the number of simple graphs on 2n labeled vertices, whose vertices have only odd degrees, is exactly* $2^{\binom{2n-1}{2}}$.

Proof:

We will find bijection between the simple graphs on (2n-1) labeled vertices and the simple graphs on 2n labeled vertices with vertices having only odd degrees.

Let be the vertices 1,2,...,2n.

Let G be a labeled graph on the vertices 1,2,...,2n-1. Then we can connect the vertices of G exactly in a unique to get a graph with only odd degrees (we connect the vertices with even degree in G with the edge 2n). If we do that, then the vertex 2n will have an odd degree, too, because in G there mut be an odd number of vertices with odd degree, thus there must be an odd number of vertices with even degree.

Conversely, if G* is a graph on the vertices 1,2,.., 2n with the desired property, then by deleting the vertex 2n with the incidental edges we get a unique graph G on the vertices 1,2,...,2n-1. QED

Secondly we will prove the following theorem, which appeared in 1979 in the Schweitzer competititon [see 2]. We will use a clever combinatorial argument in order to prove an algebraic formula about directed graphs.

The proposer of this problem was Schrijver.

Theorem 2: *If for fixed positive integers n and k we denote the number of simple strongly connected directed graphs with k edges on n labeled vertices by G(n,k), then*

$\sum_{k=n}^{n^2-n} (-1)^k G(n,k)$=*(n-1)!* .

Proof:

We will prove the statement by induction on n. For n=1 the statement of the theorem holds. Let us assume that we proved the statement for simple directed graphs with 1,2,...,n-1 vertices (n≥2). We will prove the statement for n, too.

Let 1,2,...,n be the vertices.

We will handle two distinct cases.

Case I:

If exactly two edges are incident to the vertex n, and their other endpoints coincide, then let us denote the other endpoint by w. If the graph is simple and strongly connected, then both nw and wn must be edges. Thus, in this case, if we proceed from a strongly connected graph, then by deleting the vertex n and the edges incident to it, we get a strongly connected graph with (k-2) edges on the vertices 1,2,..., (n-1). Using the induction hypothesis, our sum is in this case (n-2)!. The vertex w can be chosen in (n-1) different ways, so the sum gives (n-1)(n-2)!=(n-1)!, if two edges are incident to the vertex n, and their other endpoints are the same.

Case II:

If the vertex n does not fulfill the conditions described in Case I, then there must be different vertices u and v such that un and nv are edges of the graph (here we used that the graph is strongely connected). Let A be the set of graphs which correspond to this description and uv is an edge from them, and let B be the set of graphs which correspond to this description and uv is not an edge from them. It is easy to see that a graph G is an element of A iff (G-uv) is an element of B. Thus in this case our sum gives 0. QED

The following theorem was proposed by Dályay Pál Péter in the journal "A matematika tanítása" (see [1]), and solved in the following way by the author Borbély (this proof deviates from the official one).

Theorem 3: *For every integer greater than one holds the identity*

$$\sum_{k=0}^{n}(-1)^k \binom{n}{k}^2 k! = \sum_{k=0}^{n-2}(-1)^{k+1} \binom{n-1}{k+1}\binom{n}{k}(k+1)!.$$

Proof:

Throughout of the whole proof, the $\sum a_k$ will denote the sum of a_i's for which the sum is interpreted.

Clearly, the right hand side can be written as

$$\sum(-1)^{k+1} \binom{n-1}{k+1}\binom{n}{k}(k+1)!.$$

Let us write the right hand side in the following way:

$$\sum(-1)^{k+1} \binom{n-1}{k+1}\binom{n}{k}(k+1)! =$$

$$=\sum(-1)^{k+1} \frac{n-1}{k+1}\binom{n-2}{k}\binom{n}{k}(k+1)! =$$

$$= -(n-1)\sum(-1)^{k} \binom{n-2}{k}\binom{n}{k}(k)!.$$

Thus we have to prove the identity

$$\sum_{k=0}^{n}(-1)^k \binom{n}{k}^2 k! = -(n-1)\sum(-1)^{k} \binom{n-2}{k}\binom{n}{k}(k)!.$$

Substract from both sides the term

$$\sum(-1)^{k} \binom{n-2}{k}\binom{n}{k}(k)!.$$

So we get on the left hand side

$$\sum_{k=0}^{n}(-1)^k \binom{n}{k}^2 k! - \sum(-1)^{k} \binom{n-2}{k}\binom{n}{k}(k)! =$$

$$=\sum_{k=0}^{n}(-1)^k \binom{n}{k} k!\left(\binom{n}{k} - \binom{n-2}{k}\right) =$$

$$=\sum_{k=0}^{n}(-1)^k \binom{n}{k} k!\left(\binom{n-2}{k-1} - \binom{n-1}{k-1}\right) =$$

$$=\sum_{k=0}^{n}(-1)^k \frac{n}{k}\binom{n-1}{k-1} k!\left(\binom{n-2}{k-1} - \binom{n-1}{k-1}\right) =$$

$$=(-n)\sum(-1)^{k} \binom{n-1}{k-1}\binom{n-2}{k-1}(k-1)! +$$

$$(-n)\sum(-1)^{k} \binom{n-1}{k-1}\binom{n-1}{k-1}(k-1)! =$$

$$=(-n)\sum(-1)^{k} \binom{n-1}{k}\binom{n-2}{k}(k)! +$$

$$(-n)\sum(-1)^k\binom{n-1}{k}\binom{n-1}{k}(k)!,$$

and on the right hand side

$$-(n)\sum(-1)^k\binom{n-2}{k}\binom{n}{k}(k)!.$$

Thus we have to prove the identity

$$(-n)\sum(-1)^k\binom{n-1}{k}\binom{n-2}{k}(k)! +$$

$$+(-n)\sum(-1)^k\binom{n-1}{k}\binom{n-1}{k}(k)!=$$

$$=(-n)\sum(-1)^k\binom{n-2}{k}\binom{n}{k}(k)!.$$

Dividing both sides by (-n), we have to prove that

$$\sum(-1)^k\binom{n-1}{k}\binom{n-2}{k}k! +$$

$$+\sum(-1)^k\binom{n-1}{k}\binom{n-1}{k}k! =$$

$$=\sum(-1)^k\binom{n-2}{k}\binom{n}{k}k!.$$

For fixed positive integers r and s let $K_{r,s}$ denote the complete bipartite graph with labeled vertices and two vertex-classes having respectively r and s vertices. Let $p_k(r,s)$ be the number of k-matchings in $K_{r,s}$ (i.e. the number of matchings that cover 2k vertices). In order to construct such a k-matching, we have to choose k vertices from both of the vertex-classes and we have to decide how to establish pairs.

Thus $p_k(r,s)=\binom{r}{k}\binom{s}{k}k!$.

In order to prove our theorem we have to verify that

$$\sum(-1)^k p_k(n-1,n-2)+\sum(-1)^k p_k(n-1,n-1)=$$

$$=\sum(-1)^k p_k(n-2,n).$$

Let A and B be the two vertex-classes of the complete bipartite graph $K_{r,s}$ with |A|=r and |B|=s. Let x be a vertex in A.

The number of k-matchings, which do not cover the vertex x, is exactly

$p_k(r-1,s)$.

The number of k-matchings, which do cover the vertex x, is exactly

$(s-k+1)p_{k-1}(r-1,s)$.

Thus we have the recursion

$$p_k(r,s)=p_k(r-1,s)+(s-k+1)p_{k-1}(r-1,s).$$

Thus we get

$$\sum(-1)^k p_k(n-2,n) =$$

$$\sum(-1)^k p_k(n-2,n-1)+$$

$$+\sum(-1)^k(n-k-1)p_{k-1}(n-2,n-1)=$$

$$=\sum(-1)^k p_k(n-2,n-1)+$$

$$+\sum(-1)^{k+1}(n-k-2)\,p_k(n-2,n-1)=$$

$$=\sum(-1)^{k+1}(n-k-3)p_{k-1}(n-2,n-1).$$

On the other side we have

$$\sum(-1)^k p_k(n-1,n-2)+\sum(-1)^k p_k(n-1,n-1)=$$

$$=\sum(-1)^k p_k(n-2,n-1)+$$

$$+\sum(-1)^k p_k(n-1,n-1)=$$

$$=\sum(-1)^k p_k(n-2,n-1)+$$

$$+\sum(-1)^k p_k(n-2,n-1)+$$

$$+\sum(-1)^k(n-k)p_{k-1}(n-2,n-1)=$$

$$=\sum(-1)^k p_k(n-2,n-1)+$$

$$+\sum(-1)^k p_k(n-2,n-1)+$$

$$+\sum(-1)^{k+1}(n-k-1)p_k(n-2,n-1)=$$

$$=\sum(-1)^{k+1}(n-k-3)p_{k-1}(n-2,n-1).$$

Thus the two sides are equal, and so we proved the statement of the theorem. QED

ACKNOWLEDGMENT

We want to express our gratitude towards the Hungarian Ministry of the Human Capacities and the Óbudai Egyetem for having generously granted the research work.

REFERENCES

[1] A matematika tanítása, issue 2010/3, p.27

[2] Gábor J. Székely (editor), *Contests in higher mathematics*, Springer, 1996.

Graph Algorithm Design for a Local Transportation Application

K. Zsobrák * and L. Gugolya**
* Óbuda University – Alba Regia Technical Faculty, Székesfehérvár, Hungary
*zsobrak.krisztian@gmail.com
**gugolya.laszlo@amk.uni-obuda.hu

***Abstract*—In our modern world, the importance of mobile applications is increasing. These apps can improve our comfort, we can obtain the needed information faster, independently from our location. Such applications use more complex mathematical algorithms, like graph theory, and therefore graph algorithms.**

A special graph build algorithm will be presented in this paper, which is based on local bus transportation of Székesfehérvár. The purpose of this algorithm is to find the best route from the start bus station to the destination, even by using multiple bus lines. The bus schedule is stored in a database, in a specified format. The graph is created from this data, by an algorithm described in this paper. The search can be performed in this graph, which results in a path that contains the bus travel information. The difficulty of such route-finding algorithms, that it has to operate in both space and time dimensions, because moving from a location to another can only be performed in specified times.

I. Introduction

In our fast world we need applications, that makes our life easier. With these software we feel, we are not required to remember unnecessary information, because when we need that, it is available on our mobile device. Therefore, it came to our mind, we implement a route-search, route-plan application based on existing similar solutions, but for Székesfehérvár's local transportation.

At now, one can get the information of lines by a static website of KNYKK Company (Fig. 1).

Figure 1. – Static line's information of Székesfehérvár

Another interface is a map based route planner, where the user can select the start and the finish bus stop on the map. (Fig. 2)

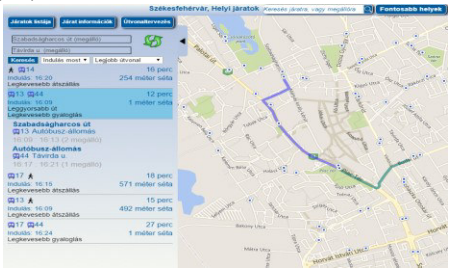

Figure 2. – Map based route planner of Székesfehérvár

But this website is not optimized to mobile devices and tablets, therefore it falters, and drastically slow on them. Also it is not responsive, and not suitable for use on the go.

Our example to follow is the BKK Futár solution, thanks to its clean design and useful functions. The Futár has a website and a mobile application, both with similar functionality for the users. It not forces the user to select the start and finish station on the map, but he or she can enter it into a text field. It can also search by street addresses.

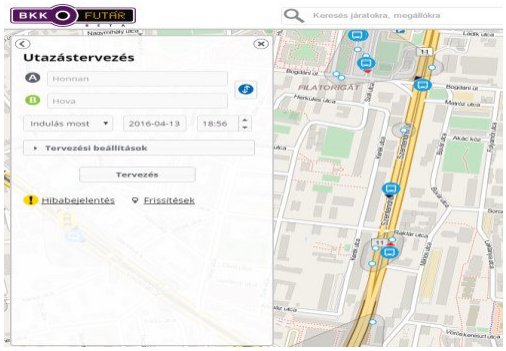

Figure 3. – Screenshot of BKK Futár website.

We choose to implement the application to Android operation system, therefore Java language and SQLite database is required.

II. Transport Information Services

Passenger information services, for example dynamic route-planning applications are designed to inform people about when and which line should they take. The base of this paper is the local transportation of Székesfehérvár, where only bus is available.

Generally, three parameters are required for the route-planner algorithm in order to generate useful data for the user: The departure location, the destination, and the departure time. The output of the algorithm is a list, from which the user can select the best. This has to contain the departure and destination time, the used lane's name, and when and where he or she should change.

Google Maps is capable of planning local transportation trips, and this feature is also available on mobile devices. The necessary GTFS based database have to be uploaded to the Google servers, and this function is accessible to everyone. But this software can be slow on older devices, which are not designed to have the requirements of the new versions of Google's software. The application mentioned in this paper (extended by many search optimization) can be faster on these devices, and independent from having an internet connection.

III. Database Plan

To create this search algorithm, the schedule data must be stored in a database. Nowadays a very popular transportation data format is the GTFS (Google Transit Feed Specification), which is very comprehensive, and can store complex schedules. Compared to Székesfehérvár's simple bus based transportation, it is easier to store data in the following database structure, but it is easily convertible to GTFS, which I plan to do after the schedule is fully uploaded.

A. Stations, Bus Stops

A *station* has a name, which is known by the passengers, and this appears in the schedule. A *stop* is a place, where the bus actually stops, and people can get on or off. The schedule does not contain the stops, but it has to be stored in order to display it on map. Because often multiple stops are belonging to a station, they create a 1:N relation. These are stored in the following relational database tables:

- Stations:
  - id
  - name
- Stops:
  - id
  - stationid
  - coordinate

B. Lanes and Lines

In Székesfehérvár people know bus *lines* by their number, which starts from 10, and ends with 44. They usually on the same route back and forth, but there are exceptions like fast lines, and circle lines. A line may include multiple *lanes*.

- Line
  Contains multiple lanes, has a publicly known number, such as 10, 11, 15. This data will be displayed to the user.
- Lane
  A lane has a well-defined path with station names, and times but there is no public identification for it. For example: Train station – Metal industry – Bus station. At least one lane is assigned to a line

They database structure is the following:

- Lines
  - id
  - name
- Lanes
  - id
  - laneid
  - mark
  - description

C. Paths

A path of a lane is simply the list of the stations where it stops, and the time it takes to get there from the departure time. These lists will be stored in a single table, because filtering by lane or station is easier.

- Path
  - id
  - laneid
  - stationid
  - minute

D. Departure times

The buses on lanes depart on specified times. These are always given in an hour-minute format. Smaller or larger time unit are unnecessary. For the simplicity, it is easier to store this time value in the number of minutes from midnight. If a p time is equal to h hours and m minutes, then p equals to h times 60 plus m.

- Departure
  - id
  - laneid
  - time
  - daytype

IV. A Sample Schedule

Because Székesfehérvár's schedule is complicated, here's a sample one (Fig. 4), in order to visualize the methods in this paper.

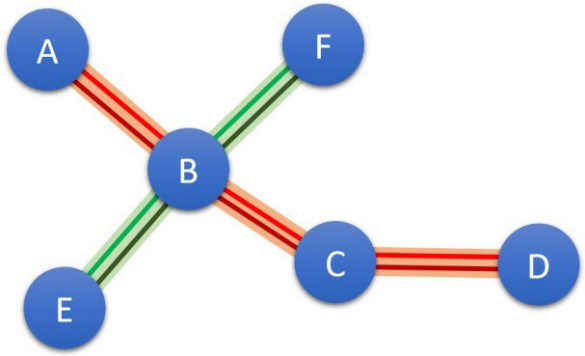

Figure 4. – A sample city

This sample city has 6 stations, labelled from A to F. There are two lines: 10 and 20. Each line has two lanes, one going forward, and the other backwards. The goal is to create an algorithm, that can easily find a route from station A to F.

A. Schedule

This is a list of the lines and lanes of the sample schedule. The list of stations and minutes are in pairs, showing the required time by the bus to get to that station from the departure time, in minutes.

- Line 10:
  - Lane 10-f:
    - Stations: A, B, C, D
    - Minutes: 0, 2, 6, 8
    - Departs: 8:00, 8:20
  - Lane 10-b:
    - Stations: D, C, B, A
    - Minutes: 0, 2, 6, 8
    - Departs: 8:10, 8:30
- Line 20:
  - Lane 20-f:
    - Stations: E, B, F
    - Minutes: 0, 2, 6

- Departs: 8:05, 8:25
- Lane 20-b:
  - Stations: F, B, E
  - Minutes: 0, 4, 6
  - Departs: 8:15, 8:35

From now on, I will use this sample data in the examples.

V. Building the Graph

Graphs in discrete mathematics, more specifically in graph theory, are mathematical abstractions, which contains two sets, nodes and edges, where a pair of nodes are interconnected by edges. A large number of graph types are extension of this definition. For example, a directed graph has edges, which node pairs are ordered, therefore a direction is assigned to it. The nodes and edges have a unique identification, usually natural numbers. This leads to assign multiple records of information to a graph object. This thesis defines this kind of graphs.

We know where a bus will be at any given time from the schedule. To display the location simpler, only one dimension is required, which will be the station identification number. Timeliness also requires only one dimension; which metric is the minute. These values are easier to present in a two-dimensional grid (Fig. 5).

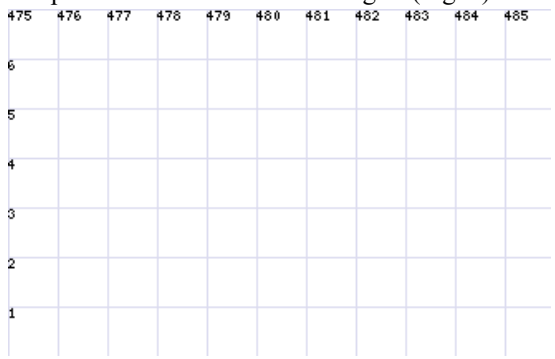

Figure 5. – Default grid

First add the nodes. We know the departure time, and where and when will the bus stop. For example, let's take lane 10-f, at 8:00 from the sample schedule. It departs from station A at 8:00. It takes 2 minutes to get to station B, therefor it is in B at 8:02, and so on. Add these nodes to the grid (Fig. 6.).

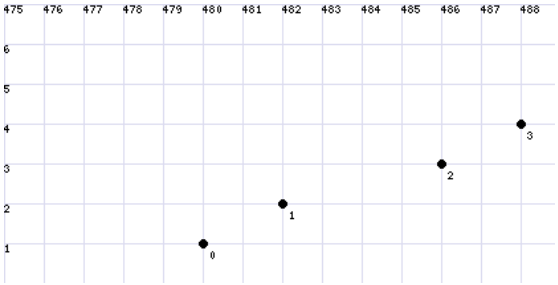

Figure 6. – Grid with a line's nodes

Connecting these nodes with directed edges will mean, that one can travel by bus between these points in space and time, but only in forward direction. The edges must contain the bus lane id data, and its weight, which is its time dimension length.

Then add all the nodes by iterating through all of the departure times, and connect them likewise. After that we got the full map of bus lines. (Fig. 7.)

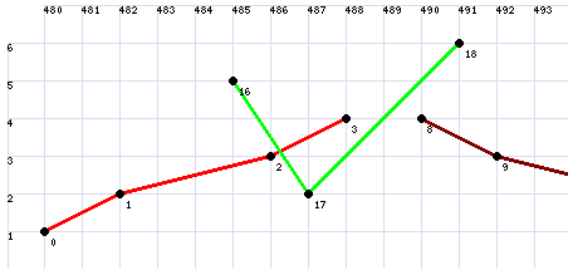

Figure 7. – The map of bus lines

Apart from that the figures are in a grid, this is a regular directed graph, with information assigned to its edges and nodes. But this is yet incomplete. For creating a simpler search algorithm, the graph must be extended by adding edges that connect station nodes in a chronologically ascending order. (Fig. 8.) These will represent the waiting at a station.

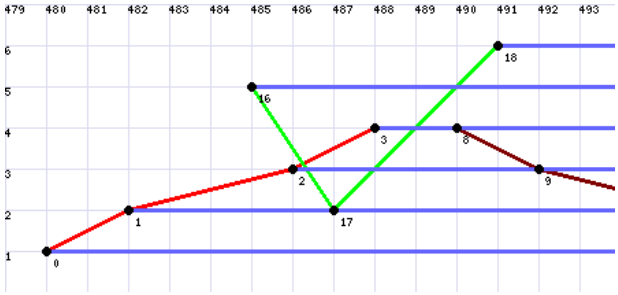

Figure 8. - The extended graph by the waiting edges

An example: Travel from station A to station F could not be done without change at station B. The shortest path would be node 0, 1, 17, 18.

VI. Graph Search

At the beginning of the search, the algorithm knows the start and finish station, and start time, but does not know the start nor the end node. For the better performance, a trip-end-time must be created, which the search algorithm cannot exceed. For example, 90 minutes from the start time. The start node is easier to find, because it will be the first that has the department station as station data, and its time data is greater or equals to the department time. The algorithm must try multiple start nodes between the start and end time to get better results.

When a start node is selected, a non-informed search has to find the nearest node, which has the arrival station as station data. The nearest node has the lowest weight path from the start node. This could be done by breadth-first search, or depth-first search.

However, this algorithm has to be fast with relatively low memory complexity, due to the mobile environment. Series of optimization has to be done on the graph build, the search algorithm, and the model of classes.

VII. Conclusion

In this solution, the mobile app is independent from other route planning services, efficient in offline mode, and gives more freedom for the developer. The application can be lightweight, and free from unnecessary services. But a possible drawback could be the lack of integration with other applications.

There are multiple designs for the search algorithm, that give the best route for the user, but they have to be

implemented and tested for memory and time complexity. Numerous optimization methods are planned, but these will be significant, when the full 100 lane schedule of Székesfehérvár is uploaded to the database, also which size is yet unknown. Based on the performance on mobile devices, the location of the calculation has to be taken into considered too. A device-based method gives the feature of offline route-planning, but the database has to be copied on modification. The server-based has the benefit of reliable calculation time, and address geocoding for departure or destination location, but slow internet connection can greatly affect the performance.

REFERENCES

[1] M. Braga, M. Y. Santos, A. Moreira, "Integrating Public Transportation Data: Creation and Editing of GTFS Data", *New Perspectives in Information Systems and Technologies, Volume 2, 2014,* pp 53-62

[2] T. Teorey, S. Lightstone, T. Nadeau, H. V. Jagadish, *Database Modeling and Design: Logical Design*, 2011

[3] R. J. Trudeau, *Introduction to Graph Theory*, 1993

[4] I. Fekete, T. Gregorics, S. Nagy, *Bevezetés a mesterséges intelligenciába*, [Introduction to Artificial Intelligence] 2006

Research on the Beach of Grand Hotel Varna

Gencho Panicharov*, Aneta Georgieva*, Marta Seebauer**
*Varna Free University "Chernorizets Hrabar", Varna, Bulgaria
**Óbuda University Alba Regia Technical Faculty, Székesfehérvár, Hungary
dr_panicharov@abv.bg, angr@abv.bg, seebauer.marta@amk.uni-obuda.hu

Abstract **— The shoreline erosion is a central problem on the Black Sea costal in the north part of Bulgaria. The aim of this paper is to describe a common project "Marina" carried out by the students of Hydraulic Engineering Department of Delft University of Technology and Varna Free University "Chernorizets Hrabar" focused on the coastal protection research on the beach of Grand Hotel Varna. The main topics of the project was the problem definition, the data collection about the real state, the selection and implementation of methodology by mathematical modeling of expected wave height, and also elaboration of an economical optimal action plan for coastal protection using mainly the available building materials.**

I. INTRODUCTION

Bulgaria is a country located along the Western Black Sea Coast in South-East Europe. Varna, the third greatest city in Bulgaria is an important economical and touristic center. This large coastal city deals with port activities, industry, beaches and tourism but the landscape is rich in natural endowments. There is a lot of information and discussions regarding the natural features and development of the Bulgarian Black Sea Coast, however the information about these projects are not organized in a systematical way. Intensive coastal and landslide protection program has taken place in the 80-ties of the last century.

II. THE SHORELINE EROSION AND THE COASTAL PROTECTION

The landscape on north Bulgarian Black Sea Coast is varied on mountains and plains, rich in surface and ground water quells. This fact and the every more intensive storms due to global heating, also the reckless human encroachments are standing changing the natural landscape. (Fig.1.)

Figure 1. The coast defended from waves by sand dune at winter time

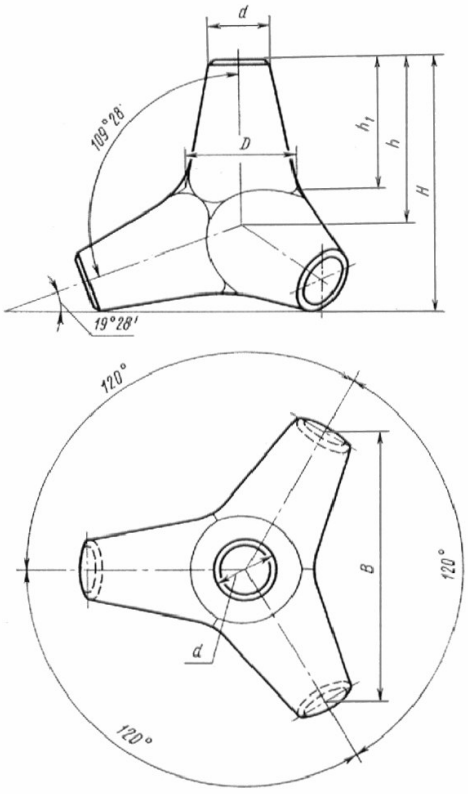

Figure 2. Tetrapod unit

At that time large number of groins and a few "marinas" were constructed. With the political and economic changes started in 1989, the state investments in coastal protection and development projects have been radical reduced. Presently, hotel owners construct small harbors and coastal protection structures attempting to maintain the beaches surrounding their property. These activities are extremely hazardous for the coastal dynamics and their effects are only partly or not at all predictable [1].

The role of coastal engineering is to maintain the shoreline, to keep it safety. Breakwaters are artificial structures built on the coasts in the reason of protect the shoreline from the effects of waves and storms. In shoreline structures as breakwaters armour units can be used several barrier materials, for example, natural shot rocks, ripraps, special concrete units.

Tetrapods are armour units in tetrahedral from used as breakwaters. A tetrapod's due to their special shape dissipate the incoming waves by allowing to flow the water around and distribute it of tetrapods to interlock as it is shown in Fig.3.

Figure 3. Breakwaters using tetrapods

Tetrapods were originally developed by Laboratoire Dauphinois d'Hydraulique (now ARTELIA) in Grenoble, France in 1950. After the patents expiration date they are produced by many contractors and widely used all over the world.

III. The Project of the Beach Grand Hotel Varna

Since 2003 a cooperation was established between the Hydraulic Engineering Department of Delft University of Technology and Varna Free University "Chernorizets Hrabar". The cooperation focuses on exchange of good practices and realization of common development projects on the coasts around Varna. Dutch and Bulgarian students get the possibility to gain experience in data collecting, processing and interpreting. Repeating this fieldwork every year in the same area will provide an overview of the coastal development in the Varna area.

The students act as consultants for local hotel owners at the Varna coast. Their work consists of measuring hydraulic aspects in the project Marina. Data collection covered the inventory of the materials near site, beach measurements, wave measurements, profile measurements, quarry analysis and a bathymetric survey. The rehabilitation plan contains the development of sub-areas in the St. Elias Marina (Fig. 4) like the peninsula, north beach, south beach and the breakwaters.

A. The problem definition

In the North of Varna, the first beach resort is established at the Bulgarian Black Sea Coast. This place is very attractive for Bulgarians and tourists.

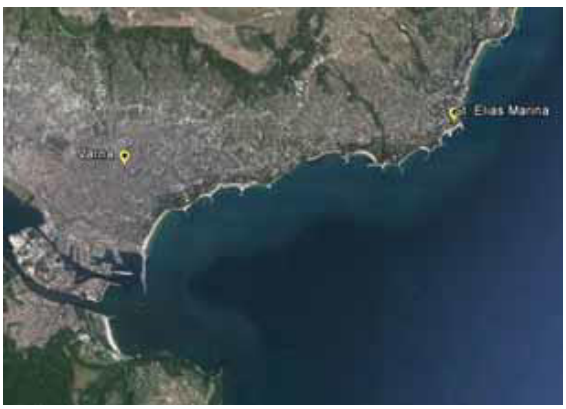

Figure 4. Sub-areas in the St. Elias Marina

Therefore, it is economically important for the whole area. Part of this resort is the, the Grand Hotel Varna Resort. It has a small marina partly constructed in the early 90-s.

Although some temporary protection work was made but by the time the defects of the port structures became visible. The one of reasons was the experimental design that was not real tested in practice. The other one was the poorly carried out work.

Attempts were made to protect the existing constructions by laying rocks in front of the existing breakwater which was constructed of 'H' shaped concrete blocks. During a big storm in 1993 this protection proved itself unstable. In result of them tons of rock - that should protect the marina - were picked up by overtopping waves and deposited in the protected area of the port.

Later on due to the neglect of this problem the damage was progressed and by now the main breakwater was totally destroyed. In 2015, a sad, abandoned and devastated port lies at the shore of Grand Hotel Varna. There is huge contrast between the beautiful coastal area, good touristic infrastructure and collapsing marine structures.

Nowadays the owner of the beach resort lacks a fully functioning port in front of his lovely resort. The circumstances now are stated that the port is severely damaged and a high probable danger to human safety [2].

Moreover, the fact that the designated area of the port is not the best place for it in the first place because there is not calm water all year around. However, these high waves and significant amount of overtopping takes place in the winter whereas the port only is operational in summer time. This means that the structure must withstand the severity of wave attacks. Furthermore, during winter time waves form the port.

B. Data collection on the beachGrand Hotel Varna

For the data collection about the materials the area was divided on 6 different sub-areas. Fig. 5 shows the different areas. The data was qualitatively and quantitatively selected, so the amount of material was estimated as well as the quality of the material.

This estimation of the quality is necessary for the reusability of the materials. Due to the bad weather and the slipperiness, the marina (area 5 and 6) was not accessible from mainland. The approach from the boat was also very hard through the danger to come nearby due to steel wire sticking out of the water. Therefore, area 6 is not discussed in this report and assumed that is has the same qualitative condition as area 5.

Figure 5. Different area's in the scope

Figure 6. Broken tetrapod units

Shores are influenced by the topography of the surrounding landscape, as well as by water induced erosion, such as waves. The geological composition of rock and soil dictates the type of shore which is created.

C. *Methodology*

The inventory and the quality check of the materials in the different areas were based on the visual inspection.

Within the total area we observed different sizes of tetrapod's, pyramid blocks, caisson slabs, rocks and a quay wall. (Fig.6) To check whether these materials are still usable at their current location or check if they're reusable at another location, it's important to know how many elements there're and how many are still intact. After this, for the areas directly influenced by the sea, calculations are made to estimate the wave heights that occurred in the last decades and predict the maximum wave height.

The broken parts and cracks were indicators for reusability of materials. A big part of units could be simple counted. When the observation was impossible due to no accessibility of the area or through the amount of units, an estimation was made [3].

The size of the units was defined by using a simple measuring tape. In case of tetrapod's, the rest of the dimensions was calculated with general formulas for tetrapod's. The size of the rocks was categorized in 4 different classes: small, medium, large and extra-large corresponding to their diameter.

For the calculation of the $D_{n,50}$, an estimation was made based on the distribution of the rock sizes. The different diameters are shown in Table 1:

TABLE I.
SIZE OF THE DIFFERENT BOXES FOR CLASSIFICATION OF THE DIFFERENT SIZES OF ROCKS.

	Diameter [m]
Small	<0,5
Medium	0,5-1,0
Large	1,0-1,5
Extra-large	>1,5

Calculations for the maximum wave heights are done with the Hudson and Van der Meer formulas. Hereby the maximum significant wave height is limited by the water depth in front of the wave protection.

We can use the dimensions of the elements on the locations to calculate which design wave height the protective structure has. We can also check which wave height certainly has occurred as some of the tetrapods are broken. For these calculations, two different formulas can be used: Van der Meer's formula and Hudson's formulas. The Hudson's formula (1) can rough estimate the needed rock weight.

$$W = \frac{\gamma_R H^3}{K_D \Delta^3 ctg\theta} \qquad (1)$$

where

- W - the weight of required riprap armour [N]
- γ_R - specific weight of the armour blocks [N/m^3],
- H - the estimated wave height [m],
- K_D - stability coefficient, experimental defined,
  - $K_D \sim 3$ for natural rocks
  - $K_D \sim 10$ for artificial blocks
- Δ - relative density of rocks,
- θ - angle with the horizontal.

This formula doesn't take wave period, damage level, permeability of structure and storm duration like the Van der Meer's formula does. The Hudson formula thereby can be only used in a preliminary design and for regular waves [4].

The Hudson formula in more simple form is

$$\frac{H}{\Delta D_{n,50}} = (K_D ctg\theta)^{\frac{1}{3}} \quad (2)$$

in them

$$D_{n,50} = \left(\frac{M_{50}}{\rho_t}\right) \qquad (3)$$

where

- $D_{n,50}$ -nominal diameter of rocks [m]
- M_{50} - median mass of rock grading given by 50% on the mass distribution curve [N],
- ρ_t - mass density of the rocks [N/m].

In this case both formulas will be used, but due to lack of specific data for the Van der Meer formula (4), the standard case situation is considered [6]. The Van der Meer formula for surging waves

$$\frac{H}{\Delta D_{n,50}} = 1.0\, P^{-0.13} \left(\frac{S}{\sqrt{N}}\right)^{0.2} \sqrt{ctg\theta}\, \xi_m^P \quad (4)$$

where

- P - notional permeability factor
- S - damage level,
- N - number of waves (storm duration)
- ξ_m - transition from plunging to surging waves.

Because not all the areas are directly influenced by the waves on the sea, only location 1, 2 and 3 are considered. Locations 4, 5, 6 are not considered due to the concrete caissons are laying here.

The maximum wave height occurring at the toe of these protective structures is limited by the depth in front of these structures. The water depth at the front of the structures is around 6 meters. Also wind induced setup of 0.5 meters is assumed.

TABLE II.
THE DIMENSIONS OF TETRAPOD'S

	C [m]	H [m]	V [m^3]	M [kg]
Small Tetrapod	0.80	1.68	1.32	3045.44
Large Tetrapod	1.08	2.26	3.25	7492.91

The maximum significant wave height is then given by:

$$H_{max} = (1+\propto * H_o)H_{const} \quad (5)$$

where

H_{max} - the maximum wave height [m],
H_o - the minimum wave height [m],
H_{const} - average wave height [m]
α - corrections coefficient

D. Results

In the total area of the Grand Hotel Varna many tetrapods are present. Most of these can be re-used for reinforcing the coast. There are two different sizes of tetrapod's available on the coast.

The dimensions of these tetrapods are determined by measuring one rib with a measuring tape. The rest of the dimensions can be determined by parameters on Fig.2 in which "h" is the height of the total tetrapod and "d" is the length of a rib.

Fig.7 shows the severely tetrapods on location 3. A lot of tetrapods on the different locations have cracks on them or have pieces that are broken off. Still most of the elements, as indicated in Table 2, are reusable. Although with moving these elements there is a danger that the tetrapod's will be damaged. Thereby a few elements at location 3 are poured in concrete and per definition cannot be moved (Fig. 7.)

Figure 7. Tetrapod's on location 3

IV. CONCLUSIONS

The first conclusion that can be made from the inventory is the lack of structure in the design of the break water and other protective structure. A lot of different materials are used and it seems that a lot of them are randomly dumped at their current location. Due to this great amount of (broken) units it will be very expensive to remove these elements. Probably the easiest and cheapest way is to demolish the elements and use them as core or fill materials for the new design of the breakwater or other structures. The tetrapods are in good shape can be used, together with new produced elements as the armour layer.

The rocks in the different locations comes in all shape and sizes. Therefore, there're a lot of possibilities reusing of these rocks. The smaller rocks are also easier to place on a different location, so there're versatile to reuse.

According to the calculations of the maximum significant wave height the break waters and other protective structures can withstand; the values are under the maximum significant wave height that can occur. This means that especially for location 1, 2 and 3 the present design is not sufficient to the wave conditions that can occur. This is confirmed by the fact that some of the tetrapods are displaced and/or broken.

REFERENCES

[1] Arkhipkin, V. S., F.N. Gippius, and K.P. Koltermann. Wind waves in the Black Sea: results of a hindcast study. Natural Hazards and Earth System Sciences, 2014.

[2] Burcharth, Hans Falk, Jacob Birk Jensen, Z. Liu, J. W. van der Meer, and K. d'Angremond. Breakage of

[3] Tetrapods. In Proceedings of the Final Workshop, Rubble Mound Breakwater Failure Modes,. Sorrento, Italy: Aalborg University, 1995.

[4] Joan Pope, U.S. Army Engineer Research and Development Center, Vicksburg, Mississippi. "Coastal Engineering Manual." 2006.

[5] Pilarczyk, K.W. Dikes and revetments, design, maintenance and safety assessment. Delft, 1998.

[6] Verhagen, H.J., K. d'Angremond, and F. van Roode. Breakwaters and closure dams. Delft: VSSD, 2009.

Software Development for a New Technology of Precision Application of Powder Coating Multifunctional Systems

D.L. Alontseva, A.L. Krasavin, O.B. Ospanov
East Kazakhstan State Technical University, 69, Protazanov Street, 070004 Ust-Kamenogorsk, Kazakhstan
dalontseva@mail.ru
alexanderkrasavin@mail.ru
ospanovolzhas@gmail.com

Abstract - **The paper presents the main results of software development for a new technology of precision application of powder coating multifunctional systems to protect surfaces of industrial products using microplasma material processing complex with the assistance of an industrial robot. The use of this technology allows receiving multifunctional systems of powder coatings with the predicted nanostructure and a complex set of properties such as microhardness and corrosion resistance. The choice of components for developing multifunctional powder coating systems and the trajectory of the plasma source and processing modes is made on the basis of the optimized condition identified by the initial experimentation and mathematical modeling. The numerical methods have been implemented for modeling of temperature fields raised by the radiation treatment of coatings. A proprietary software product has been developed to perform calculations of temperature fields in a number of industrial materials under irradiation.**

I. INTRODUCTION

Nowadays, various types of thermal spray coating processes for surface protection against temperature extremes, corrosion and wear are actively developing all over the world [1,2]. Among the different existing plasma spraying processes, the Microplasma Spraying (MPS) is particularly characterized by the low plasma power, low plasma gas flow rate, small spray spot (1...5mm), and a possibility of forming a laminar jet with the length of 100 ... 150 mm, which heats the refractory material in a stream of Ar plasma and provides low heat input into the substrate [3-6]. These properties are very beneficial for the deposition of coatings on small parts or with high accuracy. However, there are still a number of challenges, and the most important among them is a problem of the formation of coatings with the specified structure and properties.

The main prerequisites for the development of the study were the analyses of technical issues arising from the application of industrial robot for coating by plasma jets, and the desire to expand the range of tasks solved by the application of an industrial robot. The technologies of plasma spraying of coatings require accurate sustaining **of** the number of technological parameters (the distance from the plasma system nozzle to the surface of a work piece, the nozzle movement speed, etc.) during the entire processing time. Exceeding these parameters beyond the permissible limits can lead not only to rejected products, but also to an accident (a short circuit). In cases when the robot program is generated according to a given geometrical model of a processed work piece or part, the deflection of the real object shape from the model often leads to the violation of technological parameters of processing with all its undesirable consequences.

The aim of this work was to develop the software to perform calculations of temperature fields in a number of industrial materials under irradiation by **a** moving source for the deposition of coatings with the predicted nanostructure and to solve the problem of providing the desired trajectory of the plasma source. Our previous works [7, 8] dealt with the selection of relevant components for developing multifunctional powder coating systems and appropriate trajectory of the plasma source and processing modes. It was based on mathematical modeling of the optimized condition determined by our initial experimentation [9, 10].

II. EXPERIMENT

A. Materials and Methods

The research material is PG-19N-01 (Ni- based powder alloy with additives of Cr (14…20%), B (3.5%), Si (4.3%), Fe (7%), C (0.8%) deposited onto the Steel St3 (Fe – base, C - 0.25 %, Mn – 0.8 %, Si – 0.37 %, P < 0.045%) substrate by a plasma jet. In order to form the desired nanostructures in microplasma coatings we used the same powders as for plasma detonation coatings where we observed these nanostructures previously [7, 8].

The microplasma deposition of powders onto steel substrates was carried out at a pilot production site at the East-Kazakhstan State Technical University equipped with the industrial complex microplasma processing of materials on the basis of Kawasaki RS010L industrial robot (Kawasaki Robotics, Japan). The robot arm has a mounted device for the microplasma deposition of "MPN-004" powder coating (produced by Paton Institute, Ukraine), in which the powder is fed in a stream of argon

onto a substrate of any shape. Innotech Ltd, Kazakhstan, carried out the mounting of the robot. To solve the problem of providing the desired trajectory of the plasma source, we have developed the software, which converts the drawings made in AutoCAD and Compass to the robot controller by selecting the graphics primitives (line, arc, etc.) from the drawings and transferred them into the commands for the robot arm movement.

B. Model of heat propagation processes taking place during radiation treatment of coatings

The model of heat propagation processes is based on nonlinear heat conduction equation (1)

$$\nabla \cdot (k(T)\nabla T) = c(T)\frac{\partial T}{\partial t} \quad (1)$$

Let x, y, z be the moving Cartesian coordinate system, where x – axe lying along the heat source motion direction and z-axe is perpendicular to surface plane. The velocity of the coordinate system is equal to the velocity of a heat source v. In that coordinate system, the equation (1) becomes the equation (2)

$$\nabla \cdot (\mathrm{k(T)}\nabla \mathrm{T}) = \mathrm{c(T)}\left(\frac{\partial \mathrm{T}}{\partial \mathrm{t}} - \mathrm{v}\frac{\partial \mathrm{T}}{\partial \mathrm{x}}\right) \quad (2)$$

The term $\nabla \cdot (k(T)\nabla T)$ of equation (1) can be linearized using Kirchhoff's transformation

$$U(T) = \int_{T_0}^{T} k(t)\,dt \quad (3)$$

Assuming the term $\frac{\partial T}{\partial t}$ negligible small and applying Kirchhoff's transform to equation (2) we obtain a quasi-steady-state heat conduction equation (4).

$$\Delta U + vF(U)\frac{\partial U}{\partial x} = 0 \quad (4)$$

C. Boundary value problems for a quasi-steady-state equation

Let $T_1(x, y, z)$ be a quasi-steady temperature field in the coating, $T_2(x, y, z)$ - quasi-steady temperature field in the base system, and U_1 , U_2 - Kirchhoff's transforms of T_1 and T_2 respectively. Boundary conditions for nonlinear differential equations (5) and (6)

$$\Delta U_1 + vF_1(U)\frac{\partial U_1}{\partial x} = 0 \quad (5)$$

$$\Delta U_2 + vF_2(U)\frac{\partial U_2}{\partial x} = 0 \quad (6)$$

are conditions (7) - (10):

$$\left(\frac{\partial U_1}{\partial z}\right)_{z=0} = -P(x, y) \quad (7)$$

$$\left(\frac{\partial U_1}{\partial z}\right)_{z=h} = \left(\frac{\partial U_2}{\partial z}\right)_{z=h} \quad (8)$$

$$U_1|_{z=h} = U_2|_{z=h} \quad (9)$$

$$U_2|_{z=\infty} = 0 \quad (10)$$

D. Description of numerical methods

Our approach of numerical solving of boundary problems described above is based on the problem splitting into two independent problems described below.

Problem 1.Von Neumann boundary problem for a semi – infinite sheet with finite thickness h with boundary conditions (7) and (11)

$$\left(\frac{\partial U_1}{\partial z}\right)_{z=h} = -Q(x, y) \quad (11)$$

where $Q(x, y)$ is the distribution of the flat heat source.

Problem 2. Von Neumann boundary problem for half-space.

Boundary condition on the surface is:

$$\left(\frac{\partial U_2}{\partial z}\right)_{z=h} = -Q(x, y) \quad (12)$$

In our approach problems, the equations (1) and (2) are reduced to nonlinear integral equations, which are solved numerically using the iteration method.

We have developed the software that implements numerical methods described above for modeling of temperature fields raised by the radiation treatment of coatings. The program is written in Python, for the implementation of standard numerical methods a NumPy and a SciPy libraries were used.

We have simulated a number of processes taking place in the coatings with the purpose to achieve the desired precipitation from the melt phase during the deposition and cooling processes, as well as during the additional treatment by a plasma jet (Fig.1). This includes the optimum choice of the power density of a plasma source on the coating surface and also an efficient speed of the source movement. A specific temperature field in the system of a coating-substrate has been created to provide the precipitation of hardening phases in the coating during the added treatment. During this procedure the surface of the coating is melted, whereas the area of the interface of the coating with substrate is exposed to the temperature of about 400°C for several minutes. In our previous study the temperature distribution in two-layer absorbers was calculated using both: a permanent linear case model and a variable thermal parameters non-linear model [9, 10].

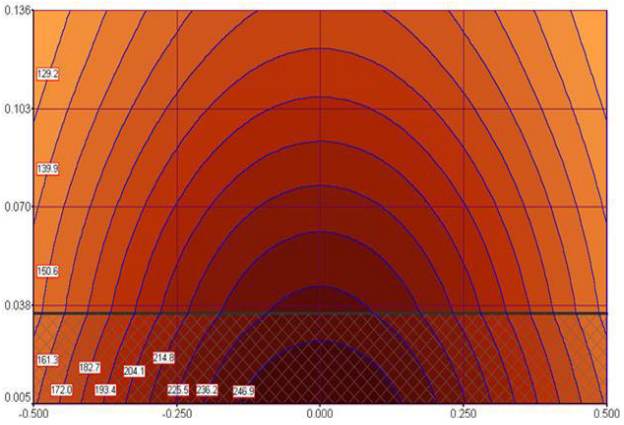

Figure 1. The contour map of the temperature field (cut perpendicular to the plane of the sample surface, the vector of the beam velocity is parallel to the plane of the cut)

E. The modes of surface treatment

Deposition and additional treatment parameters are given in Table 1. The additional treatment of the samples by a plasma jet was carried out at power density of 2.0×10^9 W/m^2.

TABLE I.
REGIMES OF COATINGS SYNTHESIS

Modes	P [W]	U[V]	I [A]	The plasma forming gas (Ar) flow rate [liter/hour]	The protective gas (Ar) flow rate [iter/hour]	The travel speed of the plasma jet [m/s]	The powder flow rate [kg/hour]	The powder utilization rate
Deposition	2	30	40	70	360	0.008	2	0.7
Additional treatment	2	30	40	60	250	0.006	-	-

F. Experimental methods of coating structures analysis

Experimental methods of analysis include Transmission Electron Microscopy (TEM) by JEM-2100 ("JEOL", Japan) with Energy Dispersive Spectrometry (EDS) INCA Energy TEM 350 ("Oxford Instruments", Great Britain), Scanning Election Microscopy (SEM) by JSM-6390LV ("JEOL", Japan), X-ray diffraction (XRD) by X'Pert PRO ("PANalytical", the Netherlands). M-691 Precision Ion Polishing System ("Gatan", USA) was used to prepare TEM foils by the Ar ion sputter etching method. Microhardness test of the samples was performed with LM-700 digital microhardness meter (LECO, Russia). Corrosion was tested using the potentiostatic method to measure the sea-water corrosion rate.

III. RESULTS

XRD methods have allowed to establish that phase compositions of the initial powder PG-19N-01 and the microplasma coating are different. A new $CrNi_3$ intermetallic phase has appeared in the coating and the volume concentration of $Cr_{13}Ni_5Si_2$ phase has decreased by 2.5 times compared to the initial powder. As TEM analysis demonstrates, the coating is mainly composed of crystallographically disoriented nanograins of Ni-based solid solution with the fcc type of crystal lattice, which precipitates nanoscale lamellae of the $CrNi_3$ intermetallic phase with the same fcc structure (Fig. 2). The EDX spectrum shows the presence of such elements as Ni, Cr, Fe, that is in a good agreement with XRD results.

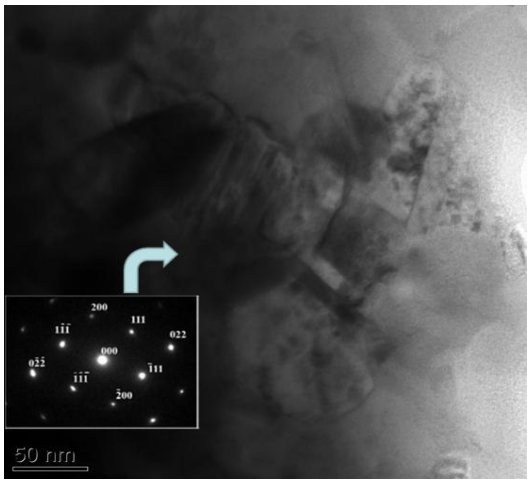

Figure 2. The TEM image of the PG-19N-01 coating with the lamellas of intermetallic phases and the corresponding micro diffraction pattern

SEM images of the coating surface show the broken powder particles (Fig. 3 a). By TEM methods we observe the twins in the substrate grains (Fig. 3 b). Probably, the twins appear for lowering the stress in the surface layer of the substrate due to impact of the plasma jet with powder particles.

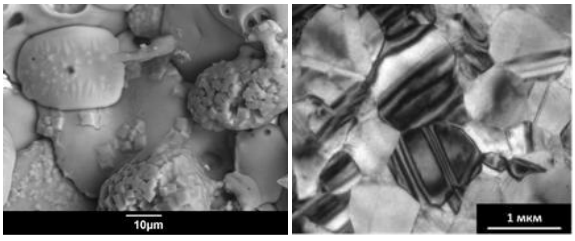

a b

Figure 3. The SEM image of the PG-19N-01 coating (a); the TEM image of the substrate Steel 3 (b)

The microhardness of the coating is 7.0 ±0.05 GPa in average. The results of the corrosion resistance test in the seawater confirm the sufficient growth of corrosion resistance for the coated samples compared to an unprotected substrate. Steel 3 substrate and PG-19N-01coating sea water corrosion potential is rather high: φ_{corr}= – 0.28 V and φ_{corr}= – 0.35 V correspondingly. Yet the substrate corrosion rate is considerably higher: i_{corr}(substrate)=3.9 mm/yr, i_{corr}(coating)=2.7 mm/yr.

To sum up, we have managed to obtain the coatings with predicted structure-phase composition and properties for specified materials. We suppose these results are quite important due to the following reasons: firstly, the structure of coatings is similar to the structure of nanocomposite, the coating consists of the ductile base with fcc lattice type which is reinforced by lamellas of hard and heat-resistant intermetallic phase. In perspective, it gives the possibility of creating a protective coating having a combination of such properties as thermal stability, high hardness and good ductility all at once, as noted also by the authors of works [2, 4, 6]. Secondly, the results indirectly confirm the correctness of the computer stimulation of temperature profiles; therefore, we have designed the correct model of the process as the whole process and the reliable software in particular. In the future, we can expand the database on thermal properties of various metals and greater use of mathematical modeling in the practice of obtaining protective coatings.

IV. CONCLUSION

A proprietary software product has been developed to perform calculations of temperature fields in a number of industrial materials under irradiation, and evidence-based recommendations have been provided on the choice of modes of surface modification by the microplasma (the trajectory and speed of the plasma source, the power density of the microplasma). The laboratory samples with protective powder coatings deposited by the microplasma according to recommended modes onto steel substrates have been obtained, and it was established experimentally that the coatings have the predicted structure-phase composition, namely the nanograin Ni-based solid solution with precipitations of strengthening intermetallic lamellas which provide the coatings high microhardness. The coatings have a good corrosion resistance in seawater. Thus, the scientific bases of the surface modification technology have been implemented by microplasma exposure and an automated pilot production site has been developed.

ACKNOWLEDGMENT

The authors thankfully acknowledge the funding provided by the Scientific Committee of the Ministry of Education and Science of the Republic of Kazakhstan for the project 0869/GF titled “Automated precision deposition of powder coating multifunctional systems”.

REFERENCES

[1] S.Kuroda, J. Kawakita, M.Watanabe, H. Katanoda, Warm spraying—a novel coating process based on high-velocity impact of solid particles, Sci. Technol. Adv. Mater. 9 (3): 033002. (2008). DOI:10.1088/1468-6996/9/3/033002.

[2] Mahmood Aliofkhazraei, Comprehensive Guide for Nanocoatings Technology, Nova Science Publishers, Properties and Development, Vol.3, NY, 2015, 481p. ISBN 978-1-63482-647-1.

[3] L.Wang, H.Wang, S.Hua, X. Cao, *Plasma Science and Technology.* 9, 52 (2007). DOI: http://dx.doi.org/10.1088/1009-0630/9/1/11.

[4] E. Lugscheider, K. Bobzin, L. Zhao and J. Zwick, Assessment of the Microplasma Spraying Process for Coating Application Advanced Engineering Materials Special Issue: Thick Coatings for Thermal, Environmental and Wear Protection Volume 8, Issue 7, 2006, p. 635–639. DOI: 10.1002/adem.200600054.

[5] L.Travis, J.Michael, Spray deposition of nanostructured metal films using hydrodynamically stabilized, high-pressure microplasmas J. Vac. Sci. Technol. A 31, 061312 (2013); http://dx.doi.org/10.1116/1.4825129.

[6] A V Andreev, I Y Litovchenko, A D Korotaev, D P Borisov Thermal Stability of Ti-C-Ni-Cr and Ti-C-Ni-Cr-Al-Si Nanocomposite Coatings 12th International Conference on Gas Discharge Plasmas and Their Applications. IOP Publishing Journal of Physics: Conference Series 652 (2015). . DOI:10.1088/1742-6596/652/1/012057.

[7] D.L. Alontseva, A.L. Krasavin, A.V. Russakova, T.A. Kolesnikova, G. S. Bektasova , *Materials Science (Medziagotyra)* 22, 2 (2016). DOI: 10.5755/j01.ms.22.2.7699.

[8] D. Alontseva, E. Ghassemieh The Structure-Phase Compositions of Powder Ni – based Coatings after Modification by DC, *Journal of Physics*, (2015) DOI:10.1088/1742-6596/644/1/012009.

[9] A.L. Krasavin, D.L. Alontseva, N.F. Denisova, Certificate of authorship No.0010558 of the Republic of Kazakhstan for the computer program (entry in the register number 1151 of August 20, 2013).

[10] D.L. Alontseva, A.L. Krasavin, T.A. Kolesnikova, A.V. Russakova, Acta Physica Polonica A 125, 6 (2014). DOI: 10.12693/ APhysPolA.125.1275.